

Exploiting aldolase variants in the synthesis of fluorinated analogues of *N*-acetyl neuraminic acid

Jennifer Ann Stockwell

Submitted in accordance with the requirements for the degree of
Doctor of Philosophy

The University of Leeds
Astbury Centre for Structural Molecular Biology
and
Department of Chemistry

September 2013

The candidate confirms that the work submitted is her own and that appropriate credit has been given where reference has been made to the work of others.

This copy has been supplied on the understanding that it is copyright material and that no quotation from the thesis may be published without proper acknowledgement.

©2013 The University of Leeds and Jennifer Ann Stockwell

The right of Jennifer Ann Stockwell to be identified as Author of this work has been asserted by her in accordance with the Copyright, Designs and Patents Act 1988.

Acknowledgements

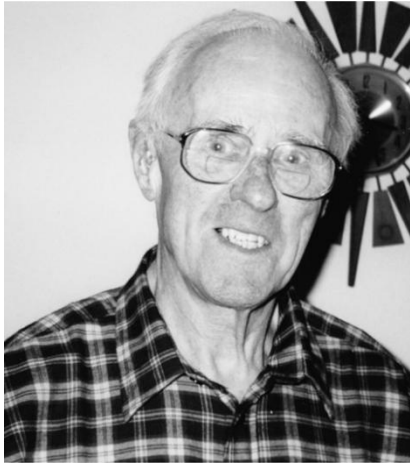
I'd like to start off by thanking my supervisors Prof. Adam Nelson and Prof. Alan Berry for all the help and guidance they have given me over the last four years. Without their support, I wouldn't be sitting here writing these acknowledgements. I'd also like to thank my industrial supervisor Dr. Keith Mulholland, it was with his support and friendship that I was able to gain confidence and realise what I wanted to do with my life. My time at AstraZeneca was brilliant and there are too many people to thank individually, so I would like to say thank you all for making me feel so welcome.

I would particularly like to thank Dr. Adam Daniels and Claire Windle for all their contributions, to Adam for his brilliant work towards greater understanding of the enzyme mechanism and to Claire for her beautiful crystal structure. I would also like to thank Dr. Tomas Lebl from the University of St. Andrews for all his help with the 2D ^{19}F NMR studies. Thank you also to the support staff at the University of Leeds; Martin Huscroft for his help with HPLC, Simon Barrett for his help with NMR and Tanya Marinko-Covell for providing the HRMS service. I'd also like to thank all the past and present members of the Nelson and Berry groups for their support and contributions.

Next I would like to thank my proof readers. Richard Doveston you have been brilliant, thank you so much for all your help. Also, thank you to my wonderful boyfriend Nathan Chapman; even though you had no idea what I was on about, you were still brilliant at picking out the times when I'd just written incomprehensible and grammatically incorrect gibberish. Also, thank you to Nathan for keeping me sane over the last few months.

I'd like to thank my family. My parents, for motivating me and for staying calm when I was at my most stressed. Finally, I'd particularly like to thank my two grandfathers who unfortunately didn't live long enough to see me fulfil my dreams, but supported me throughout my education and would be so proud to see me now.

Thank you Grandpa and Grandad



Ken Harrington

1919 - 2007



Ken Stockwell

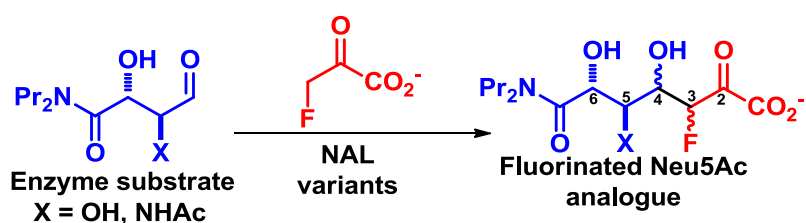
1924 - 2013

Abstract

This thesis reports the use of NAL variants to catalyse the reaction between a range of aldehyde analogues and fluoropyruvate, generating two new stereogenic centres. These reactions were catalysed by variants of *N*-acetyl neuraminic acid lyase (NAL). Wild-type NAL catalyses the aldol reaction between pyruvate and *N*-acetyl mannosamine (ManNAc) to give *N*-acetylneuraminic acid (Neu5Ac) whereas the NAL variants were evolved to catalyse the aldol reaction between pyruvate and the aldehyde analogue **DHOB** ([2*R*,3*S*]-2,3-dihydroxy-4-oxo-*N,N*-dipropylbutanamide) to give **DPAH** ([5*R*,6*R*]-7-(dipropylamino)-4,5,6-trihydroxy-2,7-dioxoheptanoic acid). This work has sought to explore the effect on the activity and stereoselectivity of the NAL variants with a broader range of substrates. A major challenge was the identification of the products of the NAL variant catalysed reactions and to determine the selectivity of each NAL variant. ¹⁹F NMR spectroscopy was invaluable in aiding characterisation of the enzyme reaction products.

Synthesis of the enzyme substrate where **X**=NHAc has been of particular focus within this work and has provided further insight into the potential importance of the *N*-acetyl group in directing the binding of the aldehyde, therefore directing the diastereoselectivity. This work has also discovered that the introduction of fluorine may have an effect on the energy barrier to the transition state leading to the (4*R*) and (4*S*)-epimers of the products. However, in the case of more sterically demanding aldehydes, the diastereoselectivity is predominantly driven by the initial binding mode.

This work has provided a more in-depth understanding of the effect of changing both the donor and acceptor substrates of the NAL-catalysed reaction. It has also evaluated the viability of using NAL variants in the synthesis of fluorinated analogues of *N*-acetyl neuraminic acid.



Contents

Acknowledgements	ii
Abstract	iv
Contents	v
List of Figures, Schemes, Tables and Charts	x
Abbreviations	xvii
Chapter 1 Introduction	1
1.1 Relevance of fluorinated sialic acid analogues in medicinal chemistry	2
1.1.1 Biological activity and applications of sialic acid analogues.....	2
1.1.2 The importance of fluorine in medicinal chemistry	4
1.1.3 The <i>gauche</i> effect in organo-fluorine molecules	5
1.1.4 Potential value of fluorinated sialic acid analogues	6
1.2 Chemical methods for the synthesis of organo-fluorine molecules	7
1.2.1 Aldol reactions of α -fluoro ketones	7
1.2.2 Carbon-fluorine bond forming reactions.....	9
1.3 Wild type <i>N</i> -Acetyl-neuraminidase (NAL).....	13
1.3.1 Mechanism of wild-type NAL.....	13
1.3.2 Substrate specificity of NAL	18
1.4 Protein engineering of NAL E192N variants	22
1.4.1 Engineering of NAL variants with modified activity	23
1.4.2 Identification of the NAL E192N variant and substrate specificity	24
1.4.3 Quantum mechanical/molecular mechanical studies of the active-site of NAL E192N	27
1.4.4 Discovery of a complementary pair of stereoselective enzymes.....	28
1.5 Thesis overview	30
Chapter 2 Synthesis of Enzyme Substrates	32

2.1. Substrate Design.....	32
2.2. Synthesis of the stable alkene precursor of DHOB.....	34
2.3. Synthesis of a stable precursors of AHOB and <i>ent</i> -AHOB	35
2.3.1. Retrosynthetic analysis of the stable precursors of AHOB/ <i>ent</i> -AHOB.....	35
2.3.2. Synthesis of AHOB utilising the Petasis reaction.....	36
2.3.3. Reactions of the lactone intermediate 33	42
2.3.4. Conversion of the lactone intermediate 35 into AHOB.....	46
Chapter 3 NAL-catalysed reactions of aldehyde analogues and pyruvate	51
3.1 NAL E192N variants in the preparation of <i>N</i> -acetyl neuraminic acid analogues ..	51
3.1.1 Preparation of NAL variants and aldehyde substrates.....	51
3.1.2 Preparative scale enzyme catalysed reactions of AHOB with pyruvate.....	53
3.1.3 Identification and characterisation of AHOB enzyme catalysed reaction products	54
3.1.4 Measuring activity of the cleavage of the products of enzyme catalysed reactions.....	56
3.2 Monitoring enzyme catalysed reactions of AHOB by 500 MHz ¹ H NMR spectroscopy	59
3.2.1 Comparison of activities and kinetic selectivity of enzyme catalysed reactions of AHOB	59
3.3 Rationalisation of the observed outcomes of enzyme catalysed reactions of AHOB	63
3.3.1 Proposed modified binding mode of AHOB compared to DHOB.....	63
3.3.2 Rationalisation of complete loss of activity of NAL E192N/T167V/S208V with AHOB	67
Chapter 4 NAL-catalysed reactions of aldehyde analogues and fluoropyruvate ...	70
4.1 Understanding and interpreting the diastereoselectivity of reactions of NAL variants with fluoropyruvate	70
4.1.1 ¹⁹ F NMR spectroscopy as a diagnostic tool	70

4.1.2 Prediction of the enzyme reaction products based on QM/MM modelling studies	73
4.2 NAL E192N variants in the preparation of 3-fluoro- <i>N</i> -acetyl neuraminic acid analogues from AHOB.....	76
4.2.1 Conditions for the enzyme catalysed reaction between 3-fluoropyruvate and AHOB	76
4.2.2 Identification and characterisation of diastereomers of enzyme catalysed reactions of AHOB and fluoropyruvate.....	79
4.3 NAL variants in the preparation of 3-fluoro- <i>N</i> -acetyl neuraminic acid analogues from DHOB	82
4.3.1 Challenges presented in the characterisation of products derived from DHOB... 82	
4.3.2 Characterisation of the products of the NAL variant-catalysed reactions of DHOB and fluoropyruvate	87
4.3.3 Summary of the products of the NAL-catalysed reaction of DHOB/ <i>ent</i> -DHOB and fluoropyruvate	99
4.4 Analysis of reactions of alternative substrates catalysed by NAL E192N variants by 296 MHz ¹⁹ F NMR spectroscopy.....	100
4.4.1 Comparison of initial rates of enzyme catalysed reactions.....	100
4.4.2 Determination of diastereoselectivity under kinetic control.....	104
4.4.3 Evaluation of the value of NAL variants in the synthesis of fluorinated <i>N</i> -acetyl neuraminic acid analogues	108
4.5 Discussion of the observed activity and diastereoselectivity of the reactions of alternative substrates catalysed by NAL variants	110
4.5.1 Evaluation of the predicted diastereoselectivity of NAL variants at the fluorine-bearing chiral centre	110
4.5.2 Structural evidence for reduced activity of the alternative donor	113
4.5.3 Structural evidence for changes in selectivity of the alternative donor	114
Chapter 5 Conclusions and future outlook	116
5.1 Overview and conclusions	116

5.2	Future outlook	119
5.2.1	Probing the proposed binding mode of new NAL substrates	119
5.2.2	Engineering NAL variants with greater activity towards fluorinated substrates	120
5.2.3	Optimisation of synthesis of <i>N</i> -acetyl neuraminic acid analogues	120
5.2.4	Design of new aldehyde substrates.....	121
Chapter 6	Materials and Methods and Experimental	122
6.1	Biological Materials and Methods.....	122
6.1.1	Buffers.....	122
6.1.2	Biological equipment.....	123
6.1.3	Purification of His Tagged NAL	124
6.1.4	SDS-PAGE	125
6.1.5	Measuring concentration of NAL.....	126
6.1.6	Measuring single point activity of NAL.....	127
6.2	General experimental	128
6.2.1	General method for ozonolysis	129
6.2.2	General method for monitoring NAL catalysed reactions by 500 MHz ¹ H NMR spectroscopy	129
6.2.3	General method for monitoring NAL catalysed reactions by 296 MHz ¹⁹ F NMR spectroscopy	129
6.3	Experimental methods and characterisation	130
6.3.1	General method for synthesis of fluorinated sialic acid analogues	152
Appendix 1	- Synthesis of non-commercial available reagents	158
A1.1	Synthesis of primary amine used in the Petasis reaction.....	158
A1.2	Optimisation of the synthesis of the selanyl acid chloride.....	158
A1.3	Synthesis of the imine used in the Mannich reaction	161
Appendix 2	- Unsuccessful reduction of enol products 50 and 51	162

Appendix 3 - Monitoring the reaction between aldehyde variants and pyruvate by 500 MHz ¹H NMR spectroscopy	165
Appendix 4 - ¹⁹F NMR spectra from the reactions of AHOB and fluoropyruvate	167
Appendix 5 - Monitoring the reaction between aldehyde variants and fluoropyruvate by 296 MHz ¹⁹F NMR spectroscopy	168
A5.1 Reactions of AHOB/ <i>ent</i> -AHOB and fluoropyruvate	168
A5.2 Reaction of DHOB/ <i>ent</i> -DHOB and fluoropyruvate	170
A5.3 Rate of NAL E192N catalysed reaction: Pyruvate Vs fluoropyruvate	173
References	174

List of Figures, Schemes, Tables and Charts

Figures:

Figure 1.1 - Structure of inhibitors of influenza neuraminidase.....	3
Figure 1.2 – Carboxamide influenza neuraminidase inhibitors	4
Figure 1.3 - Examples of two top selling fluorinated pharmaceuticals	4
Figure 1.4 - The <i>gauche</i> effect in 1,2-difluoro ethane	6
Figure 1.5 - <i>Gauche</i> preference of different conformations of 2-fluoroethylamine and 2-fluoroethanol	6
Figure 1.6 - Catalysts of asymmetric aldol reactions	8
Figure 1.7 - Transition state diagrams to rationalise the diastereoselectivity of amine catalysed aldol reaction of fluoroacetone.	9
Figure 1.8 – NFSI and general structure of Selectfluor	10
Figure 1.9 - General scheme for fluorodesilylation of allylsilanes.....	12
Figure 1.10 - Comparison of Class I and Class II aldolases.	14
Figure 1.11 – Representations of key binding interactions between ManNAc/Neu5Ac in the active site of NAL	15
Figure 1.12 - Representation of the transition state of the NAL catalysed reaction of ManNAc and pyruvate to give Neu5Ac.....	17
Figure 1.13 - Configuration of the enamine of fluoropyruvate	22
Figure 1.14 - Comparison of active-sites of wild-type NAL and the NAL E192N variant	26
Figure 1.15 – Amide derivatives accepted by NAL E192N	27
Figure 1.16 - Summary of the results of QM/MM modelling of the NAL E192N catalysed reaction between DHOB and pyruvate	28
Figure 1.17 – DPAH screening substrates.	29
Figure 2.1 - Potential acceptor substrates of the NAL variant-catalysed reaction with fluoropyruvate.	33
Figure 2.2 - Stable alkene precursors of DHOB/ <i>ent</i> -DHOB (24/ <i>ent</i> -24) and AHOB/ <i>ent</i> -AHOB (25/ <i>ent</i> -25).....	34
Figure 2.3 - Primary amine 36a and secondary amine 36b.	37
Figure 2.4 - Transition state comparisons for the aldol and Mannich reactions of the lactone 33.....	46

Figure 3.1 - SDS-PAGE during NAL E192N purification.	52
Figure 3.2 - 500 MHz ¹ H NMR spectra of the products of the NAL variant-catalysed reaction of AHOB/ <i>ent</i> -AHOB and pyruvate.	55
Figure 3.3 – 500 MHz ¹ H NMR spectroscopy time-course of the NAL E192N-catalysed reaction of AHOB and pyruvate.	60
Figure 3.4 - <i>N</i> -acetyl group built onto the C-3 hydroxyl group of the THB inhibitor in the major and minor binding modes.....	65
Figure 3.5 - Computationally modified inhibitor 56 in the minor binding mode of THB	66
Figure 3.6 - Distances between the mutated residues in the diastereoselective NAL variants E192N/T167V/S208V and E192N/T167G and the bound enzyme substrates..	68
Figure 4.1 - Ring forms of the products of the NAL E192N catalysed reactions between aldehyde substrate DHOB or AHOB and fluoropyruvate.....	71
Figure 4.2 - Geminal proton-fluorine coupling constants.....	72
Figure 4.3 - Schematic representation of relative proton-fluorine and proton-proton vicinal coupling constants	73
Figure 4.4 - Illustration of nomenclature for describing the two faces of the fluoro-enamine.....	74
Figure 4.5 - The enamine complex between K165 and fluoropyruvate in the NAL active site.....	75
Figure 4.6 - Newman projections of the "top" face of the (<i>Z</i>)-enamine attacking the <i>re</i> or <i>si</i> -face of the aldehyde	76
Figure 4.7 - 296 MHz ¹⁹ F NMR of the mass-directed reverse-phase HPLC purified product 57a.....	79
Figure 4.8 - 500 MHz ¹ H NMR spectrum of the product 57a.....	81
Figure 4.9 - 395 MHz ¹⁹ F NMR of products isolated after ion exchange of the reactions between fluoropyruvate and DHOB catalysed by NAL variants.	86
Figure 4.10 - 395 MHz ¹⁹ F NMR of products isolated after ion exchange of the reactions between fluoropyruvate and <i>ent</i> -DHOB catalysed by NAL variants.....	87
Figure 4.11 – Expansion of the 500 MHz ¹ H NMR spectrum of the product <i>ent</i> -23d	89
Figure 4.12 - NOE spectrum of <i>ent</i> -23d	90
Figure 4.13 – Separation of the products of the NAL E192N catalysed reaction of DHOB and fluoropyruvate by reverse-phase HPLC	91

Figure 4.14 – Expansion of the 500 MHz ^1H NMR spectrum of the product 23a	92
Figure 4.15 - NOE spectrum of 23a.	93
Figure 4.16 - Region of the 500 MHz ^1H NMR spectrum of the diastereomer of 23c. ...	94
Figure 4.17 – Extraction of the individual ^1H NMR spectra corresponding to each of the equilibrium species of 23c by $^1\text{H}/^{19}\text{F}$ HSQC-TOCSY.	96
Figure 4.18 - $^1\text{H}/^{19}\text{F}$ HSQC-TOCSY spectrum overlaid with $^1\text{H}/^{19}\text{F}$ HMQC spectrum of the product 23c.	97
Figure 4.19 – Time course of the reaction between DHOB and fluoropyruvate catalysed by E192N/T167V/S208V	101
Figure 4.20 – The reaction between AHOB and fluoropyruvate catalysed by NAL E192N	105
Figure 4.21 - Schematic representation of the aldehyde being attacked by the "top" face of the (Z)-fluoroenamine.	111
Figure 4.22 - Crystal structure of NAL E192N in complex with the THB inhibitor	112
Figure 4.23 - Overlaid crystal structures of wild-type NAL from <i>S. aureus</i> (saNAL) in complex with pyruvate and fluoropyruvate	114
Figure 4.24 - Overlaid crystal structures of wild-type NAL from <i>S. aureus</i> NAL (saNAL) in complex with fluoropyruvate and NAL E192N variant from <i>E. coli</i> (ecNAL) in complex with pyruvate bound to the THB inhibitor	115
Figure 5.1 - Inhibitors related to substrates of the NAL variants.	119
Figure 5.2 - Potential new NAL substrate	121
Figure 6.1 - NMR tube reaction set up for monitoring NAL-catalysed reactions by 296 MHz ^{19}F NMR.	130

Schemes:

Scheme 1.1 - Biosynthesis of <i>N</i> -acetyl neuraminic acid (Neu5Ac)	3
Scheme 1.2 – Enantioselective palladium-catalysed fluorination of a β -keto phosphate.	11
Scheme 1.3 – Organocatalysed asymmetric fluorination of aldehydes	11
Scheme 1.4 - Diastereoselective synthesis of fluorinated analogues of D-glucitol 17a and L-glucitol 17b and D-mannitol 17c	12
Scheme 1.5 – Electrophilic fluorination synthesis of protected 3-fluoro sialic acid	13

Scheme 1.6 - Wild-type NAL-catalysed reaction of ManNAc and pyruvate.....	13
Scheme 1.7 - Wild-type NAL catalysed reaction between 3-fluoropyruvate and ManNAc.....	20
Scheme 1.8 - Screening substrate DPAH.....	23
Scheme 1.9 – Principle of the standard coupled assay for determining the rate of the retro-aldol reaction by an NAL variant.	24
Scheme 2.1 - Enzyme-catalysed reaction between DHOB and pyruvate and DHOB and fluoropyruvate to give DPAH and the fluorinated product 23	32
Scheme 2.2 – Synthesis of DHOB precursor 24 from D-ribonolactone 26.....	35
Scheme 2.3 – Retrosynthetic analysis of AHOB.	36
Scheme 2.4 – Mechanism of the Petasis reaction	37
Scheme 2.5 – Petasis reaction optimisation	38
Scheme 2.6 – Unsuccessful TEMPO catalysed oxidation.....	40
Scheme 2.7 – Conversion of allyl amine 31b into oxazolidone 42.	40
Scheme 2.8 – Synthesis of the lactone 33 from (<i>S</i>)-chloropropane diol (<i>S</i>)-43.....	42
Scheme 2.9 – Conversion of the lactone 35 into the AHOB precursor 25.....	49
Scheme 2.10 – Synthesis of the <i>ent</i> -AHOB precursor <i>ent</i> -25 from (<i>R</i>)-chloropropane diol (<i>R</i>)-43.....	49
Scheme 3.1 - Conversion of stable alkene precursors 24 and 25 into the corresponding aldehydes DHOB/ <i>ent</i> -DHOB and AHOB/ <i>ent</i> -AHOB by ozonolysis.....	53
Scheme 3.2 – Principle of the standard coupled assay for determining the rate of the retro-aldol reaction of the NAL variant.....	57

Tables:

Table 1.1 - Top selling organofluorine pharmaceuticals.....	5
Table 1.2 - Diastereoselectivity of the reaction between aryl aldehydes and fluoroacetone with a selection of catalysts	8
Table 1.3 – Aldehydes accepted by wild-type NAL.....	19
Table 1.4 - Kinetic parameters of wild-type NAL for the cleavage of Neu5Ac	21
Table 1.5 - Steady-state kinetic parameters for wild-type NAL compared to the E192N variant	24

Table 1.6 - Kinetic parameters of NAL variants towards (4 <i>S</i>) and (4 <i>R</i>)-dipropylamide screening substrates (4 <i>S</i>)-DPAH and (4 <i>R</i>)-DPAH.	30
Table 2.1 – Optimisation of the Petasis reaction.....	39
Table 2.2 - Reactions of lactone 33.....	44
Table 2.3 – Optimisation of condition for opening of the lactone 35.....	48
Table 3.1 - Reactions of the NAL variants with AHOB/ <i>ent</i> -AHOB and pyruvate under preparative conditions.	54
Table 3.2 - Characterisation of the products 55a and <i>ent</i> -55b by 500 MHz ¹ H NMR spectroscopy.	56
Table 3.3 – Kinetic ratio of the NAL variants towards the aldehyde analogues calculated from the 500 MHz ¹ H NMR spectra.	62
Table 4.1 - Typical proton-proton and proton-fluorine vicinal coupling constants in six-membered rings.....	72
Table 4.2 - Conditions, estimated conversion and yield after reverse-phase HPLC purification of the reactions between AHOB and <i>ent</i> -AHOB with fluoropyruvate, catalysed by NAL variants.	78
Table 4.3 - Chemical shifts and coupling constants from the 296 MHz ¹⁹ F NMR of the observed products of the NAL variant-catalysed reactions of AHOB/ <i>ent</i> -AHOB and fluoropyruvate.	80
Table 4.4 - Characteristic chemical shifts and coupling constant of the protons of the pyranose ring of the product 57a.	81
Table 4.5 - Summary of the products of the reactions between AHOB/ <i>ent</i> -AHOB with fluoropyruvate catalysed by NAL variants.	82
Table 4.6 - Conditions, estimated conversion and yield after reverse-phase HPLC purification of the reactions between DHOB and <i>ent</i> -DHOB with fluoropyruvate, catalysed by NAL variants.	84
Table 4.7 - Characterisation by 395 MHz ¹⁹ F NMR spectroscopy of diastereomers from the NAL catalysed reactions of DHOB and <i>ent</i> -DHOB with fluoropyruvate.....	88
Table 4.8 - Diagnostic chemical shifts and coupling constants from the 500 MHz ¹ H NMR of the product 23d.....	89
Table 4.9 - Diagnostic chemical shifts and coupling constants from the 500 MHz ¹ H NMR of the product 23a.	92

Table 4.10 - Diagnostic chemical shifts and coupling constants of the equilibrium species of product 23c from extracted ¹ H NMR spectra.	98
Table 4.11 - Summary of the products of the NAL variant-catalysed reactions between DHOB and <i>ent</i> -DHOB with fluoropyruvate.	99
Table 4.12 - Calculated activity of the NAL variants towards the aldehyde analogues from the disappearance of fluoropyruvate.	102
Table 4.13 – Kinetic ratio of the products of the reactions catalysed by the NAL variants.....	107
Table 5.1 - Summary of NAL-variant catalysed reaction between the aldehyde variants and fluoropyruvate which exhibited the greatest activity and diastereoselectivity....	118
Table 6.1- Buffers	122
Table 6.2– Composition of gels for SDS-PAGE	126
Table 6.3 - SDS buffers	126

Charts:

Chart 3.1 - Single point kinetic measurements of the NAL variants against the products of the NAL E192N-catalysed reactions.....	58
Chart 3.2 - Representation of the percentage disappearance of AHOB and the percentage appearance of product 55a	60
Chart 3.3 – Kinetic ratio of the NAL variants towards the aldehyde analogues.....	63
Chart 4.1 - An example of a plot of the appearance of the product 23c and the disappearance of fluoropyruvate.....	102
Chart 4.2 - Calculated specific activity of NAL variants towards the aldehyde analogues.	103
Chart 4.3 - Specific activities calculated for the reactions of the NAL E192N variant with AHOB/ <i>ent</i> -AHOB with pyruvate and AHOB with fluoropyruvate.	104
Chart 4.4 - An example of a plot of the appearance of enzyme reaction products and disappearance of fluoropyruvate.....	105
Chart 4.5 - Ratio of products of the kinetic controlled reactions of the NAL variants and DHOB and AHOB.	108
Chart 4.6 - Activity and selectivity of NAL variant catalysed reactions of aldehyde analogues and fluoropyruvate.....	109

Chart 4.7 - Representation of the ratio of products with (3*R*):(3*S*) configurations in the reactions between the aldehyde analogues and fluoropyruvate catalysed by NAL variants.....111

Abbreviations

A₃₄₀	Absorbance at 340 nm
AHOB	[2 <i>R</i> ,3 <i>S</i>]-3-Acetamido-2-hydroxy-4-oxo- <i>N,N</i> -dipropylbutanamide
app.	Apparent
ax	Axial
COSY	Correlation spectroscopy
d	Doublet
DBU	1,8-Diazabicycloundec-7-ene
dd	Doublet of doublets
DEPT	Distortionless enhancement by polarisation transfer
DERA	2-Deoxyribose-5-phosphate aldolase
DHOB	[2 <i>R</i> ,3 <i>S</i>]-2,3-Dihydroxy-4-oxo- <i>N,N</i> -dipropylbutanamide
DIBAL	<i>Di</i> isobutylaluminium hydride
DMAP	4-Dimethylaminopyridine
DMF	Dimethylformamide
DPAH	[5 <i>R</i> ,6 <i>R</i>]-7-(Dipropylamino)-4,5,6-trihydroxy-2,7-dioxoheptanoic acid
ecNAL	<i>Escherichia coli</i> <i>N</i> -acetylneuraminic acid lyase
EDC.HCl	1-Ethyl-3-(3-dimethylaminopropyl)carbodiimide hydrochloride salt
EDTA	Ethylenediaminetetraacetic acid
ent	Enantiomer
ent-AHOB	[2 <i>S</i> ,3 <i>R</i>]-3-Acetamido-2-hydroxy-4-oxo- <i>N,N</i> -dipropylbutanamide
ent-DHOB	[2 <i>S</i> ,3 <i>R</i>]-2,3-Dihydroxy-4-oxo- <i>N,N</i> -dipropylbutanamide
eq	Equatorial
ES	Electrospray
FGI	Functional group interconversion
fur	Furanose
HCTU	<i>O</i> -(6-Chlorobenzotriazol-1-yl)- <i>N,N,N',N'</i> -tetramethyluronium hexafluorophosphate
HFIP	Hexafluoro <i>is</i> opropanol
His₆-tag	Hexa-Histidine-tag
HMBC	Heteronuclear multiple bond correlation
HMQC	Heteronuclear multiple quantum correlation
HOBt	<i>N</i> -Hydroxybenzotriazole
HPLC	High-performance liquid chromatography
HSQC	Heteronuclear single quantum correlation
IPTG	<i>iso</i> Propyl- β -D-thiogalactoside
IR	Infrared
K-selectride	Potassium tri- <i>sec</i> -butylborohydride
LC-MS	Liquid chromatography–mass spectrometry
LDH	Lactate dehydrogenase
LiHMDS	Lithium hexamethyldisilazide
m	Multiplet
m.p.	Melting point
maj	Major anomer
ManNAc	<i>N</i> -Acetyl-D-mannosamine
MeCN	Acetonitrile
min	Minor anomer

MTBE	Methyl <i>tert</i> -butyl ether
NADH	Nicotinamide adenine dinucleotide (reduced form)
NAL	<i>N</i> -Acetylneuraminic acid lyase (unless specified - assume NAL refers to <i>N</i> -acetylneuraminic acid lyase from <i>Escherichia coli</i> .)
Neu5Ac	<i>N</i> -Acetylneuraminic acid
NFSI	<i>N</i> -Fluorobenzenesulfonimide
NHAc	<i>N</i> -acetyl
NM	Not measurable
NMR	Nuclear magnetic resonance
NOE	Nuclear overhauser effect
Ns	<i>p</i> -Benzylsulfonamide
PCR	Polymerase chain reaction
PDB	Protein data bank
Petrol	Petroleum ether b.p. 40 to 60 °C
pyr	Pyranose
q	Quartet
QM/MM	Quantum mechanic/molecular mechanic
RT	Room temperature
s	Singlet
saNAL	<i>Staphylococcus aureus</i> <i>N</i> -acetylneuraminic acid lyase
SAX	Strong anion exchange
SCX	Strong cation exchange
SDS-PAGE	Sodium dodecyl sulfate polyacrylamide gel electrophoresis
Selectfluor	1-Chloromethyl-4-fluoro-1,4-diazoniabicyclo[2.2.2]octane bis(tetrafluoroborate)
t	Triplet
TBD	Triazabicyclodecene
TEMED	<i>N,N,N',N'</i> -Tetramethylethylenediamine
TFA	Trifluoroacetic acid
THB	[2 <i>R</i> ,3 <i>R</i>]-2,3,4-Trihydroxy- <i>N,N</i> -dipropylbutanamide
TOCSY	Total correlation spectroscopy
Tris.HCl	Tris(hydroxymethyl)aminomethane hydrochloride salt

Chapter 1 Introduction

Biocatalysis can be defined as the exploitation of enzymes in chemical reactions.¹ Enzymes are fantastically well suited to use in performing chemical transformation, as their diverse and complex three-dimensional structures result in highly accelerated rates of reaction and often excellent stereoselectivity.² Furthermore enzymes often operate at ambient temperatures under aqueous conditions and produce relatively little waste in comparison to traditional catalysts used in organic synthesis.³ It is therefore hardly surprising that enzymes have been increasingly used in industrial processes.⁴ Several classes of enzyme have been exploited in the preparation of pharmaceuticals and fine chemicals; examples include keto-reductases, lipases and aldolases.⁵ Synthetic applications include techniques such as dynamic kinetic resolution, for example in the preparation of chiral amines⁶ and tandem aldol reactions (DERA) used in the synthesis of statins.⁷

As organic chemists, it is often necessary to carry out a chemical transformation with substrates that do not occur naturally. In order to use an enzyme in the synthesis of a non-natural product, it may be necessary to broaden or change the substrate specificity of an enzyme. This may be done using a rational design approach where certain residues are targeted for mutation; however this approach is only an option if the structure and mechanism of the enzyme is well understood.⁸ Alternatively, directed evolution may be employed in order to introduce random mutations, using the principle of Darwinian evolution to screen and select those variants that lead to the desired changes in selectivity.^{9,4} In order for an enzyme variant to be suitable for use in large scale reactions, it may be necessary to use directed evolution to identify variants with higher stability and tolerance to organic solvents.¹

The main focus of this thesis is to investigate the application of enzyme variants in the stereoselective synthesis of chiral fluorinated compounds, in particular, fluorinated analogues of *N*-acetyl neuraminic acid. Fluorine is an atom scarcely found in natural products.¹⁰ Over 130 000 unique natural products have been characterised however only five have been identified containing a carbon-fluorine bond.¹¹ Consequently, there are very few examples of enzymes that use fluorine;^{12, 13} one of the rare examples is a fluorinase found in *Streptomyces cattleya*¹¹ which catalysed a

Chapter 1 - Introduction

substitution reaction in which a fluoride ion displaces L-methionine, forming a C-F bond.^{14, 15} There is evidence that, although Nature did not evolve many enzymes that use fluorinated ligands, some naturally occurring enzymes may also turn over a fluorinated analogue of their natural substrates.¹⁶ While fluorinated natural products are rare, fluorinated drugs are very common due to several benefits observed by the introduction of fluorine into biologically active molecules.^{17,18} Considering both the trend towards incorporation of fluorine into drugs and the growing use of biocatalysis in the synthesis of fine chemicals and pharmaceuticals; combining the two and exploiting biocatalysis in the synthesis of fluorinated molecules is a potentially exciting area of research.

The following Sections outline a number of themes that are directly relevant to this thesis. First, the value of fluorinated *N*-acetyl neuraminic acid analogues is described (Section 1.1). Secondly, traditional chemical methods for the synthesis of fluorinated small molecules is considered (Section 1.2). Finally, an overview of the development and application of *N*-acetyl neuraminic acid lyase (NAL) variants (which have been engineered using a combination of rational design and directed evolution) is provided in Section 1.3 and 1.4.

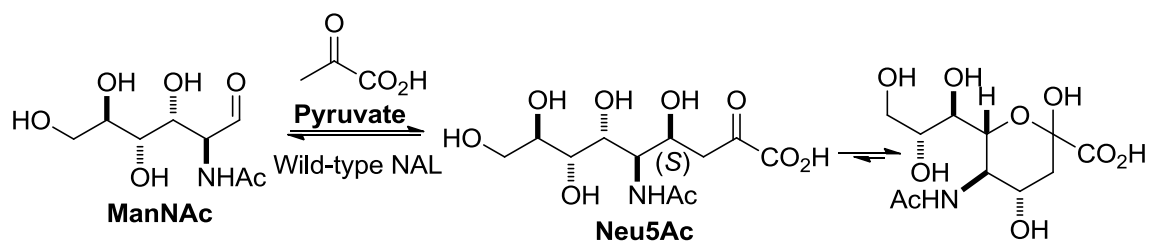
1.1 Relevance of fluorinated sialic acid analogues in medicinal chemistry

1.1.1 Biological activity and applications of sialic acid analogues

Sialic acids are a family of around 50 monosaccharides, including among others, *N*-acetylneuraminic acid (Neu5Ac).¹⁹ Neu5Ac is synthesised by *N*-acetylneuraminic acid lyase (NAL), which catalyses both the aldol (forward) and retro-aldol (cleavage) reaction between *N*-acetyl mannosamine (ManNAc) and pyruvate (Scheme 1.1)*. The reversibility of the reaction is important in preventing accumulation of toxic levels of sialic acid in the cell. Sialic acid plays several important roles in cell biology; however increased levels of sialic acid on the surface of cells, which occurs in some cancers, is believed to be a contributing factor to the detachment of cells from tumours, resulting in metastasis.²⁰

* The mechanism of this reaction is discussed in greater detail in Section 1.3.1.

Chapter 1 - Introduction



Scheme 1.1 - Biosynthesis of *N*-acetyl neuraminic acid (Neu5Ac) from *N*-acetyl mannosamine (ManNAc) and pyruvate, catalysed by *N*-acetyl neuraminic acid lyase (NAL).

The most important application of analogues of sialic acid is in the treatment of influenza. Influenza neuraminidase cleaves the terminal sialic acid from glycoconjugates preventing viral aggregation so that the virus is consequently released from infected cells.²¹ It is also believed that neuraminidase may affect respiratory tract mucus in such a way as to increase viral penetration into epithelial cells.²² Inhibition of neuraminidase has therefore become a widely employed approach for the treatment of influenza.

Several sialic acid analogues have been shown to inhibit influenza neuraminidase. Well known drugs such as Zanamivir (Relenza™)^{21,22,23} and Oseltamivir (Tamiflu™)^{24,25} are potent influenza neuraminidase inhibitors (Figure 1.1). Oseltamivir is a pro-drug; the active compound (Figure 1.1b), known as GS4071,²⁵ was discovered to be a potent inhibitor of influenza A and B neuraminidase.

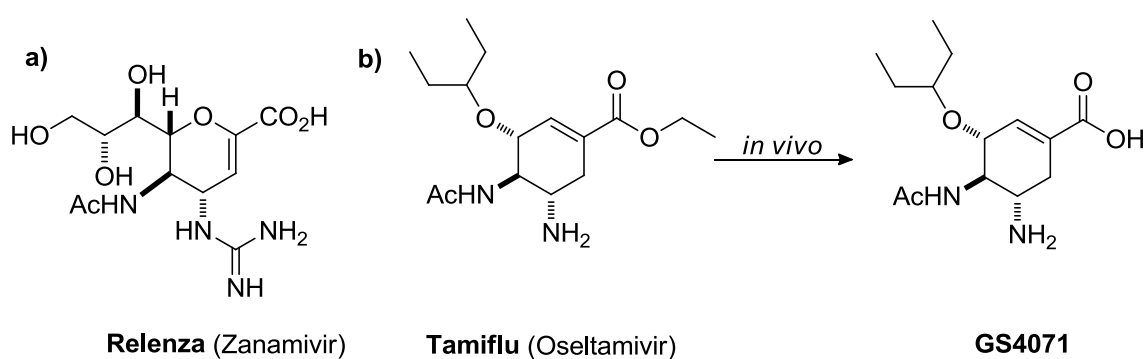


Figure 1.1 - Structure of inhibitors of influenza neuraminidase. a) Zanamivir (Relenza™). b) Oseltamivir (Tamiflu™). Oseltamivir is activated *in vivo* by hydrolysis of the ester to give GS4071.

In 1998, a new series of carboxamide type neuraminidase inhibitors containing an amide group at C-6 was discovered (Figure 1.2). Structure–activity relationships of the

Chapter 1 - Introduction

carboxamide compounds revealed that tertiary amides were more potent inhibitors than secondary amides.^{26, 27} These analogues inspired research into the engineering of NAL to accept a broader variety of substrates;²⁸ and this work will be covered in greater detail in Section 1.4.

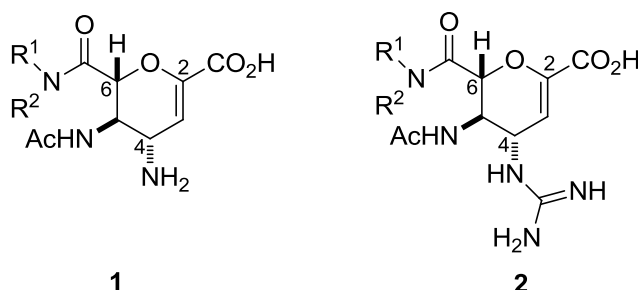


Figure 1.2 – Carboxamide influenza neuraminidase inhibitors

1.1.2 The importance of fluorine in medicinal chemistry

It was first demonstrated in 1954 that introduction of fluorine into the drug cortisol, improved its therapeutic properties. Since then, the popularity of introducing fluorine into biologically active compounds has grown rapidly and now fluorine is found in around 15-20% of new drugs licensed.^{17,18} A review of the top selling drugs in 2012²⁹ revealed several examples containing fluorine, including Crestor (Figure 1.3a), and Lipitor (Figure 1.3b) (generic name atorvastatin), this has been a top selling drug for several years and was ranked top in terms of sales (in US\$) in 2008¹⁸ and 2011.³⁰ Table 1.1 outlines the fluorine-containing drugs in the top 50 of all pharmaceuticals (based on US sales in 2012).²⁹

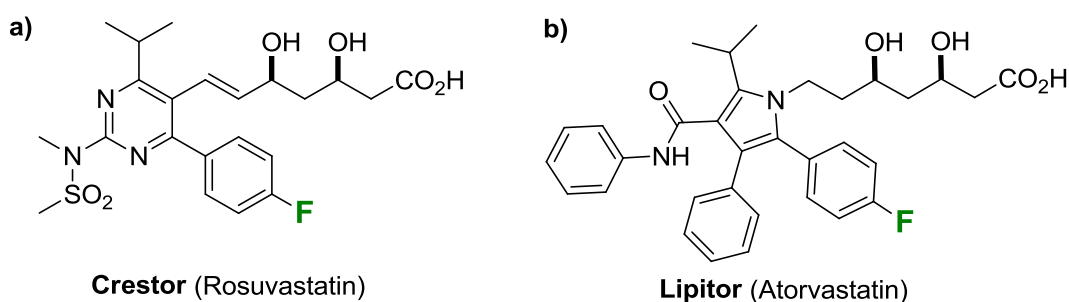


Figure 1.3 - Examples of two top selling fluorinated pharmaceuticals, both used in the treatment of high cholesterol a) Crestor and b) Lipitor

Table 1.1 - Top selling organofluorine pharmaceuticals based on US sales in US\$ in 2012²⁹

Position in sales (2012) relative to all drugs	Name	US sales in 2012 /\$ × 10 ⁹
3	Crestor	4.8
4	Advair Diskus	4.6
13	Atripla ^a	2.8
18	Januvia	2.5
20	Truvada ^a	2.2
21	atorvastatin ^b	2.1
26	Celebrex	1.9
31	Lipitor ^b	Not available
39	Zetia	1.4

a) Name for a combined therapy incorporating the fluorinated pharmaceutical emtricitabine along with other molecules. b) Atorvastatin is the generic name for Lipitor, the statistics report the sales of the generic drug and the brand named drug separately.

The popularity of incorporating fluorine into biologically active compounds is as a result of the enhanced properties of fluorine-containing drugs.³¹ The introduction of fluorine into drug molecules has an effect on several aspects of the drug's properties, such as binding, absorption through the membrane and bioavailability, distribution, metabolism, pharmacokinetic, pharmacodynamic and excretion.³² There are several cases where fluorine or trifluoromethyl groups, for example, have been used to replace other groups of similar size. The introduction of fluorine usually leads to increased lipophilicity, which can improve transport into the active site. Also, fluorine can modulate the pKa of neighbouring groups.³²

Fluorine exists naturally as the ¹⁹F isotope. This isotope is spin-active and therefore fluorine incorporation can be viewed easily by NMR spectroscopy.³³ There is a second isotope of fluorine; ¹⁸F, which is positron-emitting, and can be incorporated into drug molecules and used as a diagnostic tool to visualise uptake, transport and excretion of a drug.³¹

1.1.3 The *gauche* effect in organo-fluorine molecules

One of the properties of fluorine which makes it interesting to study is its effect on the conformation of small molecules. *Gauche* effects, where vicinal groups preferentially adopt a *gauche* conformation over an *anti* conformation, are widely

Chapter 1 - Introduction

reported in organo-fluorine compounds where a carbon-fluorine bond is vicinal to a second carbon-fluorine bond (Figure 1.4).³⁴ The energy difference between the *gauche* and *anti* conformations has been calculated to be in the region of 2-4.2 kJmol⁻¹ and the preference appears to dominate over the lone-pair repulsion between fluorine atoms.³⁴

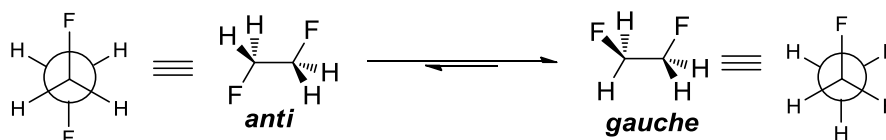


Figure 1.4 - The *gauche* effect in 1,2-difluoro ethane

The *gauche* preference is also observed between carbon-fluorine and a vicinal polarised bonds, such as carbon-oxygen or carbon-nitrogen bonds. DFT calculations have been used in order to evaluate the *gauche* preference in 2-fluoroethylamine and 2-fluoroethanol and the observations are summarised in Figure 1.5.³⁵ Rotating around the carbon-heteroatom bond reveals that when a lone-pair is pointing towards the fluorine, these conformations are less stabilised by the *gauche* effect compared to the conformation in which a proton is pointing towards the fluorine. In the corresponding ammonium and oxonium ions, the stabilisation as a result of the *gauche* effect is predicted to be greater.

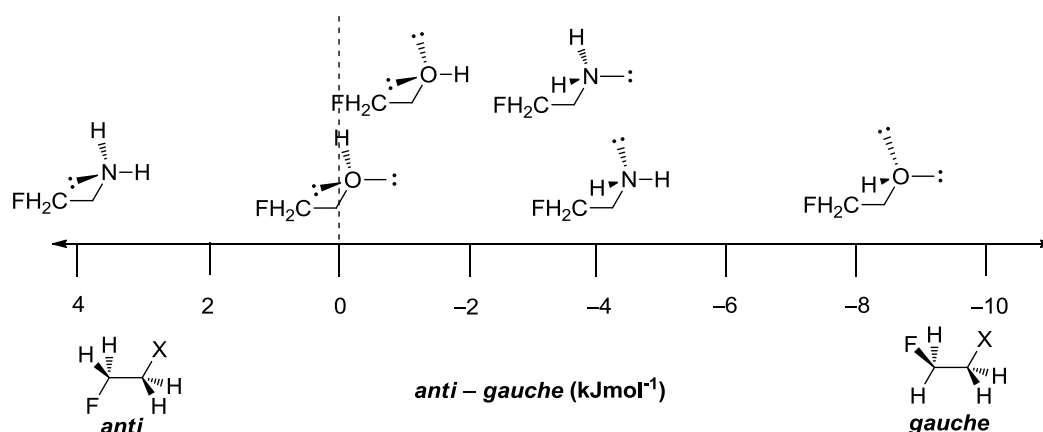


Figure 1.5 - *Gauche* preference of different conformations of 2-fluoroethylamine and 2-fluoroethanol. The scale refers to the relative stabilisation of the *gauche* conformation compared to the *anti* conformation.

1.1.4 Potential value of fluorinated sialic acid analogues

It is rare to encounter a drug with a chiral sp³ hybridised carbon attached to a fluorine atom. (The only example in Table 1.1 is the steroid derivative Advair Diskus.)

Chapter 1 - Introduction

Most of the sialic acid analogues discussed previously contained several sp^3 hybridised carbons and multiple chiral centres. The lack of fluorine-bearing chiral centres in pharmaceuticals is most likely due to the difficulty presented by stereoselectively introducing a fluorine atom into a molecule. Development of a novel method utilising enzyme variants for introducing a fluorine-bearing chiral centre with high levels of stereocontrol into sialic acid analogues may provide a new route to interesting, highly-chiral and potentially biologically active small molecules bearing multiple chiral centres.

1.2 Chemical methods for the synthesis of organo-fluorine molecules

1.2.1 Aldol reactions of α -fluoro ketones

NAL, the enzyme responsible for the biosynthesis of sialic acid is an aldolase enzyme. In the NAL active-site, the aldol reaction is accelerated by a catalytic lysine residue which forms a Schiff-base then an enamine in the active-site of the enzyme (see Section 1.3.1). This method of enamine catalysis of aldol reactions has been mimicked using chemical methods by exploiting amine catalysts.

The aldol reaction between aryl aldehydes and fluoroacetone has been evaluated with different catalysts. The diastereoselectivity of an aldol reaction is governed by both the enamine geometry and the facial selectivity. It is possible that the *gauche* effect may be a contributing factor in controlling the enamine geometry of α -fluoro-ketones (see Section 1.1.3). Catalyst **3a**³⁶ and **3b**^{37, 38} are derived from L-proline and selectively give *anti*-diastereoselectivity whereas catalyst **3c**³⁷ is a primary amine and gives *syn*-diastereoselectivity (Figure 1.6). The diastereoselectivity of the aldol reactions of fluoroacetone are presented in Table 1.1. By way of comparison, the diastereoselectivity observed for catalyst **3c** with pentan-3-one has been presented as the *gauche* effect in this case will have no impact on the enamine geometry, therefore diastereoselectivity.

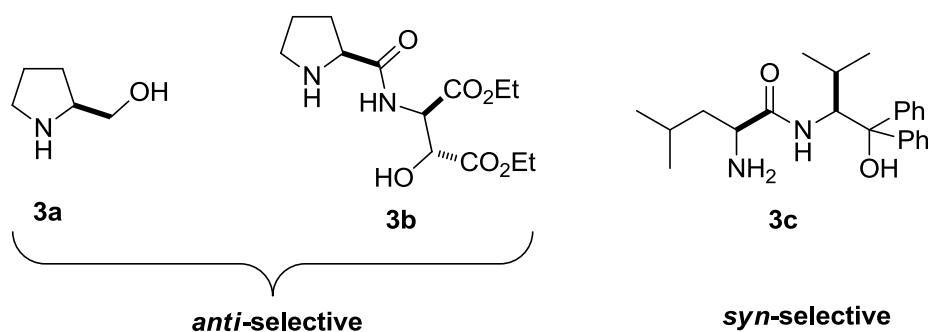
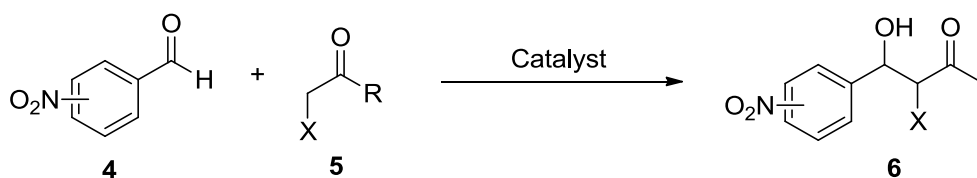


Figure 1.6 - Catalysts of asymmetric aldol reactions of aryl aldehydes and fluoroacetone (see Table 1.2)

Table 1.2 - Diastereoselectivity of the reaction between aryl aldehydes and fluoroacetone with a selection of catalysts^{36,37, 38}



Entry	Aryl	X	R	Catalyst	Yield %	d.r. (<i>anti:syn</i>)	ee %
1	<i>p</i> -NO ₂	F	CH ₃	3a (33 mol%)	82	70:30	84
2	<i>p</i> -NO ₂	F	CH ₃	3b (20 mol%)	96	67:33	95
3	<i>p</i> -NO ₂	F	CH ₃	3c (20 mol%)	45	7:93	99
4	<i>o</i> -NO ₂	F	CH ₃	3c (20 mol%)	82	<6:>94	98
5	<i>m</i> -NO ₂	Me	Et	3c (20 mol%)	82	20:80	80

The catalyst has a profound effect on the diastereoselectivity, which can be rationalised by considering the organisation of the possible transition states (Figure 1.7). The prolinol catalyst **3a** is predicted to react *via* a chair-like transition state where the facial selectivity is governed by hydrogen bonding between the hydroxyl proton and the aldehyde. The aryl and the fluorine both adopt a *pseudo*-equatorial position in order to reduce 1,3-steric interactions (Figure 1.7a).³⁶ Catalysts **3b** and **3c** are proposed to direct the facial selectivity *via* hydrogen bonding interactions between the side chain and the aldehyde. In the case of the secondary amine catalyst **3b** it is predicted that the (*E*)-enamine is preferred in order to reduce the steric clash between the fluorine and the protons of the pyrrolidine ring (Figure 1.7b)³⁸ whereas in the case of the primary amine catalyst **3c**, the (*Z*)-enamine is preferred in order to reduce steric

interaction between the fluorine and the methyl group (Figure 1.7c).³⁷ However, the *gauche* effect may be used to explain the large difference in diastereoselectivity between the reaction of fluoroacetone (Entries 3 and 4) and pentan-3-one (Entry 5).

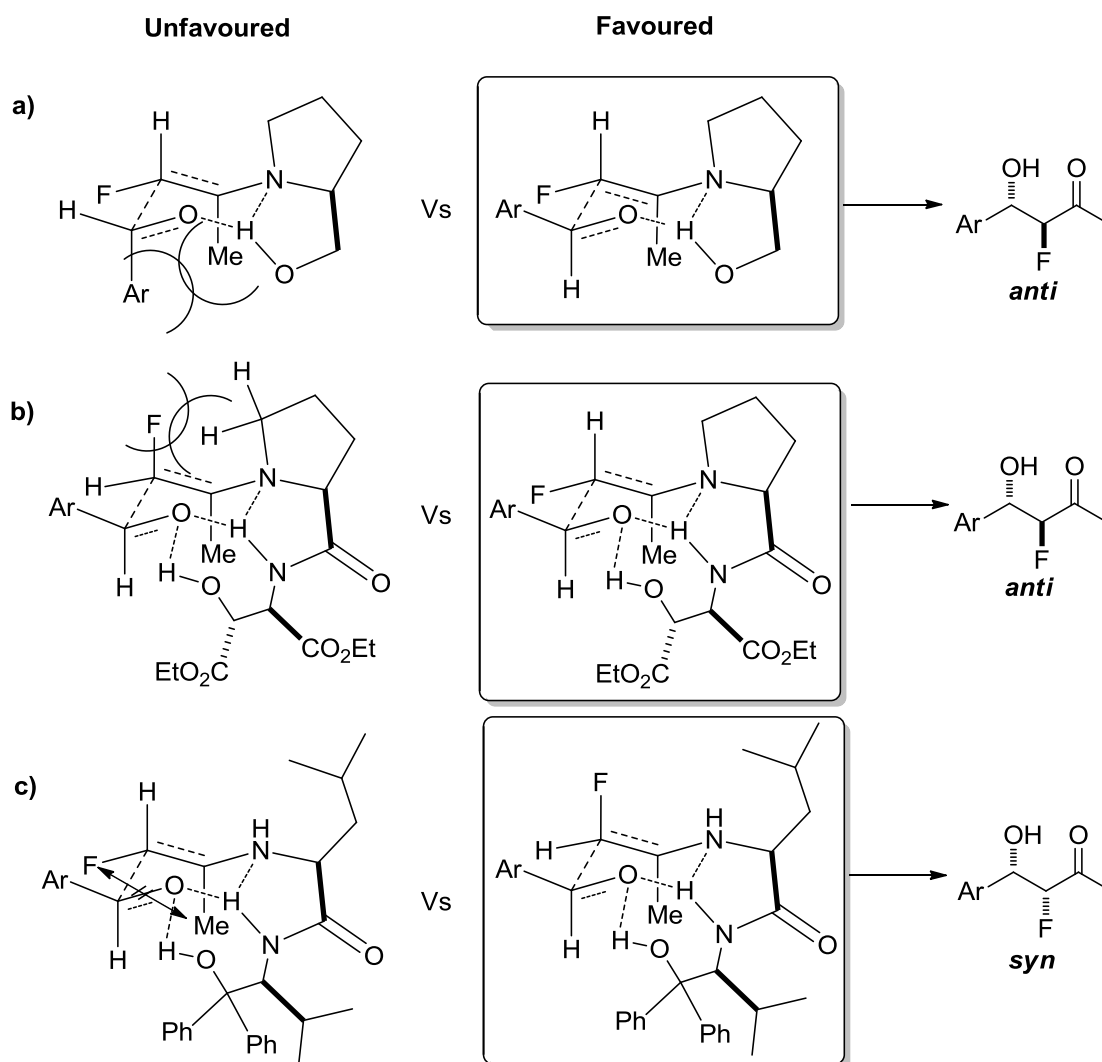


Figure 1.7 - Transition state diagrams to rationalise the diastereoselectivity of amine catalysed aldol reaction of fluoroacetone. a) Prolinol catalyst **3a** is predicted to give *anti* diastereoselectivity therefore both the aryl group and the fluorine will be in the *pseudo-equatorial* positions in the chair-like transition state. b) Secondary amine catalyst **3b** is also predicted to give *anti* diastereoselectivity *via* the (*E*)-enamine in order to reduce steric interaction with the protons of the pyrrolidine. c) Primary amine catalyst **3c** is predicted to give *syn* diastereoselectivity *via* the (*Z*)-enamine, which may be driven by steric clash with the methyl group plus the preference for fluorine to adopt a *gauche* conformation relative to a vicinal polarised bond.

1.2.2 Carbon-fluorine bond forming reactions

There are two main classes of reagents used for making carbon-fluorine bonds referred to as nucleophilic and electrophilic fluorinating reagents. There are several

Chapter 1 - Introduction

methods in the literature that exploit nucleophilic reagents for the introduction of fluorine functionality;^{39,40} one such example is in the enantioselective synthesis of a *all-syn* four vicinal fluorine motif by a series of carefully controlled S_N2 reactions with nucleophilic fluorine sources.⁴¹ Nucleophilic fluorinating reagents are important for the introduction of radioactive ^{18}F into molecules for radio-labelling studies.⁴² However, the main drawback of nucleophilic fluorinating chemistry is it does not seem to be able to provide much in the way of methods of synthesis of fluorine-bearing chiral centres from achiral starting materials. In order to look into stereoselective methods of fluorination, it is necessary to consider electrophilic fluorinating reagents.

The two most widely used electrophilic fluorinating reagents are *N*-fluorobenzenesulfonimide (NFSI) **7** and 1-alkyl-4-fluor-1,4-diazoniabicyclo[2.2.2]octane salts (Selectfluor) **8** (Figure 1.8).^{43,44} NFSI and Selectfluor have been used in conjunction with catalysts which are able to induce stereoselectivity in order to carry out asymmetric fluorination reactions.⁴⁴⁻⁴⁹

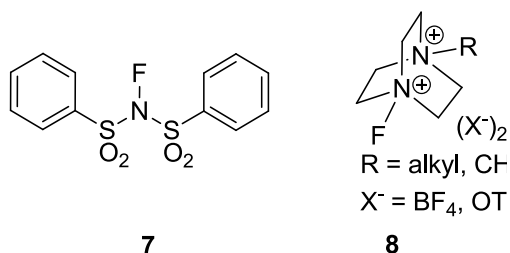
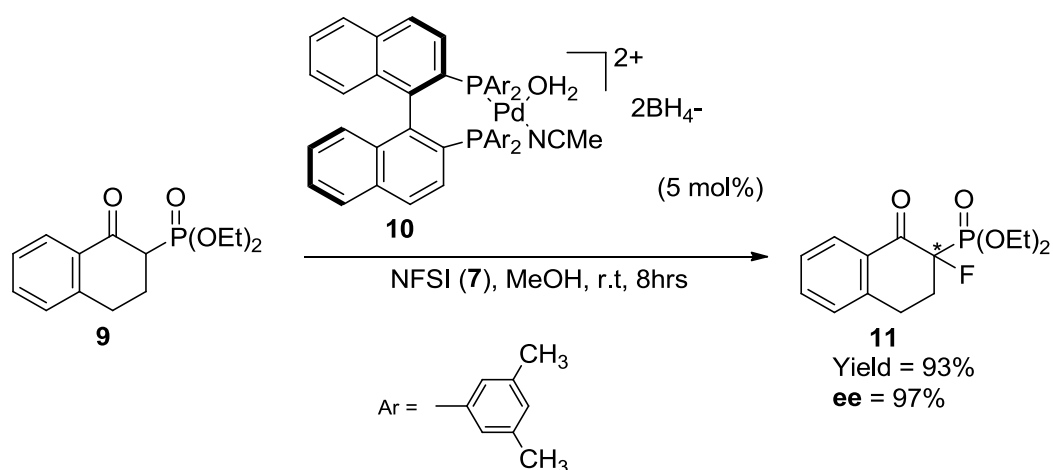


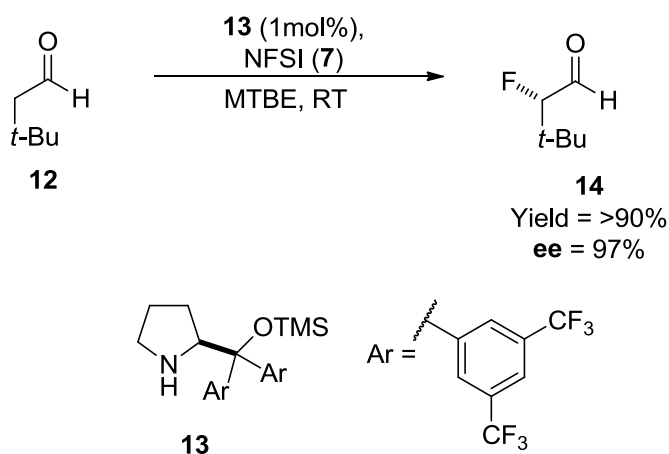
Figure 1.8 – *N*-fluorobenzenesulfonimide (NFSI) **7** and general structure of 1-alkyl-4-fluor-1,4-diazoniabicyclo[2.2.2]octane salts (Selectfluor) **8**

Asymmetric catalysis methods have taken many forms and include both metal catalyst with chiral ligands,⁴⁶ organocatalysts⁴⁸ as well as some more unusual methods including using DNA in catalysis.⁴³ An example of a metal catalysed electrophilic fluorination is the use of the palladium catalyst **10** which can be used in conjunction with NFSI **7** in order to yield chiral fluorinated products from β -keto phosphonate **9** starting materials (Scheme 1.2).⁴⁶



Scheme 1.2 – Enantioselective palladium-catalysed fluorination of a β -keto phosphate. (Absolute configuration was not stated.)

Organocatalysts can also be used to control highly enantioselective fluorination reactions. A chiral amine catalyst **13** (a proline derivative) has been used in the asymmetric fluorination of achiral aldehydes **12** *via* an enamine intermediate, which then underwent electrophilic fluorination (Scheme 1.3). This method has yielded chiral aldehydes **14** with enantiomeric excess of up to 97%.⁴⁸



Scheme 1.3 – Organocatalysed asymmetric fluorination of aldehydes.

Organosilanes, in particular allylsilanes have attracted interest in the field of electrophilic fluorination chemistry. Allylsilanes are able to undergo regioselective fluorination resulting in desilylation and translocation of the double bond (Figure 1.9). Regioselectivity is achieved as the carbocation is stabilised by hyperconjugation with silicon.⁴⁴ There are several examples in the literature of asymmetric fluorination using allylsilanes. Stereocontrol at the fluorine-bearing chiral centre in the reaction of a

Chapter 1 - Introduction

terminal organosilane may be achieved by the use of a chiral auxiliary,⁵⁰ or a chiral catalyst.⁵¹

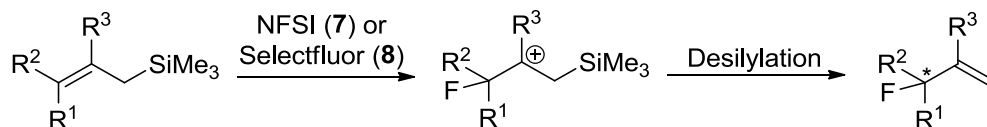
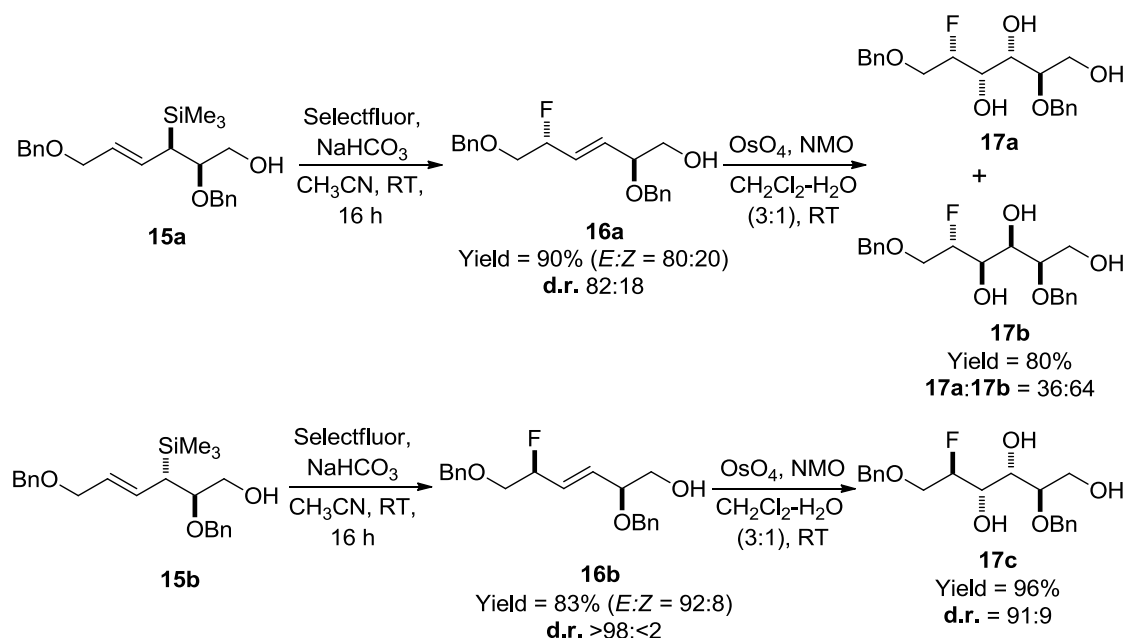


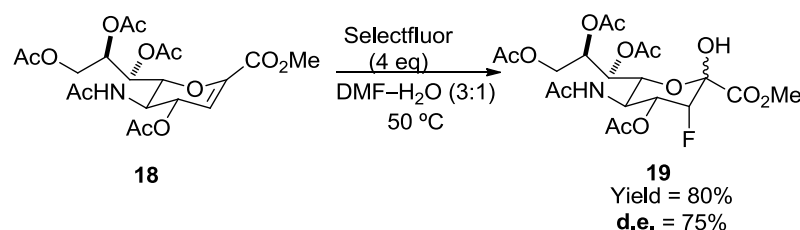
Figure 1.9 - General scheme for fluorodesilylation of allylsilanes

Secondary organosilanes may be used in the diastereoselective synthesis of fluorinated molecules. One such example is the synthesis of fluorinated carbohydrate analogues **17a**, **17b** and **17c** (Scheme 1.4). The configuration of the carbohydrate product is determined by the configuration of the allylsilane and exploits the preference for fluorination to occur *anti* to the silyl group.⁴⁵



Scheme 1.4 - Diastereoselective synthesis of fluorinated analogues of D-glucitol **17a** and L-glucitol **17b** and D-mannitol **17c**

The synthesis of 3-fluoro-sialic acid has been achieved using an electrophilic fluorination approach (Scheme 1.5).⁵² Selectfluor **8** was reacted with the protected intermediate **18** in a one-pot fluorination procedure, which is highly diastereoselective, giving only the C-3 *axial* fluorine epimer (controlled by steric effects of the ring). Later (Section 1.3.2.2), an alternative route will be discussed which demonstrates that NAL may be used in a one-step synthesis of 3-fluoro-sialic acid, avoiding the multi-step synthesis of the protected sialic acid analogue **18**.

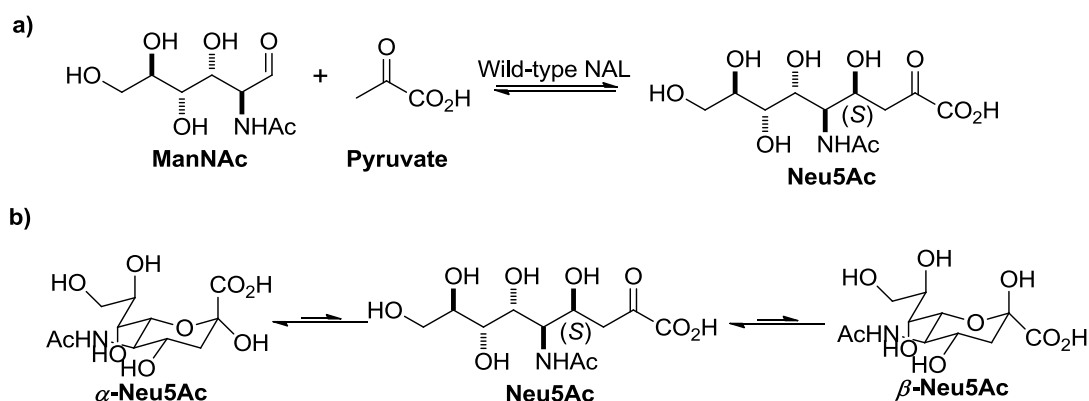


Scheme 1.5 – Electrophilic fluorination synthesis of protected 3-fluoro sialic acid **19** from protected sialic acid alkene **18**.

1.3 Wild type *N*-Acetyl-neuraminase lyase (NAL)

1.3.1 Mechanism of wild-type NAL

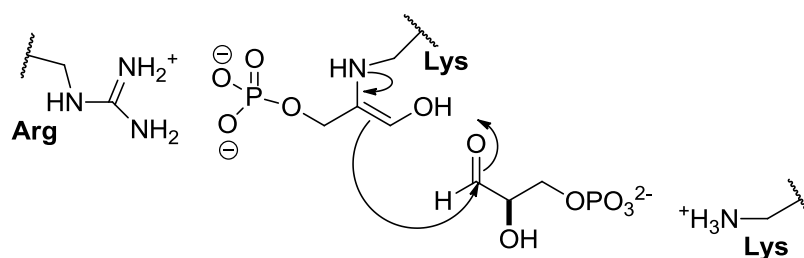
N-Acetyl-neuraminase lyase (NAL) is a Class I aldolase enzyme which catalyses the reversible aldol reaction between *N*-acetyl-D-mannosamine (ManNAc) and pyruvate to give *N*-acetylneuraminic acid (Neu5Ac) (Scheme 1.6a). This reaction sets up one new stereocentre at C-4 and wild-type NAL is highly selective for the (4*S*)-epimer. In solution, the β -anomer is predominant, but the α -anomer is the substrate for the reverse aldolase reaction (Scheme 1.6b).⁵³



Scheme 1.6 - Wild-type NAL-catalysed reaction of ManNAc and pyruvate. The sugars are drawn in open form for clarity, which will be the standard format throughout this thesis a) The NAL catalysed aldol reaction between ManNAc and pyruvate to give Neu5Ac as the (4*S*)-epimer. b) In solution, the α -Neu5Ac is in equilibrium with β -Neu5Ac.

There are two types of aldolase enzymes: Class I and Class II, which are characterised according to the mechanism by which the aldol reaction is catalysed. Class I aldolases, such as NAL, catalyse aldol reactions *via* formation of a Schiff-base, involving a lysine residue in the active site, to form an enamine intermediate.⁵⁴ Class II aldolases form an enolate intermediate stabilised by a metal cofactor (e.g. Zn²⁺) (Figure 1.10).⁵⁵

a) Class I aldolase



b) Class II aldolase

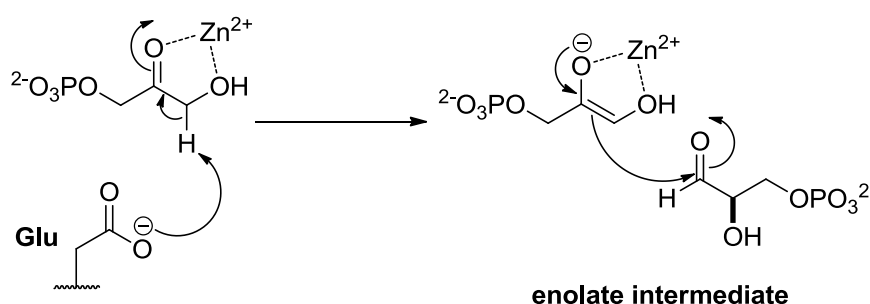


Figure 1.10 - Comparison of Class I and Class II aldolases (examples shown are DHAP-dependent aldolases). a) Class I aldolases have a catalytic lysine residue in the active site which forms a Schiff-base with the donor. b) Class II aldolases incorporate a metal cofactor (zinc in this example) into the active site, which forms an enolate with the donor.

The active site of NAL contains three residues, Glu192, Asp191 and Ser208, which form hydrogen bonding interactions with the triol chain of ManNAc/Neu5Ac while Lys165 forms the Schiff-base. This can be seen in the crystal structure of NAL from *H. influenzae* in complex with the 4-oxo-sialic acid inhibitor **20** shown in Figure 1.11.^{55, 56}

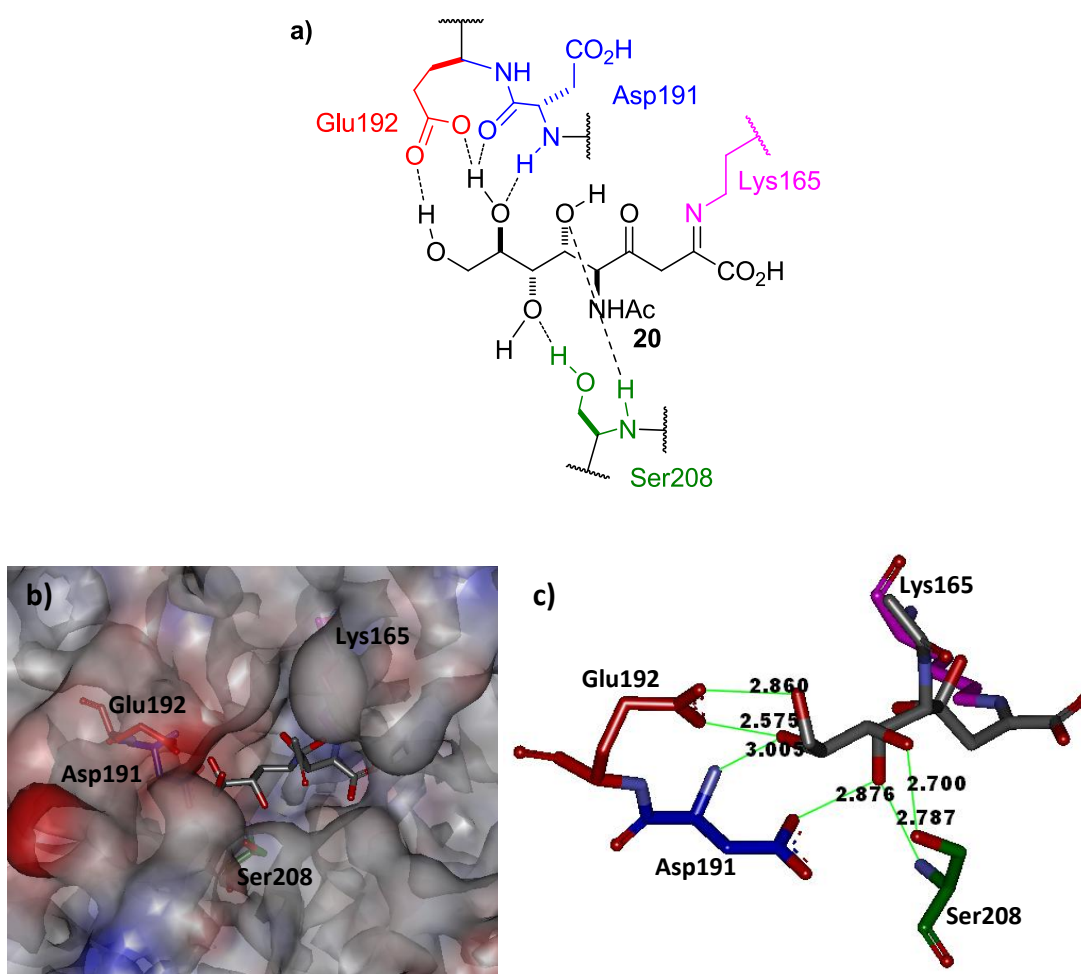


Figure 1.11 – Representations of key binding interactions between ManNAc/Neu5Ac in the active site of NAL, taken from the crystal structure of the 4-oxo-sialic acid inhibitor 20 in complex with NAL from *H. influenzae*. (PDB 1F7B)⁵⁶ (Residues are numbered according to the *E. coli*. NAL) a) Schematic representation of the active site showing the residues which may form hydrogen bonds with the triol side-chain of ManNAc/Neu5Ac. b) Surface view of the binding pocket in wild-type NAL. c) Hydrogen bond distances (Å) between residues important in recognition and the triol of ManNAc/Neu5Ac.

As mentioned previously, wild-type NAL is highly diastereoselective, giving only the (4S)-epimer of Neu5Ac. Computational QM/MM (Quantum Mechanic/Molecular Mechanic) studies have gained information about the origin of this observed diastereoselectivity.⁵⁷ The configuration is determined not only by the relative positions into which the pyruvate and the aldehyde bind in the NAL active-site, but also by the catalytic residue which is responsible for delivering a proton in the forward reaction and removing the proton in the cleavage reaction. QM/MM modelling suggests that the residue important in transferring the proton is Y137. The modelling studies also suggest that the phenolate anion is stabilised by hydrogen bonding interactions with S47 and Y110' (a tyrosine from a neighbouring subunit). The

Chapter 1 - Introduction

calculated transition state is shown in Figure 1.12a. Replacement of Y137 or S47 with alanine was highly detrimental to activity, although the Y110' was found to be less critical. In order for Y137 to be close enough to perform its role in catalysis, ManNAc has to bind in such a way that the *si*-face is presented towards the Schiff base, which is consistent with the observed stereoselectivity. It has also been postulated that T167 forms a hydrogen bond with the aldehyde of ManNAc,⁵⁸ further directing the position of the substrate in the active-site. Additionally, steric interactions between the *N*-acetyl group of ManNAc and F252 and hydrogen bonding interactions between the terminal alcohol groups of ManNAc and E192 limit the number of possible binding modes of ManNAc, resulting in high levels of stereocontrol. A schematic representation of the important interactions in the transition state is shown in Figure 1.12b.

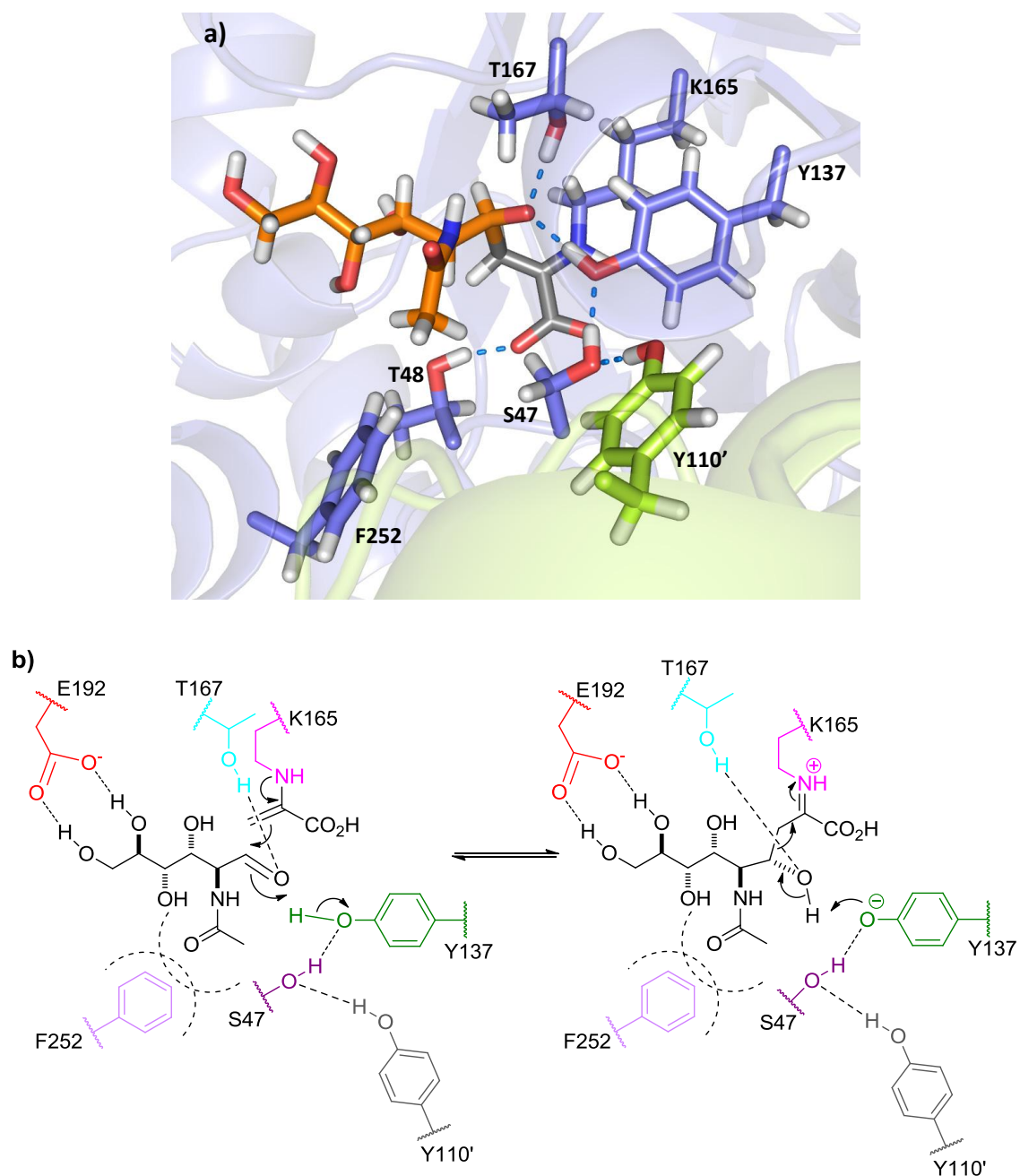
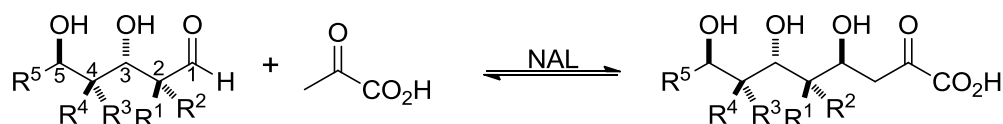


Figure 1.12 - Representation of the transition state of the NAL catalysed reaction of ManNAc and pyruvate to give Neu5Ac, based on predictions from QM/MM modelling. a) Transition state diagram (modified from reference).⁵⁷ b) Schematic representation of forward and retro aldol reactions of Neu5Ac catalysed by NAL. Y137 (green) mediates transfers of a proton to the aldehyde in the forward reaction and abstracts a proton from the alcohol in the cleavage reaction. The negative charge on Y137 (green) is stabilised by S47 (purple) and Y110' (grey). Hydrogen bonding between the aldehyde oxygen with T167 (cyan), as well as a steric clash between F252 (lilac) and the *N*-acetyl group and hydrogen bonding between E192 (red) and the terminal alcohol groups help limit the number of binding modes and direct the *si*-face of the aldehyde towards the Schiff base.

1.3.2 Substrate specificity of NAL

1.3.2.1 Acceptors

Several substrate studies have been carried out on wild-type NAL and it has been found that it will accept a variety of different sugars in place of ManNAc. Substitutions at C-2, C-4 and C-6 can be tolerated so long as the absolute configuration at these positions is not changed. A summary of some of the accepted substrates and relative rates of reaction compared to ManNAc (Entry 1) are given in Table 1.3.⁵⁴ Modification to the triol (Entries 2, 3, 4 and 6) has a moderately detrimental effect on rate of reaction, which is consistent with the structural evidence (Figure 1.11) which indicates that the triol is important in binding. Exchanging the NHAc at C-2 for an OH (Entry 5) and replacing the C-2 NHAc with a proton (Entry 7) both slightly improve the rate. However, inverting the configuration at C-2 (Entry 8) is extremely detrimental to the rate of reaction. The crystal structure shows that the C-2 substituent points out into solvent, so inverting the configuration would mean the C-2 substituent would instead potentially be pointing back towards the backbone, which may result in an unfavourable steric clash.

Table 1.3 – Aldehydes accepted by wild-type NAL⁵⁴

Entry	R ¹	R ²	R ³	R ⁴	R ⁵	Relative Rate ^a
1	AcNH	H	OH	H	CH ₂ OH	1
2	AcNH	H	OH	H	CH ₂ OAc	0.2
3	AcNH	H	OH	H	CH ₂ N ₃	0.6
4	AcNH	H	OH	H	CH ₂ F	0.6
5	OH	H	OH	H	CH ₂ OH	2
6	OH	H	OH	H	H	0.1
7	H	H	OH	H	CH ₂ OH	1.3
8	H	OH	OH	H	CH ₂ OH	0.07

a) The rates given are relative to the rate of the wild-type reaction (**Entry 1**)

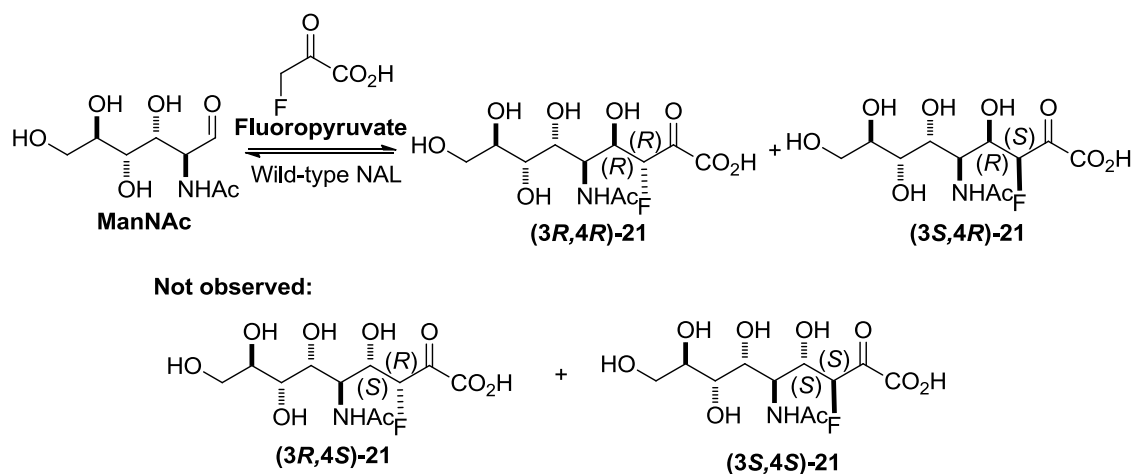
1.3.2.2 Donors

There has been some contradiction over whether or not 3-fluoropyruvate can be accepted in place of pyruvate by NAL in reaction with ManNAc. In 1996, one group concluded that 3-fluoropyruvate is not a viable substrate for wild-type NAL and therefore cannot be used to synthesise 3-fluoro-*N*-acetyl neuraminic acid (3-fluoro Neu5Ac, **21**)⁵⁹, while another group claimed that fluoropyruvate acts as a competitive inhibitor of NAL.⁶⁰ The vast majority of evidence however demonstrates that 3-fluoropyruvate is a viable substrate for wild-type NAL and the reaction between 3-fluoropyruvate and ManNAc will result in the production of 3-fluoro Neu5Ac **21** (Scheme 1.7).^{16, 57, 61, 62}

NAL, in reaction with ManNAc and pyruvate, is highly selective towards the (4S)-epimer. The NAL-catalysed reaction between ManNAc and 3-fluoropyruvate is further complicated because the reaction creates two new stereocentres at C-3 and C-4. All

Chapter 1 - Introduction

previous studies seem to be in agreement that NAL retains its C-4 stereoselectivity* and the two (4S)-epimers of 3-fluoro-Neu5Ac **21** are not observed.^{16, 57, 61, 62}



Scheme 1.7 - Wild-type NAL-catalysed reaction between 3-fluoropyruvate and ManNAc. The reaction sets up two new stereocentres so there is the possibility of forming one or more of 4 diastereomers. Previous studies have shown that only the two (4R)-epimers (3R,4R)-21 and (3S,4R)-21 are observed.

There is however disagreement over the control of the configuration at C-3 and several studies have reported different ratios of products under various reaction conditions.^{16, 61, 62} The work that directly precedes this thesis found that when using ManNAc in a 5-fold excess over 3-fluoropyruvate, after a reaction time of approximately 500 minutes (the time taken for all of the 3-fluoropyruvate to be consumed) that the ratio of products was 90:10 in favour of the product **(3R,4R)-21**. When the reaction was left for a prolonged period of time (approximately 5 weeks) with regular addition of enzyme, the ratio of products switches to 70:30 in favour of the product **(3S,4R)-21**.⁵⁷ This result suggests that the product **(3R,4R)-21** is the kinetic product and the product **(3S,4R)-21** is thermodynamically favoured.

The kinetic parameters of the wild-type NAL catalysed cleavage of the two 3-fluoro-Neu5Ac diastereomers were evaluated and compared to Neu5Ac (Table 1.4). The k_{cat} of the reaction with **(3R,4R)-21** was found to be 500-fold lower than Neu5Ac and the K_{M} four-fold higher, therefore showing that 3-fluoro-Neu5Ac **21** is a very poor substrate for NAL.⁵⁷ This data may explain why a previous study concluded that 3-fluoro-Neu5Ac **21** wasn't a substrate for NAL.⁵⁹ The product **(3S,4R)-21** was a very poor substrate, and it was not possible to determine k_{cat} or K_{M} . This was consistent with the

* In 3-fluoro-Neu5Ac, the priority of the groups surrounding C-4 changes so that the same relative configuration which for Neu5Ac would be called (4S), in 3-fluoro-Neu5Ac is called (4R).

Chapter 1 - Introduction

observed switch in selectivity over prolonged reaction times, suggesting that only the product **(3R,4R)-21** is able to undergo the cleavage reaction so the product **(3S,4R)-21** accumulated over time.

Table 1.4 - Kinetic parameters of wild-type NAL for the cleavage of Neu5Ac, (3R,4R)-21 and (3S,4R)-21. Determined using a standard LDH-coupled assay (see Section 1.4.1) at 30 °C.⁵⁷

NAL substrate	$k_{\text{cat}} / \text{min}^{-1}$	K_{M} / mM	$k_{\text{cat}} / K_{\text{M}} / \text{min}^{-1} \text{mM}^{-1}$
Neu5Ac	510 ± 11	2.0 ± 0.1	260
(3R,4R)-21	0.91 ± 0.03	8.4 ± 0.7	0.11
(3S,4R)-21	- ^a	- ^a	- ^a

a) Not measurable under the conditions

The observed diastereoselectivity of the wild-type NAL-catalysed reactions between ManNAc and fluoropyruvate indicate that the preferred enamine geometry is the (*Z*)-enamine. This may be related to the *gauche* effect discussed in Section 1.1.3. Previous gas phase computational modelling studies of 3-fluoropyruvate forming a Schiff-base with a truncated lysine have shown that there is a preference of 35.3 kJ mol⁻¹ for fluorine to adopt a *gauche* configuration, resulting in a preference for the (*Z*)-enamine (Figure 1.13a).⁵⁷ Since then, a crystal structure of fluoropyruvate bound in the active-site of wild-type NAL from *S. aureus* has shown that the fluorine does adopt a *gauche* configuration (Figure 1.13b).⁶³

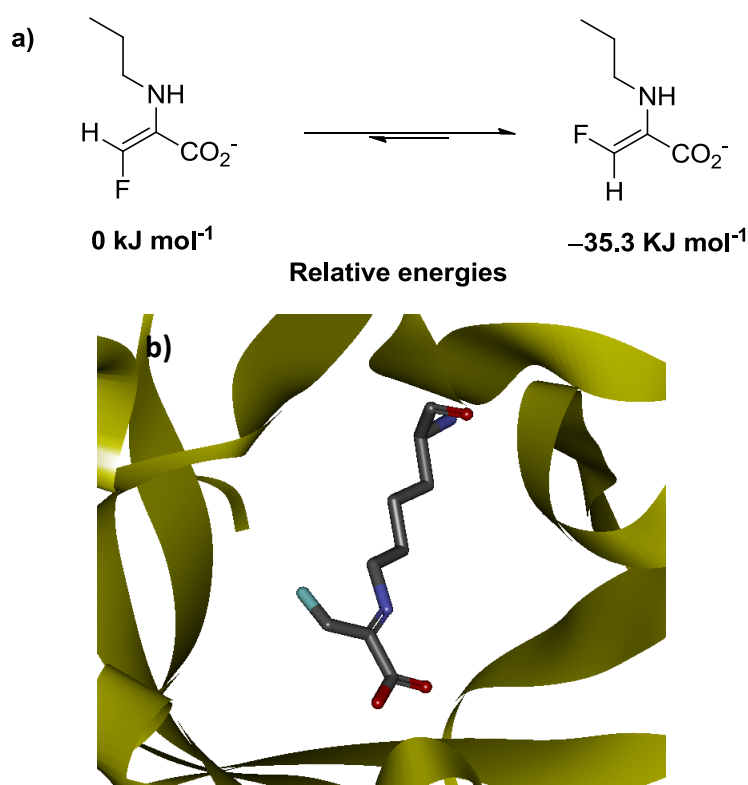


Figure 1.13 - Configuration of the enamine of fluoropyruvate a) Gas phase optimised calculated relative energies of the (*E*) and (*Z*)-fluoroenamines form of the complex between 3-fluoropyruvate and a truncated lysine residue. b) Crystal structure of 3-fluoropyruvate bound to K165 of NAL from *S. aureus* showing the fluorine atom adopting a *gauche* relationship relative to the carbon-nitrogen bond.⁶³

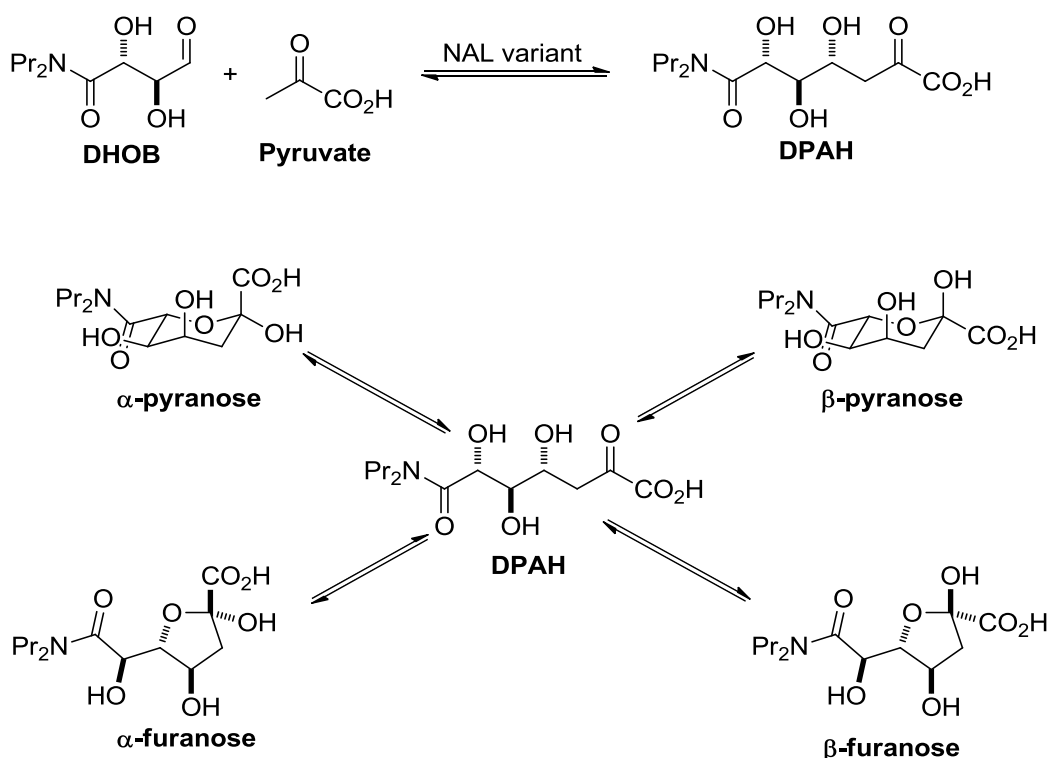
Section 1.2.2 describes an alternative method in which a protected precursor **19** of 3-fluoro-sialic acid **21** is synthesised chemically in a multi-step procedure. The application of wild-type NAL may provide a viable alternative to this chemical method as it allows access to fluorinated sialic acid **21** in a single step from commercially available materials.

1.4 Protein engineering of NAL E192N variants

Mutagenesis methods have previously been used to engineer variants of NAL with high specificity for C-6 amide sialic acid analogues.⁶⁴ The NAL variants to stem from mutagenesis studies have also been shown to be useful in the parallel synthesis of sialic acid analogues, with a range of different amides.²⁸ The following Section will outline the methodology by which NAL variants with modified substrate specificity were identified and optimised. In addition, the evolution of a pair of complementary NAL variants with opposing stereoselectivity is discussed.

1.4.1 Engineering of NAL variants with modified activity

Engineering of NAL variants aimed to identify an NAL variant capable of catalysing the reaction between the dipropylamide aldehyde **DHOB** ([2*R*,3*S*]-2,3-dihydroxy-4-oxo-*N,N*-dipropylbutanamide) and pyruvate. In order to screen for desired activity, it was necessary to synthesise chemically **DPAH** ([5*R*,6*R*]-7-(dipropylamino)-4,5,6-trihydroxy-2,7-dioxoheptanoic acid) which is the product of the reaction between **DHOB** and pyruvate (Scheme 1.8).⁶⁵ In solution, the open chain of **DPAH** cyclises to give a mixture of four equilibrium species.*



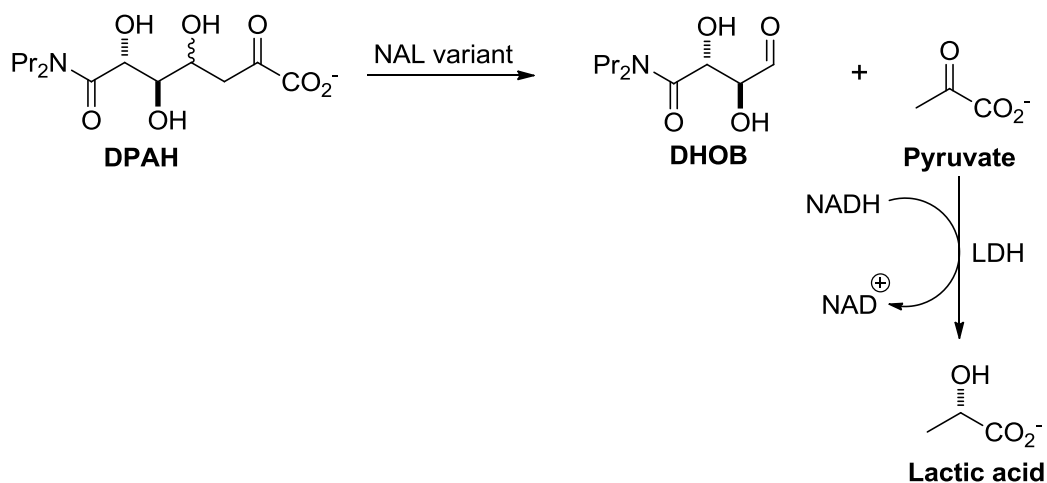
Scheme 1.8 - Screening substrate DPAH used in the discovery of E192N. DPAH can be synthesised by the aldol reaction between DHOB and pyruvate. DPAH exists as a mixture of the 6 member ring (pyranose) and 5 member rings (furanose), each of which can exist as the α or β -anomer.

In order to alter the substrate specificity of NAL, Glu192, Asp191 and Ser208 were chosen targets for saturation mutagenesis, as these residues were known to form hydrogen bonding interactions with the triol of ManNAc/Neu5Ac.⁶⁴ Variants with modified specificity were identified by using a standard coupled assay in which the rate of the retro-aldol reaction was measured. The standard coupled assay works by

* α - and β -anomers of furanose and pyranose rings.

Chapter 1 - Introduction

indirectly measuring the rate of pyruvate formation in the retro-aldol reaction. (Scheme 1.9).⁶⁴



Scheme 1.9 – Principle of the standard coupled assay for determining the rate of the retro-aldol reaction by an NAL variant.

1.4.2 Identification of the NAL E192N variant and substrate specificity

After saturation mutagenesis and screening, mutants with substitutions at each of the target residues were evaluated. In the case of Asp191 substitution, very low activity with sialic acid was observed and little improved selectivity for **DPAH** was observed. Substitutions of Ser208 also showed decreased activity with sialic acid and little improvement in selectivity for **DPAH**. However, substitution of Glu192 with asparagine did yield a mutant enzyme (E192N) with 640-fold greater selectivity for **DPAH** than for sialic acid (Table 1.5).²⁸

Table 1.5 - Steady-state kinetic parameters for wild-type NAL compared to the E192N variant²⁸

NAL substrate	Wild-type NAL			NAL E192N		
	k_{cat} /min ⁻¹	K_M /mM	k_{cat}/K_M /min ⁻¹ mM ⁻¹	k_{cat} /min ⁻¹	K_M /mM	k_{cat}/K_M /min ⁻¹ mM ⁻¹
Neu5Ac	260 ± 6	4.4 ± 0.3	74 ± 4	170 ± 10	38 ± 5	4.4 ± 0.6
DPAH	11 ± 1	6.9 ± 1.0	6.9 ± 1.0	130 ± 3	0.39 ± 0.04	340 ± 30

The drastic change in substrate specificity can be explained by examining the crystal structures of the closely related NAL from *H. influenzae* bound to the 4-oxo-sialic acid

Chapter 1 - Introduction

inhibitor **20** (Figure 1.14a)⁵⁶ compared to *E. coli* NAL E192N bound to the **THB** ([2*R*,3*R*]-2,3,4-trihydroxy-N,N-dipropylbutanamide) inhibitor, which is closely related to **DHOB** (Figure 1.14b and c).⁶⁶ The glutamic acid at position 192 forms a hydrogen bonding interaction with the triol of Neu5Ac, whereas when the glutamic acid is exchanged for an asparagine, hydrogen bonding with the triol of Neu5Ac is no longer possible. The hydrophobic pocket created by this mutation is instead able to accommodate the hydrocarbon chains of the greasy dipropylamide group.

The NAL E192N variant, unlike the wild-type NAL was found to exhibit poor diastereoselectivity at the newly formed chiral centre, giving a 74:26 mixture of the (4*S*) and (4*R*)-epimers of **DPAH**.⁶⁷ The crystal structure of the **THB** inhibitor in complex with NAL E192N revealed two different binding modes, the major binding mode where the hydroxyl group of C-3 was orientated towards the core of the enzyme (Figure 1.14b) and the minor binding mode where the same hydroxyl group is pointing towards the bulk solvent (Figure 1.14c).⁶⁶ The crystal structure of the **THB** inhibitor in complex with NAL E192N was used as a starting point for QM/MM studies to understand the observed ratio of epimers in the NAL E192N catalysed reaction of **DHOB** and pyruvate (Section 1.4.3).⁵⁷

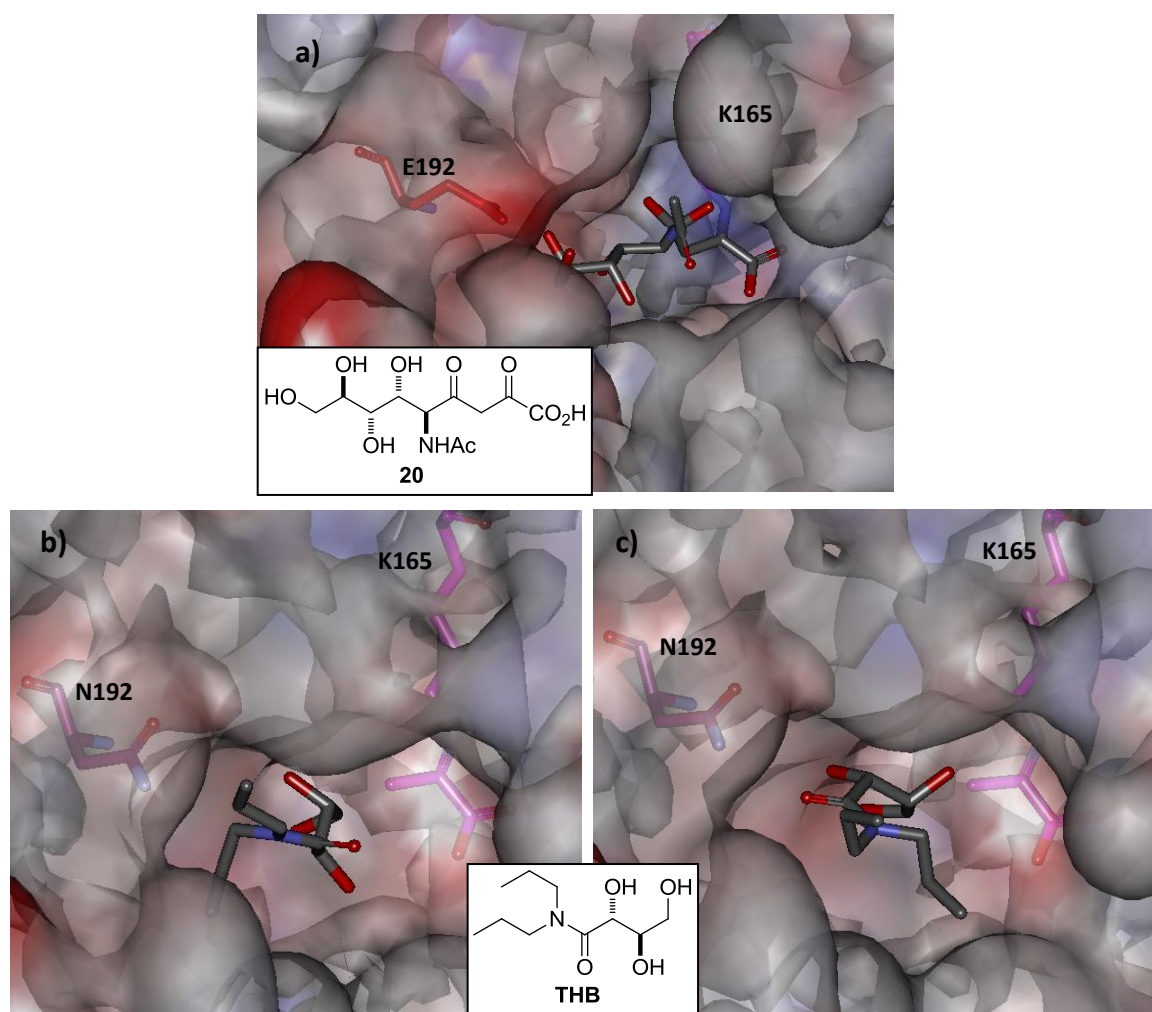


Figure 1.14 - Comparison of active-sites of wild-type NAL and the NAL E192N variant a) Wild-type NAL from *H. influenzae* bound to the 4-oxo-sialic acid inhibitor **20** (PDB 1F7B)⁵⁶ and b) *E. coli* NAL E192N bound to the **THB** inhibitor in the major binding orientation observed in subunits A, C and D (PDB 2WPB). c) *E. coli* NAL E192N bound to the **THB** inhibitor in the minor binding orientation observed in subunit B (PDB 2WPB)⁶⁶

In order to examine the modified specificity of E192N towards other amide sialic acid analogues **22a-22g**, a further series of amides was synthesised and evaluated using the standard coupled assay (Scheme 1.9) in order to determine the scope of substrates NAL E192N would accept. It was found that NAL E192N had greater catalytic activity for more hydrophobic derivatives and the rate of turnover of dibutylamide derivative was even faster than **DPAH (22a)**. Figure 1.15 shows the amides screened in order of catalytic activity with E192N. The pyrrolidine derivative, which was amongst the most polar, is positioned on the far left as the rate of the retro-aldol reaction by NAL E192N was slowest. The dibutylamide derivative, which is the least polar, is positioned on the far right as the rate of the retro-aldol reaction by NAL E192N was fastest.⁶⁴

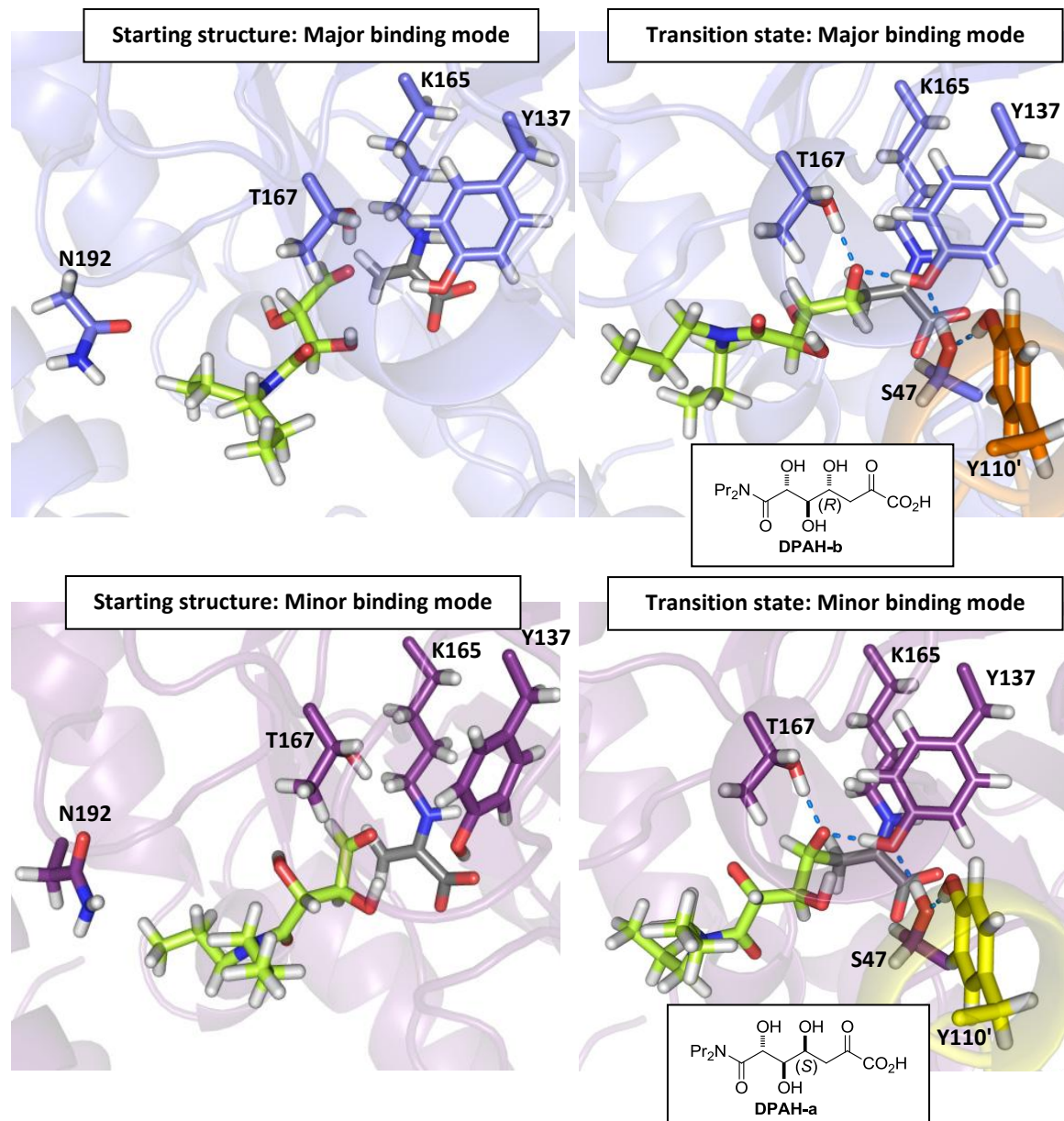


Figure 1.16 - Summary of the results of QM/MM modelling of the NAL E192N catalysed reaction between DHOB (green) and pyruvate (grey). As in wild-type NAL, Y137 acts as a base to transfer the proton to the aldehyde of DHOB and the negative charge is stabilised by S47 and Y110'

Left pane: Starting structure for umbrella sampling of DHOB in the major (top left) and minor (bottom left) binding mode

Right pane: Approximate transition states structures of the lowest energy reaction pathways. The transition state for the major binding mode (top right) is organised to give the (4R)-epimer of DPAH and the minor binding mode (bottom right) is organised to give the (4S)-epimer of DPAH. (Figure adapted from reference)⁵⁷

1.4.4 Discovery of a complementary pair of stereoselective enzymes

As mentioned previously (Section 1.4.2), the NAL E192N exhibits poor diastereoselectivity at the newly formed chiral centre of **DPAH**, therefore further mutagenesis studies were carried out in order to engineer a complementary pair of NAL E192N variants with high levels of stereoselectivity at C-4.⁶⁷ Screening substrates

Chapter 1 - Introduction

DPAH-a and **DPAH-b** were synthesised to be used in the standard coupled assay as described previously (Figure 1.17).⁶⁵

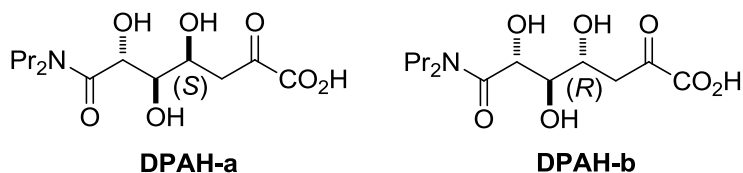


Figure 1.17 – DPAH screening substrates used in the discovery of NAL mutants with modified C-4 selectivity.

At the time the diastereoselective NAL variants were evolved, the mechanism by which the C-4 configuration is controlled was not understood; so error prone PCR (EP-PCR) was used to randomly introduce mutations.⁶⁷ Mutant libraries from EP-PCR were screened using the standard coupled assay as described previously (Section 1.4.1). Mutants that showed enhanced selectivity towards one or other diastereomer were screened using substrates **DPAH-a** and **DPAH-b**, identifying a series of potentially important residues. Site-directed mutagenesis experiments were then carried out in order to identify which residues were most important in determining the configuration of the product. It was discovered that three residues, Ala10, Thr48 and Ser208, all of which are in direct contact with the substrate when it is bound in the active site were the most important. In addition, Thr167 was reasoned to also be important as the corresponding residue in another aldolase (2-keto-3-deoxygluconate aldolase) makes a hydrogen bond to the C-4 hydroxyl of its product⁶⁸ (and it has since been found that this hydrogen bonding interaction is also found in NAL.)⁵⁷ The NAL variant E192N/T167G was found to be highly selective for the (4S)-epimer and the NAL variant E192N/T167V/S208V was found to be highly selective for the (4R)-epimer. The kinetic parameters for the (4S) and (4R)-selective variants are outlined in Table 1.6. These enzymes can be used in synthesis of C-6 amide-substituted sialic acid analogues with the desired configuration at C-4 with high diastereoselectivity.⁶⁷

Table 1.6 - Kinetic parameters of NAL variants towards (4S) and (4R)-dipropylamide screening substrates DPAH-a and DPAH-b.

	NAL Wild-type	NAL E192N	NAL E192N/T167V/S208V	NAL E192N/T167G
DPAH-a	$k_{\text{cat}} / \text{min}^{-1}$	230 ± 6	450 ± 14	0.1 ± 0.003
	K_{M} / mM	12 ± 1	0.8 ± 0.07	8.5 ± 0.4
	$k_{\text{cat}}/K_{\text{M}}$	19	563	0.012
	$/\text{min}^{-1} \text{mM}^{-1}$			10
DPAH-b	$k_{\text{cat}} / \text{min}^{-1}$	73 ± 4	130 ± 3	1.1 ± 0.04
	K_{M} / mM	11 ± 2	0.4 ± 0.04	1.9 ± 0.2
	$k_{\text{cat}}/K_{\text{M}}$	6.6	325	0.58
	$/\text{min}^{-1} \text{mM}^{-1}$			< 0.2
Ratio of $k_{\text{cat}}/K_{\text{M}}$ (4S):(4R)	74:26	63:37	2:98	>98:<2

a) Not measurable under the conditions

1.5 Thesis overview

The primary aim of this thesis is to study the NAL-catalysed reaction between fluoropyruvate and a series of aldehyde substrates in order to access fluorinated analogues of sialic acid. NAL E192N was engineered to be highly active towards **DPAH**, however it was found to exhibit poor stereocontrol, which led to the evolution of the diastereoselective variants NAL E192N/T167V/S208V and E192N/T167G. This work aims to evaluate these NAL variants in greater detail, to discover whether the activity and diastereoselectivity they were designed to exhibit is retained when the donor and acceptor are changed.

These aims were achieved initially by the development of a new synthetic route towards the synthesis of a broader range of potential enzyme substrates, as outlined in Chapter 2. The main priority was the synthesis of an enzyme substrate in which the *N*-acetyl functionality present in ManNAc was retained. Chapter 3 compares the new aldehyde analogues with the previously studied enzyme substrate **DHOB** in the NAL variant-catalysed reaction with pyruvate. The QM/MM modelling studies, outlined in Section 1.4.3, have been invaluable in rationalising the outcomes of the NAL-catalysed reactions of the new aldehyde substrates. Significantly, the QM/MM modelling studies indicate a link between the initial binding mode and the energy barrier of the two possible pathways leading to the two C-4 epimer. This link may be validated by higher

Chapter 1 - Introduction

levels of stereocontrol in the NAL-catalysed reactions of aldehydes bearing a sterically demanding group which directs the binding.

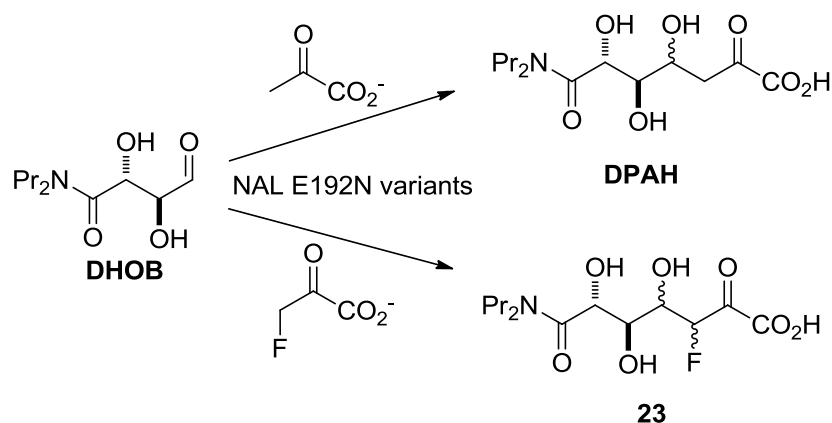
Chapter 4 describes the NAL-catalysed reaction of aldehyde analogues with fluoropyruvate, in the synthesis of fluorinated sialic acid analogues. This added an extra level of complexity because two stereocentres are formed in the reaction. It was therefore necessary to understand the factors that controlled the selectivity at both positions. The underlying reason for the diastereoselectivity of the NAL variants E192N/T167V/S208V and E192N/T167G was not fully understood; therefore it was unclear whether these variants would retain their diastereoselectivity with fluoropyruvate as the donor. The aim was to discover whether fluorine was merely a bystander or if it was somehow directing the diastereoselectivity at both positions.

Finally, the potential scope of using NAL variants in the synthesis of fluorinated analogues of sialic acid has been considered. In order for the NAL variants to be synthetically useful, it is important that they exhibit both high levels of selectivity as well as activity. The NAL variants identified with both of these qualities may be used as a starting point for further optimisation.

Chapter 2 Synthesis of Enzyme Substrates

2.1. Substrate Design

Wild-type NAL is known to catalyse the reaction between ManNAc and fluoropyruvate.¹⁶ The initial aim of this thesis was to determine whether the NAL variants (E192N, E192N/T167V/S208V and E192N/T167G), which were evolved to catalyse the reaction **DHOB** ([2*R*,3*S*]-2,3-dihydroxy-4-oxo-*N,N*-dipropylbutanamide) with pyruvate to give **DPAH** ([5*R*,6*R*]-7-(dipropylamino)-4,5,6-trihydroxy-2,7-dioxoheptanoic acid) (see Section 1.4), will also accept fluoropyruvate as an alternative donor to give the fluorinated product **23** (Scheme 2.1). In extension to this, further potential acceptor substrates were studied to further probe the activity and selectivity of the NAL variants; the synthesis of which will be discussed within the following Sections. The reaction between **DHOB** and pyruvate results in the formation of one new stereocentre, whereas the reaction between **DHOB** and fluoropyruvate results in the formation of two new stereocentres. This work has sought to evaluate both the activity of the NAL variants towards alternative donors and acceptor substrates, and also the diastereoselectivity exhibited by the NAL variants.



Scheme 2.1 - Enzyme-catalysed reaction between **DHOB** ([2*R*,3*S*]-2,3-dihydroxy-4-oxo-*N,N*-dipropylbutanamide) and pyruvate and **DHOB** and fluoropyruvate to give **DPAH** ([5*R*,6*R*]-7-(dipropylamino)-4,5,6-trihydroxy-2,7-dioxoheptanoic acid) and the fluorinated product **23**

In order to further probe the promiscuity of the NAL variants, along with **DHOB**, a series potential acceptor substrates were designed which were used in the NAL-catalysed reaction with fluoropyruvate (Figure 2.1). The substrates were chosen

Chapter 2 - Synthesis of Enzyme Substrates

because it was proposed that they would provide interesting insight into the mechanism and selectivity of the NAL variants.

It had previously been shown that NAL variants catalyse the reaction between **ent-DHOB** and pyruvate.⁶⁹ In the case of E192N and E192N/T167G the activity of **ent-DHOB** compared to **DHOB** was reduced 10 to 20-fold, however in the case of E192N/T167V/S208V the rate was increased 6-fold compared to **DHOB**. These results have demonstrated that it is important to consider both enantiomeric series when designing potential enzyme substrates. Previous work has not considered the combined effect of changing both the donor substrate and the enantiomeric series of the acceptor substrate.

E192N, E192N/T167V/S208V and E192N/T167G have all been evolved to have optimised activity where the acceptor is **DHOB**. Analogues of **DHOB** have since been studied, including the 3-deoxy analogue,⁷⁰ which exhibited diminished enzyme activity and stereocontrol. ManNAc bears an *N*-acetyl group adjacent to the aldehyde group, and this functional group combination is replicated in the potential substrate **AHOB** ([2*R*,3*S*]-3-acetamido-2-hydroxy-4-oxo-*N,N*-dipropylbutanamide). Until now it has not been possible to study **AHOB** as no suitable synthetic route had been developed. **AHOB** was considered an important substrate to study due to its structural similarity to ManNAc and **AHOB** has provided information about the significance of the *N*-acetyl functionality in controlling the relative configuration of the product (to be discussed in Section 3.3). Furthermore, the introduction of a nitrogen atom provides a synthetic handle for further modification and diversification.

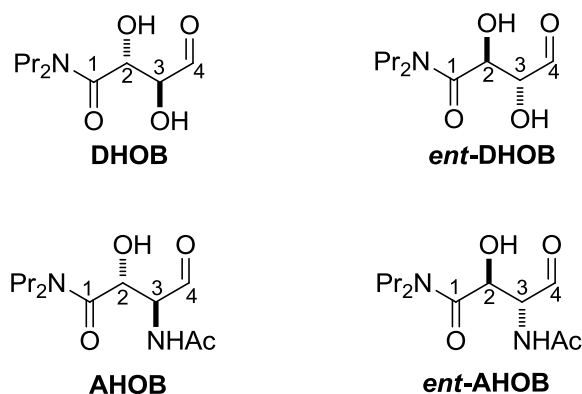


Figure 2.1 - Potential acceptor substrates of the NAL variant-catalysed reaction with fluoropyruvate.

Chapter 2 - Synthesis of Enzyme Substrates

The following Sections will describe only the synthesis of stable precursors of the enzyme substrate **DHOB**, *ent*-**DHOB**, **AHOB** and *ent*-**AHOB**. The aldehydes themselves decompose within days, therefore for reasons of practicality, the enzyme substrates were stored as alkene precursors of the type **24** and **25** (Figure 2.2), which were converted to the corresponding aldehyde by ozonolysis when required and used immediately (Section 3.1.1).

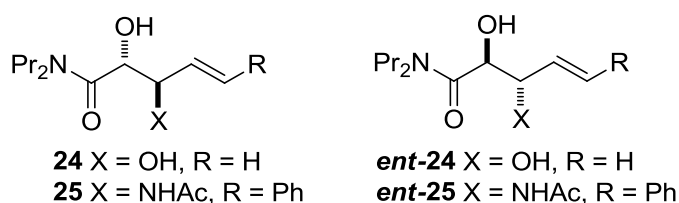
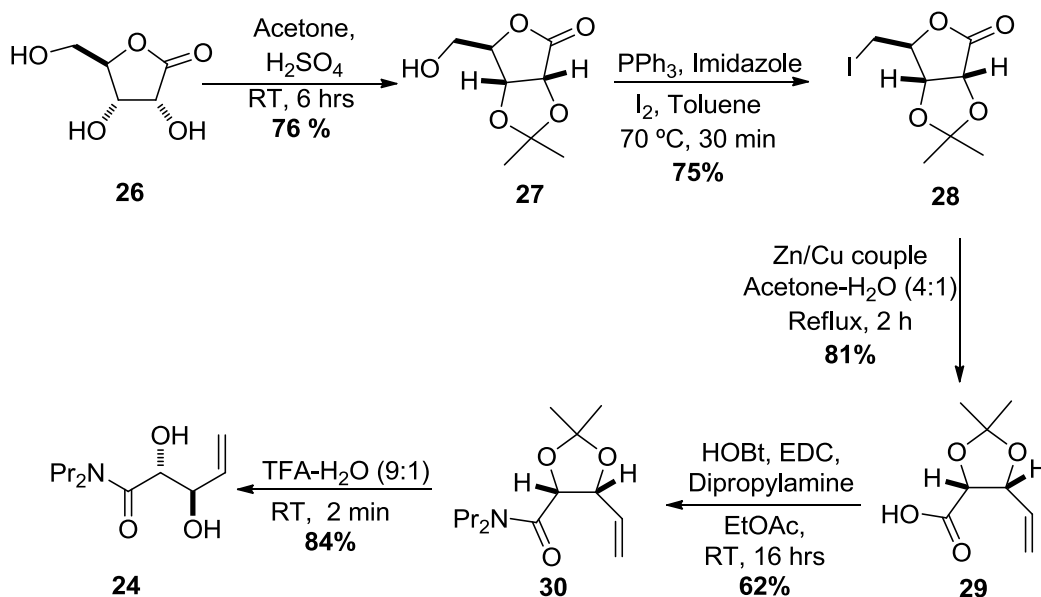


Figure 2.2 - Stable alkene precursors of the potential NAL substrates of **DHOB**/*ent*-**DHOB** (**24**/*ent*-**24**) and **AHOB**/*ent*-**AHOB** (**25**/*ent*-**25**).

2.2. Synthesis of the stable alkene precursor of **DHOB**

The **DHOB** precursor **24** was synthesised in 6 steps from *D*-ribonolactone **26** in an overall yield of 24% using a previously established method (Scheme 2.2).⁶⁵ The secondary alcohols of *D*-ribonolactone **26** were protected by acetonide formation to give **27**. The primary alcohol of **27** was then reacted with triphenylphosphine, imidazole and iodine, to yield the corresponding iodide **28**, which was then eliminated and the lactone opened under Lewis-acidic conditions to give the corresponding carboxylic acid **29**. The carboxylic acid **29** was then activated for amide coupling by HOBT and EDC, to give the acetonide protected dipropylamide **30** which, after acid-mediated cleavage of the acetonide protecting group gave the **DHOB** precursor **24**. *ent*-**DHOB** can be synthesised by an analogous method starting from *D*-lyxose,⁷¹ although for this work, a sample of the *ent*-**DHOB** precursor *ent*-**24** was kindly provided by Thomas Harman.⁶⁹

Chapter 2 - Synthesis of Enzyme Substrates



Scheme 2.2 – Synthesis of DHOB precursor 24 from D-ribonolactone 26

2.3. Synthesis of a stable precursors of AHOB and *ent*-AHOB

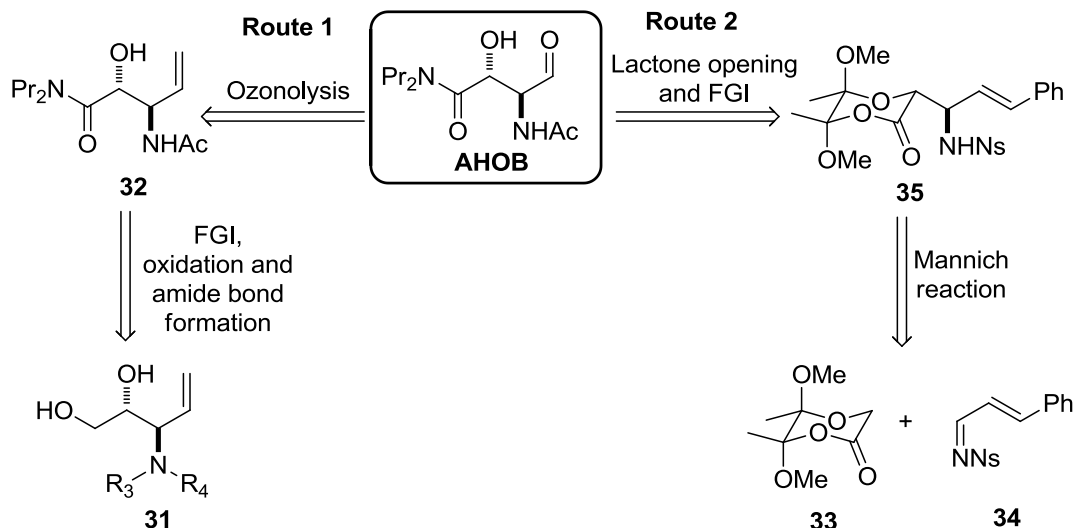
2.3.1. Retrosynthetic analysis of the stable precursors of AHOB/*ent*-AHOB

Several methods were considered for the synthesis of the stable alkene precursors of **AHOB** and *ent*-**AHOB**. The method needed to be reliable to allow the synthesis of multiple grams of substrate, preferably in both enantiomeric series. Scheme 2.3 outlines the different routes considered.

Route 1 would utilise a Petasis reaction to construct intermediate **31**. It was envisioned that the primary alcohol of intermediate **31** could be selectively oxidised, followed by amide coupling and finally functional group interconversion to give the **AHOB** precursor **32**. The absolute configuration could be controlled by the use of a single enantiomer of glyceraldehyde for the Petasis reaction.

Route 2 would exploit the lactone **33** as a key intermediate in the synthesis. The lactone **33** could be synthesised in three steps from a single enantiomer of chloropropane diol by a previously well-established method.⁷² Both enantiomers of chloropropane diol are commercially available so both enantiomers of the lactone **33** can be accessed by analogous routes. The lactone **33** would then be exploited in a

Mannich reaction to give the lactone **35** which, on opening with dipropylamine and introduction of an acetyl group, would give the **AHOB** precursor **25**.



Scheme 2.3 – Retrosynthetic analysis of AHOB. Two routes were considered; route 1 would utilise the Petasis reaction to construct intermediate **31** diastereoselectively and route 2 would utilise the lactone **33** as a key intermediate.

2.3.2. Synthesis of AHOB utilising the Petasis reaction

The Petasis reaction is a three component reaction between an aldehyde, vinyl or aryl boronic acid and an amine to give an allyl or phenyl amine.⁷³ When a chiral α -hydroxy-aldehyde is used, the reaction is diastereoselective in favour of the product with an *anti*-relationship between the α -hydroxyl group and the amine. Scheme 2.4 shows the proposed mechanism of the Petasis reaction between an α -hydroxy aldehyde and a vinyl boronic acid. The mechanism is based on DFT calculations⁷⁴ which predicted that the rate-determining step was C-C bond formation, which occurs by an intramolecular transfer of the vinyl group from a tetra-coordinated borate intermediate. The borate is coordinated to the top face of the imine (as drawn), therefore the vinyl group is delivered to the top face of the imine.



Scheme 2.4 – Mechanism of the Petasis reaction and the role of the α -hydroxyl group in control of the diastereoselectivity

Two amines were considered, the primary amine **36a**,⁷⁵ (see Appendix 1 for synthesis), and the commercially available diallylamine **36b**⁷⁶ (Figure 2.3). Both amines had previously been shown to be suitable substrates for the Petasis reaction.^{75, 76} Previous reaction development studies have shown that secondary amines tend to give higher yields than primary amines.⁷⁷ In addition, studies have shown that using hexafluoroisopropanol (HFIP) as a co-solvent with dichloromethane leads to faster reaction times, especially with secondary amines.⁷⁸ When the Petasis reaction was originally reported,⁷³ a boronic acid was used, however it was found that vinyl boronic acid is unstable⁷⁵ so therefore the corresponding dialkyl ester was used. The boronic ester had to be activated by addition of water to the reaction solvent and required elevated reaction temperatures (24 °C up to 50 °C) and longer reaction times (up to 72 h).

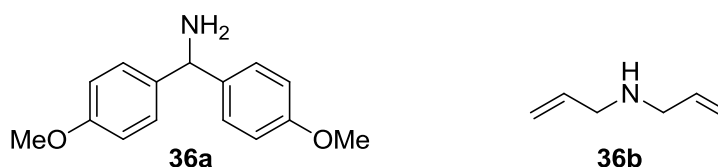


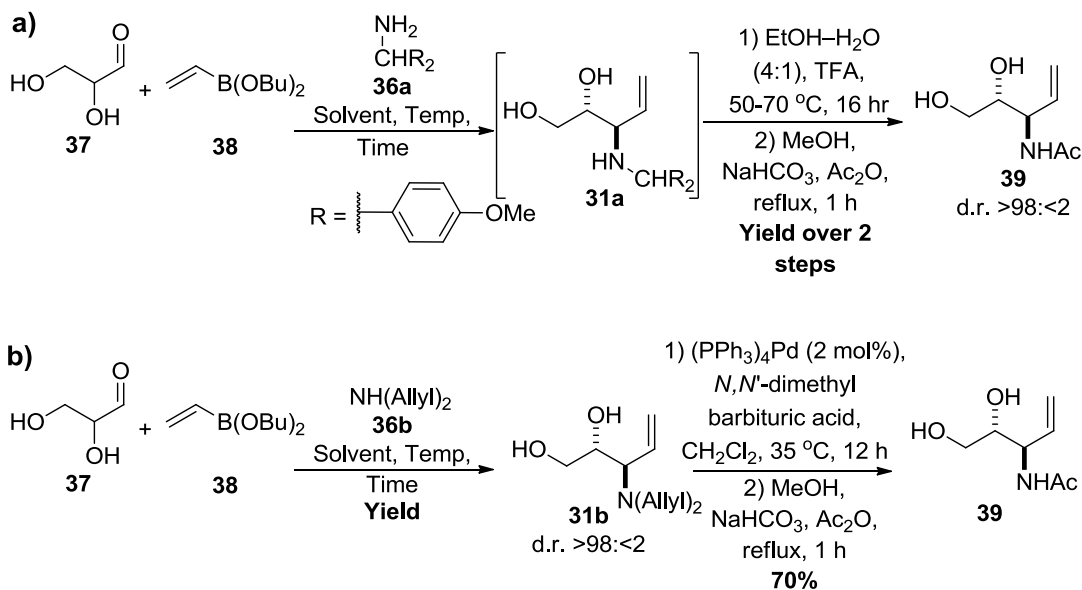
Figure 2.3 - Primary amine **36a** and secondary amine **36b** used in optimisation of the Petasis reaction.

For the purpose of reaction development, the racemic aldehyde **37** was used. Several conditions for the Petasis reaction (Scheme 2.5) were screened in order to optimise the synthesis of the diol **39** and these conditions are outlined in Table 2.1. Entries 1-3 outline the conditions screened for the primary amine **36a**. The crude product, **31a**, of the Petasis reaction was converted directly into the diol **39** by removal of the bis-*p*-methoxyphenyl protecting group under acidic conditions followed by acetylation.⁷⁹ The yields quoted in Table 2.1 are based on the quantity of the diol **39** obtained (Scheme 2.5a). Entries 4-7 outline the conditions screened for the secondary amine **36b**. In this case, the intermediate amine **31b** was purified by flash column chromatography so the yields quoted in Table 2.1 are based on the yield of the diallylamine **31b**. The

diallylamine **31b** was converted into the diol **39** by deprotection with *N,N'*-dimethylbarbituric acid and catalytic tetrakis(triphenylphosphine) palladium(0) in dichloromethane, followed by reaction with acetic anhydride in refluxing methanol to give the diol **39** in a 70% yield over 2 steps from the diallylamine **31b** (Scheme 2.5b).

In Entry 1, the literature conditions were replicated however the reported yield of 60%⁷⁹ was not found to be reproducible. Despite increasing the reaction temperature, the best yield achieved with ethanol–water as the solvent was 9% (Entry 2). Switching to 9:1 dichloromethane–HFIP improved the yield to 38% (Entry 3).

After the mixed success with primary amine **36a**, diallylamine **36b** was considered as an alternative (Entries 4-7). As observed previously, using HFIP as a co-solvent greatly improved the yield (Entries 6 and 7). However, when the scale was increased, the yield decreased significantly and the product became more difficult to purify (Entry 7).



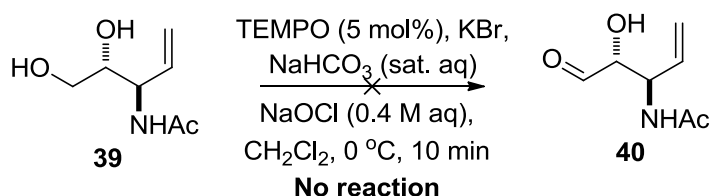
Scheme 2.5 – Petasis reaction optimisation varying amine 36, solvent, reaction temperature, reaction time and relative equivalents of DL-glyceraldehyde 37, amine 36 and vinyl boronic acid 38 a) Reactions of primary amine **36a** (Table 2.1, Entries 1-3). Yield of the diol **39** (based on the limiting reagent) is reported. b) Reactions of the secondary amine **36b** (Table 2.1, Entries 4-7). Yield of diallylamine **31b** (based on the limiting reagent) is reported.

Table 2.1 – Optimisation of the Petasis reaction

Entry	Amine	Solvent	Temp	Scale /mmol 37	Equivalents 37:36:38	Reaction time /day	Yield % (d.r.) ^a
1	36a	EtOH–H ₂ O (4:1)	50 °C	5	1:1:2	4	6 ^b (>98:<2)
2	36a	EtOH–H ₂ O (4:1)	70 °C	3.3	1.5:1.5:1	4	9 ^b (>98:<2)
3	36a	CH ₂ Cl ₂ –HFIP (9:1)	Reflux	3	1.5:1.5:1	3	38 ^b (>98:<2)
4	36b	EtOH–H ₂ O (4:1)	Reflux	5.55	1.5:1.5:1	1	20 ^c (>98:<2)
5	36b	EtOH–H ₂ O (4:1)	RT	5.55	1.5:1.5:1	7	36 ^c (>98:<2)
6	36b	CH ₂ Cl ₂ –HFIP (9:1)	Reflux	5.55	1.5:1.5:1	1	71 ^c (>98:<2)
7	36b	CH ₂ Cl ₂ –HFIP (9:1)	Reflux	11.1	1.5:1.5:1	1	36 ^c (>98:<2)

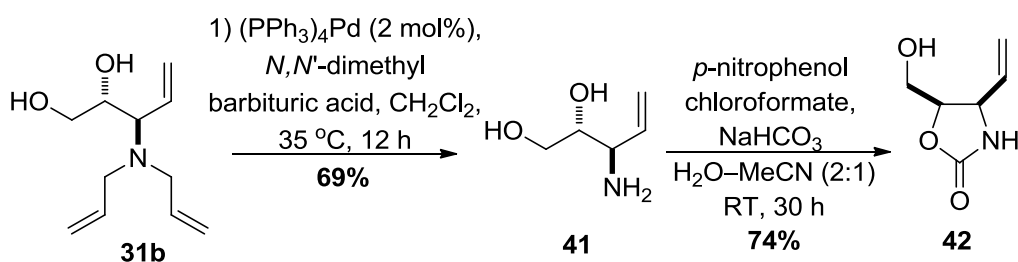
a) Diastereomeric ratio determined by 500 MHz ¹H NMR spectroscopy b) Yield of the diol **39** c) Yield of the diallylamine **31b**

The next stage was to oxidise the primary alcohol of the diol **39** to the corresponding carboxylic acid. There are very few methods for selective oxidation of a primary alcohol, particularly a 1,2-diol. It was decided to investigate a protocol which had previously been successful⁷⁶ in which sodium hypochlorite and catalytic TEMPO in dichloromethane at 0 °C were expected to selectively oxidise the primary alcohol to the corresponding aldehyde **40** (Scheme 2.6). Unfortunately after several attempts, no reaction was observed.



Scheme 2.6 – Unsuccessful TEMPO catalysed oxidation of the diol **39** to the corresponding aldehyde **40**.

After the lack of success selectively oxidising the primary alcohol of the diol **39**, the secondary alcohol was selectively protected by formation of an oxazolidinone **42** so only the primary alcohol was available for reaction. The diallylamine **31b** was deprotected as described previously with *N,N'*-dimethylbarbituric acid and catalytic tetrakis(triphenylphosphine) palladium(0) in dichloromethane, however the primary amine intermediate **41** was purified by SCX ion exchange and was isolated in a 69% yield. The primary amine **41** was then successfully converted in a 74% yield into the oxazolidinone **42** by reaction with *p*-nitrophenol chloroformate (Scheme 2.7).



Scheme 2.7 – Conversion of allyl amine **31b** into oxazolidone **42**.

The oxazolidone **42** was subjected to two sets of oxidation conditions. The first oxidant investigated was Dess–Martin periodinane in dichloromethane at room temperature, however no product was observed despite the starting material being consumed. The same problem occurred under a one-pot direct oxidation to the acid, in which it was expected that the oxazolidinone **42** would be oxidised to the aldehyde by sodium hypochlorite and catalytic TEMPO, immediately followed by a second oxidation to the corresponding acid with sodium chlorite and 2-methyl-2-butene in monosodium phosphate buffered aqueous solution at pH 6 to 7.

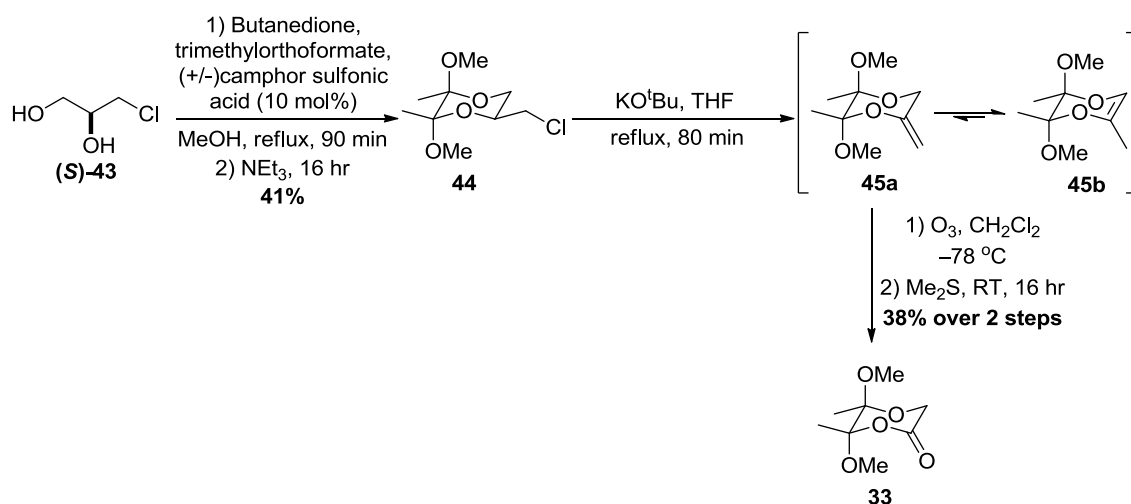
The route was abandoned as suitable oxidation conditions for the diol **39** or the oxazolidinone **42** could not be found. This, along with the problems encountered with yield and purification on scale-up of the Petasis reaction, resulted in the conclusion

Chapter 2 - Synthesis of Enzyme Substrates

that this route was unsuitable. Further problems were encountered when trying to find a reputable source of single enantiomers of glyceraldehyde, which would be necessary if the route had been optimised. Consequently, the second route considered for the synthesis of **AHOB** was investigated.

2.3.3. Reactions of the lactone intermediate **33**

The lactone **33** was synthesised in 3 steps from chloropropane diol **43**.⁷² (*S*)-Chloropropane diol (**S**)-**43** was first reacted with butanedione and trimethylorthoformate in methanol with catalytic camphorsulfonic acid to give the chlorolactone **44** in a 41% isolated yield after chromatography. Upon treatment with potassium *tert*-butoxide in refluxing THF, the chlorolactone **44** underwent elimination to the corresponding exocyclic alkene **45a**. Over prolonged reaction times, isomerisation to the endocyclic alkene **45b** occurred. The alkene **45a** was then ozonolysed to give the lactone **33** in a 38% yield and an overall yield of 16% over 3 steps (Scheme 2.8). By telescoping all three steps and only carrying out purification by chromatography after the ozonolysis reaction, the overall yield was improved to up to 25% over 3 steps.

Scheme 2.8 – Synthesis of the lactone **33** from (*S*)-chloropropane diol (**S**)-**43**

It was envisioned that the lactone **33** could be used as a key intermediate in the synthesis of the **AHOB** precursor **25**. A range of reactions of the lactone **33** were investigated and are summarised in Table 2.2. The general protocol was to generate the enolate by deprotonation with lithium hexamethyldisilazide (LiHMDS) in THF at –78 °C, followed by addition of one of the following electrophiles: an aldehyde (aldol reaction),⁸⁰ an acid-chloride (Claisen-type reaction)⁸⁰ or an imine (Mannich-type reaction)⁸¹ followed by filtration through silica and purification by column chromatography.

Chapter 2 - Synthesis of Enzyme Substrates

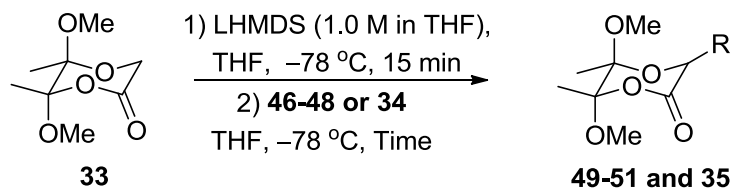
Entry 1 shows the reaction between the lactone **33** and the allyl aldehyde **46** to give the lactone **49**. The lactone **49** could be opened with dipropylamine to give an *anti*-1,2-diol similar to the **DHOB** precursor **24** described in Section 2.2. Although the aldol reaction proceeded successfully, it was not considered a practical intermediate for the synthesis of **AHOB** as a double inversion of the configuration of the alcohol group of the lactone **49** would be required to give the correct relative configuration for the conversion into **AHOB**.

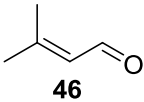
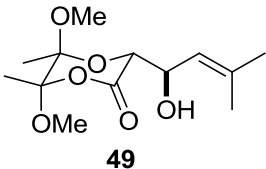
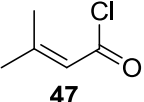
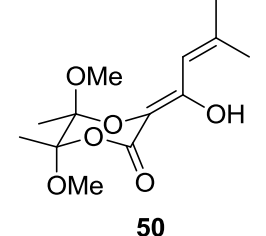
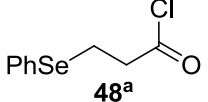
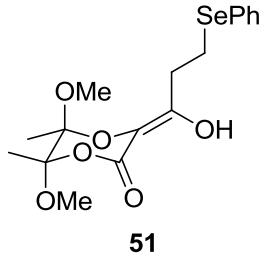
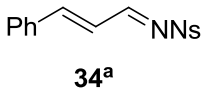
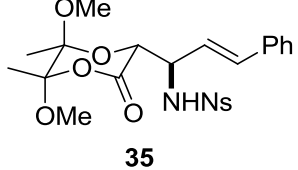
Entries 2 and 3 show a Claisen-type condensation of the lactone **33** with an acid chloride. It was previously shown that for bulky alkyl acid chlorides, a single condensation would occur to give an enol, which would then undergo reduction by tetrabutylammonium borohydride to give the epimer of the product **49**.⁸⁰ The acid chlorides **47** (Entry 2) and **48** (Entry 3) were both investigated.* Reaction with the acid chloride **47** installed the required alkene functionality directly whereas selenide-ethers have previously been shown to act as "masked" double bonds.⁸² Both acid chlorides **47** and **48** underwent a Claisen-type reaction to give the corresponding enol intermediates **50** and **51** respectively however the isolated yields were poor. Furthermore the carbon-selenium bond of the enol **51** was not very stable, leading to rapid decomposition. Suitable conditions for the reduction of the enol intermediates **50** and **51** were not found. Despite screening several different conditions (see Appendix 2), in all cases either conjugate reduction products were observed, or the enol was seen to decompose and a complex mixture was observed.

Entry 4 shows a Mannich type reaction between the sulfonyl-imine **34** (for synthesis, see Appendix 1) and the lactone **33**. This installed the amine group directly without the requirement for substitution and inversion. The lactone **35** was chosen as a suitable intermediate in the synthesis of **AHOB**.

* The synthesis of the none commercially available acid chloride **48** is discussed in Appendix 1

Table 2.2 - Reactions of lactone 33



Entry	Reaction partner	Reaction Time	Product	Yield % (d.r.)
1	 46	5 min	 49	85 (d.r. >98:<2) ^b
2	 47	1 hr	 50	37
3	 48^a	1 hr	 51	65 ~50:50 enol:keto
4	 34^a	2 hr	 35	78 (d.r. 83:17) ^c

a) Not commercially available, see Appendix 1 and experimental Section 6.3 for synthesis b) Configuration was proven by comparison with the previously reported data. c) Absolute configuration was confirmed by analysis of downstream products (Section 3.1.3).

The aldol reaction (Entry 1) and the Mannich reaction (Entry 4) both result in the formation of two new stereocentres (therefore four possible diastereomers could be observed) and the products **49** and **35** drawn in Table 2.2 were observed as the major diastereomers. The aldol reaction was diastereoselective (d.r. >98:<2)^{*} whereas the Mannich-type reaction gave an 83:17 mixture of diastereomers. Rationalisation for the observed stereocontrol of both reactions is shown in Figure 2.4. In both cases, the pair of diastereomers in which the electrophile attacks into the axial position of the lactone **33** would be highly unfavoured due to a 1,3-steric clash with the methoxy group (Figure 2.4a). The aldol reaction (Figure 2.4b) is likely to proceed *via* a chair-like transition state with the lithium coordinating to the negative charge of the oxygen on the lactone **33** and the lone pair of the aldehyde **46** oxygen. The electrophile attacks in the equatorial position of the lactone **33** and the bulkiest group is positioned in a *pseudo*-equatorial position in the transition state, with the hydrogen occupying the *pseudo*-axial position in order to minimise steric interaction with the methoxy groups of the lactone.⁸⁰ In the case of the Mannich reaction (Figure 2.4c), in order for the nitrogen lone pair to be available to interact with the lithium and the reaction to proceed *via* a chair-like transition state, the imine **34** would have to adopt the (*Z*) configuration to give the observed major diastereomer of the lactone **35**.⁸¹ It is likely however that the imine adopts the (*E*) configuration predominantly, therefore it may also be possible that the reaction proceeds *via* an open transition state to give the observed major diastereomer of the lactone **35**. The (*E*)-imine would be unlikely to react *via* a chair-like transition state due to unfavourable steric interactions between the phenyl group of imine **34** and the methoxy groups of the lactone **33**. This added level of complexity may account for the reduction in diastereoselectivity observed in the Mannich-type reaction.

^{*} Within the error of NMR integral measurements

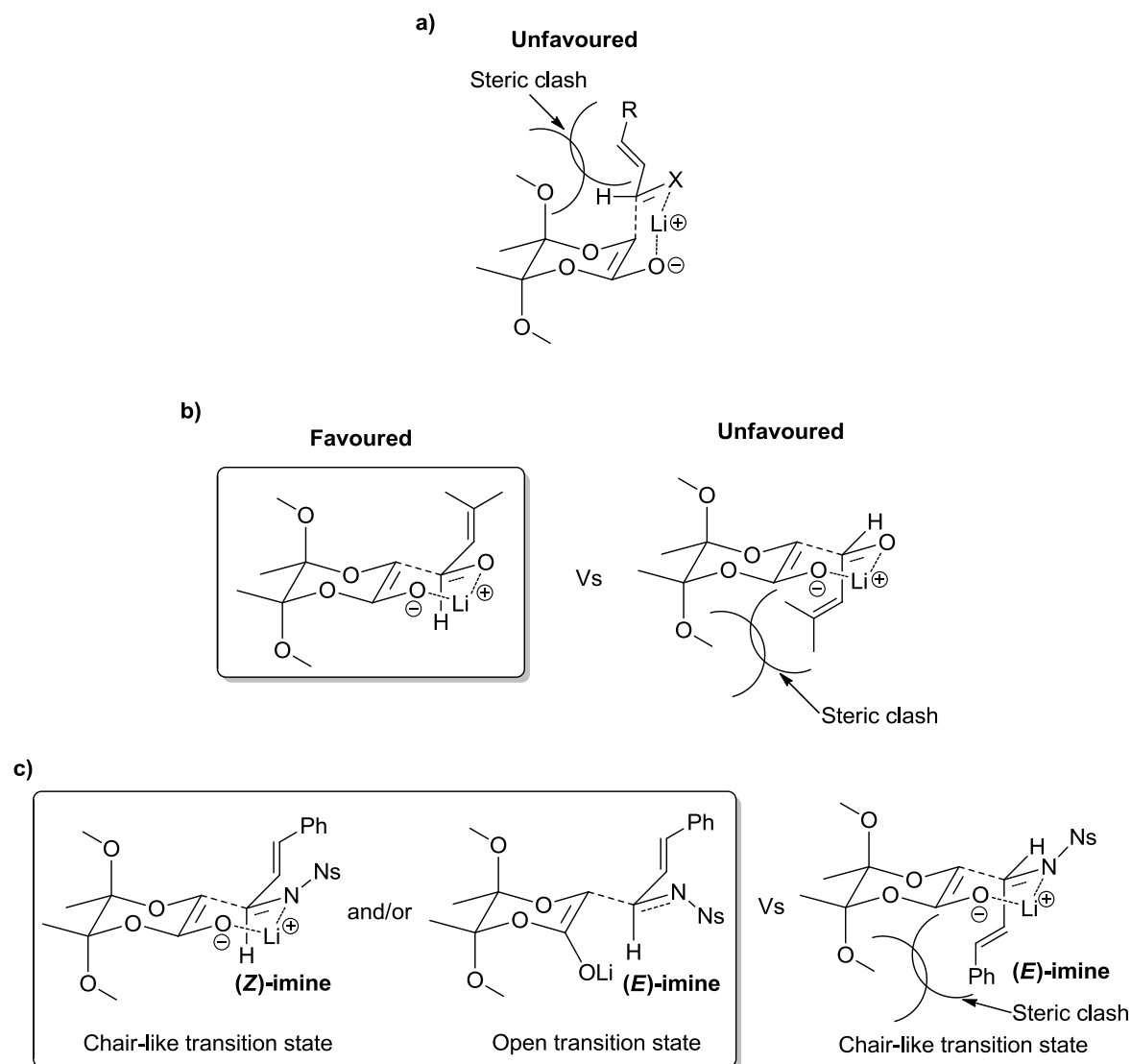


Figure 2.4 - Transition state comparisons for the aldol and Mannich reactions of the lactone 33 a) Unfavoured attack of the electrophile into the axial position of the lactone b) The aldol reaction between the aldehyde 46 and the lactone 33 and c) The Mannich reaction between the sulfonyl-imine 34 and the lactone 33.

2.3.4. Conversion of the lactone intermediate 35 into AHOB.

In order to convert the intermediate **35** into the **AHOB** precursor **25**, the following synthetic steps were necessary: opening of the lactone **35**, the introduction of the dipropylamide functionality and conversion of the sulfonamide into an acetamide. The acetyl group was introduced in the last step so that it would be possible to add different functional groups to the amine if required in the future, without having to redesign the synthesis.

The step which proved to be most challenging was the opening of the lactone **35** and the conditions investigated are outlined in Table 2.3. The protected intermediate **52** was difficult to purify due to its instability on silica, however it was necessary to ensure

Chapter 2 - Synthesis of Enzyme Substrates

removal of all unreacted dipropylamine as any contaminating dipropylamine in the acetal cleavage reaction resulted in poor or no conversion to the deprotected sulfonamide **53**.

Entries 1-3 use dipropylamine as the solvent, making its subsequent removal very difficult. Under these conditions, it was found to also be necessary to use a catalyst, as the uncatalysed reaction (Entry 1) resulted in no reaction taking place. Both TBD and DMAP at 30 mol% loading, heating to 75 °C (Entries 2 and 3) gave a similar yield with no epimerisation (the d.r. of the lactone **35** is 83:17) but significant elimination of *p*-benzenesulfonamide as a by-product was observed.* The mechanism of this elimination is unclear as no lactone-containing by-product partner was isolated. Despite careful removal of the *p*-benzenesulfonamide by-product,[†] the yields of isolated product were disappointing at only 22%.

Amines activated by forming the aluminium salt have previously been shown to open lactones under milder conditions.^{83, 84} Two aluminium sources were considered, trimethylaluminium in dichloromethane at 40 °C (Entries 4 and 6)⁸³ and DIBAL in THF at room temperature (Entry 5).⁸⁴ Activating with aluminium allowed for much lower dipropylamine loadings to be used; therefore removal of dipropylamine simply by aqueous extraction became possible. It was found by crude NMR that under the DIBAL activated conditions (Entry 5) that significant epimerisation had occurred, with the d.r. reduced from 83:17 to 67:33, however the yield was improved to 52% of the protected intermediate **52** after chromatography. Under the trimethylaluminium activated conditions (Entry 4), the crude NMR showed little to no epimerisation had taken place, however the yield after chromatography was reduced to only 28%. However, examination of the 500MHz ¹H NMR spectrum of the unpurified product **52**, after an aqueous work-up, contained very little unreacted dipropylamine or other impurities. The crude product was dissolved in acetonitrile–water (1:1) and the *O*-acetal protecting group was hydrolysed by the addition of trifluoroacetic acid. The sulfonamide **53** was isolated in a much improved 68% yield over 2 steps with little to

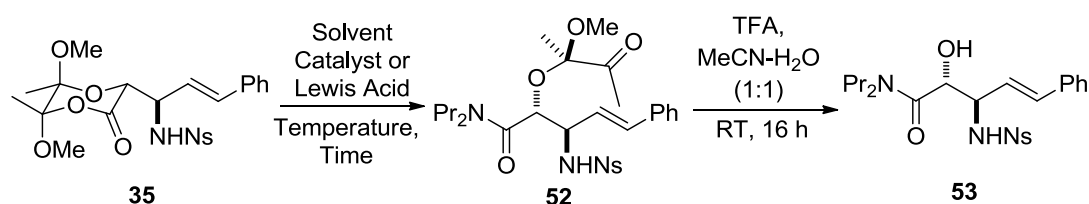
* By careful removal of the *p*-nitrobenzenesulfonamide after the Mannich reaction, it was found that the *p*-nitrobenzenesulfonamide was being eliminated during opening of the lactone **35** under the conditions outlined in Table 2.3, Entries 2 and 3 rather than being carried through the synthesis.

[†] The *p*-nitrobenzenesulfonamide by-product could be removed by dissolving the contaminated product in chloroform after chromatography, followed by removal of the *p*-benzenesulfonamide by filtration.

Chapter 2 - Synthesis of Enzyme Substrates

no epimerisation observed and with the reaction time of the lactone opening reaction reduced to only 2 hours (Entry 6).

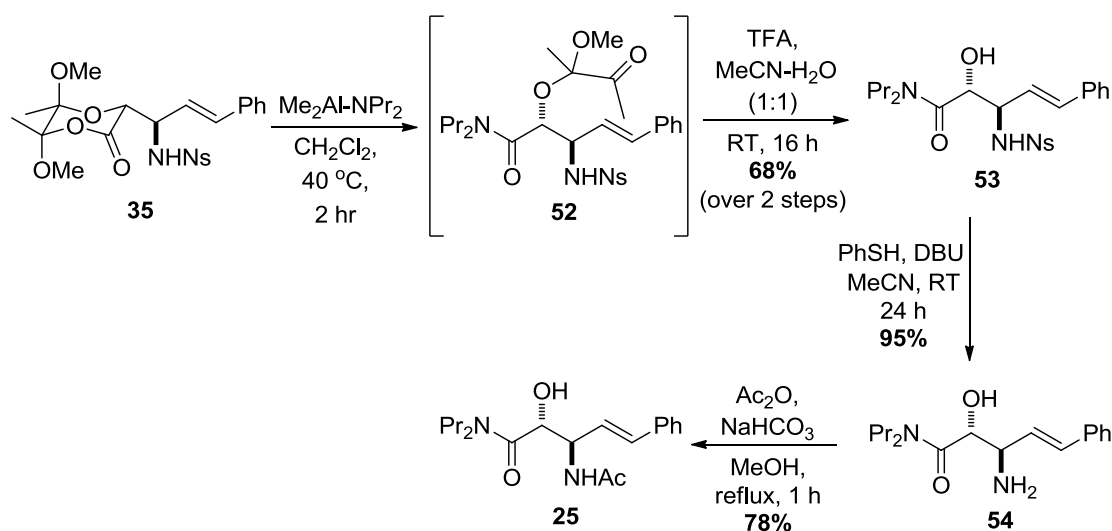
Table 2.3 – Optimisation of condition for opening of the lactone 35



Entry	Solvent	Catalyst/ Lewis acid	Eq. HNPr ₂	Temp. /°C	Time /h	Yield of 52 % (d.r)	Yield of 53 %
1	HNPr ₂	-	>20	100	-	No reaction	-
2	HNPr ₂	TBD (30 mol%)	>20	75	2	22 (83:17)	36
3	HNPr ₂	DMAP (30 mol%)	>20	75	2	22 (83:17)	-
4	CH ₂ Cl ₂	Me ₃ Al	1	40	24	28 (83:17)	-
5	THF	DIBAL	2.5	RT	24	52 (67:33)	-
6	CH ₂ Cl ₂	Me ₃ Al	2	40	2	Not isolated	68 (2 steps)

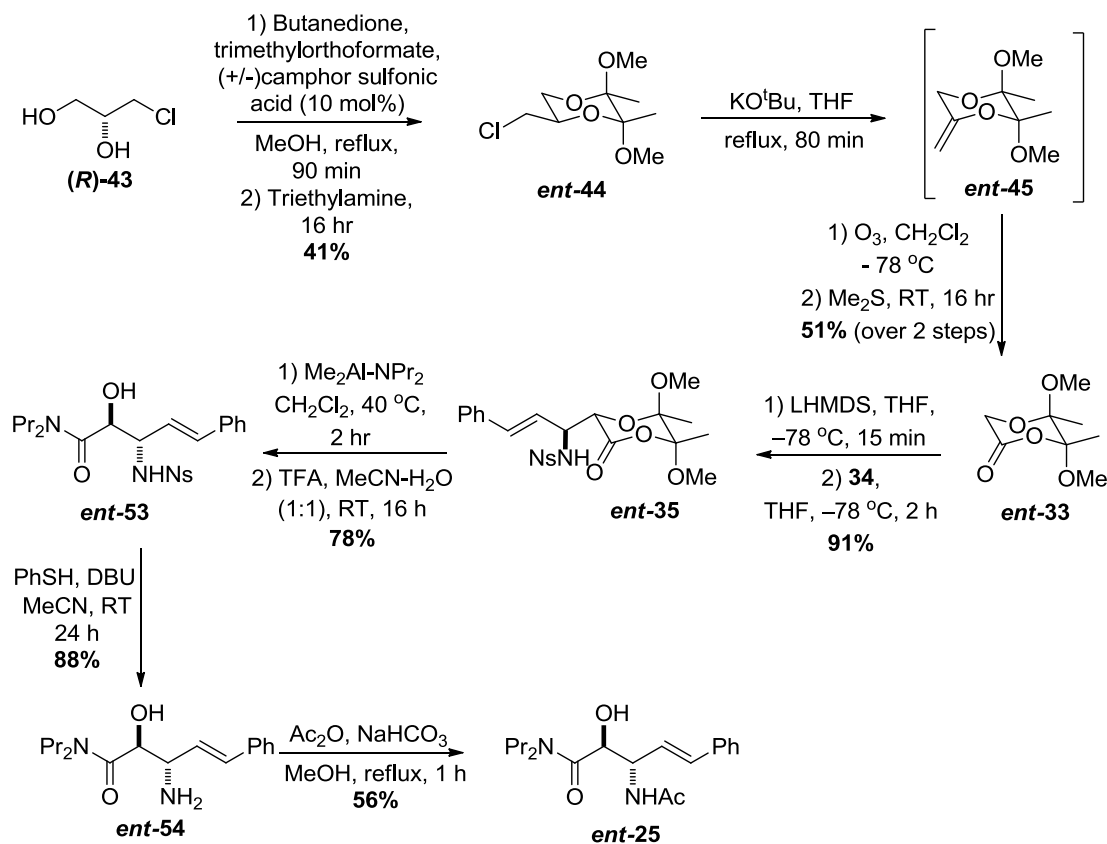
The final synthetic route employed for the latter stages of a multi-gram synthesis of the **AHOB** precursor **25** is outlined in Scheme 2.9. The lactone **35** was opened under the optimised conditions described previously to give the protected dipropylamide **53**, which is then deprotected in over 90% yield with thiophenol and DBU at room temperature in acetonitrile. The resulting primary amine **54** was reacted with acetic anhydride in refluxing methanol to give the **AHOB** precursor **25** as a single enantiomer in a 10% overall yield from the commercially available (*S*)-chloropropane diol (**S**)-**43**.

Chapter 2 - Synthesis of Enzyme Substrates



Scheme 2.9 – Conversion of the lactone **35** into the AHOB precursor **25** by aluminium mediated lactone opening, followed by deprotection and *N*-acetylation.

The enantiomeric precursor, **ent-25**, was synthesised by an analogous route starting from (*R*)-chloropropane diol (**R-43**) (Scheme 2.10). The yields obtained at each stage were similar to those observed for the enantiomeric series.



Scheme 2.10 – Synthesis of the *ent*-AHOB precursor **ent-25** from (*R*)-chloropropane diol (**R-43**).

Chapter 2 - Synthesis of Enzyme Substrates

In summary, stable alkene precursors of the four potential NAL substrates discussed in Section 2.1 have been successfully synthesised in sufficient quantities for use in the enzyme catalysed reaction between NAL and pyruvate or fluoropyruvate. The method for synthesis of the **DHOB** precursor **24** was successfully replicated and a new synthetic route for accessing different potential NAL substrates has been established.

The Petasis reaction proved to be unsuccessful due to problems with selective oxidation of the primary alcohol **39** or the oxazolidinone **42**. Furthermore, the yield of the Petasis reaction appeared to decrease when the scale was increased, and the purification became more challenging. Furthermore, the intermediates formed in the Petasis route are limiting in terms of the potential to introduce further diversity or adapt the route to access a greater range of potential enzyme substrates.

The method developed utilising the lactone **33** is not only a very reliable route to access the **AHOB** precursor **25**, the lactone **33** may be used in other types of reaction to produce several other synthetically useful intermediates. The route that has been developed could be easily adapted to access further substrates to probe the NAL active site.

Chapter 3 NAL-catalysed reactions of aldehyde analogues and pyruvate

3.1 NAL E192N variants in the preparation of *N*-acetyl neuraminic acid analogues

The analysis of the NAL variant-catalysed reactions has been separated into two sections; the reactions of pyruvate and the reactions of fluoropyruvate. This Chapter focuses only on the NAL-catalysed reaction of pyruvate, in which one new stereocentre is formed in the reaction. The reaction of **DHOB** and *ent*-**DHOB** with pyruvate have previously been studied in detail^{67, 69} so this Chapter will only evaluate the NAL variant-catalysed reactions of the aldehyde substrate **AHOB** ([2*R*,3*S*]-3-acetamido-2-hydroxy-4-oxo-*N,N*-dipropylbutanamide) and its enantiomer *ent*-**AHOB**. The main objective of this study was to determine whether the NAL variants (E192N, E192N/T167V/S208V and E192N/T167G) would tolerate the introduction of an *N*-acetyl group and what the effect would be on the diastereoselectivity of the reaction.

3.1.1 Preparation of NAL variants and aldehyde substrates

His₆-tagged NAL variants were expressed in *E. coli* grown in 2×TY media from glycerol stocks prepared previously.⁵⁷ The NAL variants were obtained by collecting the pellet, lysing the cells, centrifugation to remove the cell debris and purification from the supernatant using nickel affinity chromatography. Figure 3.1 shows a typical example of an SDS-PAGE gel analysing the purification process. The second lane shows the crude cell extract with a very intense band at 33.5 kDa, which corresponds to the molecular weight of His-tagged NAL.⁸⁵

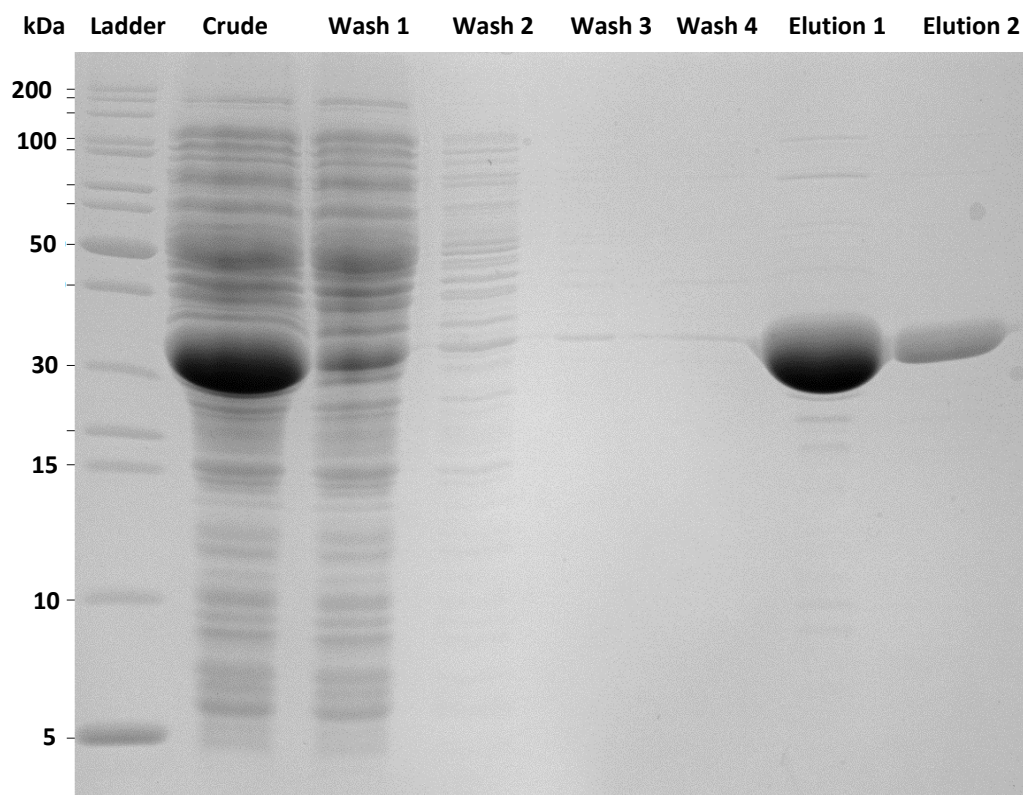
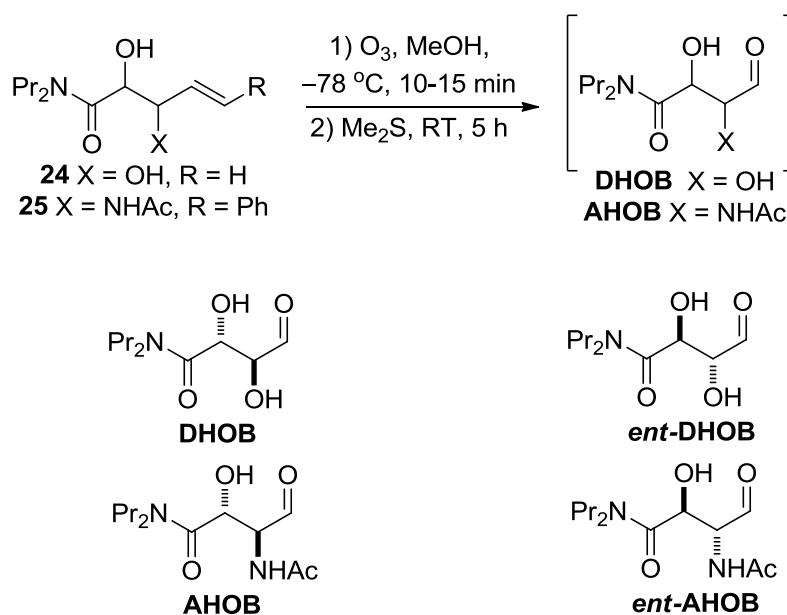


Figure 3.1 - SDS-PAGE during NAL E192N purification. From left to right, lane 1 corresponds to the molecular weight marker, lane 2 shows the crude cell extract, clearly showing the large band corresponding to over-expression of NAL. Wash 1-4 corresponds to washing contaminated proteins off the nickel resin while NAL was bound to the resin. Elution 1 and 2 correspond to purified NAL after being eluted from the nickel resin with imidazole.

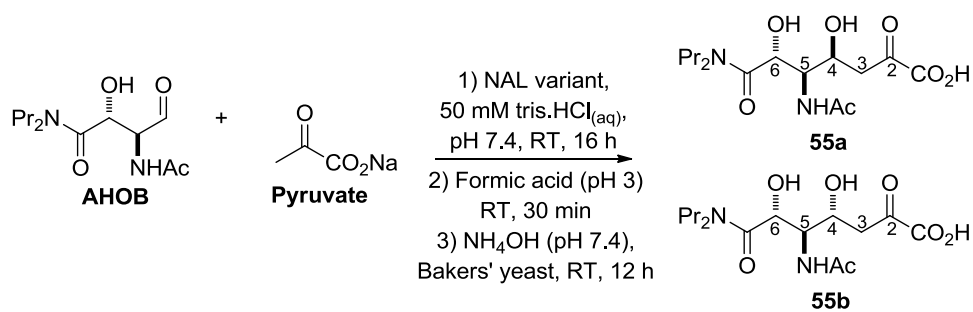
The previous Chapter outlined the development of a synthetic route to a series of stable precursors of potential substrates of the NAL variants. The potential substrates were stored as their corresponding alkene precursors **24** and **25**, which were converted into the aldehyde substrates by ozonolysis as they were required (Scheme 3.1).⁶⁵ The methodologies for preparation of NAL variants and aldehyde substrates described within this Section were applied throughout.



Scheme 3.1 - Conversion of stable alkene precursors **24** and **25** into the corresponding aldehydes **DHOB/ent-DHOB** and **AHOB/ent-AHOB** by ozonolysis.

3.1.2 Preparative scale enzyme catalysed reactions of **AHOB** with pyruvate

AHOB and **ent-AHOB** were subjected to reaction with pyruvate, catalysed by the NAL variants E192N, E192N/T167V/S208V and E192N/T167G. Typically, the NAL-catalysed reactions were carried out in 50 mM Tris.HCl at pH 7.4, followed by addition of formic acid after 16 hours in order to denature the NAL variant and stop the reaction. The pH was then returned to 7.4 and Bakers' yeast was added in order to break down excess pyruvate to acetaldehyde. Initial purification was carried out by Dowex[®] ion exchange. Table 3.1 outlines the isolate yields and observed diastereoselectivity (measured by 500 MHz ¹H NMR; Section 3.1.3 and Appendix 3) of the NAL variant-catalysed reactions. The NAL E192N/T167V/S208V variant was found to be completely inactive towards **AHOB** under the reaction conditions (Entry 2). The NAL E192N-catalysed reaction of **AHOB** and pyruvate (Entry 1) gave a single diastereomer, **55a**, which did not require further purification. The NAL E192N/T167G variant also gave product **55a** selectively (Entry 3). The NAL E192N-catalysed reaction of **ent-AHOB** gave a 76:24 mixture of **ent-55b** and **ent-55a** (Entry 4). The products **55a** and the mixture of **ent-55a** and **ent-55b** were further purified by mass-directed reverse-phase HPLC.

Table 3.1 - Reactions of the NAL variants with AHOB/*ent*-AHOB and pyruvate under preparative conditions.

Entry	Aldehyde	NAL variant	Equivalents of aldehyde:pyruvate	Yield %	d.r
1	AHOB	E192N	1:2	41 ^a	>98:<2 55a
2	AHOB	E192N/T167V/ S208V	1:2	0	-
3	AHOB	E192N/T167G	1:2	11 ^b	>98:<2 55a
4	<i>ent</i> -AHOB	E192N	1:2	9 ^b	24:76 <i>ent</i> -55a: <i>ent</i> -55b

a) Yield after ion exchange chromatography b) Yield after mass-directed reverse-phase HPLC purification

3.1.3 Identification and characterisation of AHOB enzyme catalysed reaction products

The reaction between **AHOB**/*ent*-AHOB and pyruvate sets up one new stereocentre; therefore there are two possible products in the reaction, resulting from *re* or *si*-face attack of the aldehyde. Figure 3.2a is a 500 MHz ¹H NMR spectrum of the HPLC purified product **55a**. Figure 3.2b shows the 500 MHz ¹H NMR spectrum of the mixture of isolated products *ent*-55b and *ent*-55a (76:24).

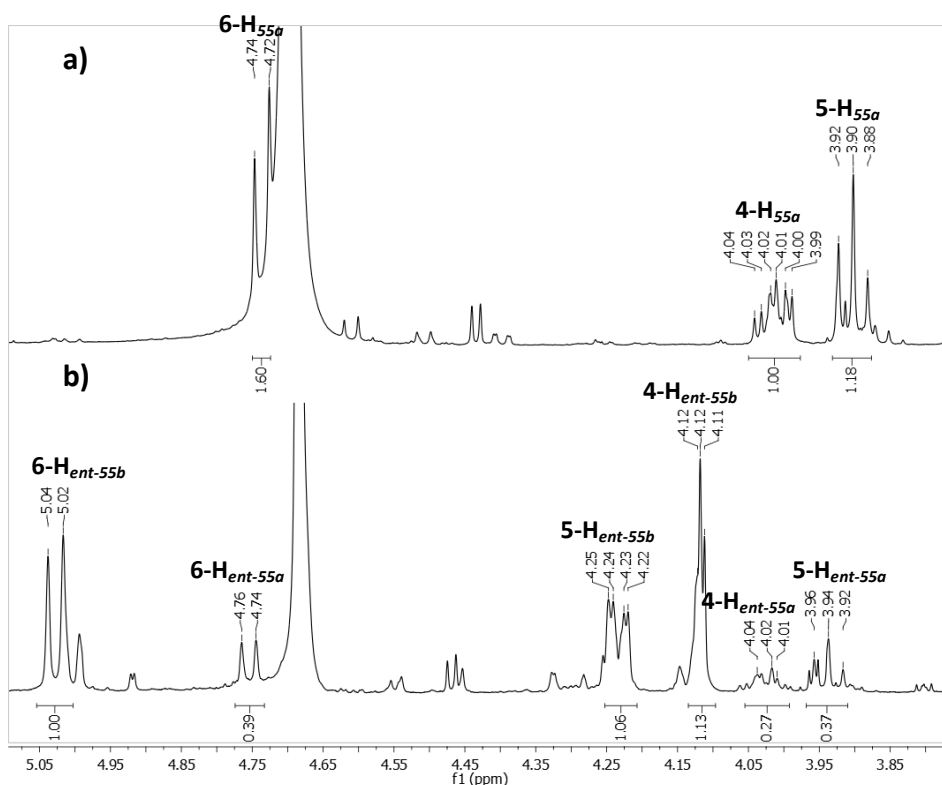
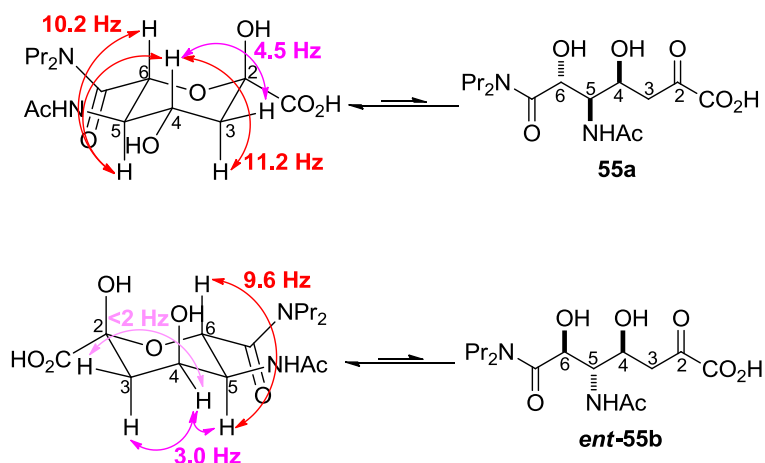


Figure 3.2 - Diagnostic region of the 500 MHz ^1H NMR spectra of the mass-directed reverse-phase HPLC purified products of the NAL variant-catalysed reaction of AHOB/*ent*-AHOB and pyruvate. a) HPLC purified product **55a b) HPLC purified 76:24 mixture of products *ent*-**55b** and *ent*-**55a**.***

The diagnostic peaks in the 500 MHz ^1H NMR spectrum of the products **55a** and *ent*-**55b** were analysed and characterised (Table 3.2). The configuration of the products was assigned by careful analysis of the signals corresponding to 5-H. Due to the configuration of the starting materials, and the preference for the largest substituents to adopt the equatorial positions of a pyranose ring, 5-H and 6-H will always be axial. The structure of product **55a** was confirmed because the signal for 5-H appeared as a triplet with a coupling constant of 10.2 Hz, indicating that H-4, H-5 and H-6 are all axial in a pyranose ring. The structure of product *ent*-**55b** was confirmed because 5-H appeared as a doublet of doublets with a coupling constant to 6-H of 10.6 Hz and a coupling constant to 4-H of 3.1 Hz, indicating that 5-H and 6-H were axial and H-4 was equatorial in a pyranose ring.

* The NMR spectra were recorded without suppression of the water peak, as suppression resulted in diminished resolution of signals close to the water peak, and in some cases disappearance of signals.

Table 3.2 - Characterisation of the products **55a** and *ent*-**55b** by 500 MHz ¹H NMR spectroscopy.

Product	δ_{H} (500 MHz, D ₂ O) /ppm	Multiplicity	³ J /Hz	Identity	Configuration at C-4
55a	4.83	d	10.3	6-H	(S)
	4.11	td	11.2, 10.9 and 4.5	4-H	
	4.00	t	10.2	5-H	
<i>ent</i> - 55b	5.03	d	9.6	6-H	(S)
	4.23	dd	10.6 and 3.1	5-H	
	4.12	t	3.0	4-H	

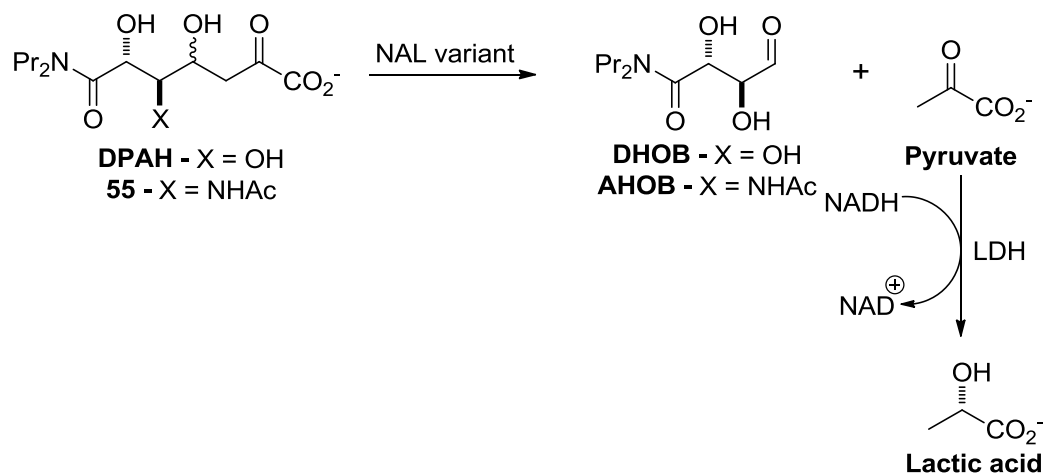
3.1.4 Measuring activity of the cleavage of the products of enzyme catalysed reactions

The activity of the NAL variants in the cleavage of the products **55** and *ent*-**55** was analysed in comparison to the cleavage of **DPAH** (the product of the NAL variant-catalysed reaction of **DHOB** and pyruvate) using the coupled assay* (Scheme 3.2). Due to only small quantities of material being available, single concentration kinetic measurements were taken at low concentrations (1 mM of substrate with 0.06 mg/ml of NAL) of products **55**, *ent*-**55** and **DPAH**. At low substrate concentrations, the enzyme is unlikely to be saturated therefore the observed rates are likely to correlate with k_{cat}/K_M .⁸⁵ Chart 3.1 shows the activity of the NAL variants recorded as the decrease in absorbance at 340 nm per minute for each of the NAL variants and substrates.

* For more details of the standard coupled assay, see Section 1.4.1 and the experimental Section 6.1.6

Chapter 3 - NAL-catalysed reactions of aldehyde analogues and pyruvate

Compound **55a** was evaluated as a single diastereomer, whereas **ent-55** and **DPAH** were tested as a mixture of diastereomers.



Scheme 3.2 – Principle of the standard coupled assay for determining the rate of the retro-aldol reaction of the NAL variant

Chapter 3 - NAL-catalysed reactions of aldehyde analogues and pyruvate

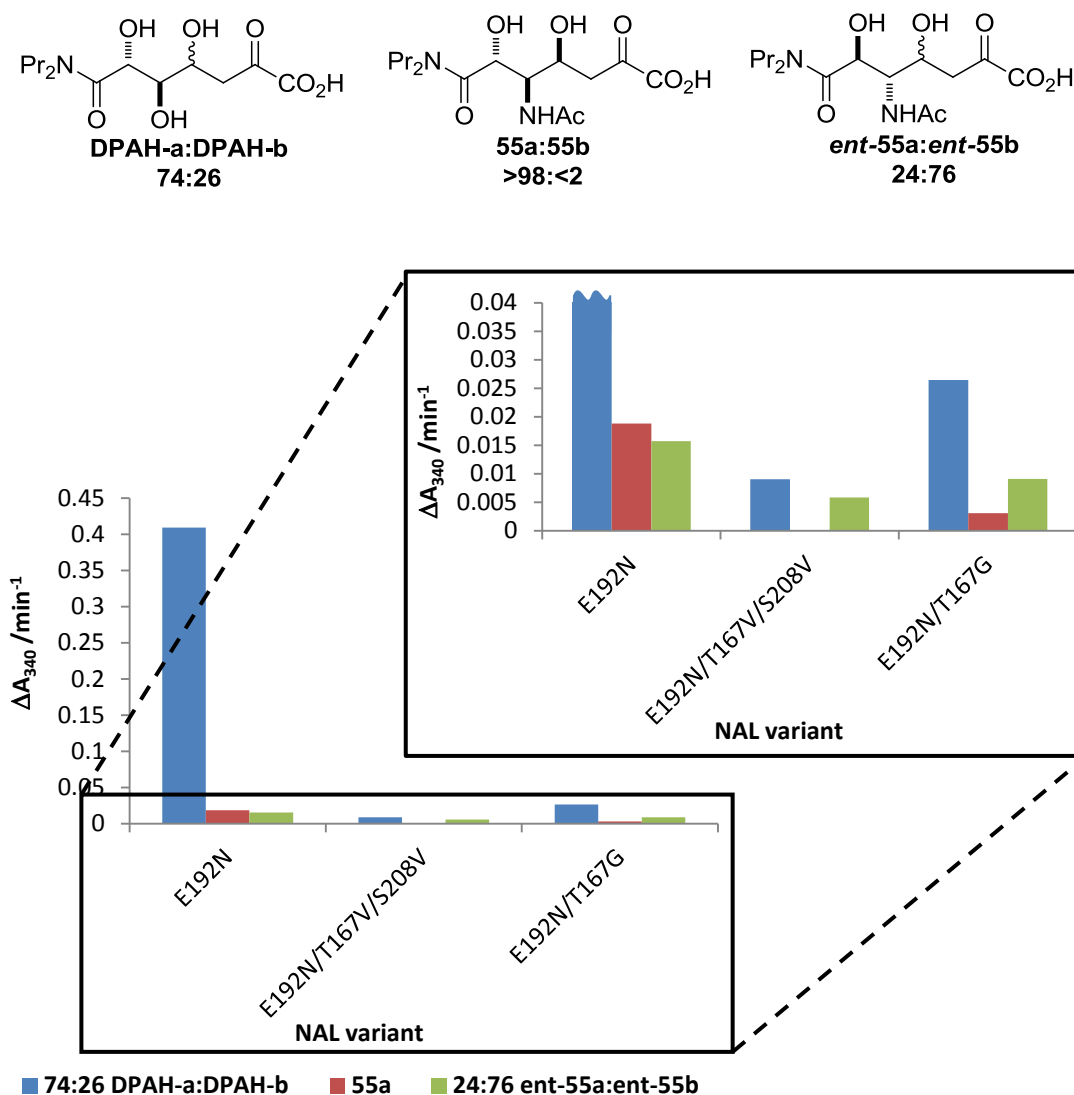


Chart 3.1 - Single point kinetic measurements of the NAL variants against the products of the NAL E192N-catalysed reactions (1 mM of substrate with 0.06 mg/ml of NAL); DPAH (blue), which was used as a 74:24 mixture of (4S) and (4R)-epimers, 55a (red) and ent-55 (green), which was used in a 76:24 mixture of (4S) and (4R)-epimers. Insert shows an enlargement of the lower level activity measurements.

DPAH was found to be by far the most active in the cleavage direction for all the NAL variants. The NAL E192N variant is over 20 times more active towards the cleavage of DPAH compared to the cleavage of the product 55a. As discussed in the previous Section, NAL E192N/T167V/S208V was inactive towards AHOB, therefore it was not surprising to find that it was also inactive in the cleavage of the product 55a.

The NAL E192N/T167V/S208V and E192N/T167G variants are both poorly active towards cleavage of ent-55. NAL E192N is known from previous studies to be 20 times less active towards the enantiomeric form of DPAH,⁶⁴ and is also seen to be less active towards ent-55 compared to 55. However, as observed for the enantiomeric series of

DPAH, NAL E192N/T167V/S208V was found to be more active towards *ent*-**55** compared to **55**.⁶⁹

3.2 Monitoring enzyme catalysed reactions of AHOB by 500 MHz ¹H NMR spectroscopy

3.2.1 Comparison of activities and kinetic selectivity of enzyme catalysed reactions of AHOB

The forward reactions, catalysed by the NAL variants, with **AHOB**/*ent*-**AHOB** were monitored by 500 MHz ¹H NMR spectroscopy in order to evaluate the kinetic selectivity of the enzyme-catalysed reactions. Figure 3.3 shows a selection of the time points of the NAL E192N-catalysed reaction between **AHOB** and pyruvate. The peaks highlighted in red, which correspond to **AHOB**, disappear and the peaks corresponding to diastereomer **55a**, highlighted in blue, appear over time.* The areas highlighted in green correspond to the regions of the spectra where the peaks corresponding to **55b** would appear. It was found that the product **55b** (the (4*R*)-epimer of the product of the reaction of **AHOB** and pyruvate) was not observed under the conditions investigated. Chart 3.2 shows a plot of the appearance of the product **55a** and the disappearance of **AHOB** over time.

* Due to deuterium incorporation as a result of keto-enol tautomerisation of pyruvate, the chemical shifts and multiplicities of the peaks change compared to the preparative scale reaction.

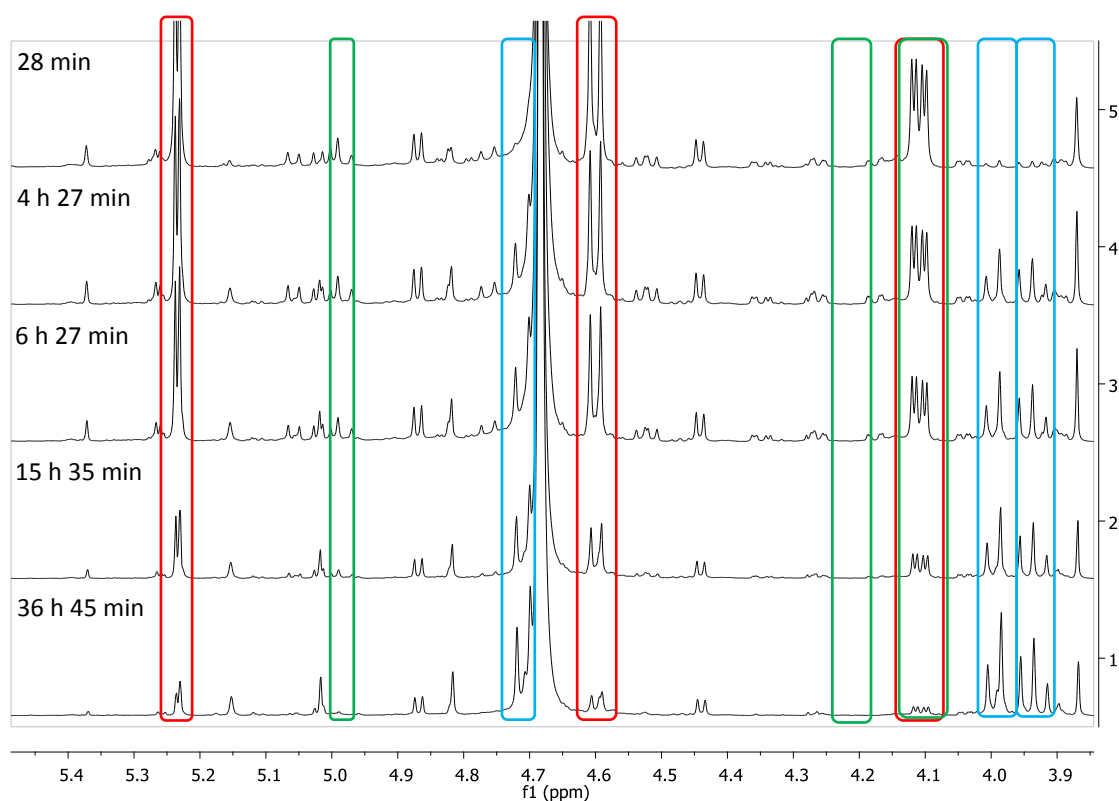


Figure 3.3 – 500 MHz ^1H NMR spectroscopy time-course of the NAL E192N-catalysed reaction of AHOB and pyruvate. AHOB (red) 55a (blue) region of the spectra where 55b would appear (green). (Conditions for time-course: 0.1 mmol of aldehyde, 0.2 mmol of pyruvate and 0.56 mg of NAL in 0.7 ml of deuterated sodium phosphate buffer, pH 7.4)

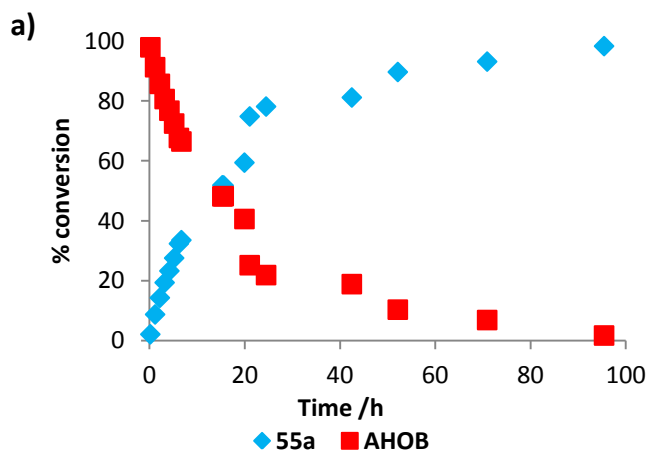


Chart 3.2 - Representation of the percentage disappearance of AHOB and the percentage appearance of product 55a over the full reaction time.

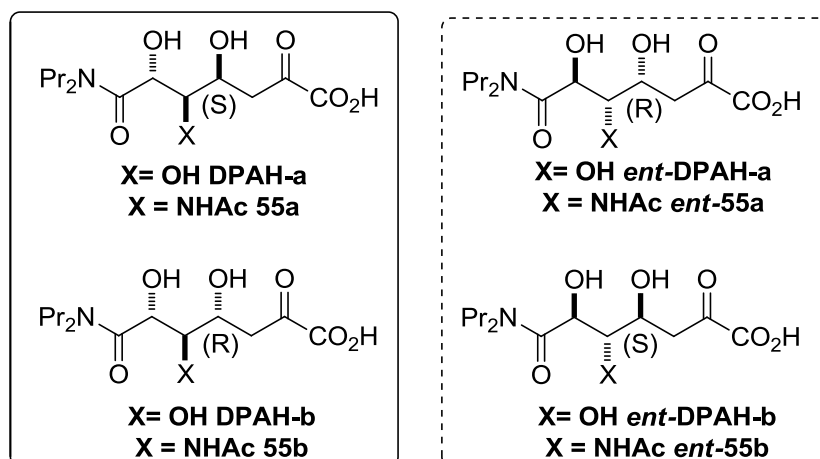
The selectivity data of the kinetically controlled reactions is shown in Table 3.3, along with the known selectivities of the NAL-catalysed reaction of **DHOB** and *ent*-**DHOB**.⁶⁹ This data is further illustrated in Chart 3.3. The most remarkable result is that regardless of the enantiomer of **AHOB**, the NAL E192N variant exhibits high levels of C-4 selectivity, which is in direct contrast with the selectivity observed for **DHOB/ent-DHOB**, where the C-4 selectivity is very poor.⁶⁹ The NAL E192N/T167G-catalysed

Chapter 3 - NAL-catalysed reactions of aldehyde analogues and pyruvate

reaction of **AHOB** was also found to be selective for the (4S)-epimer, product **55a**. At the time NAL E192N/T167V/S208V and E192N/T167G were evolved, very little was known about the different reaction pathways leading to the two diastereomers of **DPAH** in the NAL E192N-catalysed reaction.⁶⁷

Chapter 3 - NAL-catalysed reactions of aldehyde analogues and pyruvate

Table 3.3 – Kinetic ratio of the NAL variants towards the aldehyde analogues calculated from the 500 MHz ¹H NMR spectra. (Conditions for time-course: 0.1 mmol of aldehyde, 0.2 mmol of pyruvate and 0.56 mg of NAL in 0.7 ml of deuterated sodium phosphate buffer)



Aldehyde	NAL variant	Ratio of products a:b	Ratio of products by configuration at C-4 (4R):(4S)
DHOB ^a	E192N	79:21	79:21
	E192N/T167V/S208V	>13:<87	>13:<87
	E192N/T167G	<95:>5	<95:>5
<i>ent</i> -DHOB ^a	E192N	57:43	43:57
	E192N/T167V/S208V	<83:>17	>17:<83
	E192N/T167G	64:36	36:64
AHOB	E192N	>98:<2	>98:<2
	E192N/T167V/S208V	-	-
	E192N/T167G	>98:<2 ^b	>98:<2 ^b
<i>ent</i> -AHOB	E192N	<2:>98 ^b	>98:<2 ^b
	E192N/T167V/S208V	-	-
	E192N/T167G	NM	NM

a) Reported from previously recorded experiments⁶⁹ for the purpose of comparison. b) See Appendix 3 for time course data used to calculate kinetic ratios.

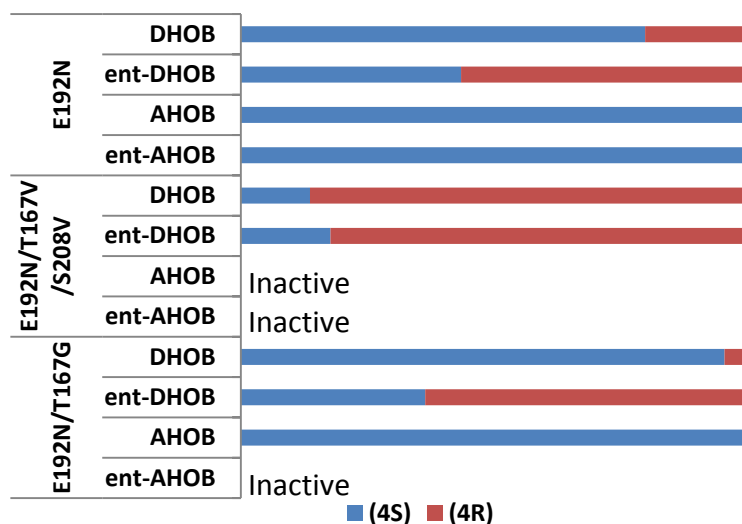


Chart 3.3 – Kinetic ratio of the NAL variants towards the aldehyde analogues calculated from the 500 MHz ^1H NMR spectra. Expressed in terms of the absolute configuration at C-4.

3.3 Rationalisation of the observed outcomes of enzyme catalysed reactions of AHOB

NAL E192N has previously been shown to exhibit poor diastereoselectivity with **DHOB**, however it was found to be highly selective for **AHOB**, giving only the product resulting from attack of the *si*-face of the aldehyde, product **55a**. Unfortunately, NAL E192N was found to be significantly less active towards **AHOB** and the NAL E192N/T167V/S208V variant was completely inactive towards **AHOB**. The following Section aims to discuss the possible reason for this improved diastereoselectivity but loss of activity. The QM/MM modelling studies into the mechanism of facial selectivity in NAL E192N⁵⁷ has been used to form the basis of the rationalisation presented within this Section.

3.3.1 Proposed modified binding mode of AHOB compared to DHOB

Predictions with regards the binding of **AHOB**^{*} were based upon analysis of the crystal structure of NAL E192N in complex with the inhibitor **THB** (which is closely related to **DHOB**)⁶⁶ since there is no crystal structure of an analogue of **AHOB** in complex with NAL. It has previously been shown that **DHOB** has two possible binding modes. The major binding mode, in which the C-3 hydroxyl group is pointing back towards the core of the enzyme, and the minor binding mode, where the C-3 hydroxyl

* There are no crystal structures for the enantiomeric series of the aldehyde substrates so it is not possible to analyse the potential binding modes of **ent-AHOB**.

group is pointing out into the solvent.⁶⁶ It has also been predicted using QM/MM modelling that the major binding mode preferentially leads to *re*-face attack of the aldehyde and that the minor binding mode preferentially leads to *si*-face attack of the aldehyde (see Section 1.4.3).⁵⁷ In the reactions of **AHOB** and *ent*-**AHOB**, the reaction products have (4*S*)-configuration, which means that the *si*-face of the aldehyde is attacked.

In order to gain understanding of how **AHOB** may bind in the NAL active-site, the crystal structure of the **THB** inhibitor in complex with the NAL E192N variant was computationally modified so that the C-3 hydroxyl group was exchanged for an *N*-acetyl group using the building function of Accelrys Discovery Studio Visualizer 3.0. This was done without changing the position of any of the residues or the inhibitor, with the aim of understanding whether **AHOB** could potentially adopt similar binding modes in the NAL E192N variant active site as is predicted for **DHOB**. The *N*-acetyl group was built into both the major and minor binding modes (Figure 3.4). The *N*-acetyl group is much larger than the hydroxyl group that it replaces; when the *N*-acetyl group was built into the major binding mode of **THB** (Figure 3.4a), the *N*-acetyl group came into close contact with the tyrosine residue at position 190. This potential steric clash led to the conclusion that **AHOB** would be unlikely to bind in the NAL E192N active-site in this way. When the *N*-acetyl group was built into the minor binding mode (Figure 3.4b), this steric clash was removed and the *N*-acetyl group was in a space where it was not obviously clashing with any of the residues around the active-site. It is therefore predicted that the minor binding mode of the **THB** inhibitor is a closer representation of the true binding mode of **AHOB** than the major binding mode of the **THB** inhibitor. The minor binding mode of **DHOB** is predicted to favour the pathway leading to *si*-face attack of the aldehyde⁵⁷ so if **AHOB** is binding in a manner similar to the minor binding mode of **DHOB**, this may explain why the product resulting from the *si*-face attack of **AHOB** is observed predominantly.

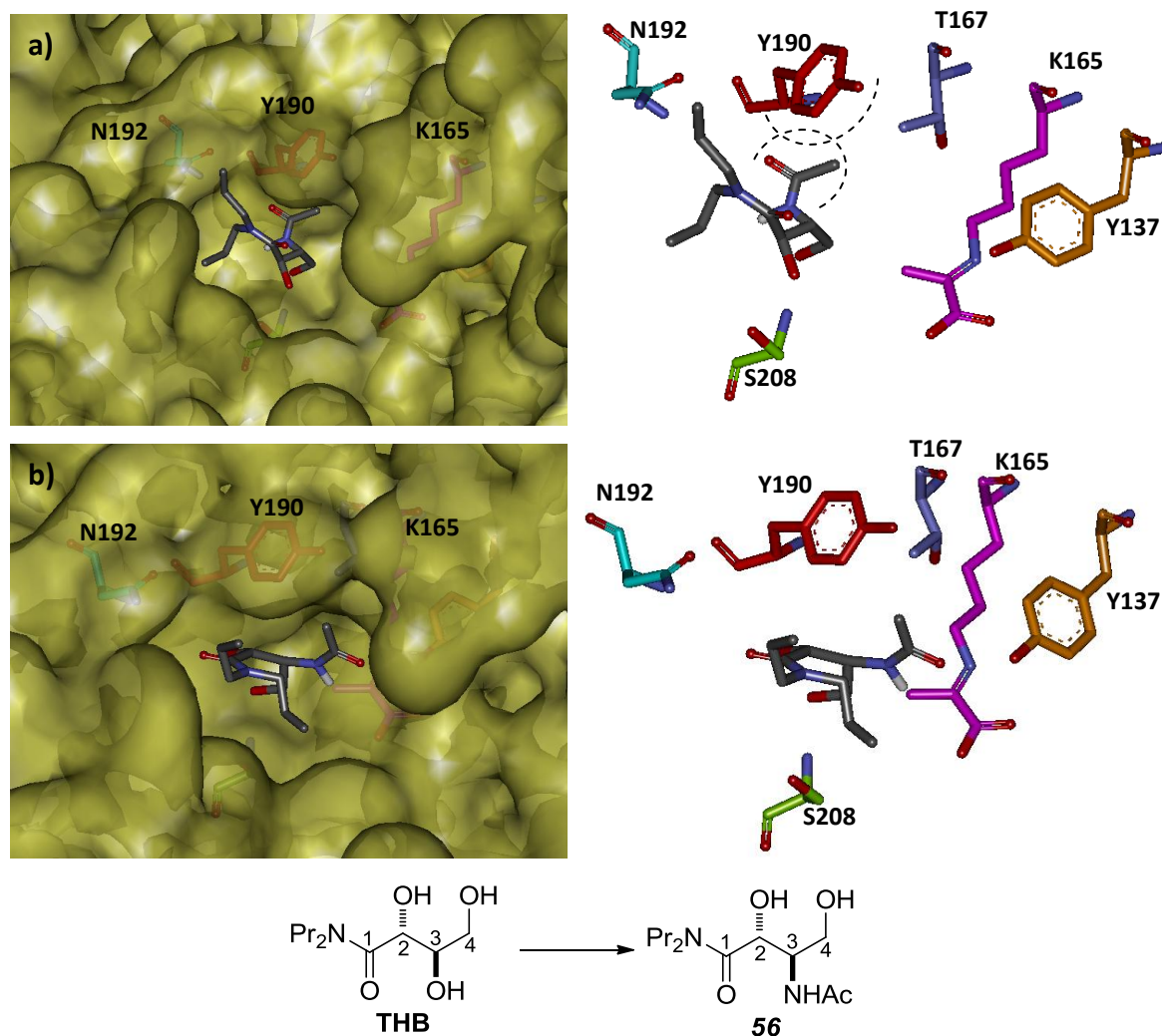


Figure 3.4 - *N*-acetyl group built onto the C-3 hydroxyl group of the THB inhibitor in the major and minor binding modes. In the major binding mode, there is predicted to be a steric clash between the *N*-acetyl group and Y190 (red) (PDB 2WPB)⁶⁶. a) Computation modified inhibitor **56 in the major binding mode of THB, surface view shows (left) shows the *N*-acetyl comes into close contact with the density surrounding the Y190 residue, which is further illustrated with the surface removed (right). b) Computation modified inhibitor **56** in the minor binding mode of THB, surface view (left) shows that the *N*-acetyl group is now pointing out into solvent and with the surface removed (right), the *N*-acetyl group is clearly seen rotated away from the Y190 residue.**

ManNAc, the natural substrate of NAL, has an *N*-acetyl group in the same position relative to the aldehyde as **AHOB**. Considering the region of the NAL active-site occupied by the *N*-acetyl group of ManNAc gave some indication as to whether the predicted binding mode of **AHOB** was a reasonable estimation of the true binding mode. The computationally modified inhibitor **56** (green), in the minor binding mode in the NAL E192N active site⁶⁶ has been overlaid with the crystal structure of the inhibitor **20** (pink) in complex with the NAL from *H. influenza*⁵⁶ (Figure 3.5). The carbon chain does not line up as the **THB** inhibitor sits slightly higher than the inhibitor **20**. However, looking just at the position of the *N*-acetyl group in both inhibitors, it

points out into the same area of solvent but the *N*-acetyl group of the inhibitor **20** is rotated out and away from the K165 residue. The true binding mode of **AHOB** is likely to be somewhere in between the minor binding mode of **DHOB** and the binding mode of ManNAc.

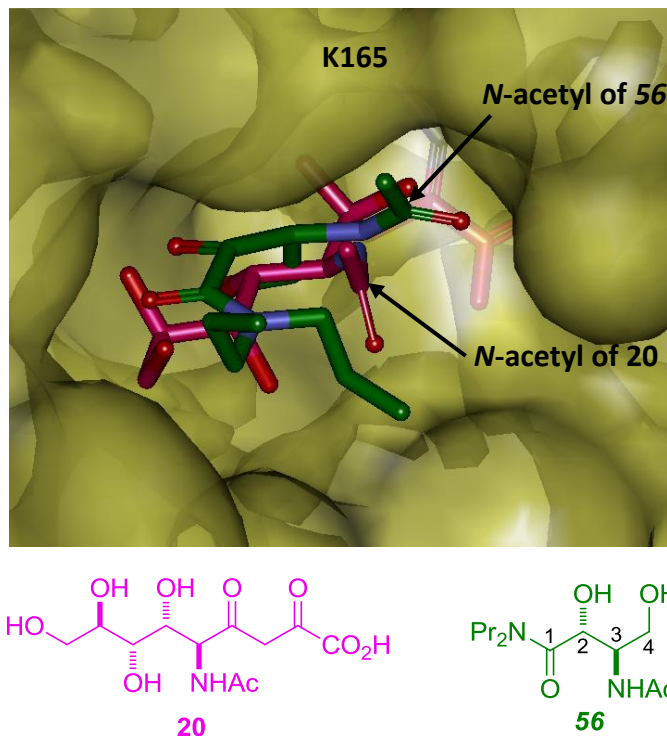


Figure 3.5 - Computationally modified inhibitor **56** (green) in the minor binding mode of THB in the active site of NAL E192N in complex with pyruvate overlaid with the 4-oxo-sialic acid inhibitor **20** (pink) in complex with the NAL from *H. influenza* (1F7B).⁵⁶ The surface corresponds to the surface of the NAL E192N crystal structure (PDB 2WPB).⁶⁶

To summarise, the wild-type NAL reaction between ManNAc and pyruvate results in attack of the *si*-face of the aldehyde (therefore the new stereocentre has the (*S*)-configuration). The reaction between **AHOB** and pyruvate also only resulted in attack of the *si*-face of the aldehyde. In order to reduce unfavourable steric interactions, **AHOB** is predicted to bind similarly to the minor binding mode of **DHOB**, which means that the *N*-acetyl group will point out into solvent, similarly to the *N*-acetyl group of ManNAc/Neu5Ac. It is predicted from QM/MM modelling studies that the minor binding mode of **DHOB** favours attack of the *si*-face of the aldehyde and it is known experimentally that the *si*-face of ManNAc is attacked in the wild-type reaction. This evidence together provides justification for the observed stereoselectivity in the reactions between **AHOB** and pyruvate, catalysed by the NAL variants.

3.3.2 Rationalisation of complete loss of activity of NAL E192N/T167V/S208V with AHOB

It is not clear why the NAL E192N/T167V/S208V, under the reaction conditions, is inactive towards **AHOB**. In the reaction with **DHOB**, the NAL E192N/T167V/S208V preferentially forms the product resulting from attack of the *re*-face of the aldehyde, therefore suggesting that NAL E192N/T167V/S208V may direct **DHOB** into the major binding mode. However the mechanism by which this occurs is unknown.⁵⁷ It has already been postulated that **AHOB** cannot adopt the major binding mode of **DHOB**, which was the justification of the selectivity observed in NAL E192N (Section 3.3.1). This proposal however does not fully explain why **AHOB** is not a substrate for NAL E192N/T167V/S208V.

The mutation which may hold the most clues about why the NAL E192N/T167V/S208V variant is inactive is the mutation at position 208. In the wild-type reaction, residue S208 forms a hydrogen bond with the C-7 hydroxyl group of Neu5Ac over a distance of 2.7 Å (**Figure 3.6a**).⁵⁶ In the **THB** inhibitor, the equivalent C-7 hydrogen-bond acceptor is the amide oxygen. In both the major and minor binding modes of the **THB** inhibitor, the distance between the S208 residue and the amide-oxygen is too long for a hydrogen bond interaction at 6.4 Å and 5.5 Å respectively (**Figure 3.6b and c**).⁶⁶ The distance is shorter in the minor binding mode, which is the binding mode predicted to most closely resemble the true binding mode of **AHOB**. Since the binding mode of **AHOB** is not exactly known, it is possible that in the true binding mode of **AHOB** that this distance is short enough that hydrogen bonding between S208 and the amide-oxygen occurs. Therefore, when this interaction is not possible, as in the NAL E192N/T167V/S208V variant, no measurable activity is observed.

The NAL E192N/T167G variant also has very poor activity towards **AHOB** compared to the NAL E192N variant, so it is possible that both the T167 and S208 residues are important in binding **AHOB**. Removing the hydrogen bond donors from just the 167 position is very detrimental to activity, and removing both hydrogen bond donors is so detrimental to binding that the activity is completely lost.

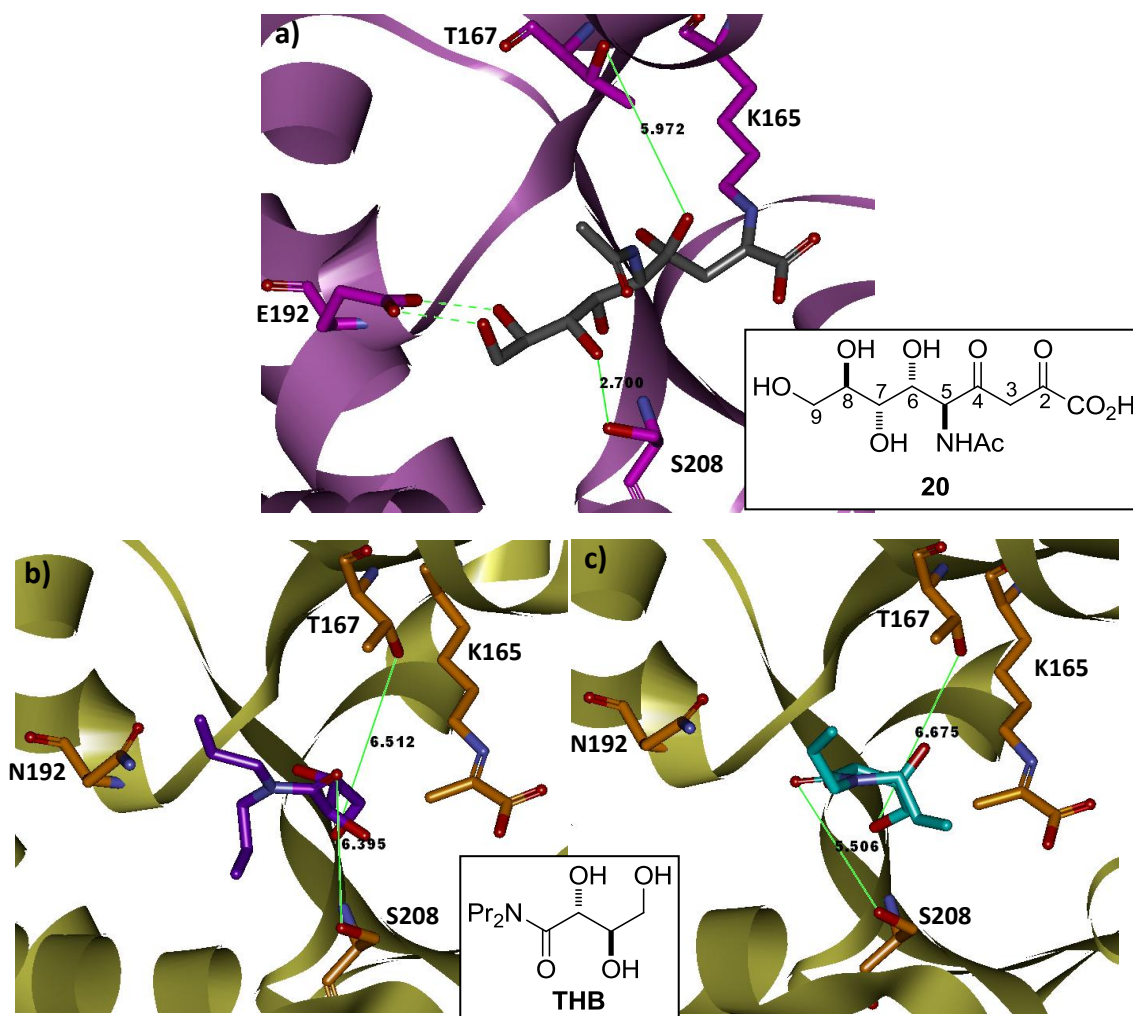


Figure 3.6 - Distances between the mutated residues in the diastereoselective NAL variants **E192N/T167V/S208V** and **E192N/T167G** and the bound enzyme substrates. a) Wild-type NAL from *H. influenza* in complex with the 4-oxo-sialic acid analogue **20** (PDB 1F7B).⁵⁶ b) Major binding mode of the THB inhibitor bound in the active site of NAL E192N in complex with pyruvate. c) Major binding mode of the THB inhibitor bound in the active site of NAL E192N in complex with pyruvate (PDB 2WPB).⁶⁶

In conclusion, in the true binding mode of **AHOB**, it is possible that the amide-oxygen forms a hydrogen bond with S208; consequently S208 plays a more important role in directing the binding of **AHOB** compared to **DHOB**. If this is the case, the NAL variant **E192N/T167V/S208V**, in which the serine at 208 is replaced with a valine, cannot form a hydrogen bond with the amide-oxygen of **AHOB**, which may be the cause for the insignificant activity of this variant. There are multiple binding modes in the NAL active-site and the lowest energy binding mode is most likely controlled by a combination of the substrate conformation and the active site residues (i.e. the sequence of amino acids of the NAL variant) and their conformation. Consequently, it is difficult to predict which changes to the substrate may be tolerated by the enzyme variants. This Chapter has however highlighted some of the subtleties that need to be

Chapter 3 - NAL-catalysed reactions of aldehyde analogues and pyruvate

understood before protein engineers can truly claim to be able to rationally design enzymes.

Chapter 4 NAL-catalysed reactions of aldehyde analogues and fluoropyruvate

4.1 Understanding and interpreting the diastereoselectivity of reactions of NAL variants with fluoropyruvate

The previous Chapter described the NAL-catalysed reactions of **AHOB** and pyruvate. In these reactions only one new stereocentre was formed, hence only two diastereomers were possible. In the reaction between the aldehyde analogues and fluoropyruvate, two stereocentres are formed, adding an extra level of complexity both to identifying and characterising enzyme reaction products and to understanding what the results mean in terms of the mechanism of the enzyme. These challenges presented in characterisation of enzyme reaction products were overcome by exploiting ^{19}F NMR spectroscopy and the mechanistic understanding gained from the QM/MM modelling studies carried out previously.⁵⁷ ^{19}F NMR spectroscopy is a very useful diagnostic tool and was used to gain information about the diastereoselectivity of the NAL variants. The insights gained through computational modelling studies have been used to rationalise the diastereoselectivity at the fluorine-bearing chiral centre of the products of the NAL catalysed reactions.

4.1.1 ^{19}F NMR spectroscopy as a diagnostic tool

In order to evaluate the diastereoselectivity of the NAL variants, it must be possible to identify which diastereoisomers are formed in each NAL-catalysed reaction. In the NAL-catalysed reaction between the aldehyde analogues and fluoropyruvate, four diastereomers are possible. However, the reaction products may cyclise in solution. In the simple case of **AHOB**, where **X**=NHAc, it is only possible to get pyranose species; however both α - and β -anomers are possible (Figure 4.1b). In the case of **DHOB**, where **X**=OH, the analysis is further complicated by the additional possibility of α - and β -furanose species* (Figure 4.1a).

* Throughout this Chapter, “products” refers to the diastereomeric outcomes of the NAL-catalysed reaction of the aldehyde variants and fluoropyruvate and “species” refers to the equilibrium ring forms of the “products”.

Chapter 4 - NAL-catalysed reactions of aldehyde analogues and fluoropyruvate

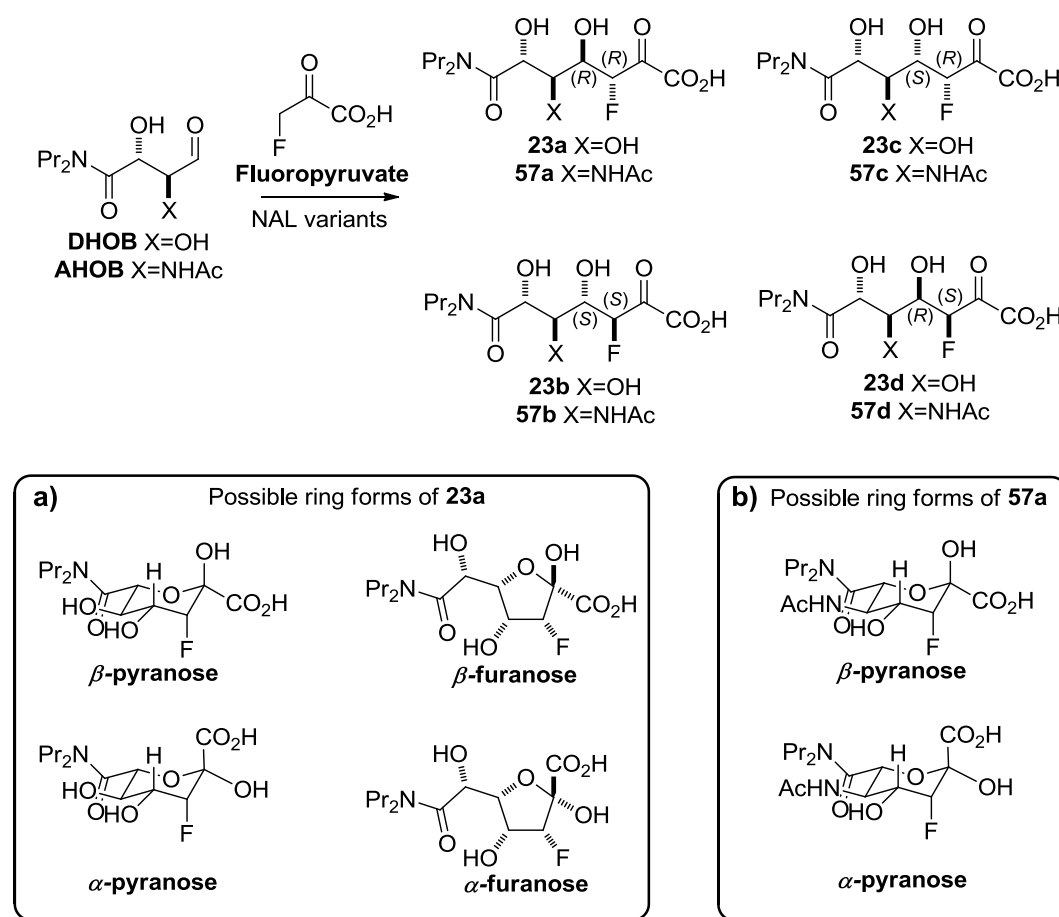


Figure 4.1 - Ring forms of the products of the NAL E192N catalysed reactions between aldehyde substrate DHOB or AHOB and fluoropyruvate. a) Pyranose and furanose ring forms of the products of the NAL variant-catalysed reaction DHOB and fluoropyruvate. The example given here is product **23a** b) Pyranose only ring forms of the products of the NAL variant-catalysed reactions of AHOB and fluoropyruvate. The example given here is product **57a**.

If the NAL variant is unselective, or the position of the equilibrium does not favour one ring form, the ^1H NMR spectrum of the enzyme reaction product(s) would be very complicated. However, each product contains one fluorine atom, therefore there will only be one peak in the fluorine NMR spectrum per equilibrium species. ^{19}F NMR proved to be an extremely useful diagnostic tool for identifying and characterising the enzyme reaction products. Each of the individual species of the products of the enzyme-catalysed reactions between the aldehyde analogues and fluoropyruvate are characterised by a doublet of doublets in the ^{19}F NMR spectrum. The two coupling constants correspond to a proton-fluorine geminal coupling and a proton-fluorine vicinal coupling, each of which is characteristic of the species.

The geminal proton-fluorine coupling constant provides information about whether the carbon attached to fluorine is part of a five or a six-membered ring. The geminal coupling for a five-membered ring is 3-4 Hz larger than the geminal coupling in a six-

membered ring, which is around 49 Hz. The chemical shift also provides information about whether the fluorine is in the axial or equatorial position of a six-membered ring, an axial fluorine has a chemical shift upfield from an equatorial fluorine (Figure 4.2).³³

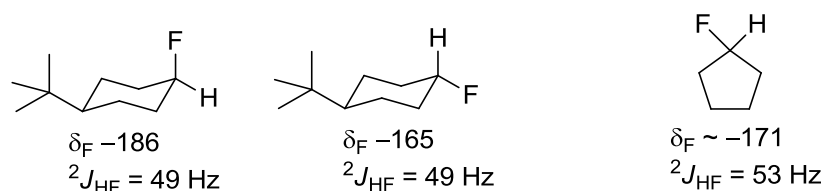


Figure 4.2 - Geminal proton-fluorine coupling constants in six-membered rings are generally slightly smaller than five-membered rings³³

Just as for vicinal proton-proton coupling constants, vicinal proton-fluorine coupling constants can be described by the Karplus relationship, which defines the relationship between the dihedral angle between vicinal substituents and the coupling constant.⁸⁶ This relationship serves as a guide to predict the coupling constants of the pyranose forms of each of the possible products. Coupling constants in six-membered rings are generally well defined and can therefore be used to evaluate the relationship between vicinal substituents. Proton-fluorine coupling constants are typically much larger than proton-proton coupling constants as outlined in Table 4.1, which shows the range of expected vicinal proton-proton and proton-fluorine coupling constants in six membered rings.

Table 4.1 - Typical proton-proton and proton-fluorine vicinal coupling constants in six-membered rings^{33, 87}

Vicinal proton				
	Range of ${}^3J_{\text{HH}}$	Range of ${}^3J_{\text{HF}}$	Range of ${}^3J_{\text{HH}}$	Range of ${}^3J_{\text{HF}}$
	X=H /Hz	X=F /Hz	X=H /Hz	X=F /Hz
H-axial	8-11	25-35	3-6	10-25
H-equatorial	3-6	10-25	0-4	0-10

An understanding of the Karplus relationship was applied to predict ranges of the diagnostic vicinal proton-fluorine and proton-proton coupling constants for a pyranose

ring form each of the four possible diastereomers of the enzyme reaction products, as shown in Figure 4.3. The pyranose ring forms of the products **23/57a** will have the 3-F and 4-H in the axial position and will have the largest proton-fluorine vicinal coupling constant. The products **23/57b**, which have an equatorial 3-F and an equatorial 4-H, will have the smallest proton-fluorine vicinal coupling constant. The products **23/57c** and **23/57d** cannot be distinguished from the proton-fluorine coupling constant alone, as they may be similar, and can only be distinguished by the proton-proton vicinal coupling constants. The 5-H of **23/57** will always be axial in a pyranose ring due to the structure of the starting material and a preference for the largest substituents to be in the equatorial positions, therefore the vicinal coupling constant between the 4-H and 5-H is very diagnostic. This coupling constant will be largest when the 4-H is axial, as in product **23/57d**, and smaller when the 4-H is equatorial, as in product **23/57c**.

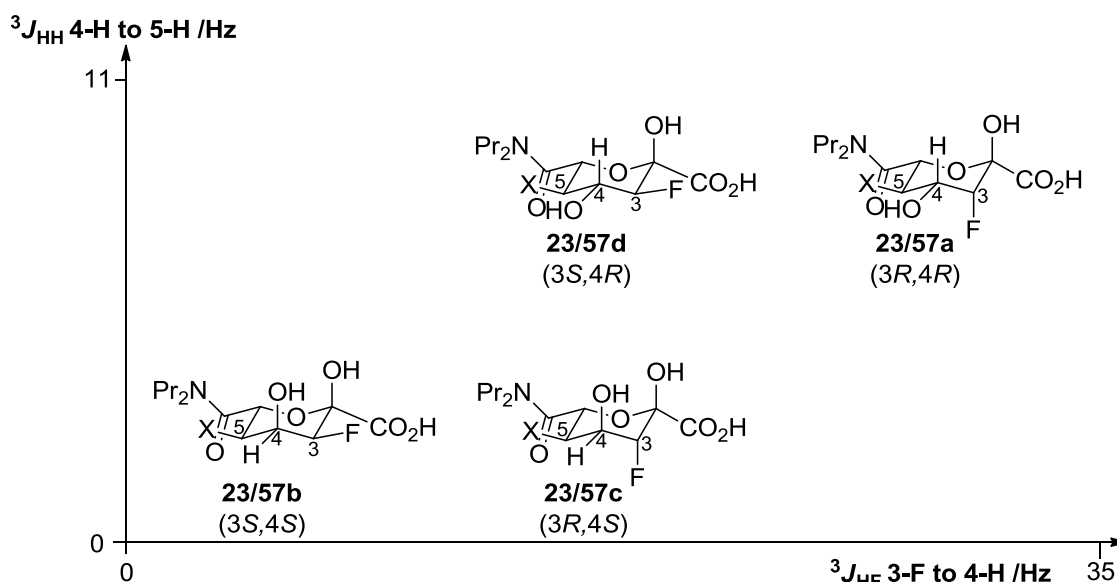


Figure 4.3 - Schematic representation of relative proton-fluorine and proton-proton vicinal coupling constants of the pyranose rings in each of the four possible diastereomeric products from the reaction between DHOB/AHOB and fluoropyruvate.

4.1.2 Prediction of the enzyme reaction products based on QM/MM modelling studies

In the reaction between the aldehyde analogues and fluoropyruvate, catalysed by the NAL variants, there are three factors to consider: the face of the enamine which attacks the aldehyde, the face of the aldehyde which is attacked and the geometry of the enamine. For the purpose of simplifying the explanation of the diastereoselectivity, the faces of the enamine will be referred to as the "top" and "bottom", which means, if

the enamine is orientated so that the lysine residue is in the back right quadrant, "top" refers to the aldehyde coming in from above and "bottom" refers to the aldehyde coming in from below (as the enamine is drawn in Figure 4.4).

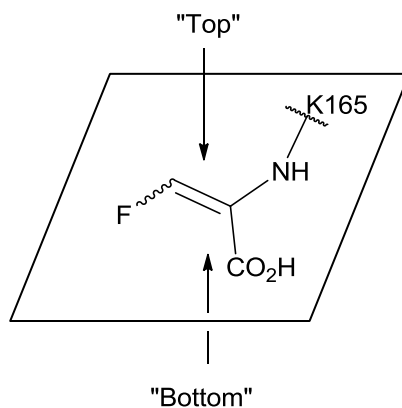


Figure 4.4 - Illustration of nomenclature for describing the two faces of the fluoro-enamine

The Y137 residue is believed to transfer the proton to the aldehyde.⁵⁷ In order for Y137 to be close enough to the substrate to carry out the proton transfer, it is predicted that the aldehyde has to be attacked from the "top" face of the enamine. Furthermore, it is known from the crystal structure of fluoropyruvate in complex with NAL from *S. aureus*⁶³ that the fluoroenamine adopts the (*Z*)-configuration in complex with K165 (Figure 4.5a) This observation was consistent with the modelling studies carried out on the complex between *n*-butylamine and fluoropyruvate, which predicted the (*Z*)-configuration to be 35.2 kJ mol⁻¹ lower in energy than the (*E*)-configuration⁵⁷ (Figure 4.5b).

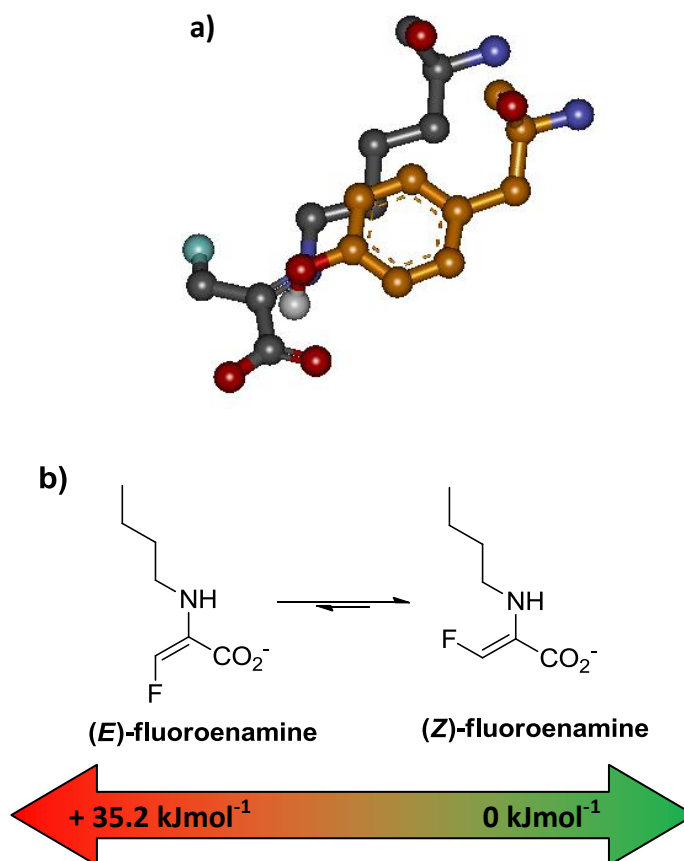


Figure 4.5 - The enamine complex between K165 and fluoropyruvate in the NAL active-site preferentially adopts the (Z)-configuration and the attack on the aldehyde comes from the "top" face of the enamine. a) Y137 (gold) is positioned above the "top" face of the (Z)-fluoroenamine, therefore it is predicted that the aldehyde can only be protonated from the "top" face of the (Z)-enamine.⁶³ b) The (Z)-configuration was calculated to be 35.2 kJmol⁻¹ lower in energy than the (E)-configuration.⁵⁷

The "top" face of the (Z)-enamine can attack either the *si* or *re*-face of the aldehyde, which is illustrated using Newman projections in Figure 4.6. This mode of attack can lead to only the two diastereomers with the (3*R*)-configuration. The two diastereomers with the (S)-configuration at C-3 can only be accessed by either attack from the "bottom" face of the (Z)-enamine or attack from the "top" face of the (E)-enamine, both of which are predicted to be unfavoured. It was hypothesised that the diastereomers with (3*R*,4*R*) and (3*R*,4*S*)-configurations would be observed most frequently in the NAL variant-catalysed reactions of the aldehyde analogues and fluoropyruvate. In Section 4.5.1, this hypothesis is evaluated along with further discussion into the diastereoselectivity of NAL variants towards reactions of fluoropyruvate.

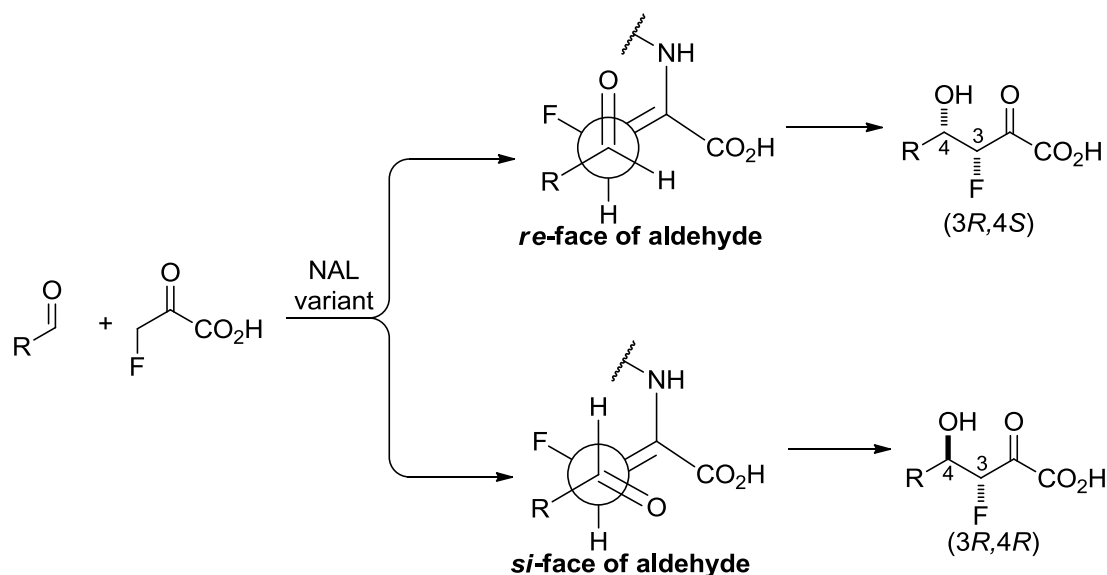


Figure 4.6 - Newman projections of the "top" face of the (Z)-enamine attacking the *re* or *si*-face of the aldehyde, leading to the formations of diastereomers with (3R)-configuration.

4.2 NAL E192N variants in the preparation of 3-fluoro-*N*-acetyl neuraminic acid analogues from AHOB

4.2.1 Conditions for the enzyme catalysed reaction between 3-fluoropyruvate and AHOB

AHOB and *ent*-**AHOB** were generated by ozonolysis of the alkene precursors **25** and *ent*-**25** as described previously (Section 3.1.1) and used immediately without purification. The conditions used for the preparative scale reaction between fluoropyruvate and **AHOB** were different from those for the reaction between pyruvate and **AHOB** (Section 3.1.2). In the reactions of fluoropyruvate, the aldehyde was generally used either in excess or equimolar equivalents and Bakers' yeast was not used. The conditions were altered because there is evidence that fluoropyruvate may act as an inhibitor to NAL⁶⁰ and it has previously been found that using excess fluoropyruvate results in formation of several by-products.⁵⁷

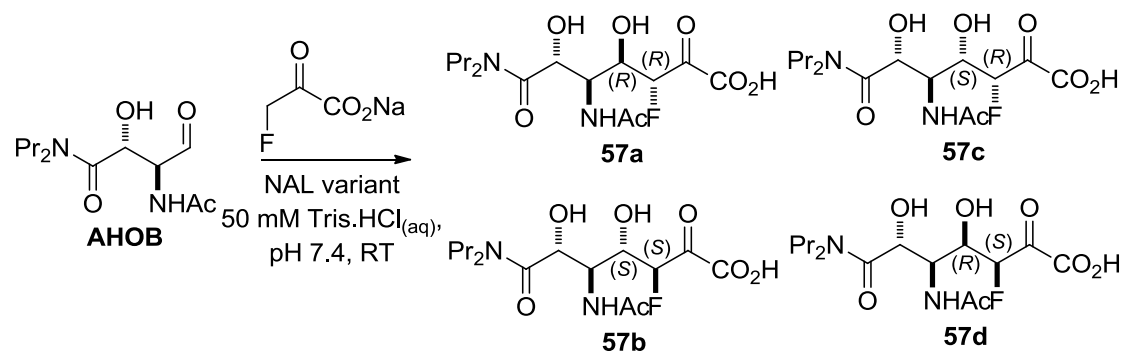
The preparative scale reactions between fluoropyruvate and **AHOB/ent**-**AHOB** are summarised in Table 4.2. Carrying out the reaction with fluoropyruvate as the limiting reagent made it possible to estimate the conversion by measuring the relative integrals of fluoropyruvate and product peaks in the 296 MHz ¹⁹F NMR spectrum before HPLC purification. It was therefore possible to ascertain whether low yields

Chapter 4 - NAL-catalysed reactions of aldehyde analogues and fluoropyruvate

were due to low conversions or difficulty in purification. The products were purified initially by Dowex® ion exchange and in the cases where sufficiently high conversion was observed, reverse-phase mass-directed HPLC was used to remove the unreacted fluoropyruvate. In all cases, the conversions and yields were very low and only the reaction between **AHOB** and fluoropyruvate, catalysed by NAL E192N (Entry 1), gave enough product to warrant HPLC purification. In order to find out if the reaction could be carried out with an excess of fluoropyruvate, five equivalents of fluoropyruvate were used in the NAL E192N catalysed reaction of **AHOB** (Entry 2), however although the conversion was estimated to be improved, the yield after HPLC purification was not significantly increased. NAL E192N/T167V/S208V, as previously, was found to be inactive towards both enantiomers of **AHOB**. Some of the reactions were left for more than two days (Entries 2, 6 and 7), in the hope of improving the yield however **AHOB** is not very stable and decomposes over the course of two days, so it is unlikely that longer reaction times would lead to an improvement in the overall conversion/yield. Remarkably, the reactions were all highly selective and the following Sections outline how the relative configurations of the products were assigned.

Chapter 4 - NAL-catalysed reactions of aldehyde analogues and fluoropyruvate

Table 4.2 - Conditions, estimated conversion and yield after reverse-phase HPLC purification of the reactions between AHOB and *ent*-AHOB with fluoropyruvate, catalysed by NAL variants.



Entry	Aldehyde	NAL variant	Equivalents of aldehyde: F-pyruvate	Reaction time /days	Conversion ^a %	Yield after HPLC %	Products observed
1	AHOB	E192N	1:1	2	21	5	57a and 57d (98:2)
2	AHOB	E192N	1:5	5	50 ^b	7	57a and 57d (98:2)
3	AHOB	E192N/ T167V/ S208V	1:0.75	2	0	-	-
4	AHOB	E192N/ T167G	1:0.75	2	0.3	c	57a (>98:<2)
5	<i>ent</i> -AHOB	E192N	1:0.75	2	5.6	c	<i>ent</i> -57d (>98:<2)
6	<i>ent</i> -AHOB	E192N/ T167V/ S208V	1:1	7	0	-	-
7	<i>ent</i> -AHOB	E192N/ T167G	1:1	7	4.7	c	<i>ent</i> -57a (>98:<2)

a) Conversions were calculated by measuring the relative integrals in the 296 MHz ¹⁹F NMR of the products after purification by ion exchange. b) Fluoropyruvate was used in excess so estimating the conversion from 296 MHz ¹⁹F NMR integrals would have had a much larger error. c) HPLC purification was not carried out due to low conversion.

4.2.2 Identification and characterisation of diastereomers of enzyme catalysed reactions of AHOB and fluoropyruvate

The 296 MHz ^{19}F NMR spectra of the NAL variant-catalysed reactions of **AHOB/ent-AHOB** and fluoropyruvate were recorded (see Appendix 4) and the ^{19}F NMR spectrum of the HPLC purified product **57a** is shown in Figure 4.7 as an example. The chemical shifts and coupling constants of the peaks observed by ^{19}F NMR were measured and the configurations at C-3 and C-4 were assigned (Table 4.3). The peaks at -207.8 ppm and -218.5 ppm had vicinal coupling constants of 29.1 Hz and 28.8 Hz respectively, which was within the range expected for the diastereomer where the 3-F and 4-H are both axial, therefore this product was proposed to be **57a**. The two peaks correspond to the major and minor anomers, which were observed in a ratio of 98:2. The product **57d/ent-57d** was characterised by a peak at -199.2 ppm with a vicinal coupling constant 10.4 Hz, which is at the bottom end of the range of predicted coupling constants for an axial-equatorial relationship between the fluorine and the vicinal proton. Unfortunately, due to low conversion, it was not possible to acquire a good ^1H NMR spectrum of the product **ent-57d**. The configuration was assigned by correlation of the data with a compound with the same configuration which was purified (see characterisation of product **ent-23d** in Section 4.3.2.1).

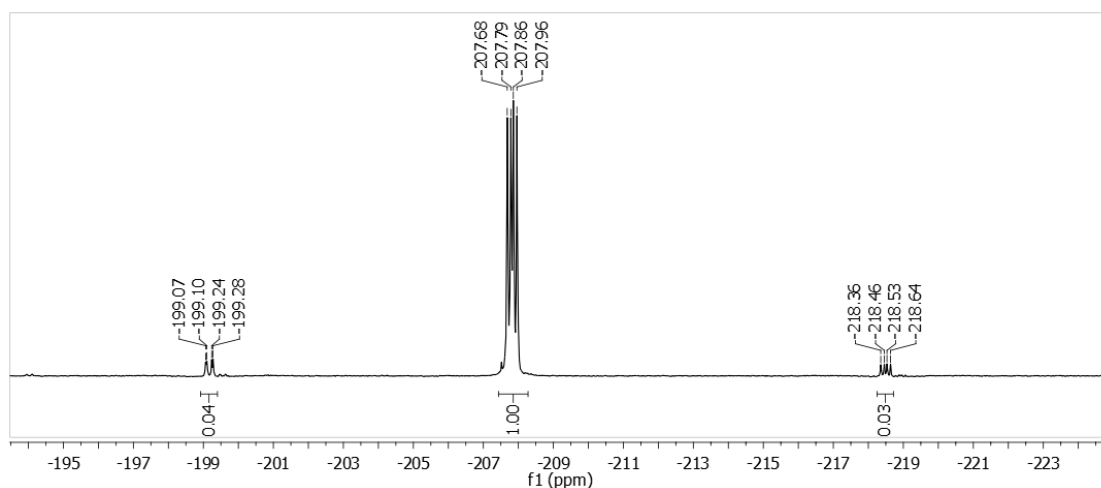
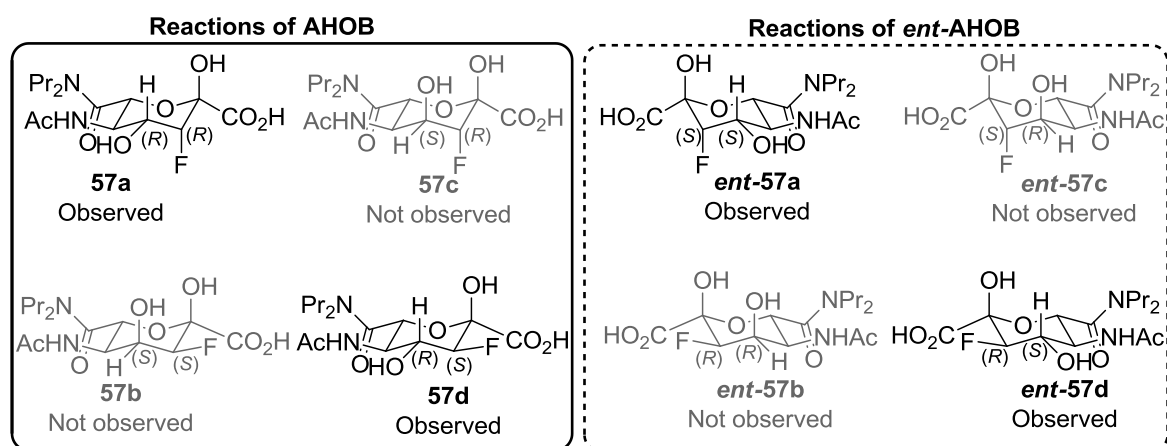


Figure 4.7 - 296 MHz ^{19}F NMR of the mass-directed reverse-phase HPLC purified product **57a**.

Table 4.3 - Chemical shifts and coupling constants from the 296 MHz ¹⁹F NMR of the observed products of the NAL variant-catalysed reactions of AHOB/*ent*-AHOB and fluoropyruvate.

Product	δ_F (295 MHz, D ₂ O) /ppm	J /Hz	Predicted ring form	Ratio of equilibrium species	Configuration at C-3 and C-4
57a	-207.8	49.0 and 29.1	Pyranose	98:2	(3 <i>R</i> ,4 <i>R</i>)
	-218.5	50.2 and 28.8	Pyranose		[(3 <i>S</i> ,4 <i>S</i>) - <i>ent</i> -57a]
57d	-199.2	49.3 and 10.4	Pyranose	>98:<2	(3 <i>S</i> ,4 <i>R</i>) [(3 <i>R</i> ,4 <i>S</i>) - <i>ent</i> -57d]

In order to further confirm the configuration of the product **57a**, the 500 MHz ¹H NMR spectrum of the mass-directed reverse-phase HPLC purified material was recorded. The 500 MHz ¹H NMR spectrum (Figure 4.8), provided all of the proton-proton diagnostic coupling constant around the pyranose ring, which are recorded and characterised in Table 4.4. The large coupling constant of 10.0 Hz between 5-H and 4-H and the smaller coupling constant of 2.2 Hz between 4-H and 3-H are consistent with the expected coupling constants of the product **57a**.

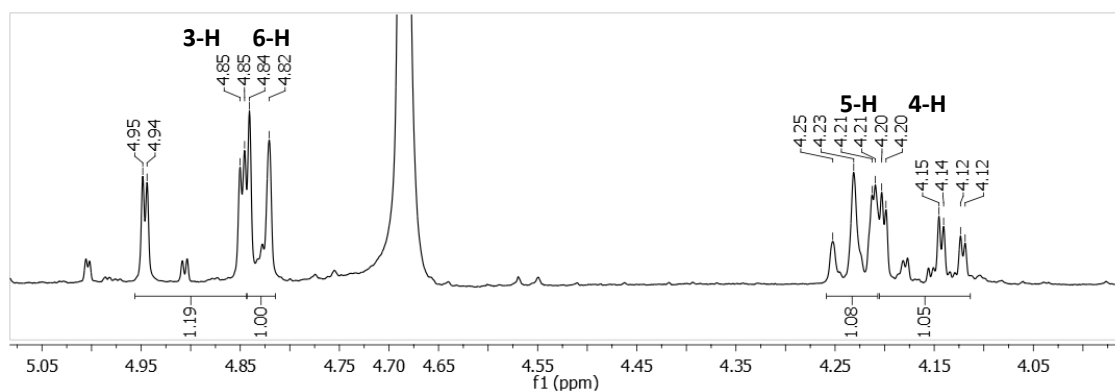
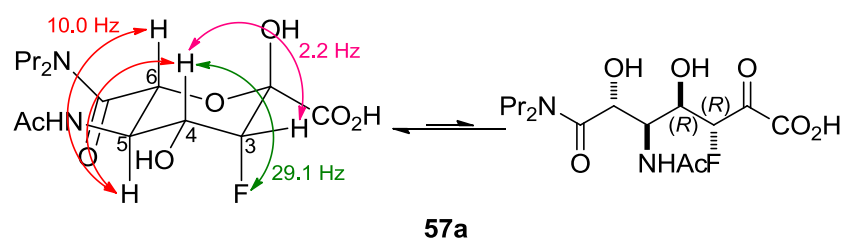


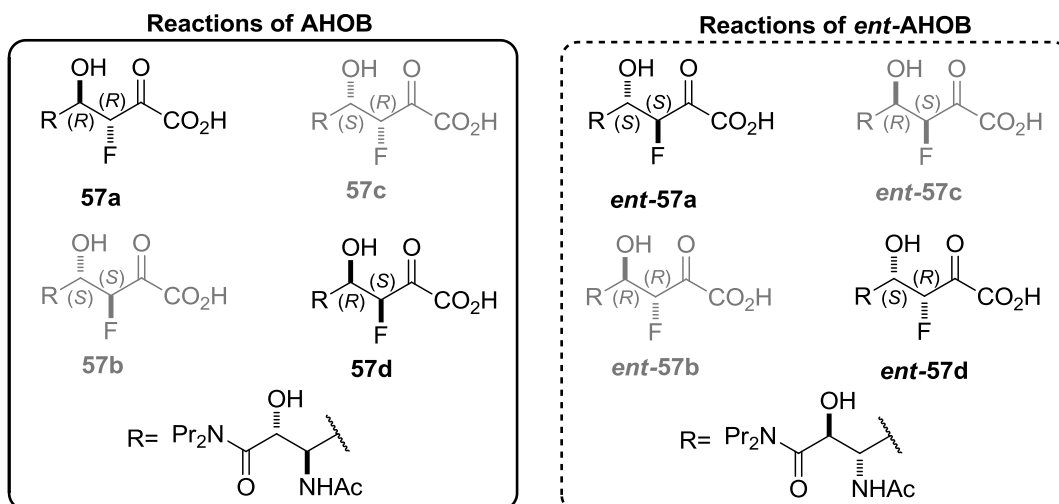
Figure 4.8 - 500 MHz ^1H NMR spectrum of the product 57a. The product was purified by mass-directed reverse-phase HPLC in order to remove excess fluoropyruvate

Table 4.4 - Characteristic chemical shifts and coupling constant of the protons of the pyranose ring of the product 57a.



δ_{H} (500 MHz, D_2O) /ppm	Multiplicity	$^2J_{\text{HF}}$ /Hz	$^3J_{\text{HF}}$ /Hz	$^3J_{\text{HH}}$ /Hz	Identity
4.90	dd	49.2	-	2.2	3-H
4.83	d	-	-	10.0	6-H
4.23	t	-	-	9.9	5-H
4.16	ddd	-	29.1	10.9 and 2.2	4-H

The overall selectivity of NAL E192N and E192N/T167G towards **AHOB** and **ent-AHOB** in the reaction with fluoropyruvate is summarised in Table 4.5. Generally, as predicted in Section 4.1.2, the (3R)-epimer is almost exclusively preferred and the only exception is the NAL E192N/T167G-catalysed reaction of **ent-AHOB**, which appears to give a product with (3S)-configuration but the conversion in this reaction was very low (4.7% conversion) and will be discussed later (Section 4.5.1).

Table 4.5 - Summary of the products of the reactions between AHOB/*ent*-AHOB with fluoropyruvate catalysed by NAL variants.

Aldehyde	NAL variant	Products observed	Ratio of products a:b:c:d	Ratio of products by configuration at C-3 and C-4
				(3 <i>R</i> ,4 <i>R</i>):(3 <i>S</i> ,4 <i>S</i>): (3 <i>R</i> ,4 <i>S</i>):(3 <i>S</i> ,4 <i>R</i>):
AHOB	E192N	57a and 57d	98:0:0:2	98:0:0:2
	E192N/T176G	57a	100:0:0:0	100:0:0:0
<i>ent</i> -AHOB	E192N	<i>ent</i> -57d	0:0:0:100	0:0:100:0
	E192N/T176G	<i>ent</i> -57a	100:0:0:0	0:100:0:0

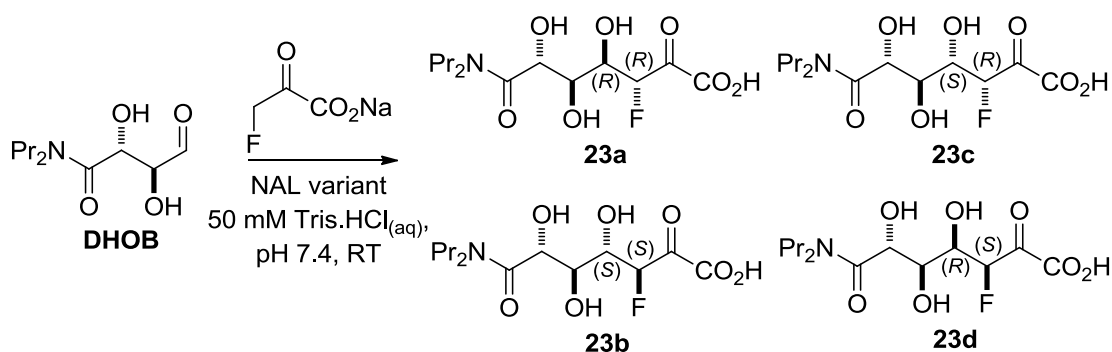
4.3 NAL variants in the preparation of 3-fluoro-*N*-acetyl neuraminic acid analogues from DHOB

4.3.1 Challenges presented in the characterisation of products derived from DHOB

DHOB and *ent*-DHOB were generated by ozonolysis from the alkene precursors **24** and *ent*-**24** as described previously (Section 3.1.1) and used immediately without further purification. The reactions between **DHOB**/*ent*-**DHOB** and fluoropyruvate catalysed by the NAL variants were carried out in much the same way as the reactions of **AHOB**, with equimolar equivalents of aldehyde and fluoropyruvate or an excess of aldehyde. The conversions and yields achieved in the reactions were considerably higher compared to **AHOB** and the conditions and conversions are given in Table 4.6. The reactions were carried out in aqueous 50 mM Tris.HCl buffer at pH 7.4, since neither the buffer nor the solvent contain any fluorine atoms, it was possible to

Chapter 4 - NAL-catalysed reactions of aldehyde analogues and fluoropyruvate

perform ^{19}F NMR on the reaction mixtures rather than on purified product. It was therefore possible to analyse the conversion and diastereoselectivity of the enzyme reactions without the need to purify the products of every reaction. For the reactions that were not purified the conversion is given but not the yield. While the yields were higher compared to the reactions of **AHOB**, the selectivity was greatly reduced in the case of NAL E192N and E192N/T167G, which led to greater difficulty in identifying and characterising the reaction products. Notably, product **23a**, the minor product of the NAL E192N-catalysed reaction of **DHOB** and fluoropyruvate, was only ever observed in a mixture with **23c**.

Table 4.6 - Conditions, estimated conversion and yield after reverse-phase HPLC purification of the reactions between DHOB and *ent*-DHOB with fluoropyruvate, catalysed by NAL variants.

Entry	Aldehyde	NAL variant	Equivalents of aldehyde: F-pyruvate	Reaction time /days	Conversion %	Yield ^a %	Products observed ^d
1	DHOB	E192N	2:1	2	>99	53	23a and 23c (40:60)
2	DHOB	E192N/T167V/S208V	2:1	2	94	41	23c (>98:<2)
3	DHOB	E192N/T167G	1:1	6 ^b	79	-	23a, 23c and 23d (28:70:2)
4	<i>ent</i> -DHOB	E192N	1:1	6 ^b	45	-	<i>ent</i> -23a and <i>ent</i> -23d (8:92)
5	<i>ent</i> -DHOB	E192N/T167V/S208V	1:1	1	NM ^c	52	23d (>98:<2)
6	<i>ent</i> -DHOB	E192N/T167G	1:1	6 ^b	38	-	<i>ent</i> -23a and <i>ent</i> -23d (10:90)

a) Yield after purification by ion exchange b) Reaction mixture was not purified. The reactions were monitored by ¹⁹F NMR and the conversions given were after 6 days of reaction. c) NM = Not measured d) Products observed by 395 MHz ¹⁹F NMR of purified products (where products were purified) and crude products (where products were not purified).

Figure 4.9 shows the 395 MHz ¹⁹F NMR spectra of the reactions between DHOB and fluoropyruvate catalysed by NAL E192N (Figure 4.9a), E192N/T167V/S208V (Figure 4.9b) and E192N/T167G (Figure 4.9c). In the NAL E192N-catalysed reaction of DHOB, two different diastereomers are observed. The minor diastereomer, identified as product 23a (indicated in red), existed predominantly as one ring form characterised by the peak at -206.0 ppm, with a small amount of the minor ring form characterised

Chapter 4 - NAL-catalysed reactions of aldehyde analogues and fluoropyruvate

by the peak at -216.8 ppm. This same diastereomer, product **23a**, is also observed as the minor product in the NAL E192N/T167G catalysed reaction. In all three reactions, the product identified as **23c** (indicated in blue) is always observed as the major diastereomer. Product **23c** exists as a complex mixture of four equilibrium species in a ratio of 37:23:29:11. In the NAL E192N/T167V/S208V-catalysed reaction of **DHOB**, the product **23c** is the only diastereomer observed. Finally, there is a very small amount of the product identified as **23d** (indicated in green), characterised by a peak at -199.8 ppm, which under the reaction conditions, is only observed as a product of the NAL E192N/T167G-catalysed reaction.

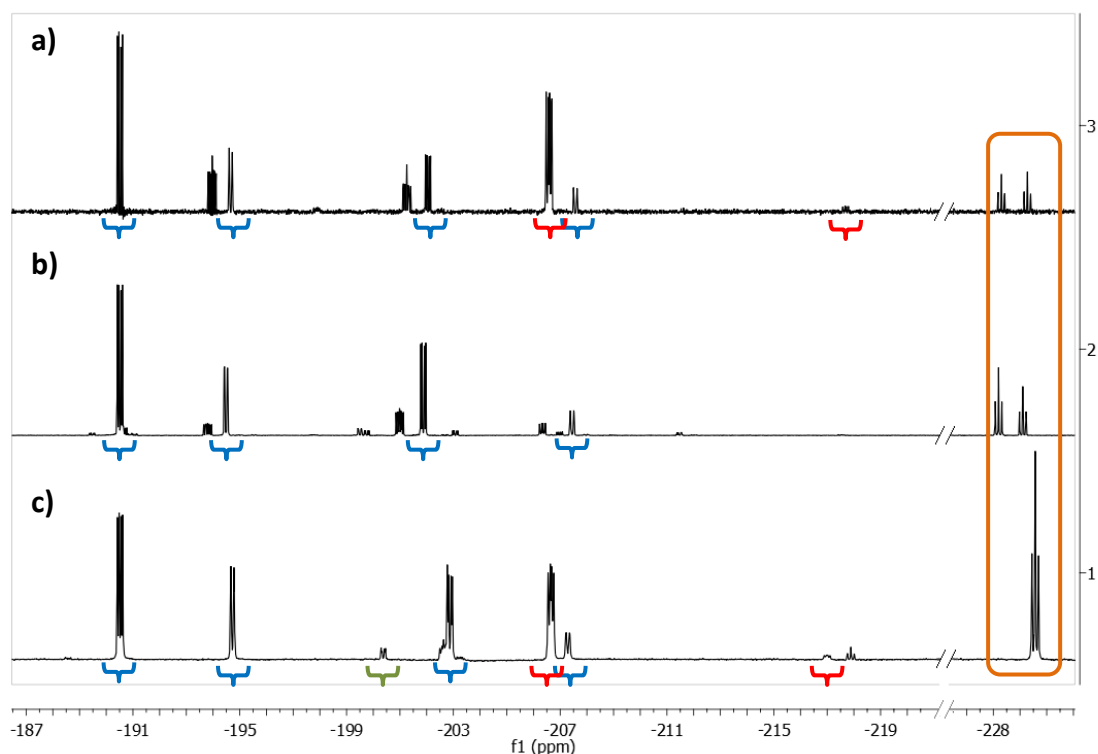
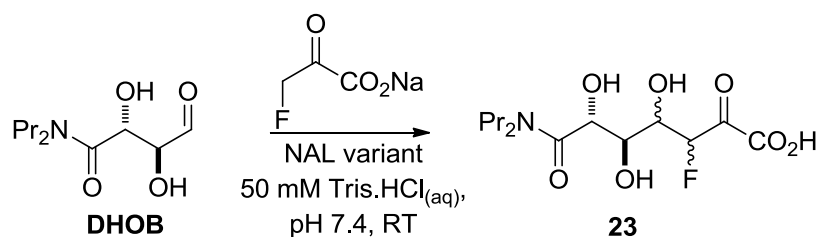


Figure 4.9 - 395 MHz ^{19}F NMR of products isolated after ion exchange of the reactions between fluoropyruvate and DHOB catalysed by NAL variants. Product peaks are indicated in blue (product **23c**), red (product **23a**) and green (product **23d**). The multiplets observed at -193.8 ppm and -201.0 ppm were found to correspond to a by-product which was removed upon further purification. a) E192N catalysed reaction between DHOB and fluoropyruvate b) E192N/T167V/S208V catalysed reaction of DHOB and fluoropyruvate c) E192N/T167G catalysed reaction of DHOB and fluoropyruvate. The spectrum of the E192N/T167G was recorded on the un-purified reaction mixture, so some of the chemical shifts are slightly different due to a difference in pH and the presence of salts from the reaction buffer, however the coupling constants are consistent across all three experiments.

The reactions of *ent*-DHOB are rather more selective and the 395 MHz ^{19}F NMR spectra of each the products are shown in Figure 4.10. All three NAL variants give one major diastereomer, identified as product *ent*-**23d** (indicated in green), which is characterised by a peak at -199.8 ppm. NAL E192N/T167V/S208V, in the reaction with *ent*-DHOB, appears to be completely selective (Figure 4.10b). NAL E192N (Figure 4.10a) and E192N/T167G (Figure 4.10c) both gave a small amount of the diastereomer characterised by a peak at -206.0 ppm, identified as *ent*-**23a** (highlighted in red).

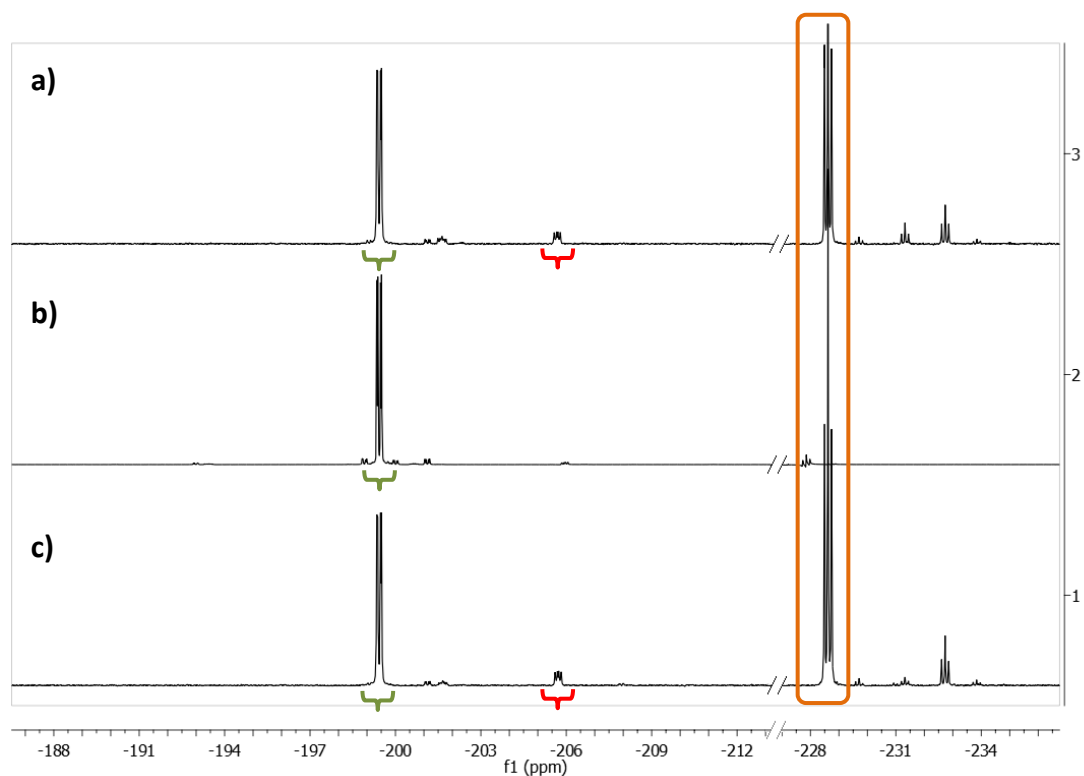
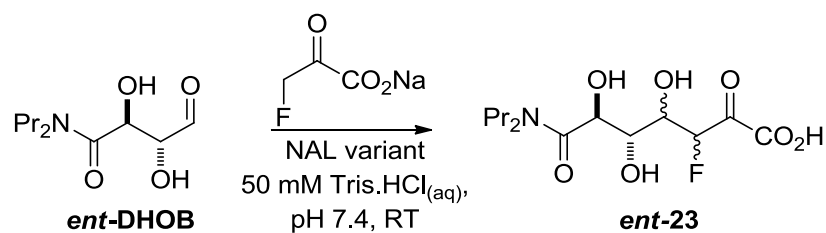
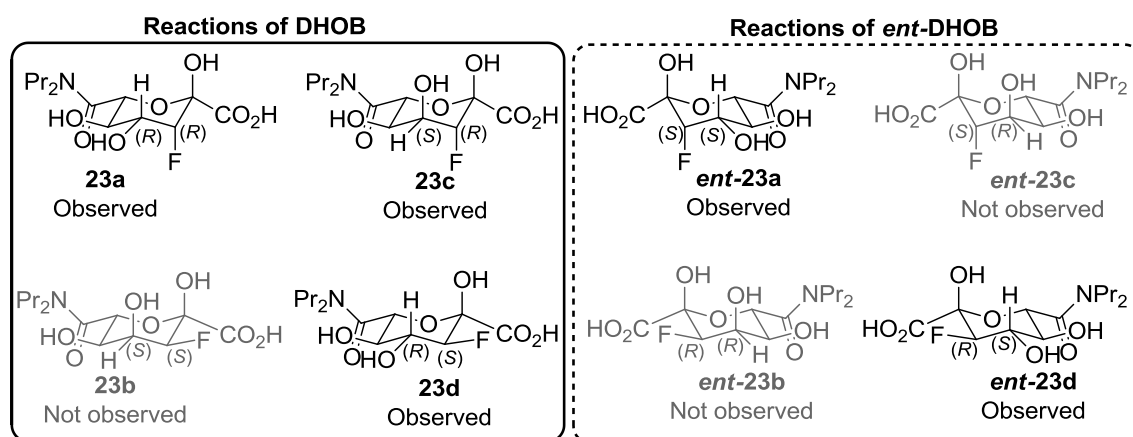


Figure 4.10 - 395 MHz ^{19}F NMR of products isolated after ion exchange of the reactions between fluoropyruvate and *ent*-DHOB catalysed by NAL variants. a) E192N catalysed reaction between *ent*-DHOB and fluoropyruvate b) E192N/T167V/S208V catalysed reaction of *ent*-DHOB and fluoropyruvate c) E192N/T167G catalysed reaction of *ent*-DHOB and fluoropyruvate

4.3.2 Characterisation of the products of the NAL variant-catalysed reactions of DHOB and fluoropyruvate

Table 4.7 outlines the peaks and coupling constants which correspond to each of the observed products of the NAL variant-catalysed reactions of **DHOB/ent-DHOB** and fluoropyruvate. This highlights a second challenge in the characterisation of products of the reactions of **DHOB/ent-DHOB**; the product **23c** exists as a complex mixture of equilibrium species. This is compounded by the problem identified previously that the product **23a** is only observed in a mixture of diastereomers with **23c**. The following sections explain how each of the diastereomers were individually characterised by exploiting further purification techniques and advanced NMR experiments.

Table 4.7 - Characterisation by 395 MHz ^{19}F NMR spectroscopy of diastereomers from the NAL catalysed reactions of DHOB and *ent*-DHOB with fluoropyruvate

Products observed	δ_{F} (395 MHz, D_2O) /ppm	J /Hz	Predicted ring form	Ratio of equilibrium species	Configuration at C-3 and C-4
23a	-206.0	49.9 and 32.5	Pyranose	92:8	(3 <i>R</i> ,4 <i>R</i>)
	-216.8	51.4 and 32.8	Pyranose		[(3 <i>S</i> ,4 <i>S</i>) – <i>ent</i> -23a]
23c	-190.5	50.5 and 24.0	Pyranose	37:23:29:11	(3 <i>R</i> ,4 <i>S</i>)
	-194.5	43.7 and 4.7	Furanose		
	-201.9	53.1 and 18.7	Pyranose		
	-207.4	48.5 and 10.1	Furanose		
23d	-199.8	49.3 and 13.3	Pyranose	>98:<2	(3 <i>S</i> ,4 <i>R</i>) [(3 <i>R</i> ,4 <i>S</i>) – <i>ent</i> -23d]

4.3.2.1 Characterisation of the product of the NAL E192N/T167V/S208V-catalysed reaction of *ent*-AHOB and fluoropyruvate

The product of the NAL E192N/T167V/S208V catalysed reaction of *ent*-DHOB and fluoropyruvate is characterised by a peak in the ^{19}F NMR at -199.8 ppm and has been identified as the product *ent*-23d. The enantiomer of this product (**23d**) is also observed in the NAL E192N/T167G catalysed-reaction of DHOB and pyruvate. Since this product could be isolated without the need to separate mixtures of diastereomer

and existed predominantly as one ring form, it was characterised without need for further purification or advanced analytical techniques. The 500 MHz ^1H NMR spectrum was recorded (Figure 4.11) and the structure was confirmed by careful analysis of the coupling constants of the protons attached to the carbons in the pyranose ring (Table 4.8). The coupling constant between the 5-H and 4-H is 9.5 Hz and the 5-H appears as a triplet, which indicated that the 4-H, 5-H and 6-H were all axial. Furthermore, the coupling constant between 4-H and 3-H is 9.3 Hz, which indicated that both of these protons are axial, which means that the fluorine must be equatorial, therefore confirming the identity of this product as **ent-23d**.

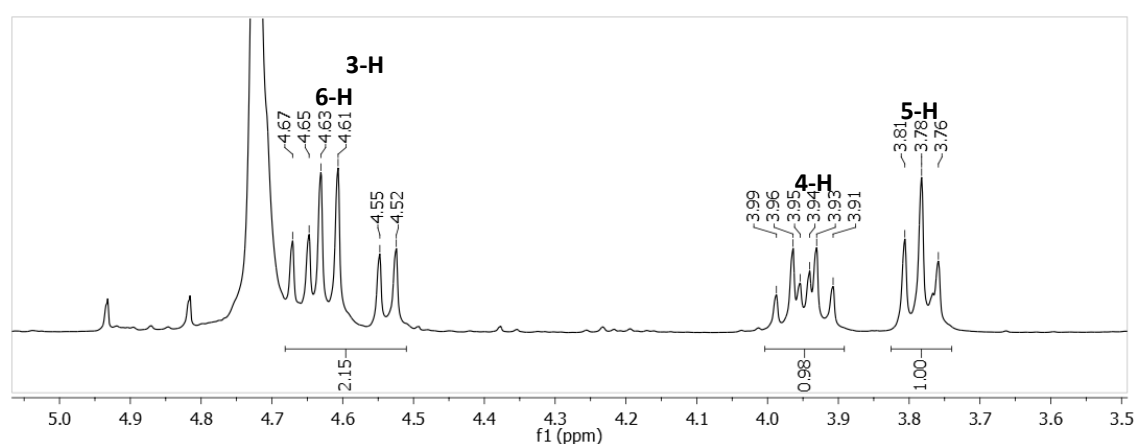
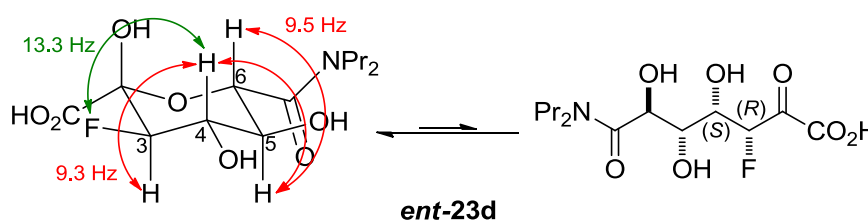


Figure 4.11 – Expansion of the 500 MHz ^1H NMR spectrum of the product **ent-23d**

Table 4.8 - Diagnostic chemical shifts and coupling constants from the 500 MHz ^1H NMR of the product **23d**



δ_{H} (500 MHz, D_2O) /ppm	Multiplicity	$^2J_{\text{HF}}$ /Hz	$^3J_{\text{HF}}$ /Hz	$^3J_{\text{HH}}$ /Hz	Identity
4.62	d	-	-	9.7	6-H
4.60	dd	49.3	-	9.3	3-H
3.95	dt	-	13.3	9.4	4-H
3.78	t	-	-	9.5	5-H

The characterisation of **ent-23d** has assumed that the major equilibrium species of this diastereomers is a pyranose ring. This was confirmed by recording an NOE spectrum. The peak at 3.95 ppm (corresponding to 4-H) was irradiated and correlation was observed with the peak at 4.62 ppm, which corresponds to 6-H (Figure 4.12).

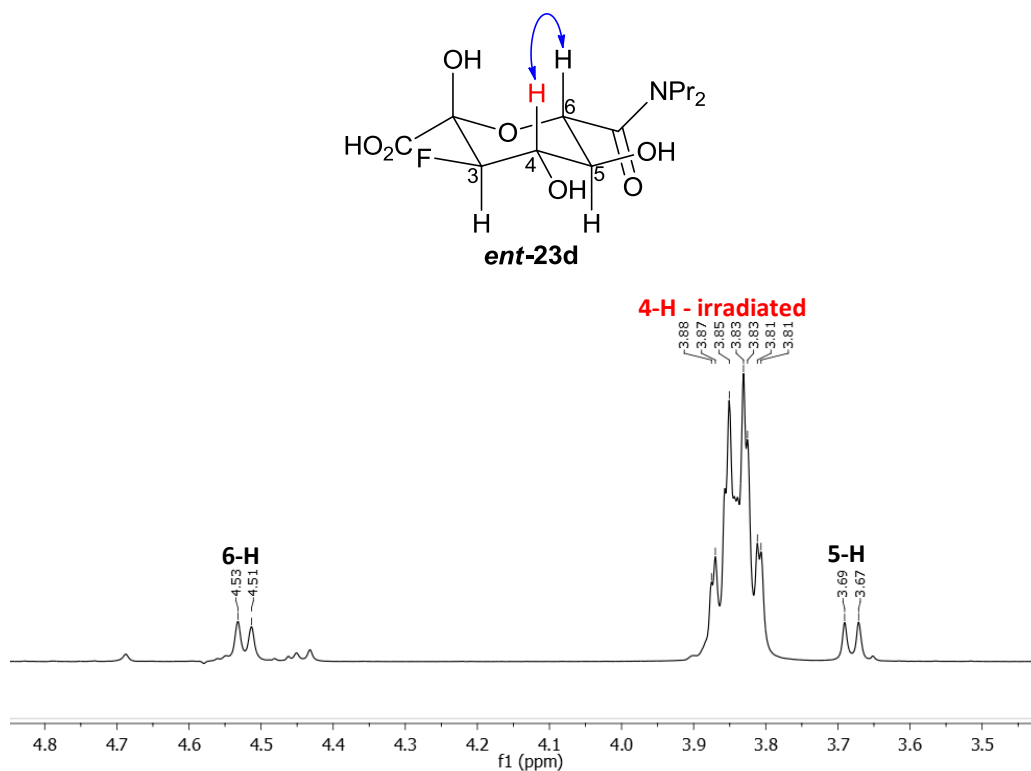


Figure 4.12 - NOE spectrum of **ent-23d** provided evidence that the major equilibrium species was a pyranose ring. Predicted to be observed as a positive NOE due formation of non-covalent polymerised lattices resulting in slower tumbling.

4.3.2.2 Separation of mixtures of diastereomers

In the NAL E192N catalysed reaction of **DHOB** and fluoropyruvate, a mixture of two diastereomeric products was observed, products **23a** and **23c**. The mixture was difficult to separate, however it was possible to prepare a small quantity of each of the diastereomers by semi-preparative reverse-phase HPLC (Figure 4.13a). Product **23a** was eluted after 28.7 minutes (Figure 4.13b), was confirmed to exist predominantly as one equilibrium species, which is characterised by a peak at -206.0 ppm. While the vicinal proton-fluorine coupling constant indicated that this peak corresponded to the diastereomer in which the 3-F and 4-H were axial, in order to be sure it was necessary to acquire a ^1H NMR spectrum. Product **23c** was eluted after 31.0 minutes (Figure

4.13c) and was observed as a complex mixture of equilibrium species and the characterisation of this diastereomer will be discussed in Section 4.3.2.3.

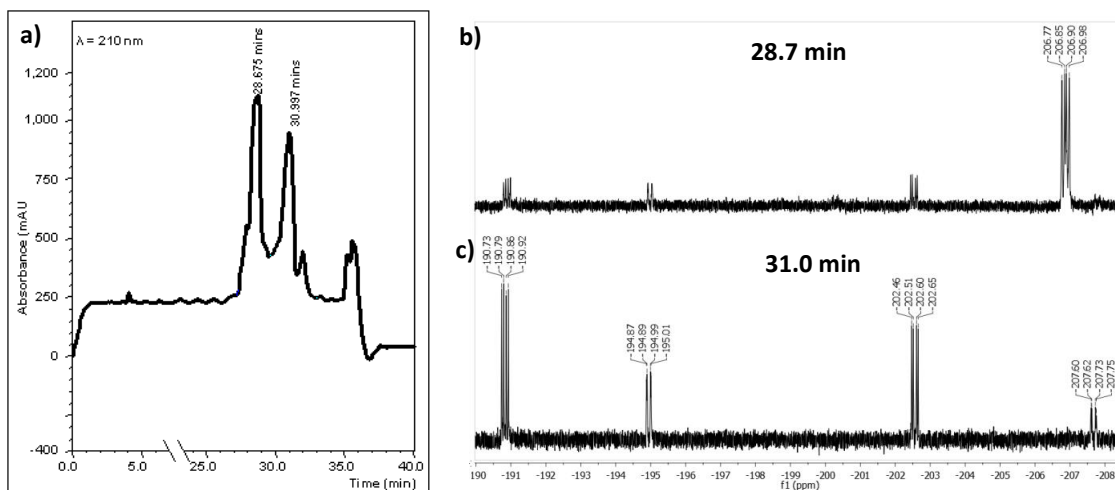
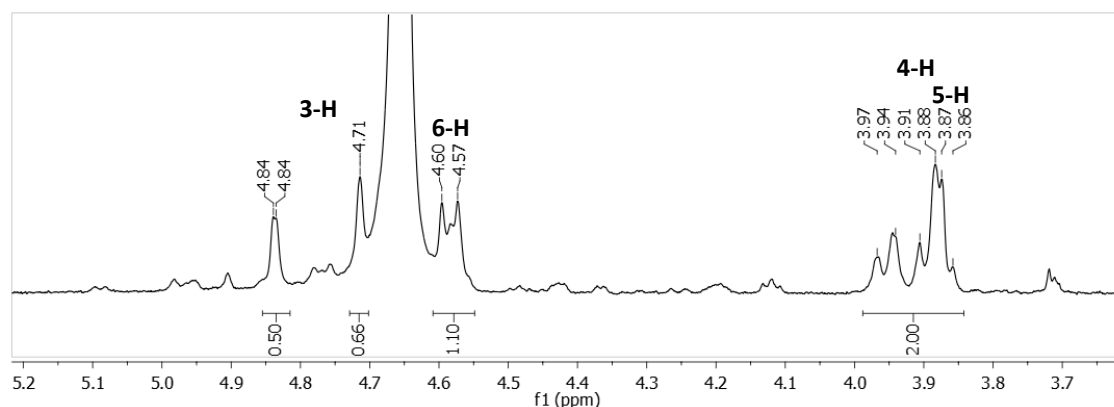
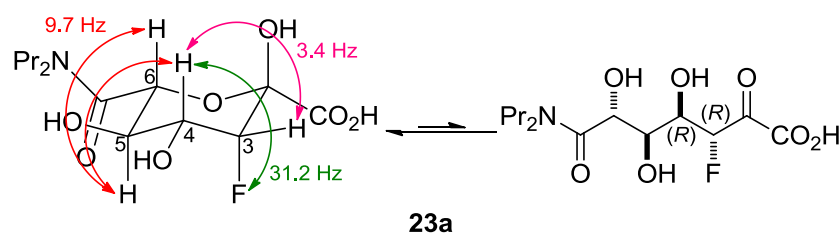


Figure 4.13 – Separation of the products of the NAL E192N catalysed reaction of DHOB and fluoropyruvate by reverse-phase HPLC a) UV-Vis trace 210 nm from the reverse-phase HPLC purification. Two peaks are observed at 28.7 minutes and 31.0 minutes. b) 395 MHz ^{19}F NMR spectrum of the product **23a** was eluted after 28.7 minutes c) 395 MHz ^{19}F NMR spectrum of product **23c** was eluted after 31.0 minutes. Some contamination from the product **23c** can still be observed in the spectrum of product **23a**.

Having separated the mixture of diastereomers, it was possible to obtain a 500 MHz ^1H NMR spectrum (Figure 4.14) and confirm the structure of product **23a**. The configuration of product **23a** was confirmed by careful analysis of the coupling constants of the protons attached to the carbons in the pyranose ring (Table 4.9). Most importantly, the vicinal coupling constant between the 4-H and 5-H was measured to be 9.7 Hz, which indicated that both of these protons are axial in a pyranose ring. It was therefore concluded that the minor diastereomer of the NAL E192N-catalysed reaction between **DHOB** and fluoropyruvate was the product **23a**.

Figure 4.14 – Expansion of the 500 MHz ^1H NMR spectrum of the product **23a**Table 4.9 - Diagnostic chemical shifts and coupling constants from the 500 MHz ^1H NMR of the product **23a**.

δ_{H} (500 MHz, D_2O)	Multiplicity	$^2J_{\text{HF}}$ (Hz)	$^3J_{\text{HF}}$ (Hz)	$^3J_{\text{HH}}$ (Hz)	Identity
4.78	dd	49.9	-	3.4	3-H
4.75	d	-	-	9.2	6-H
3.97-3.90	m	-	31.2*	9.7 and 3.4†	4-H
3.88	t	-	-	9.7	5-H

*Measured from the 395 MHz ^{19}F NMR spectrum †Estimated coupling constants based on coupling constants observed for neighbouring protons.

The predicted pyranose ring form of **23a** was confirmed by NOE. The peak at 4.75 ppm (corresponding to 6-H) was irradiated and correlation was observed with the peak corresponding to 4-H and the peak corresponding to the protons of the propyl chain closest to the nitrogen (Figure 4.15).

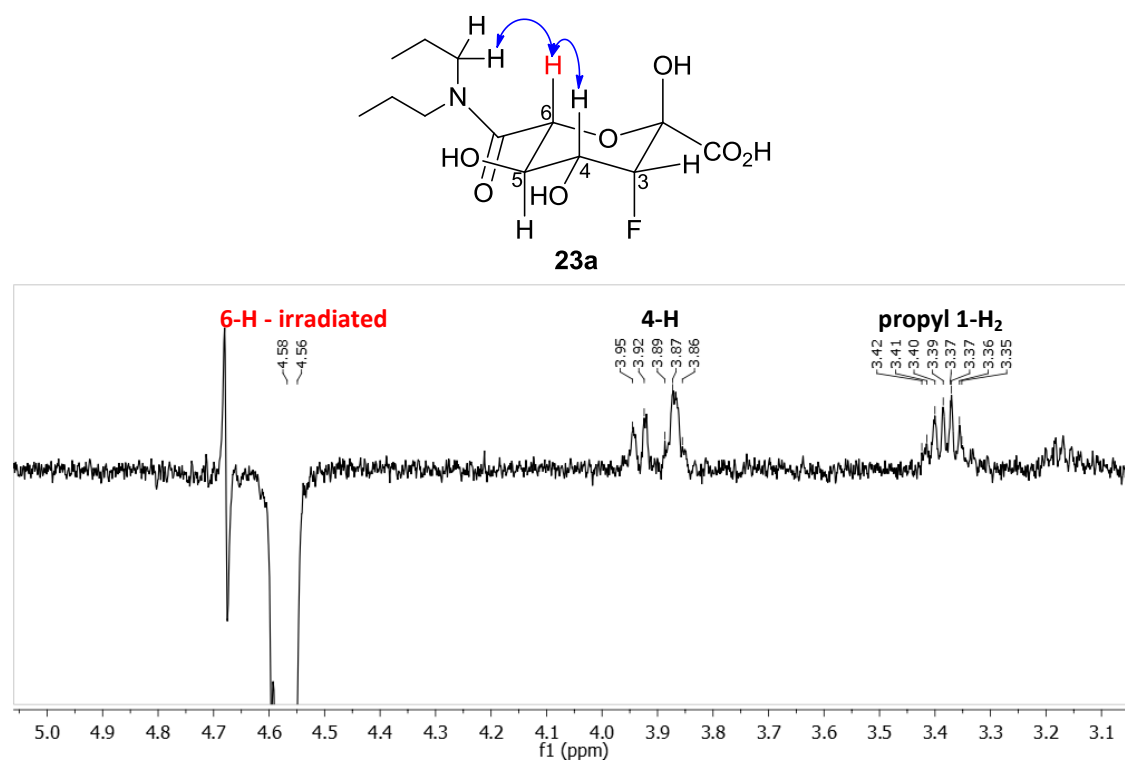


Figure 4.15 - NOE spectrum of **23a** provided evidence that the major equilibrium species was a pyranose ring.

4.3.2.3 Application of $^1\text{H}/^{19}\text{F}$ HSQC-TOCSY in the characterisation of complex mixtures of equilibrium species

The product **23c** existed as a mixture of equilibrium species, therefore it was difficult to confirm by ^1H NMR the configuration of this product. Figure 4.16 shows the 500 MHz ^1H NMR spectrum of **23c**, in which the peaks corresponding to the four equilibrium species overlap. The proton-fluorine vicinal coupling constants for each species were determined by 395 MHz ^{19}F NMR spectroscopy which confirmed an axial-equatorial relationship between 3-F and 4-H in the pyranose form, but no gave no indication of whether the 3-F or the 4-H was the axial substituent. It was therefore necessary to employ two-dimensional NMR techniques, which were carried out in collaboration with Dr. Tomas Lebl,^{*} in order to deconvolute the spectra of the species.

^{*} University of St. Andrews, UK

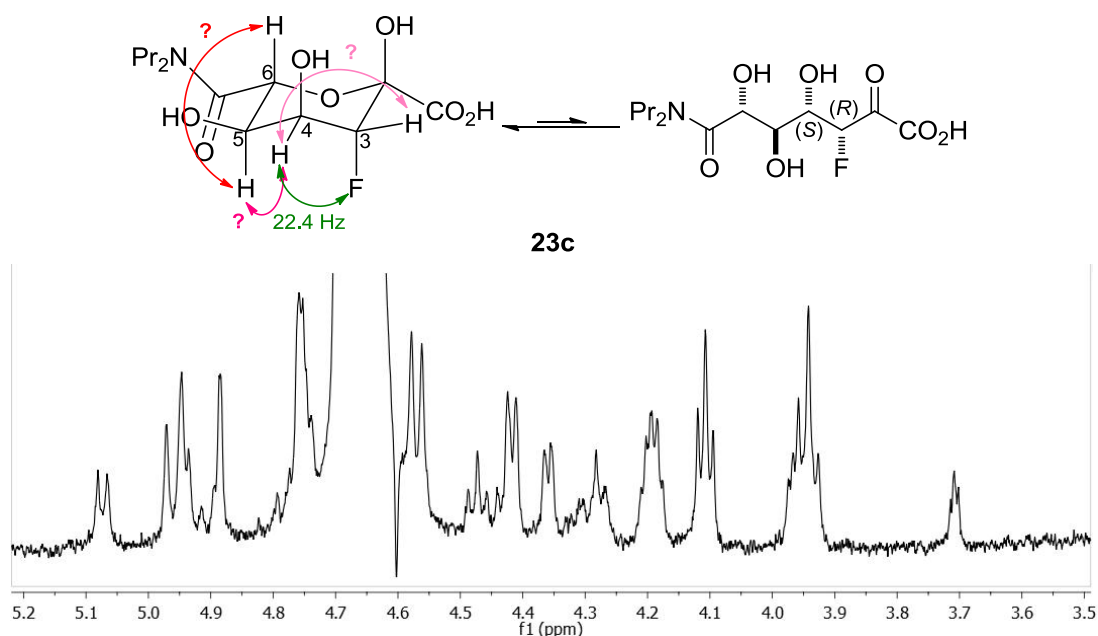


Figure 4.16 - Region of the 500 MHz ^1H NMR spectrum of the diastereomer **23c.**

While the ^1H NMR spectrum of **23c** is very complicated, the ^{19}F NMR spectrum of the HPLC-purified product has four clear peaks corresponding to each of the four equilibrium species. It was therefore decided to extract the ^1H NMR spectrum of each of the equilibrium species using a two-dimensional $^1\text{H}/^{19}\text{F}$ experiment ($^1\text{H}/^{19}\text{F}$ HSQC-TOCSY).

TOCSY (TOtal Correlation Spectroscopy) is a homonuclear two-dimensional technique in which cross-peaks between signals corresponding to nuclei in the same spin system are observed. HSQC (Heteronuclear Single Quantum Coherence spectroscopy) is a second two-dimensional technique that is used to evaluate coupling between protons and other nuclei.⁸⁷

Figure 4.17a shows the 4 possible equilibrium forms of **23c** and Figure 4.17b shows the recorded $^1\text{H}/^{19}\text{F}$ HSQC-TOCSY spectrum. The vertical axis shows the four peaks in the ^{19}F NMR spectrum corresponding to each equilibrium species. By taking a slice through the centre of each row, it was possible to measure both the chemical shifts and the coupling constants of the proton peaks corresponding to each of the equilibrium species. The extracted ^1H NMR spectra of the equilibrium species are shown in Figure 4.17c. It should be noted that the integration of the peaks relates the efficiency with which magnetisation was transferred around the ring.

Chapter 4 - NAL-catalysed reactions of aldehyde analogues and fluoropyruvate

In order to observe correlation between ^{19}F and the most distance protons, this techniques was complemented by recording the $^1\text{H}/^{19}\text{F}$ HMQC (Heteronuclear Multiple Quantum Coherence) spectrum (blue) which was overlaid onto the $^1\text{H}/^{19}\text{F}$ HSQC/TOCSY (red) (Figure 4.18) in order to show the cross-peaks corresponding to the protons furthest from the fluorine. The contour of the peaks in the HMQC does not have the same level of resolution as the HSQC/TOCSY spectrum, so no further information could be gained about coupling constants.

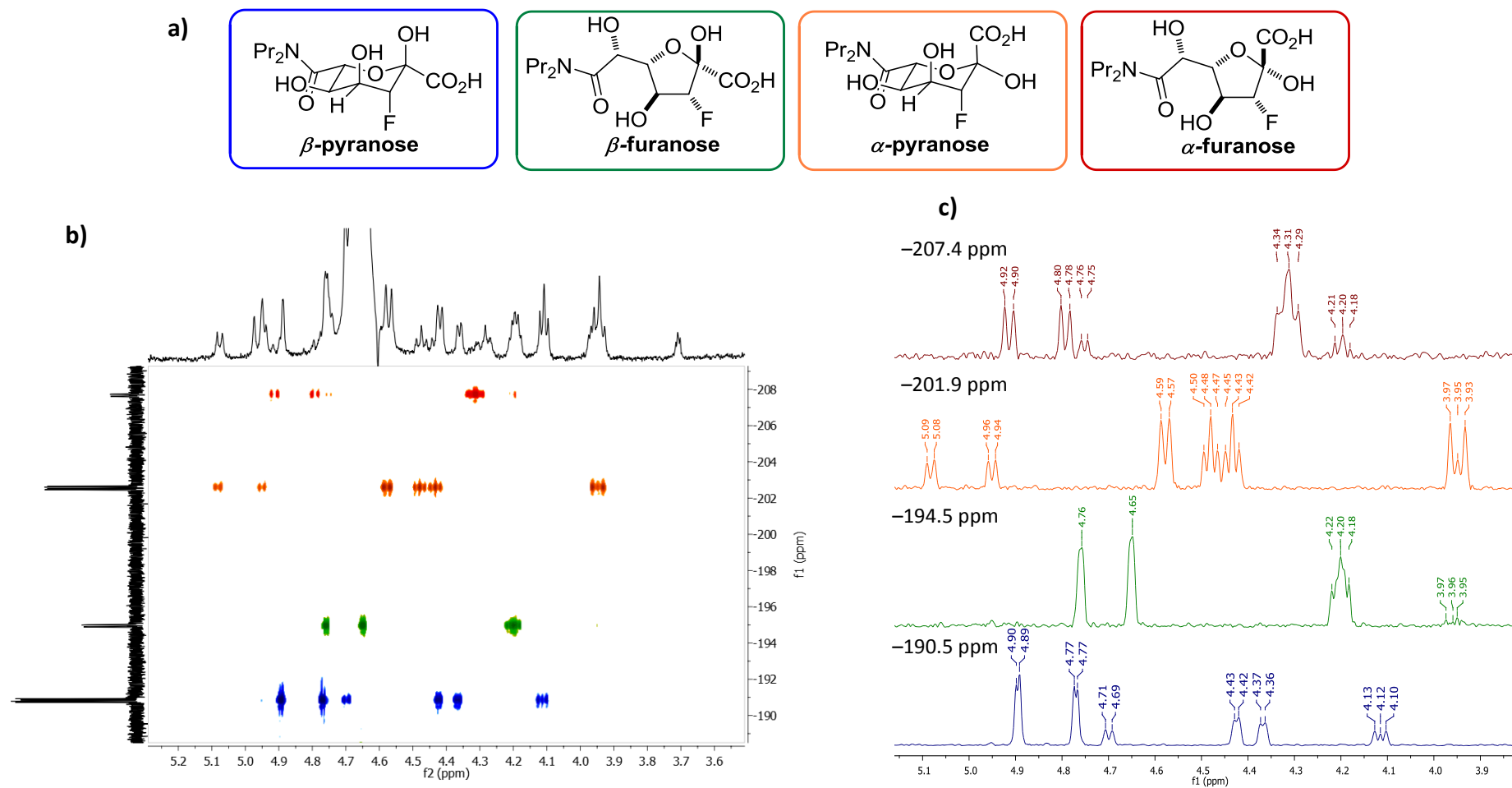


Figure 4.17 – Extraction of the individual ^1H NMR spectra corresponding to each of the equilibrium species of **23c** by $^1\text{H}/^{19}\text{F}$ HSQC-TOCSY. a) Equilibrium forms of **23c**. b) $^1\text{H}/^{19}\text{F}$ HSQC-TOCSY spectrum of the product of the reaction between DHOB and fluoropyruvate catalysed by E192N/T167V/S208V. The cross-peaks show the protons in the same spin system as each of the fluorine environments. c) Extracted ^1H NMR spectra from the $^1\text{H}/^{19}\text{F}$ HSQC-TOCSY spectrum of the reaction between DHOB and fluoropyruvate.

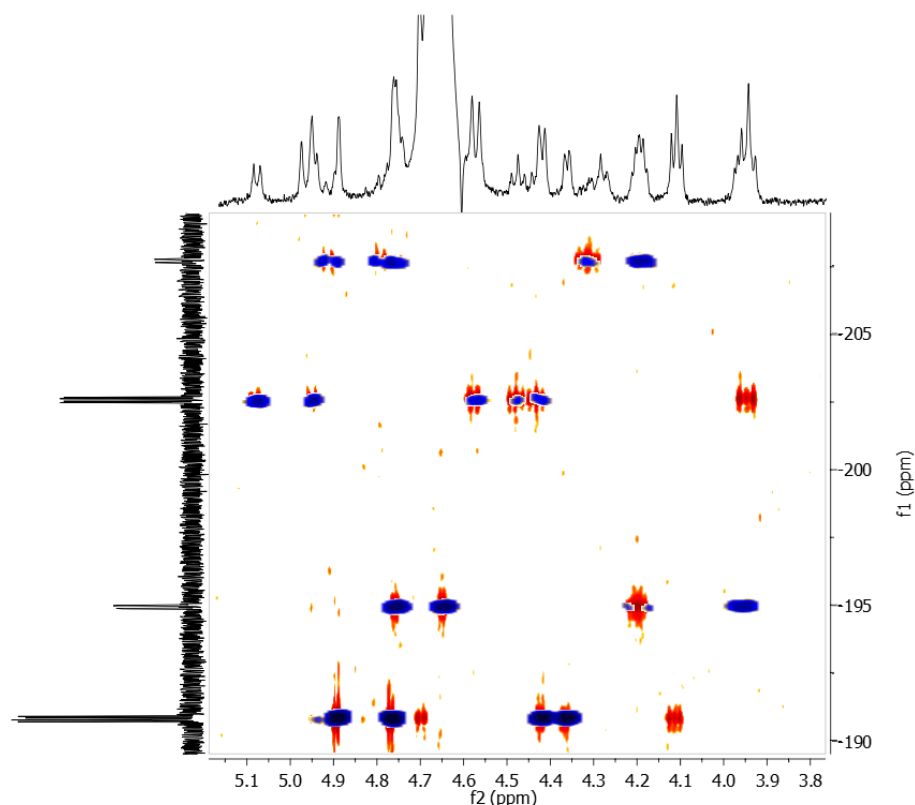


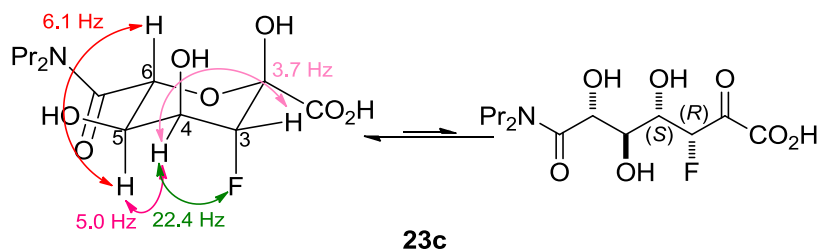
Figure 4.18 - $^1\text{H}/^{19}\text{F}$ HSQC-TOCSY spectrum (red cross-peaks) overlaid with $^1\text{H}/^{19}\text{F}$ HMQC spectrum (blue cross-peaks) of the product **23c**. The HMQC identifies cross-peaks which are weak in the HSQC-TOCSY spectrum.

With all the information gathered together from the two-dimensional NMR experiments (Table 4.10), it was possible to assign the spectra and identify the structure of **23c** by careful analysis of the coupling constants of the pyranose species. In the previously characterised pyranose species the geminal proton-fluorine coupling constants have always been measured at 49-50 Hz, therefore it was predicted that the pyranose species were those characterised by a peaks in the ^{19}F NMR spectrum at -190.5 ppm (blue) and -201.9 ppm (yellow). Unfortunately, due to the complexity of the ^1H NMR spectrum it was not possible to acquire a NOE spectrum to confirm this prediction. The configuration of **DHOB** dictated that 5-H and 6-H must be both axial, however the coupling constants measured between these two protons were quite small. Furthermore the proton-fluorine vicinal coupling constants of the pyranose species were surprisingly large. The deviation of the magnitude of the proton-proton coupling constants may be a consequence of flattening of the pyranose rings, perhaps due to an unfavourable 1,3-diaxial interaction between the C-4 hydroxyl and the C-2 substituent. This may also explain why this diastereomer was observed as an

Chapter 4 - NAL-catalysed reactions of aldehyde analogues and fluoropyruvate

equilibrium mixture of ring forms because unfavourable steric interactions occur in all of the possible ring forms.

Table 4.10 - Diagnostic chemical shifts and coupling constants of the equilibrium species of product 23c from extracted ^1H NMR spectra.

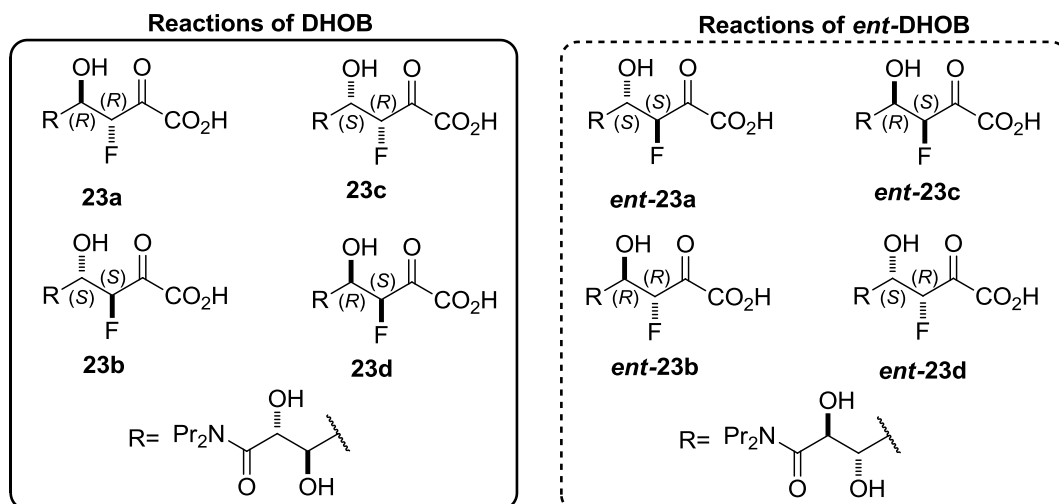


δ_{F} (395 MHz, D_2O) /ppm	δ_{H} (500 MHz, D_2O) /ppm	Multiplicity	$^2J_{\text{HF}}$ /Hz	$^3J_{\text{HF}}$ /Hz	$^3J_{\text{HH}}$ /Hz	Identity
Major pyranose						
-190.5	4.85	dd	49.7	-	4.8	3-H
	4.65	d	-	-	6.1	6-H
	4.39	dd	-	22.4	3.7	4-H
	4.12	t	-	-	5.0	5-H
Major furanose						
-194.5	4.72	dd	44.2	-	1.7	3-H
	4.02	app. t	-	5.9	7.4	4-H
	3.96	m	-	-	-	5-H
Minor pyranose						
-201.9	5.03	dd	52.0	-	5.5	3-H
	4.57	d	-	-	7.2	6-H
	4.46	dt	-	18.7	5.6	4-H
	3.95	t	-	-	6.4	5-H
Minor furanose						
-207.4	4.86	dd	48.1	-	7.3	3-H
	4.75	d	-	-	5.4	6-H
	4.30	td	-	8.7	3.4	4-H
	4.18	dd	-	-	8.6 and 5.1	5-H

4.3.3 Summary of the products of the NAL-catalysed reaction of DHOB/*ent*-DHOB and fluoropyruvate

The products of the NAL catalysed reaction of **DHOB**/*ent*-**DHOB** and fluoropyruvate more difficult to characterise. The products of the *ent*-**DHOB** reactions with fluoropyruvate were less challenging to characterise as all three NAL variants gave predominantly one diastereomer, which existed as one major equilibrium species. By the application of separation techniques and informative two-dimensional NMR experiments, it was possible to identify and characterise the products of the **DHOB** reactions (summarised in Table 4.11). As previously observed for the reactions of **AHOB**, the (3*R*)-epimers are by far the most common as predicted in Section 4.1.2.

Table 4.11 - Summary of the products of the NAL variant-catalysed reactions between DHOB and *ent*-DHOB with fluoropyruvate.



Aldehyde	NAL variant	Products observed	Ratio of	Ratio of products by
			products a:b:c:d	configuration at C-3 and C-4 (3 <i>R</i> ,4 <i>R</i>):(3 <i>S</i> ,4 <i>S</i>): (3 <i>R</i> ,4 <i>S</i>):(3 <i>S</i> ,4 <i>R</i>):
DHOB	E192N	23a and 23c	40:0:60:0	40:0:60:0
	E192N/T167V/S208V	23c	0:0:100:0	0:0:100:0
	E192N/T176G	23a , 23c and 23d	28:0:70:2	28:0:70:2
<i>ent</i> - DHOB	E192N	<i>ent</i> - 23a and <i>ent</i> - 23d	8:0:0:92	0:8:92:0
	E192N/T167V/S208V	23d	0:0:0:100	0:0:100:0
	E192N/T176G	<i>ent</i> - 23a and <i>ent</i> - 23d	10:0:0:90	0:10:90:0

4.4 Analysis of reactions of alternative substrates catalysed by NAL E192N variants by 296 MHz ¹⁹F NMR spectroscopy

The preparative-scale enzyme-catalysed reactions discussed previously have provided some information about the potential value of the NAL variants in the synthesis of fluorinated analogues of Neu5Ac, however many of the results are qualitative. In order to better understand the activity of the enzyme variants, further experiments were carried out in order to make direct comparison between the enzyme-catalysed reactions which can be quantified. Furthermore, in order to fully understand the diastereoselectivity of the NAL variants, it is important to analyse the kinetic ratios of products.

In order to answer these questions, a series of reactions were carried out on a small scale and monitored by 296 MHz ¹⁹F NMR spectroscopy. The reactions were driven by excess aldehyde (5 molar equivalents). With fluoropyruvate as the limiting reagent, it was possible to calculate the conversion of fluoropyruvate to product at each time point over the course of 35 hours and plot the disappearance of fluoropyruvate and appearance of products over time. It was possible in this way to simultaneously compare the initial rates of reaction and evaluate the kinetic selectivity. The most constructive way to understand the stereocontrol imparted by the NAL-variants is to consider the absolute configuration of C-3 and C-4. The colour-coding used in presentation of the data throughout the following Sections is related to the configuration at C-3 and C-4 rather than pairs of enantiomers.

4.4.1 Comparison of initial rates of enzyme catalysed reactions

In order to monitor the rate of the enzyme-catalysed reactions, a series of reactions were carried out in NMR tubes. In order for the NMR machine to lock, it is necessary to have a small amount of deuterated solvent in the NMR tube; however adding deuterium oxide to the buffer directly would have resulted in deuterium incorporation into the products. In order to overcome this problem, a sealed capillary tube containing deuterium oxide was placed inside the NMR tube so the deuterium oxide would not be in direct contact with the reaction mixture.

Chapter 4 - NAL-catalysed reactions of aldehyde analogues and fluoropyruvate

296 MHz ^{19}F NMR spectra were recorded at suitable intervals over a period of 35 hours. Figure 4.19 shows a stacked-plot of 5 time points taken from the reaction between **DHOB** and fluoropyruvate, catalysed by NAL E192N/T167V/S208V as an example. It is clear to see the intensity of the peaks corresponding to product (highlighted in blue) relative to fluoropyruvate (highlighted in orange) increased over time. The fluoropyruvate appeared as two triplets, this is because in an aqueous solution, the fluoropyruvate was in equilibrium between the ketone and hydrate form.

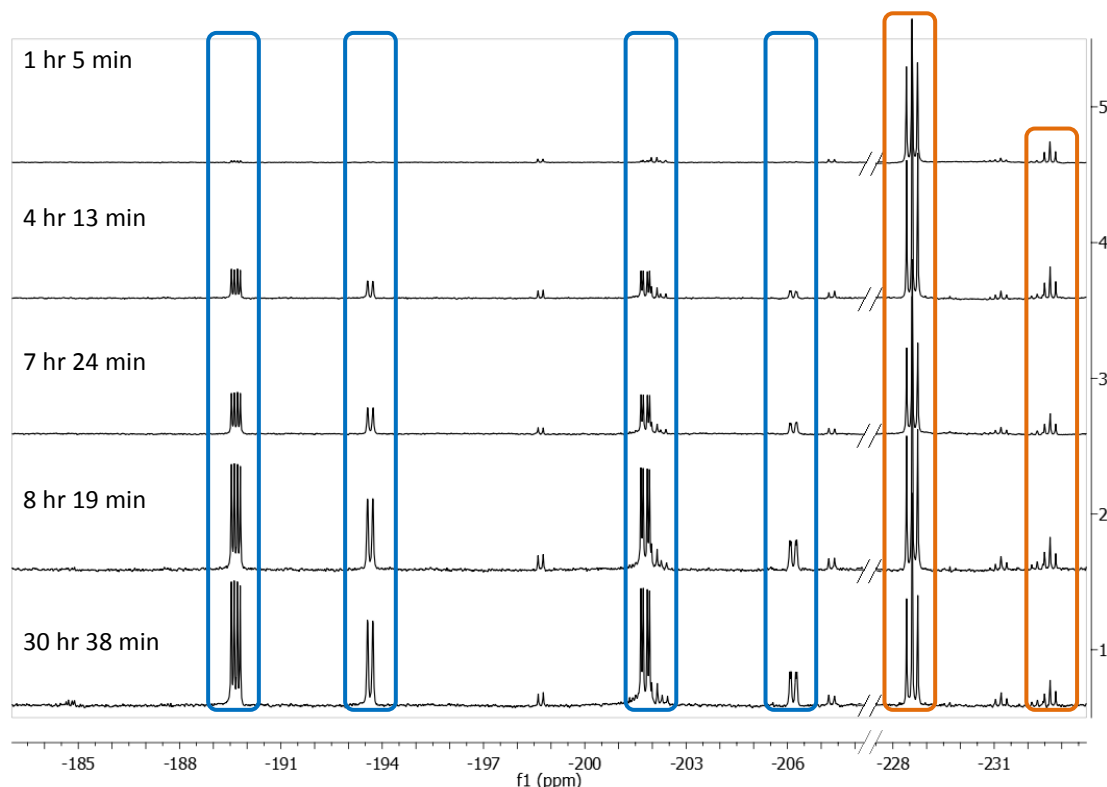


Figure 4.19 – Time course of the reaction between DHOB and fluoropyruvate catalysed by E192N/T167V/S208V

By measuring the relative integrals of reaction product (blue) compared to fluoropyruvate (orange) over time, it was possible to plot the appearance of product and disappearance of fluoropyruvate as shown in Chart 4.1a and the initial rates of reaction was calculated (Chart 4.1b). Time course reactions were carried out for each of the NAL-variant and aldehyde combinations and the results are shown in Table 4.12. (For full raw data sets, see Appendix 5)

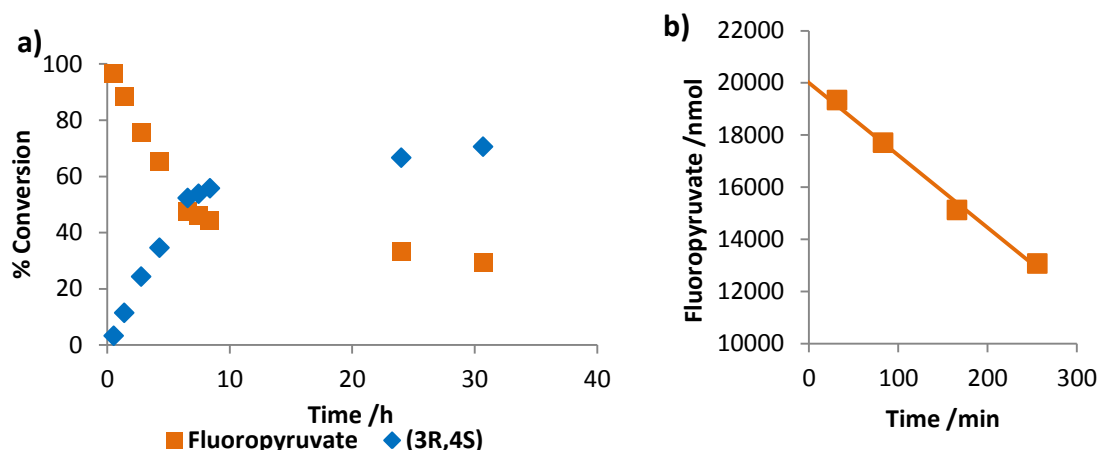


Chart 4.1 - An example of a plot of the appearance of the product 23c of the NAL E192N/T167V/S208V-catalysed reaction of DHOB and fluoropyruvate and the disappearance of fluoropyruvate. The conversion was calculated from the relative integrals of the 296 MHz ^{19}F NMR spectra recorded at suitable time intervals. a) Representation of the percentage disappearance of fluoropyruvate and the percentage appearance of product over the full reaction time. b) Linear points of the disappearance of fluoropyruvate. The initial gradient was used to calculate the initial rate of the reaction. In this reaction, the fluoropyruvate is disappearing at a rate of 27.7 nmol/min. For plots for all the combinations of NAL variants and aldehydes see Appendix 5.

Table 4.12 - Calculated activity of the NAL variants towards the aldehyde analogues from the disappearance of fluoropyruvate.

NAL variant	Aldehyde	Rate of disappearance of pyruvate /nmol min ⁻¹	Quantity of enzyme in the NMR tube /nmol	Specific activity /min ⁻¹
E192N	DHOB	236	28.8	9.12
	<i>ent</i> -DHOB	13.3	28.8	0.46
	AHOB	30.25	28.8	1.05
	<i>ent</i> -AHOB	1.88	28.8	0.07
E192N/T167V/S208V	DHOB	27.7	49.0	0.56
	<i>ent</i> -DHOB	0.76	25.9	0.03
	AHOB	0	-	0
	<i>ent</i> -AHOB	0	-	0
E192N/T167G	DHOB	3.15	52.7	0.06
	<i>ent</i> -DHOB	6.18	52.7	0.12
	AHOB	1.77	52.7	0.03
	<i>ent</i> -AHOB	1.52	52.7	0.03

Chart 4.2 is a graphical representation of the data in Table 4.12. Most of the focus of discussion will be on the NAL variants E192N and E192N/T167V/S208V as the E192N/T167G variant is 35 times less active than the NAL E192N variant towards

AHOB and over 300 times less active than NAL E192N towards **DHOB**. The NAL E192N variant was found to be around 9 times more active towards **DHOB** compared to **AHOB** and the NAL E192N/T167V/S208V variant was found to be inactive towards **AHOB**. In the case of both NAL E192N and E192N/T167V/S208V, switching enantiomeric series resulted in a 15-20 fold decrease in activity.

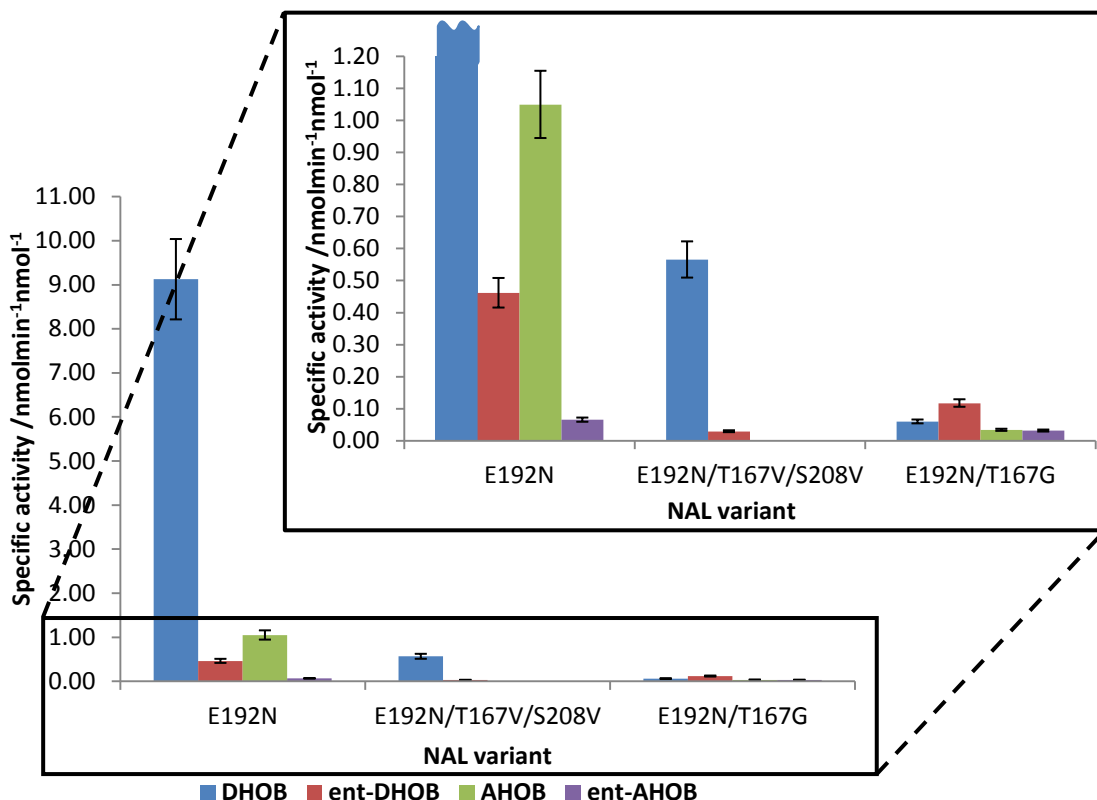


Chart 4.2 - Calculated specific activity of NAL variants towards the aldehyde analogues. Calculations based on the disappearance of fluoropyruvate, which was calculated by measuring relative integrals of ¹⁹F NMR spectra recorded at regular time intervals. Insert shows an enlargement of the lower levels of activity.

The NAL E192N-catalysed reaction of **AHOB** and fluoropyruvate was carried out under identical conditions to the reactions of **AHOB/ent-AHOB** with pyruvate described in Section 3.2.1. Chart 4.3 shows the relative activities measured for these experiments which revealed that switching donor from pyruvate to fluoropyruvate resulted in a 4-fold decrease in activity.

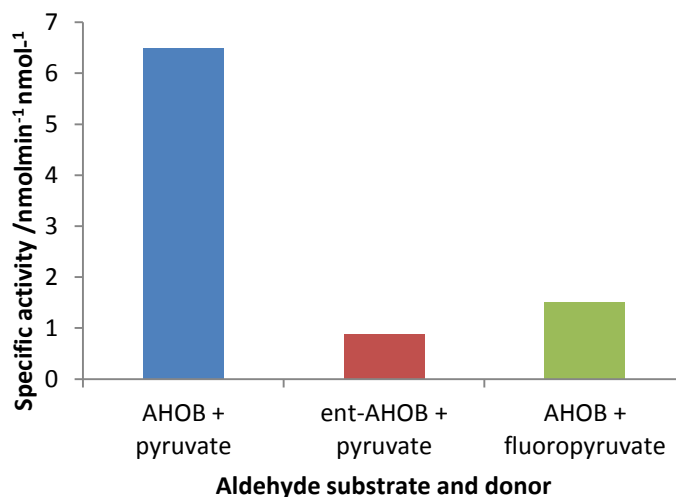


Chart 4.3 - Specific activities calculated for the reactions of the NAL E192N variant with AHOB/*ent*-AHOB with pyruvate and AHOB with fluoropyruvate. (For data used to calculate these results, see Appendix 5)

4.4.2 Determination of diastereoselectivity under kinetic control

It is not necessarily the case that the enzyme variants will display the same diastereoselectivity under kinetic conditions as under the preparative conditions described in Section 4.3.3. This became evident during the course of acquiring the data to measure the initial rates of reaction. For example, Figure 4.20 shows a selection of time points from the NAL E192N-catalysed reaction of **AHOB** and fluoropyruvate. In the preparative reaction conditions (Section 4.2.2) the product **57a** was isolated in a 98:2 excess over the **57d** diastereomer, however under kinetic control, the diastereomers were observed in a 56:44 ratio **57a:57d**.

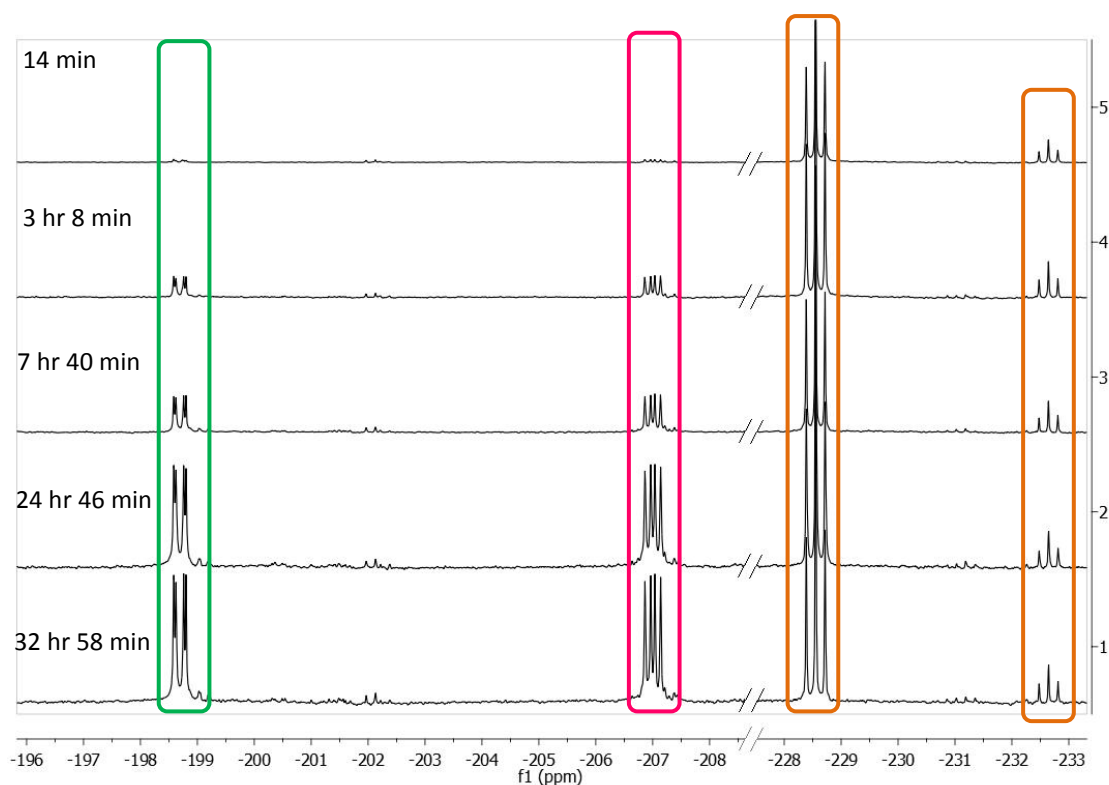


Figure 4.20 – The reaction between AHOB and fluoropyruvate catalysed by NAL E192N was selective under the preparative conditions described previously but gave a mixture of products under kinetic control.

In the case of reactions in which more than one diastereomer was formed, the ratio between the products was measured. The plot of the NAL E192N catalysed reaction between AHOB and fluoropyruvate is shown as an example in Chart 4.4.

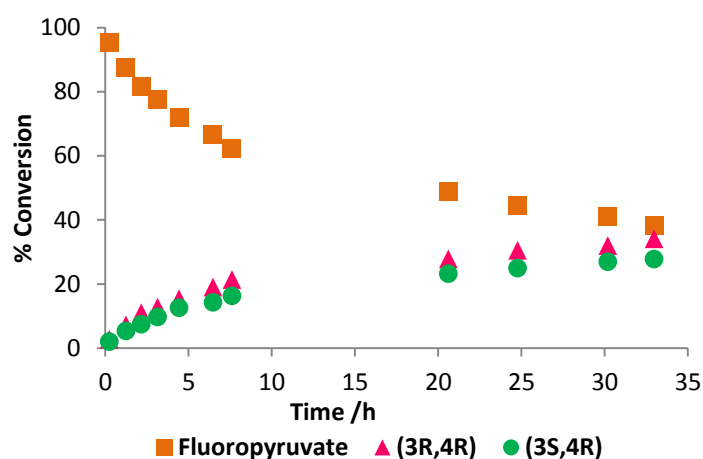
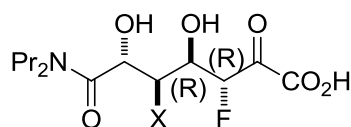


Chart 4.4 - An example of a plot of the appearance of enzyme reaction products (where two or more products are formed) and disappearance of fluoropyruvate generated from monitoring the enzyme catalysed reaction between the aldehyde analogues and fluoropyruvate. This example is the NAL E192N-catalysed reaction of AHOB and fluoropyruvate.

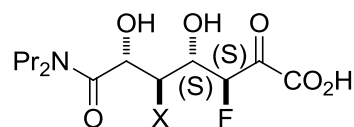
Chapter 4 - NAL-catalysed reactions of aldehyde analogues and fluoropyruvate

Table 4.13 shows the combined selectivity data for each combination of NAL variants and aldehyde analogues and the results are summarised in Chart 4.5. The two most prevalent colours on this chart are blue and pink which correspond to the two (3*R*)-epimers of the enzyme reaction products. This result is in agreement with the QM/MM modelling studies discussed in Section 4.1.2.⁵⁷ Surprisingly, the NAL E192N/T167G variant, which was evolved to favour attack of the *si*-face of the aldehyde in the reaction with **DHOB** and pyruvate, appears to be no longer selective in the reaction with **DHOB** and fluoropyruvate. Furthermore, the NAL E192N variant switched selectivity from favouring the product resulting from *si*-face attack of the aldehyde in reaction with **DHOB** and pyruvate, to favouring the product resulting from *re*-face attack of the aldehyde in reaction with **DHOB** and fluoropyruvate.

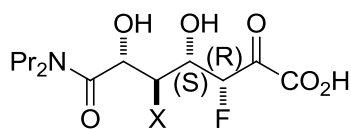
Table 4.13 – Kinetic ratio of the products of the reactions catalysed by the NAL variants.



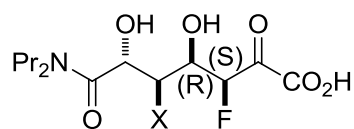
X= OH 23a
X = NHAc 57a



X= OH 23b
X = NHAc 57b



X= OH 23c
X = NHAc 57c



X= OH 23d
X = NHAc 57d

Aldehyde	NAL variant	Ratio of products a:b:c:d	Ratio of products by configuration at C-3 and C-4
			(3 <i>R</i> ,4 <i>R</i>):(3 <i>S</i> ,4 <i>S</i>): (3 <i>R</i> ,4 <i>S</i>):(3 <i>S</i> ,4 <i>R</i>)
DHOB	E192N	41:0:52:7	41:0:52:7
	E192N/T167V/S208V	0:0:100:0	0:0:100:0
	E192N/T167G	7:0:90:2	7:0:90:2
<i>ent</i> -DHOB	E192N	9.5:0:0:90.5	0:9.5:90.5:0
	E192N/T167V/S208V	0:0:0:100	0:0:100:0
	E192N/T167G	24:0:0:76	0:24:76:0
AHOB	E192N	56:0:44:0	56:0:44:0
	E192N/T167V/S208V	-	-
	E192N/T167G	100:0:0:0	100:0:0:0
<i>ent</i> -AHOB	E192N	27:0:0:73	0:27:73:0
	E192N/T167V/S208V	-	-
	E192N/T167G	100:0:0:0	0:100:0:0

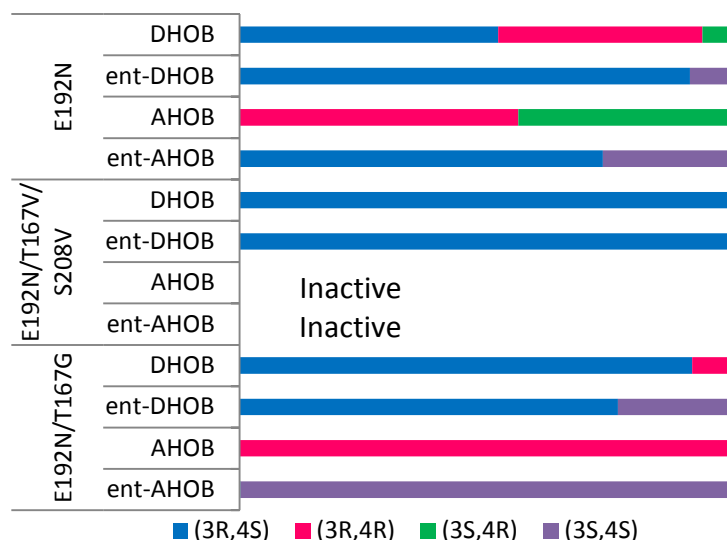


Chart 4.5 - Ratio of products of the kinetic controlled reactions of the NAL variants and DHOB and AHOB. The colour-coding corresponds to the relative configuration at C-3 and C-4.

4.4.3 Evaluation of the value of NAL variants in the synthesis of fluorinated *N*-acetyl neuraminic acid analogues

In order for the enzyme-catalysed reactions evaluated within this thesis to be synthetically useful, it is important that the enzymes are active enough to give useful yields of product, with high diastereoselectivity. The kinetically controlled reactions made it possible to compare simultaneously activity and diastereoselectivity as illustrated in Chart 4.6. By comparing the reactions in this way, it has been shown that while the NAL E192N-catalysed reaction with **DHOB** was by far the most active enzyme-substrate combination, and so from a catalytic efficiency point of view the most suitable candidate for use in synthesis, the diastereoselectivity was very poor. However, there were three further enzyme-substrate combinations which were much less active than the NAL E192N-catalysed reaction of **DHOB**, however did exhibit sufficient levels of activity and diastereoselectivity that they were considered to be good starting points for future development of improved NAL variants.

The first of these potentially interesting reactions is the NAL E192N catalysed reaction of **AHOB** and fluoropyruvate. In the preparative scale reaction (Section 4.3.3), the reaction was completely selective for product **57a** (98:2), however, under kinetic control, a mixture of the products **57a** and **57d** (56:44) was observed. It may be

possible to optimise the NAL E192N-catalysed reaction of **AHOB** to improve the yield and selectivity. The second interesting reaction is the NAL E192N/T167V/S208V catalysed reaction of **DHOB** and fluoropyruvate, which was found to be completely selective for the product **23c**. Furthermore, the isolated yield in the preparative conditions of this reaction was 40%. Finally, the NAL E192N catalysed reaction of *ent*-**DHOB** gave predominantly a single diastereomer *ent*-**23d** (d.r. 90:10). The NAL E192N variant was generally found to exhibit good activity with a broad range of substrates.

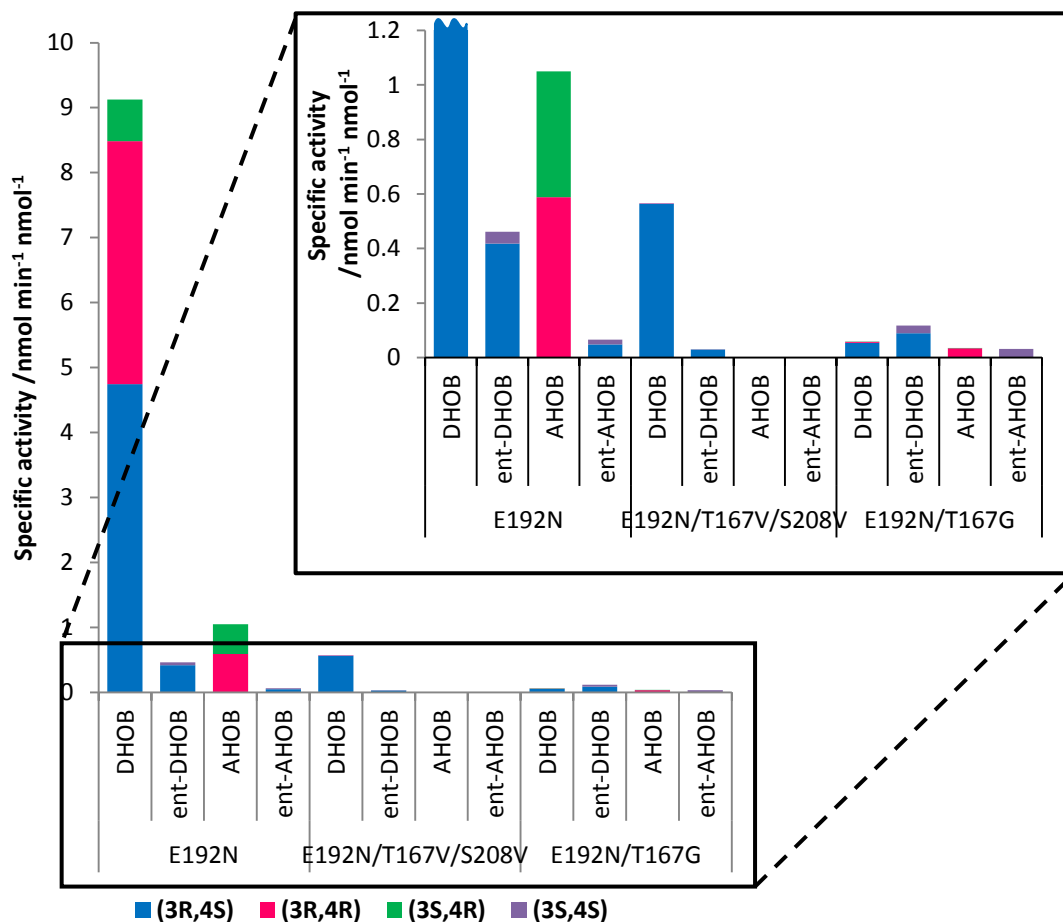


Chart 4.6 - Activity and selectivity of NAL variant catalysed reactions of aldehyde analogues and fluoropyruvate. Insert is an expansion of the region 1.2 nmol min⁻¹ nmol⁻¹ and below.

The NAL variants E192N/T167V/S208V and E192N/T167G have been engineered to be complementary and selective to give the diastereomers resulting from *re*-face and *si*-face attack of the aldehyde respectively, in the reaction between **DHOB** and pyruvate. However, the diastereoselective variants were a factor of 10 less active compared to the NAL E192N variant.⁶⁷ This initial high level of activity may account for why the NAL E192N variant is more tolerant to a broader range of substrates. Furthermore,

changing the donor from pyruvate to fluoropyruvate resulted in loss of diastereoselectivity in the case of the NAL E192N/T167G variant.

4.5 Discussion of the observed activity and diastereoselectivity of the reactions of alternative substrates catalysed by NAL variants

The previous Sections have explained the experimental outcome of various reactions of NAL variants with aldehyde analogues and fluoropyruvate. In order to take these results forward and make suggestions about the future direction of this work, it is important to understand what has been learnt about the mechanism of NAL from these experiments. QM/MM modelling studies⁵⁷ and the crystal structures of saNAL in complex with fluoropyruvate⁶³ were used to predict the selectivity the NAL variants might exhibit at the fluorine-bearing chiral centre (Section 4.1.2).

Justifying the C-4 selectivity of the NAL variants is rather more difficult, as is explaining the decrease in activity observed in the reaction of fluoropyruvate compared to pyruvate. There are two factors to consider; firstly, the introduction of fluorine may have an effect on the active-site geometry, therefore resulting in a reduction in activity because the catalytic residues are no longer in the right position relative to the donor or acceptor. Alternatively, the electronegative nature of fluorine may cause the enamine of fluoropyruvate to be a poorer nucleophile in comparison to pyruvate and change the transition state energy barriers leading to formation of the (4*R*) and (4*S*)-epimers. The NAL crystal structures may be used to evaluate whether there are any structural differences between complexes of fluoropyruvate and complexes of pyruvate, however further QM/MM modelling studies would be required to evaluate the significance of the differences in electronic properties between pyruvate and fluoropyruvate.

4.5.1 Evaluation of the predicted diastereoselectivity of NAL variants at the fluorine-bearing chiral centre

At the beginning of this Chapter (Section 4.1.2), it was predicted that in the NAL-catalysed reactions of the aldehyde analogues and fluoropyruvate, the diastereomers with (3*R*) configuration would be formed preferentially. These

predictions were based on the crystal structure of fluoropyruvate in complex with NAL from *S. aureus*,⁶³ which showed the fluorine preferentially forms the (Z)-enamine and the QM/MM modelling studies which showed that Y137 is responsible for proton transfer⁵⁷ and is positioned above the "top" face of the Schiff-base (Figure 4.21).

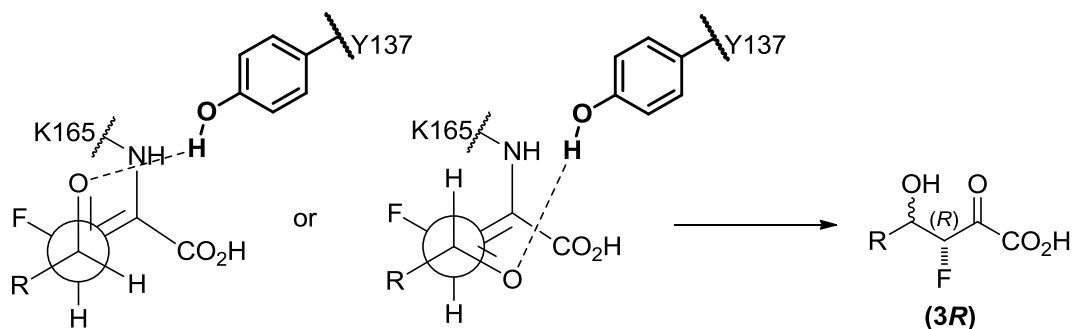


Figure 4.21 - Schematic representation of the aldehyde being attacked by the "top" face of the (Z)-fluoroenamine. The Y137, which is responsible for mediating proton transfer, is above the "top" face of the Schiff-base complex. The reaction products therefore have the (3R) configuration.

Chart 4.7 shows the (3R) versus (3S) selectivity observed for each of the NAL variant catalysed reaction of the aldehyde analogues and fluoropyruvate under kinetic control. In the vast majority of the experiments, the (3R)-epimers were seen as the major products, agreeing with the predictions made based on the structural and computational evidence. The only enzyme-substrate combination which goes against the expected C-3 selectivity is the NAL E192N/T167G catalysed reaction of **ent-AHOB**, however the NAL E192N/T167G variant is very inactive towards fluoropyruvate.

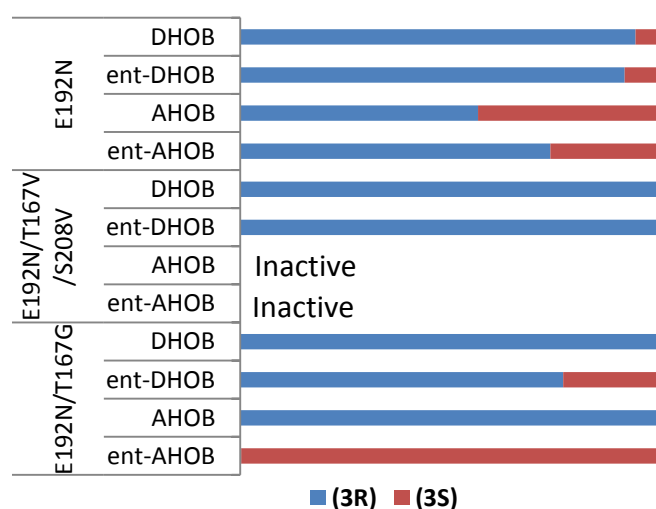


Chart 4.7 - Representation of the ratio of products with (3R):(3S) configurations in the reactions between the aldehyde analogues and fluoropyruvate catalysed by NAL variants.

While in most cases, the (3*R*)-epimers were observed as the major products of the NAL variant-catalysed reactions of the aldehyde analogues and fluoropyruvate, there were some examples in which the (3*S*)-epimers were observed. However, were these products the result of reaction with the "bottom" face of the enamine, or reaction with the (*E*)-enamine? Figure 4.22 shows the crystal structure of the NAL E192N variant in complex with the **THB** inhibitor.⁶⁶ From the surface view, it is possible to clearly see the cavity into which the inhibitor/aldehyde fits, and at the base of that pocket, the enamine is visible with the "top" face presented towards the cavity. Furthermore, the Y137 (gold) residue, which is believed to be responsible for proton transfer to the aldehyde oxygen, and the T167 (lilac) residue, which is believed to form a hydrogen bond with the aldehyde oxygen (and is therefore important in substrate recognition),⁵⁷ are both positioned above the "top" face of the enamine. From these observations it can be concluded that the aldehyde cannot be attacked by the "bottom" face of the enamine so the experiments in which the (3*S*)-epimers were observed resulted from attack from the "top" face of the (*E*)-enamine.

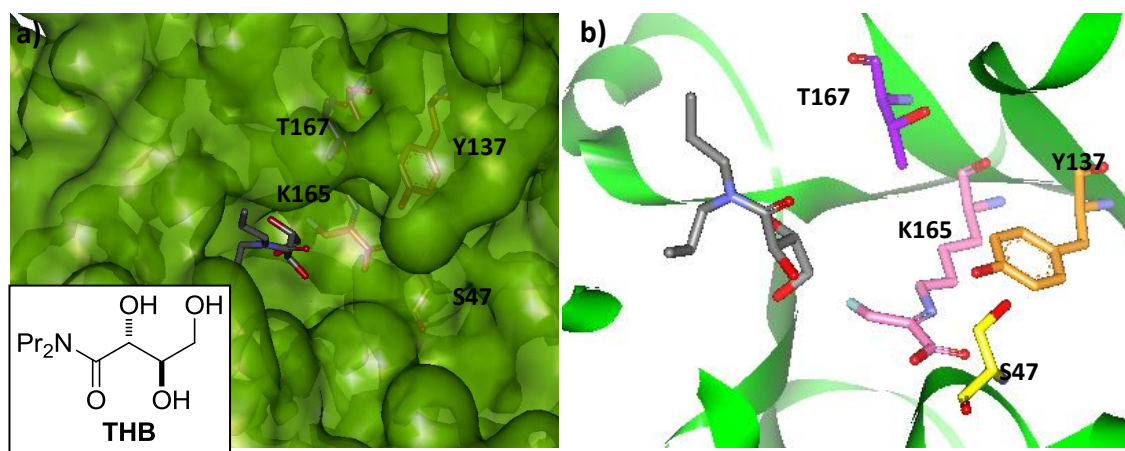


Figure 4.22 - Crystal structure of NAL E192N in complex with the THB inhibitor (PDB 2WPB)⁶⁶ (K165/fluoropyruvate complex superimposed from the crystal structure of wild-type NAL from *S. aureus*)⁶³. The Y137 (gold), S47 (yellow) and T167 (lilac) residues, which were predicted to be important in aldehyde recognition and catalysis, are all positioned above the "top" of the K165 Schiff-base complex (pink). Furthermore, the shape of the binding pocket meant that the aldehyde entered the binding pocket onto the "top" of the enamine. a) Surface view shows the shape of the binding pocket and the "top" face of the enamine presented towards the cavity. b) Ribbon view shows more clearly the relative positions of the key catalytic residues and the K165 Schiff-base complex.

In most cases, switching enantiomeric series did not change the selectivity at C-3 of the NAL variants and generally the (3*R*)-epimers were observed. The exception was the NAL E192N/T167G-catalysed reaction of *ent*-AHOB, which gave the (3*S*)-epimer, however the measured activity was very poor. Switching enantiomeric series

significantly decreased the activity of NAL variants, which may be due to binding efficiency. The enantiomer of **THB** has never been studied but it may be that it does not bind efficiently and is therefore is a poor inhibitor in comparison with **THB**.

4.5.2 Structural evidence for reduced activity of the alternative donor

Switching from pyruvate to fluoropyruvate results in a drop in activity of the NAL variants in the reactions of the alternative substrates (Section 4.4.1) but also wild-type NAL in the reaction with ManNAc.⁵⁷ NAL from *S. aureus* (saNAL) has been crystallised in complex with fluoropyruvate.⁶³ The saNAL is structurally very similar to the NAL from *E. coli* (ecNAL) (RMSD of 2.717 Å) which has been used throughout this thesis, so the observations in the crystal structures of saNAL are highly relevant to ecNAL. In order to rationalise the decrease in activity, it is important to know if switching from pyruvate to fluoropyruvate disrupts the local environment of the NAL active site.

Figure 4.23 shows two crystal structures of wild-type saNAL superimposed, one in complex with pyruvate⁸⁸ (pink) and one in complex with fluoropyruvate⁶³ (cyan). This comparison was used to look for any differences in the overall structure of the protein caused by changing the donor from pyruvate to fluoropyruvate. Figure 4.23a shows the ribbon-type representation of the backbone of one subunit of saNAL. The backbone superimposes closely (RMSD of only 0.322 Å), so changing the donor apparently makes little difference to the tertiary structure of the protein. Figure 4.23b shows just the active-site, in particular the Schiff-base complex between K165 and the donor. Directed evolution identified T167 and S208 as important residues in control of configuration⁶⁷ and the QM/MM modelling studies identified Y137, S47 and T167 as residues important in catalysis.⁵⁷ As can be seen from the superimposed structures, there is very little difference in the relative positions of these key residues in the active-site and in particular, the position of the Schiff-base complex does not change significantly. Therefore, it is likely that the lower activity is brought about by the enamine of fluoropyruvate being a poor nucleophile in comparison to the enamine of pyruvate due to the electronegative character of fluorine.

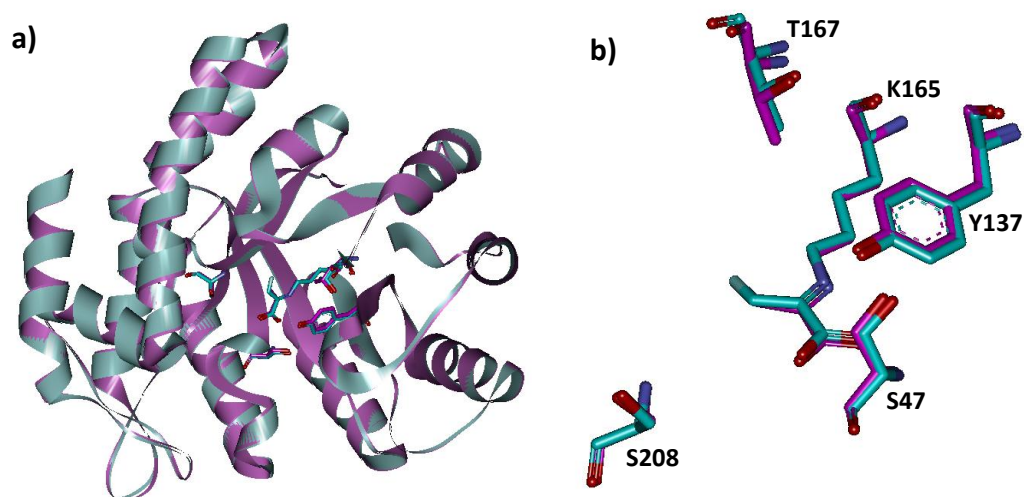


Figure 4.23 - Overlaid crystal structures of wild-type NAL from *S. aureus* (saNAL) in complex with pyruvate (pink, PDB 4AH7)⁸⁸ and fluoropyruvate (cyan).⁶³ a) Ribbon view shows the overall protein structure of the saNAL is the same regardless of whether pyruvate or fluoropyruvate is bound, i.e. the introduction of the unnatural fluorinated ligand in place of the natural ligand has no effect on the tertiary structure of saNAL. b) Active site of saNAL showing the residues known to be important in catalysis and stereocontrol and the Schiff-base complex. The residues and the Schiff-base complex overlay closely, showing that in terms of the active-site geometry, introduction of the unnatural-fluorinated ligand is only very subtly different to the natural ligand.

4.5.3 Structural evidence for changes in selectivity of the alternative donor

In the reaction between **DHOB** and pyruvate, the product resulting from attack of the *si*-face of the aldehyde is the major product, however in the reaction between **DHOB** and fluoropyruvate, the product resulting from the attack of the *re*-face of the aldehyde is the major product. The binding mode of the aldehyde is known to be important in dictating the C-4 selectivity in the NAL-catalysed reaction.⁵⁷ In order to look into potential structural differences in the active-site geometry in greater detail, the crystal structure of wild-type saNAL in complex with fluoropyruvate (cyan)⁶³ was superimposed with the crystal structure of ecNAL E192N variant in complex with pyruvate and the **THB** inhibitor⁶⁶ (pink) in the major (Figure 4.24a) and minor (Figure 4.24b) binding modes. The key residues again appear to have very similar relative positions in the structure with pyruvate (pink) and the structure with fluoropyruvate (cyan), and there does not appear to be any significant difference in the positions of the key residues between the two binding modes. The differences in selectivity between pyruvate and fluoropyruvate most likely occur as a result of the electronic properties of fluoropyruvate, which may have a profound effect on the energy barriers to the transition states leading to the two C-4 epimers.

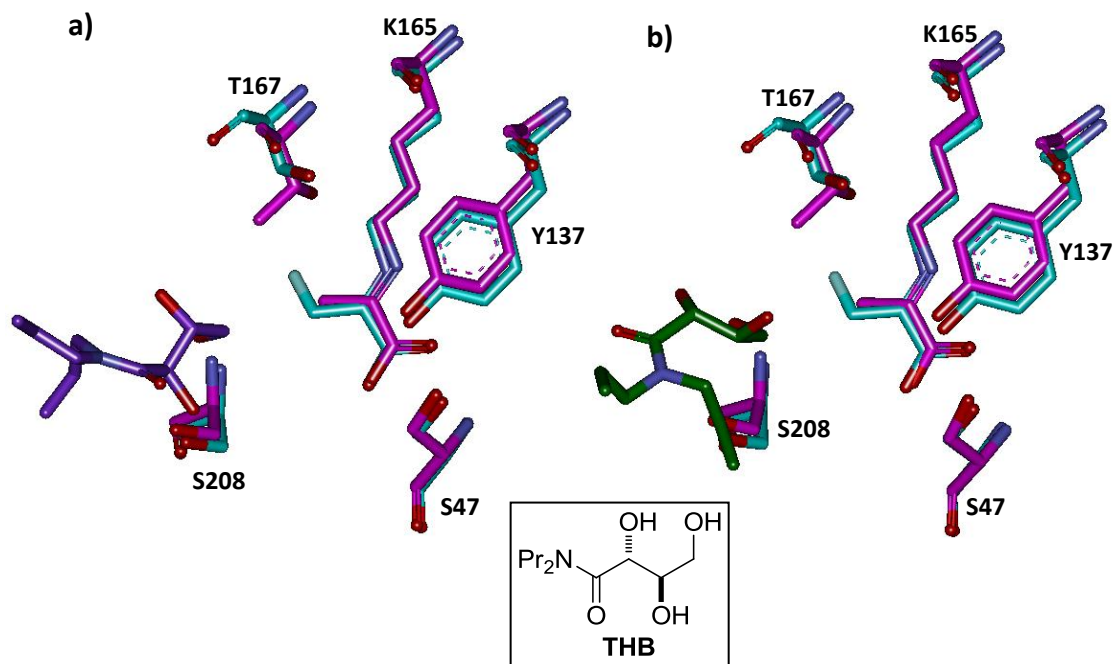


Figure 4.24 - Overlaid crystal structures of wild-type NAL from *S. aureus* NAL (saNAL) in complex with fluoropyruvate⁶³ (cyan) and NAL E192N variant from *E. coli* (ecNAL) in complex with pyruvate bound to the THB inhibitor (pink, PDB 2WPB).⁶⁶ The positions of the important catalytic residues are only subtly different between the two structures, and there is no difference between the relative positions of the residues in the two binding modes of the THB inhibitor. There is no evidence that the possible binding modes of the aldehyde should be any different in the case of reactions of fluoropyruvate compared to the reactions of pyruvate. a) Major binding mode of the THB inhibitor (purple) b) Minor binding mode of the THB inhibitor (green).

In Section 3.3.1, it was reasoned that the NAL E192N-catalysed reaction between **AHOB** and pyruvate was selective for the product resulting from *si*-face attack of the aldehyde because **AHOB** was unable to adopt the major binding mode seen in the crystal structure of the **THB** inhibitor bound to NAL E192N. Since the shape of the binding pocket was unchanged by changing the donor from pyruvate to fluoropyruvate, the argument that **AHOB** was more limited in terms of the binding modes it can adopt was equally valid in this case. Regardless of whether the donor used in the reaction is pyruvate or fluoropyruvate, the C-4 selectivity in the NAL catalysed reactions of **AHOB** was unchanged. This provides some evidence that the initial binding mode is still important in determining diastereoselectivity whether the donor is pyruvate or fluoropyruvate.

Chapter 5 Conclusions and future outlook

5.1 Overview and conclusions

This work primarily sought to evaluate the potential value of NAL variants in the synthesis of fluorinated analogues of *N*-acetyl neuraminic acid. This has been achieved by synthesis of a series of aldehyde analogues which have been used in the NAL variant-catalysed reaction with fluoropyruvate. The products were analysed by ^{19}F NMR spectroscopy. Two-dimensional $^1\text{H}/^{19}\text{F}$ experiments were used in order to aid characterisation of the most complex reaction products.

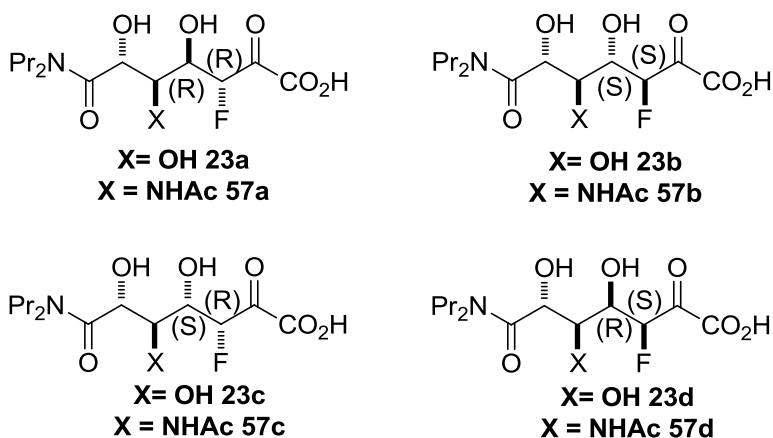
Chapter 2 outlined the development of a new synthetic route to access the new aldehyde substrate **AHOB**, which was used to further probe the activity and selectivity of the NAL variants. The route used to access **AHOB** was more modular in its approach compared to the previously developed route employed in the synthesis of **DHOB**.⁶⁵ The new route utilising the lactone **33** could be modified to access further potential NAL substrates for example by utilising different reaction of the lactone **33**^{72, 80, 81, 89} or by introducing different functionalities later in the synthesis.

Chapter 3 described the evaluation of the NAL variant-catalysed reactions of the new aldehyde **AHOB** in reaction with pyruvate compared to **DHOB**. It was found that while **AHOB** is significantly less active than **DHOB**, the selectivity at C-4 is greatly improved with only the product resulting from attack of the *si*-face of the aldehyde (the (4*S*)-epimer) observed. The crystal structure of NAL E192N in complex with the **THB** inhibitor⁶⁶ provided evidence that the selectivity may occur as a result of the **AHOB** adopting a binding mode similar to the minor binding mode of **DHOB**, which was found by QM/MM modelling studies to favour the formation of the (4*S*)-epimer.⁵⁷ Furthermore, the NAL E192N/T167V/S208V variant, which directs attack onto the *re*-face of **DHOB**,⁶⁷ was found to be inactive towards **AHOB**, which may provide some evidence of the mechanism of selectivity of the NAL variants, E192N/T167V/S208V and E192N/T167G.

Chapter 5 - Conclusions and future outlook

Chapter 4 described the evaluation of the activity and selectivity of the NAL variant-catalysed reactions of the aldehyde analogues and fluoropyruvate. The activity of the NAL variants towards fluoropyruvate was found to be lower compared to pyruvate. The crystal structure of saNAL⁶³ provided no evidence which may explain this loss of activity, therefore it was concluded that the drop in activity was due to the enamine formed from fluoropyruvate being a poor nucleophile. The selectivity at the C-3 position was found to be controlled by the preference for the fluoropyruvate-K165 enamine complex to adopt the (*Z*)-configuration,⁵⁷ which may be due to the *gauche*-effect.³⁵ The selectivity at the C-4 position was predicted to be controlled partially by the initial binding mode as evident by the observation that the *si*-face of **AHOB**, which is predicted to be restricted in terms of the binding modes it can adopt, is always attacked regardless of the donor. The C-4 selectivity of the **DHOB** reaction catalysed by NAL E192N switched with fluoropyruvate and was lost in the reaction catalysed by NAL E192N/T167G, which may be due to differences in the electronic properties of fluoropyruvate, resulting in changes in the energy profile of the reactions leading to the (*4R*) and (*4S*)-epimers.

In conclusion, the work within this thesis has demonstrated that NAL variants may be used in the synthesis of fluorinated analogues of Neu5Ac with high levels of stereocontrol. The most promising examples, which may be used as a starting point for future development are outlined in Table 5.1. The examples were chosen based on superior enzyme activity (particularly in the case of entry 1), and in the cases of entries 3 and 4, high levels of stereocontrol. However, further development is required in order to improve the activity of the NAL variants towards reactions of fluoropyruvate, for example by further directed evolution studies.

Table 5.1 - Summary of NAL-variant catalysed reaction between the aldehyde variants and fluoropyruvate which exhibited the greatest activity and diastereoselectivity.

Entry	NAL variant	Aldehyde	Specific activity ^a /nmolmin ⁻¹ nmol ⁻¹	D.r (a:b:c:d) ^b
1	E192N	DHOB	9.12	41:0:52:7
2	E192N	AHOB	1.05	56:0:44:0
3	E192N	<i>ent</i> -DHOB	0.46	9.5:0:0:90.5
4	E192N/T167V/S208V	DHOB	0.56	0:0:100:0

a) Based on the activity calculated from the initial rate of the forward reaction (Section 4.4.1). b) Based on diastereoselectivity under kinetic control (Section 4.4.2)

This work has also revealed some interesting insights into the mechanism of the C-4 selectivity of the NAL variants and may have provided some evidence to validate the QM/MM modelling studies.⁵⁷ When the diastereoselective NAL variants (E192N/T167V/S208V and E192N/T167G) were evolved, the mechanism of C-4 selectivity was not understood⁶⁷ and the diastereoselective variants have been found to lose their activity and diastereoselectivity when the substrate was changed. This is an example of one of the limitations of directed evolution in that ultimately, "you get what you screen for"⁹⁰ and sometimes a bit more. The greater insight into the mechanism of stereocontrol of NAL, provided by the QM/MM modelling studies⁵⁷ and validated experimentally within this work, may be used to direct the development of improved diastereoselective NAL variants with broader substrate specificity.

5.2 Future outlook

5.2.1 Probing the proposed binding mode of new NAL substrates

The NAL E192N variant was found to only direct attack onto the *si*-face of **AHOB** regardless of the donor used. This was predicted to occur as a result of the binding mode of **AHOB** being more restricted in order to accommodate the *N*-acetyl group (Section 3.3.1). There is no crystallographic evidence to back up this hypothesis; however the basis for the proposed binding mode came from the crystal structure of the **THB** inhibitor bound in the active site of NAL E192N.⁶⁶ In order to evaluate the possible binding modes of **AHOB**, the *N*-acetyl group was built onto the **THB** inhibitor *in silico*, however if the modified inhibitor **56** was synthesised (Figure 5.1), it could be crystallised with NAL E192N in order to provide an experimental comparison to back up the predictions made within this thesis. Furthermore, it was hypothesised that, based on the interaction observed between the C-7 hydroxyl group of Neu5Ac⁵⁶ and the S208 residue, that the presence of a hydrogen-bond donor at position 208 may be important in stabilising the binding. If, in the crystal structure of the new inhibitor **56**, it was found that the distance between the equivalent hydrogen-bond acceptor and S208 was comparable to the distance measured in the wild-type NAL, this may provide evidence to explain the lack of activity observed in NAL E192N/T167V/S208V towards **AHOB**.

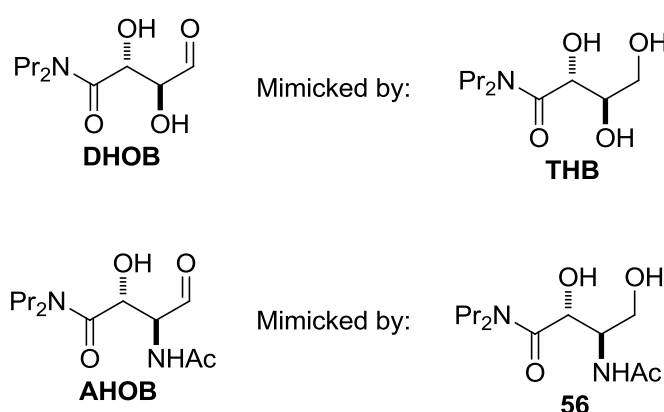


Figure 5.1 - Inhibitors related to substrates of the NAL variants.

5.2.2 Engineering NAL variants with greater activity towards fluorinated substrates

There is no evidence in the crystal structure of fluoropyruvate bound into the saNAL active-site⁶³ to suggest why the introduction of fluorine results in a reduction in enzyme activity. The reason for the reduction in activity may be related to the energy barrier to the reactive species or to the transition state of the carbon-carbon bond forming reaction. There are two complementary approaches which could be used in order to improve the activity of NAL variants towards fluoropyruvate.

The first approach would be to use QM/MM modelling studies, such as those used to study the reaction pathways of **DHOB** and pyruvate in NAL E192N.⁵⁷ This may provide some insight into the difference in energy barriers in the carbon-carbon bond forming reaction with the enamine of fluoropyruvate compared to the enamine of pyruvate.

The second approach is to use directed evolution to screen for NAL variants with greater activity towards fluoropyruvate.¹¹ If a fluoropyruvate-selective variant were to be identified, this variant may then be studied using the QM/MM modelling techniques in order to understand why the new variant is more active towards fluoropyruvate.

5.2.3 Optimisation of synthesis of *N*-acetyl neuraminic acid analogues

The yields achieved in the NAL variant-catalysed reactions were poor, particularly in the reaction of **AHOB**. It was seen that in the NAL E192N catalysed reaction of **AHOB** and fluoropyruvate, the conversion estimated by the ¹⁹F NMR spectrum before purification was much higher than the yield recorded after HPLC purification. Furthermore in the NAL E192N-catalysed reactions of **DHOB**, the reaction went to complete conversion as calculated from the ¹⁹F NMR spectrum, although this was not reflected in the isolated yields. It may therefore be possible with optimisation of the reaction conditions and the purification techniques to improve the isolated yields of products.

This may be complemented by work carried out to engineer NAL variants which are more active towards fluoropyruvate. The drop in activity resulting from switching from pyruvate to fluoropyruvate was around four-fold in the NAL E192N-catalysed reaction

of **AHOB**, so by improving the activity of NAL variants towards fluoropyruvate, the isolated yield of the fluorinated Neu5Ac analogues may be improved.

5.2.4 Design of new aldehyde substrates

Switching enantiomeric series of the aldehyde substrate resulted in a decrease in activity of the NAL variants of around 15-20 fold (Section 3.1.4 and 4.4.1).⁶⁹ It would however be interesting to know whether switching the configuration of just one of the stereocentres of the aldehyde would also result in a similar decrease in activity. It may be that switching the configuration of one of the stereocentres is tolerated better than switching the other. Two further pairs of enantiomers could be synthesised as shown in Figure 5.2. These *syn*-diastereomers could be subjected to in the NAL variants-catalysed reactions with pyruvate and fluoropyruvate in the same way as discussed for the *anti*-diastereomers in order to understand which NAL active-site interactions are the most important.

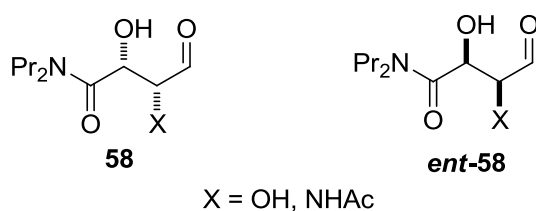


Figure 5.2 - Potential new NAL substrate which may be used to probe which position is most critical in control of diastereoselectivity and enzyme activity.

Chapter 6 Materials and Methods and Experimental

6.1 Biological Materials and Methods

6.1.1 Buffers

The buffers used throughout this thesis are outlined in Table 6.1. Unless otherwise stated, the buffer components were dissolved in deionised water. The pH was adjusted by the addition of aqueous hydrochloric acid or sodium hydroxide.

Table 6.1- Buffers used for protein purification, storage and enzyme catalysed reactions.

Buffer/pH	Component	Concentration
Washing - pH 7.4	Tris.HCl	50 mM
	Imidazole	20 mM
	Sodium chloride	0.5 M
Elution - pH 7.4	Tris.HCl	50 mM
	Imidazole	0.5 M
	Sodium chloride	0.5 M
Dialysis - Tris.HCl - pH 7.4	Tris. HCl	50 mM
	Sodium chloride	50 mM
Dialysis - Ammonium acetate - pH 7.4	Ammonium acetate	20 mM
Deuterated sodium phosphate - pH 7.4	Disodium hydrogen phosphate	15.5 mM
	Monosodium dihydrogen phosphate	4.5 mM
	Sodium chloride	20 mM
	Deuterium oxide	-

6.1.1.1 Preparation of deuterated 20 mM sodium phosphate buffer:

Deuterated buffer was prepared by initially preparing a 50 ml solution of 20 mM sodium phosphate buffer pH 7.4 (see Table 6.1) in water, which was then concentrated *in vacuo*. The residue was then dissolved in deuterium oxide (20 ml) and concentrated *in vacuo*. The process of re-dissolving in deuterium oxide and concentrating the residue was repeated a total of 5 times. The residue was then dissolved in deuterium oxide to a total volume of 50 ml.

6.1.2 Biological equipment

6.1.2.1 2×TY Bacterial growth medium and bacterial strains and plasmids

Bacterial cultures were grown in 2×TY medium. One litre of 2×TY medium contains 16 g tryptone, 10 g yeast extract and 5 g NaCl. The p*KnanA*-His6 plasmid, encoding NAL⁶⁴ was used and the bacterial strain used for high level protein expression was *E. coli* BL21 (DE3) (B F– *dcm ompT hsdS*(rB– mB–) *gal* λ(DE3)), purchased from Agilent Technologies, Cheshire, UK. The NAL variants were provided by Adam Daniels.⁵⁷

6.1.2.2 Enzymes

L-Lactate dehydrogenase from rabbit muscle was purchased from Roche, Mannheim, Germany.

6.1.2.3 Chromatographic media

Chelating Sepharose Fast Flow™ resin charged with Ni²⁺ was used for purification of His-tagged NAL and was purchased from Amersham Biosciences, Buckinghamshire, UK. Resins were stored in ethanol in 50 ml Falcon tubes without Ni²⁺ bound and were activated by decanting off the ethanol, washing with water then washing buffer (see Table 6.1). A 0.2 M NiCl₂ aqueous solution was poured onto the resin which was placed on a roller at 4 °C for 1 hour. The NiCl₂ solution was decanted and the Ni²⁺-activated resin was washed twice with water then twice with washing buffer.

6.1.2.4 Aseptic technique

Standard aseptic techniques were used throughout. Sterilisation of media and heat resistant materials was carried out using an autoclave at 110 °C. Heat labile solutions were sterilised by filtration through 0.22 µm MiniSart® filters (Sartorius AG, Goettingen, Germany).

6.1.2.5 Determination of pH

The pH of buffer solutions was determined using a Jenway 3020 pH meter, calibrated according to the manufacturer's instructions.

6.1.2.6 Spectrophotometry

Absorbances were measured using a Kontron Instruments UVIKON 930 spectrophotometer.

6.1.2.7 Centrifugation

Centrifugation was performed using a Beckman Coulter Avanti® J-26 XP Series high-performance centrifuge. Unless otherwise stated, centrifugation was performed at 4 °C.

6.1.2.8 Cell lysis

Cell lysis was carried out using a cell disruptor supplied by Constant Cell Disruption System, Nothants UK. The cells were lysed at 20 kpsi.

6.1.2.9 Dialysis

NAL samples were dialysed against 50-100 times the volume of the relevant buffer for two 8-16 hr periods at 4 °C. Dialysis tubing (12-14 kDa molecular weight cut-off) was purchased from Medicell International Ltd., London, UK.

6.1.2.10 Concentrating NAL

Concentration of NAL solutions were carried out using 15 ml centrifuge filters (Regenerated cellulose 10 000 NMWL) purchased from Amicon Ultra – IS. Centrifuge filters were prepared by washing with water, followed by centrifugation (2187g, 10 min) then three times with buffer (depending on which buffer the protein to be concentrated is dissolved into) followed by centrifugation (2187g, 10 min). The protein solution was then transferred to the filter and centrifuged (2187g) until the required volume/concentration was achieved.

6.1.3 Purification of His Tagged NAL

E. coli cells expressing the NAL E192N mutant⁸⁵ (see Section 6.1.2.1) were grown in day cultures containing 5 ml 2xTY media, 5µl glycerol solution containing the *E. coli* cells and 5 µl of 100 mg/ml ampicillin solution for 6-8 hr at 37 °C. Day cultures were then transferred to night cultures, which were grown at 37 °C in 2xTY media

Chapter 6 - Materials and Methods and Experimental

supplemented with 50 µg/ml ampicillin and 0.1 mM IPTG. The cells were harvested by centrifugation (9 000g, 20 min) and the pellet was re-suspended in washing buffer (see Table 6.1) using a homogeniser. The cells were lysed and the cell debris was collected by centrifugation (30 000g, 45 min). The supernatant was loaded onto chelating sepharose resin (pre-equilibrated with the wash buffer, see Section 6.1.2.3), in a 50 ml Falcon tube. The suspension was placed on a roller for 1 h. The suspension was then centrifuged (4000g, 5 min, 4 °C) and the supernatant was removed; washing buffer (30 ml) was added to the resin and the suspension placed on a roller for 15 mins followed by centrifugation (4000g, 5 min). Contaminating proteins were removed by washing the resin a further 3 times with washing buffer (roll for 15 min, followed by centrifugation at 4000g for 5 min). Elution buffer (see Table 6.1) (30 ml) was added to the resin and placed on a roller for 1 hr. The suspension was centrifuged (4000g, 5 min) and the eluted His-tagged NAL enzyme dissolved in the supernatant was decanted from the resin. The resin was then washed for a second time with elution buffer and rolled (15 mins) followed by centrifugation (4000g, 5 min) and the supernatant was collected. The eluted NAL was then dialysed (12 h, 4 °C) into Tris.HCl pH 7.4 dialysis buffer (see Table 6.1 and Section 6.1.2.9). The dialysis tubes containing eluted NAL were then transferred to fresh Tris.HCl pH 7.4 dialysis buffer and left to dialyse (4 h, 4 °C). The dialysed solution was then sterile filtered into Falcon tubes and stored at 4 °C. For longer-term storage, the NAL was dialysed into ammonium acetate buffer (see Table 6.1) and freeze-dried. Freeze-dried protein was re-dissolved into a suitable buffer depending on the experiment required.

6.1.4 SDS-PAGE

Protein purity was determined by SDS page. The composition of the running gel and stacking gel are given in Table 6.2 and the buffers are given in Table 6.3. The ladder was provided by Fermentas. Protein samples were mixed with sample buffer (1:1), heated to 100 °C for 3 min before loading onto the gel (20 µl). The gel was stained (methanol (50% v/v), acetic acid (10% v/v), Coomassie Brilliant Blue (0.25% v/v) and water (39.75% v/v)) and destained (methanol (50% v/v), acetic acid (10% v/v), and water (40% v/v)).

Table 6.2– Composition of gels for SDS-PAGE

Gel	Component	Quantity (μl)
Running	Acrylamide (30%)	7500
	1.5 M Tris-HCl	3750
	SDS (10%)	150
	Water	3500
	APS (Ammonium persulfate) (50 mg in 200 μl) (25%)	50
	TEMED (Tetramethylethylenediamine)	5
	Acrylamide (30%)	625
Stacking	1.5 M Tris-HCl	625
	SDS (10%)	50
	Water	3650
	APS (Ammonium persulfate) (50 mg in 200 μl) (25%)	50
	TEMED (Tetramethylethylenediamine)	5

Table 6.3 - SDS buffers

Buffer	Component	Quantity
2 × SDS sample buffer	Dithiothreitol	154 mg
	10% (w/v) SDS	2.0 ml
	Glycerol	1.0 ml
	1 M Tris.HCl (pH 6.8)	170 ml
	Water	1.63 ml
	0.2% (w/v) bromophenol blue	200 μl
SDS running buffer	Tris.HCl	3.0 g
	Glycine	14.4 g
	SDS	1.0 g
	β-mercaptoethanol	0.14 ml
	water	1000 ml

6.1.5 Measuring concentration of NAL

Concentration was determined by transferring 900 μl 100 mM Tris.HCl buffer (pH 7.4) into a 1 ml quartz cuvette (path length 1 cm) as a blank to calibrate the spectrometer. 100 μl dialysed NAL solution was added to the buffer and the

Chapter 6 - Materials and Methods and Experimental

absorbance measured at 280 nm. The extinction coefficient of His₆-tagged NAL is 24870 M⁻¹cm⁻¹,⁹¹ which according to the Beer-Lambert Law ($A=\epsilon cl$) gives a protein concentration of 1 mg/ml when $A_{280} = 0.743$.

6.1.6 Measuring single point activity of NAL

Activity was measured using the reverse-coupled assay by monitoring disappearance over 1 minute of NADH⁺ by UV-Vis spectroscopy at a wavelength of 340 nm.^{64, 85} 50 mM Tris.HCl buffer (pH 7.4) was used as a blank. To 50 mM Tris.HCl buffer (sufficient to make the final volume 1000μl) was added a solution of substrate (of known concentration in 50 mM Tris.HCl buffer, pH 7.4), NADH⁺ (0.2 mM), LDH (2 μl) and finally a solution of NAL (of known concentration in 50 mM Tris.HCl, pH 7.4). The final concentration of substrate and enzyme in the cuvette were 1.0 mM and 0.06 mg/ml respectively.

6.2 General experimental

Unless otherwise stated, all non-aqueous reactions were carried out under a nitrogen atmosphere. Solvents were evaporated under reduced pressure using a Büchi rotary evaporator attached to a vaccubrand PC2001 Vario diaphragm pump with the water bath set at 40 °C. Flash column chromatography was carried out using silica (35-70µm) particles and thin layer chromatography was carried out using pre-coated aluminium plates. Ion exchange chromatography was carried out using Dowex® 1×8 200-400 resin or Discovery SAX or SCX pre-packed cartridges. Ozone for ozonolysis was generated using a Welsbach generator at 0.4-0.6 psi. The machine was purged for at least 15 min before and after use with oxygen gas (0.4-0.6 psi) and the reaction mixture was also purged with oxygen (0.4-0.6 psi) before and after ozonolysis. Starch-iodide paper was used to test that the quenching reaction of trioxolane intermediate by Me₂S has gone to completion. Unless otherwise stated, petrol refers to petroleum ether (b.p. 40-60 °C) and ether refers to diethyl ether. NMR chemical shifts are quoted in parts per million (ppm) downfield of trimethylsilane and *J* coupling values are quoted in hertz (Hz). NMR spectra were recorded on Bruker Avance DPX 300, Avance 500 or DRX 500 spectrophotometer and the spectra were processed using MestraReNova NMR processing software. Semi prep-HPLC of **23a**, **23c** and *ent*-**23d** was carried out on an Agilent Technologies 1200 series instrument. Optimum conditions for separation were found to be reverse-phase C18 Hyperclone column with a gradient elution 0:100 → 20:80 acetonitrile-TFA (0.1% v/v):water-TFA (0.1% v/v) over 30 min, a flow rate of 3.0 ml/min and an injection volume of 20 µl of a 23 -25 mg/ml of enzyme reactions product in water. Mass directed prep-HPLC was carried out by the University of Leeds HPLC services. HRMS was carried out by the University of Leeds Mass Spectrometer services using a Bruker MicrOTOF mass spectrometer. Melting points were recorded on a Reichert hot stage microscope and optical rotations (where provided) were recorded on a A.A-1000 Polarmeter or a Schmidt + Haensch Polartronic hr 532 polarmeter (units for $[\alpha]_D$ are 10⁻¹ deg cm² g⁻¹).

6.2.1 General method for ozonolysis

Unless otherwise stated, ozonolysis was carried out under the following conditions. The alkene was dissolved in methanol (0.1 mmol of alkene per 0.5 ml of MeOH), cooled to $-78\text{ }^{\circ}\text{C}$, purged with O_2 for at least 10 min and then exposed to ozone. Once a blue colour was observed, excess ozone was purged from the reaction with O_2 . Me_2S (0.15 ml per 0.1 mmol of alkene) was added and the reaction was allowed to stir under nitrogen until all peroxides were quenched (starch-iodide paper).

6.2.2 General method for monitoring NAL catalysed reactions by 500 MHz ^1H NMR spectroscopy

For each experiment 0.1 mmol of alkene was cleaved by standard ozonolysis conditions. After quenching, the solution was transferred to an NMR tube and concentrated by blowing nitrogen over the solution to remove all volatile components. The NMR tube was then placed in a drying tube on the high-vacuum line over-night to remove all trace of volatile contaminants. A 1 M solution of sodium pyruvate in 20 mM deuterated sodium phosphate buffer pH 7.4 (see Section 6.1.1.1) (200 μl , 0.2 mmol) was added followed by NAL in 20 mM deuterated sodium phosphate buffer pH 7.4 (500 μl). (NAL concentrations: E192N - 1.12 mg/ml, E192N/T167G - 1.59 mg/ml). The experiment was kept at room temperature and re-submitted for 500 MHz ^1H NMR spectroscopy initially at 1 h intervals for the first 7 h, then at 3-6 h intervals thereafter up to 36 h. Conversions were calculated by comparing the relative integrals of the product peaks to the aldehyde peaks such that when the aldehyde peaks were no longer visible in the NMR spectrum the reaction was assumed to have gone to completion.

6.2.3 General method for monitoring NAL catalysed reactions by 296 MHz ^{19}F NMR spectroscopy

For each experiment 0.1 mmol of alkene was cleaved by standard ozonolysis conditions. After quenching the solution was transferred to an NMR tube and concentrated by blowing nitrogen over the solution to remove all volatile components. The NMR tube was then placed in a drying tube on the high-vacuum line over-night to remove all trace of volatile contaminants. A 1 M solution of sodium fluoropyruvate in 50 mM Tris-HCl buffer pH 7.4 (20 μl , 0.02 mmol) was added followed by NAL in 50 mM

Chapter 6 - Materials and Methods and Experimental

Tris.HCl buffer pH 7.4 (980 μ l). (NAL concentrations: E192N - 1.00 mg/ml, E192N/T167V,S208V - 0.90 mg/ml, E192N/T167G - 1.82 mg/ml). A sealed capillary tube containing deuterium oxide was placed inside the NMR tube (Figure 6.1). The experiment was kept at room temperature and re-submitted for 296 MHz ^{19}F NMR spectroscopy initially at 1 h intervals for the first 7 h, then at 3-6 h intervals thereafter up to 36 h. Conversions were calculated by comparing the relative integrals of the product peaks to the fluoropyruvate peaks such that when the fluoropyruvate peaks were no longer visible in the NMR spectrum, the reaction was assumed to have gone to completion.

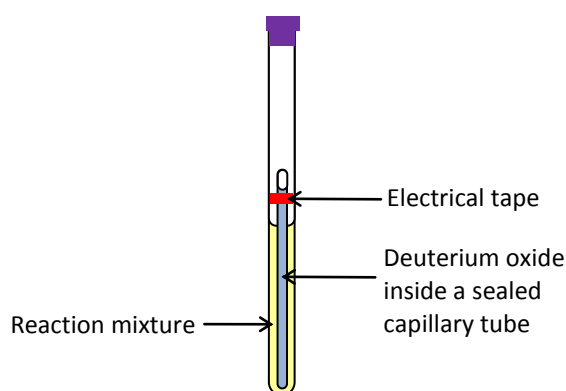
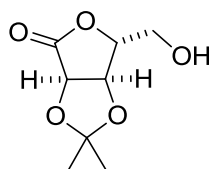


Figure 6.1 - NMR tube reaction set up for monitoring NAL-catalysed reactions by 296 MHz ^{19}F NMR. Deuterium oxide is required for the machine to lock onto the signal but sealing the D_2O inside a tube prevents it coming into contact with the reaction mixture. The electrical tape wrapped around the top of the capillary tube holds the tube in the centre of the NMR tube and prevents it from rattling.

6.3 Experimental methods and characterisation

2,3-*O*-Isopropylidene-D-ribo-1,4-lactone **27**⁶⁵

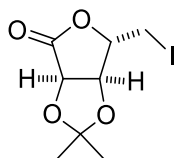


Concentrated sulfuric acid (4 ml) was added to a solution of D-ribo-1,4-lactone (4.80 g, 32.4 mmol) in acetone (250 ml) and stirred for 5 h 45 min. Solid sodium carbonate (20 g) was added and the solution was left to neutralise over night. The solution was dried (MgSO_4), filtered and the solvent removed *in vacuo* to give a crude product which was recrystallised from petrol–EtOAc to give the lactone **27**⁶⁵ (4.61 g, 76%) as colourless prisms; m.p. 136.5-138 $^\circ\text{C}$ (EtOAc–petrol) [lit. 137-139 $^\circ\text{C}$]; R_f : 0.72 (EtOAc);

Chapter 6 - Materials and Methods and Experimental

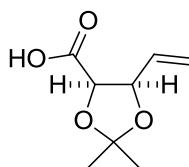
$[\alpha]_D^{24}$ -71.6 (c. 0.60 in chloroform) [lit. -66.0 (c. 1.0 in chloroform)]; δ_H (400 MHz; $CDCl_3$) 4.77 (1H, d, J 5.6, H-2), 4.72 (1H, d, J 5.6, H-3), 4.57 (1H, t, J 2.0, H-4), 3.99 (1H, dd, J 12.3 and 2.3, H-5_A), 3.74 (1H, dd, J 12.3 and 1.7, H-5_B), 1.98 (1H, s, OH), 1.41 (3H, s, Me_A), 1.32 (3H, s, Me_B); m/z (ES) $[MNa]^+$ 211.0 (100%, $[MNa]^+$).

5-Deoxy-5-iodo-2,3-O-isopropylidene-D-ribo-1,4-lactone **28**⁶⁵



Iodine (13.0 g, 51.0 mmol) was added to a solution of the lactone **27** (5.44 g, 24.0 mmol), imidazole (5.00 g, 73.0 mmol) and triphenylphosphine (18.0 g, 69.0 mmol) in dry toluene (100 ml) and stirred under nitrogen at 75 °C for 30 min. The reaction was quenched with aqueous sodium thiosulfate (50 ml of a 1 M solution) then extracted with ethyl acetate (3 × 150 ml) and the combined organic layers were washed with brine (100 ml), dried ($MgSO_4$), and the solvent removed *in vacuo* to give the crude product which was purified by flash column chromatography (gradient elution 5:95 → 50:50 EtOAc–petrol) to give the iodo-lactone **28**⁶⁵ (5.39g, 75%) as colourless needles; m.p. 95-96 °C (EtOAc–petrol) [lit. 89.0-91.0 °C]; R_f : 0.31 (4:1 petrol–EtOAc); $[\alpha]_D^{23}$ -27.2 (c. 1.00 in chloroform) [lit. -33.1 (c. 1.05 in chloroform)]; δ_H (300 MHz; $CDCl_3$) 4.94 (1H, d, J 6.0, 2-H), 4.59-4.54 (2H, m, 3-H and 4-H), 3.36 (2H, d, J 6.1, 5-H), 1.41 (3H, s, Me_A), 1.33 (3H, s, Me_B); HRMS Found: 320.9594, $[C_8H_{11}IO_4Na]^+$ requires 320.9600.

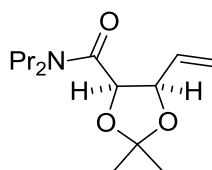
(2*R*, 3*R*)-2,3-O-Isopropylidene-pent-4-enoic acid **29**⁶⁵



Zinc/copper couple (9.32 g) was added to a solution of the iodo-lactone **28** (5.32 g, 18 mmol) in acetone–water (4:1) which was heated under reflux for 2 h. The reaction was cooled to room temperature then filtered through Celite®. The filtrate was evaporated under reduced pressure. The residue was dissolved in 97:3 $CHCl_3$ –formic acid (50 ml),

which was washed with brine (40 ml). The aqueous layer was then re-extracted with chloroform (3 × 50 ml). The combined organic phases were dried (MgSO₄) and the solvent removed *in vacuo* to give the acid **29**⁶⁵ (2.48 g, 81%) as a colourless oil; *R_F*: 0.6 (1:99 AcOH–EtOAc); $[\alpha]_D^{23}$ –13.6 (c. 1.00 in chloroform) [lit. –24.6 (c. 1.56 in chloroform)]; δ_H (300 MHz; CDCl₃) 5.80 (1H, ddd, *J* 17.1, 10.3 and 6.9, 4-H), 5.48 (1H, dd, *J* 17.1 and 1.1, 5-H_A), 5.33 (1H, d, *J* 10.4, 5-H_B), 4.86 (1H, app. t, *J* 7.2, 3-H), 4.71 (1H, d, *J* 7.4, 2-H), 1.64 (3H, s, Me_A), 1.43 (3H, s, Me_B).

(2*R*,3*R*)-2,3-*O*-Isopropylidene-pent-4-enoic acid dipropylamine **30⁶⁵**



Method 1

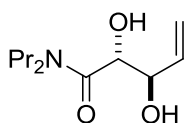
A solution of the acid **29** (0.20 g, 1.16 mmol), dipropylamine (0.24 ml, 2.32 mmol) and triethylamine (1.29 ml, 9.28 mmol) in dry DMF (20 ml) was added over 8 h to a solution of 2-chloro-1-methyl-pyridinium iodine (1.19 g, 4.64 mmol) in dry DMF (40 ml) at 85 °C. The solution was stirred for a further 8 h, cooled to room temperature and diluted with ethyl acetate (60 ml) and water (150 ml). The layers were separated, and the aqueous phase was extracted with ethyl acetate (3 × 50 ml) and the combined organic phases were washed with brine (3 × 100 ml) and aqueous HCl (50 ml, 0.5 M), the solvent removed *in vacuo* and the product was purified by flash column chromatography (petrol–EtOAc 4:1) to give the protected dipropylamide **30**⁶⁵ (0.26 g, 88%) as a pale yellow oil; *R_F*: 0.31 (2:1, petrol–EtOAc); $[\alpha]_D^{23}$ –36.0 (c. 2.0 in chloroform) [lit. –28.6 (c. 0.91 in chloroform)]; δ_H (500 MHz; CDCl₃) 5.80 (1H, ddd, *J* 17.2, 10.1 and 8.2, 4-H), 5.40 (1H, d, *J* 17.1, 5-H_A), 5.25 (1H, d, *J* 10.2, 5-H_B), 4.94 (1H, d, *J* 7.2, 3-H), 4.78 (1H, t, *J* 7.7, 2-H), 3.50 (3H, dt, *J* 13.3 and 7.8, propyl 1-H_A), 3.14–2.96 (3H, m, propyl 1-H_B and propyl 1-H₂), 1.67 (3H, s, Me_A), 1.63–1.48 (4H, m, 2 × propyl 2-H₂), 1.41 (3H, s, Me_B), 0.91 (3H, t, *J* 7.2, propyl 3-H_{3,A}), 0.88 (3H, t, *J* 7.2, propyl 3-H_{3,B}).

Method 2

Diisopropylethylamine (DIPEA) (0.85 ml, 11.6 mmol), HCTU (2.41 g, 5.81 mmol) and dipropylamine (0.43 ml, 5.7 mmol) were added to a solution of the acid **29** (0.90 g, 5.81 mmol) in dry DMF (50 ml) and stirred at room temperature for 18 h. The reaction was diluted with water (100 ml) and extracted with ethyl acetate (3 × 100 ml). The combined organic layers were washed with sat. aqueous sodium carbonate (2 × 50 ml) and brine (3 × 100 ml). Solvents were removed *in vacuo* and the crude product was purified by flash column chromatography (petrol–EtOAc (2:1) to give the protected diproylamide **30**⁶⁵ (0.43 g, 29%) as a pale yellow oil; Spectroscopically identical to that obtained previously.

Method 3

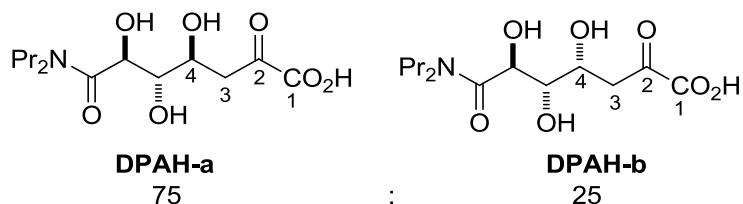
EDC (0.46 ml, 4.52 mmol), HOBt (0.60 g, 4.52 mmol) and dipropylamine (0.31 ml, 4.56 mmol) were added to a solution of the acid **29** in EtOAc (160 ml) and stirred for 16 h. The reaction mixture was washed with water (160 ml) and the aqueous layer was extracted with EtOAc (2 × 120 ml). Combined organic layers were dried (MgSO₄) and the solvent removed *in vacuo* and the residue was purified by flash chromatography (1:1 petrol–EtOAc) to give the protected diproylamide **30**⁶⁵ (0.48 g, 62%) as a pale yellow oil; Spectroscopically identical to that obtained previously.

(2R,3R)-2,3-Dihydroxy-N,N-dipropylpent-4-enamide **24⁶⁵**

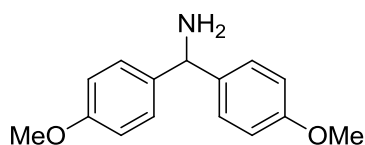
The protected diproylamine **30** (0.43 g, 1.68 mmol) was dissolved in a solution of 9:1 trifluoroacetic acid–water (34 ml) and swirled for 2 min, the solvents were then removed *in vacuo* and the residue was purified by flash column chromatography (60:40 petrol–ethyl acetate) to give the diol **24**⁶⁵ (0.30 g, 84%) as colourless needles; m.p. 78.6–79.8 °C (EtOAc–petrol) [lit. 77.4–79.1 (CH₂Cl₂)]; *R_F*: 0.17 (1:1, petrol–EtOAc); [α]_D²⁵ 22.2 (c. 0.90 in chloroform) [lit. 17.1 (c. 0.84 in chloroform)]; δ_{H} (300 MHz; CDCl₃) 5.81 (1H, ddd, *J* 17.1, 10.5 and 5.8, 4-H), 5.34 (1H, dt, *J* 17.2 and 1.5, 5-H_A), 5.25 (1H, dt, *J* 10.5 and 1.4, 5-H_B), 4.45 (1H, dd, *J* 8.8 and 4.1, 2-H), 4.23 (1H, ddd, *J* 9.6, 5.5 and 4.2,

3-H), 3.71 (1H, d, J 8.78, 2-OH), 3.65-3.52 (1H, m, propyl 1-H_A), 3.42-3.29 (1H, m, propyl 1-H_B), 3.22-3.10 (1H, m, propyl 1-H_C), 3.11-2.99 (1H, m, propyl 1-H_D), 3.06 (1H, d, J 9.34, 3-OH), 1.73-1.47 (4H, m, 2 × propyl 2-H₂), 0.94 (3H, t, J 7.4, propyl 3-H_{3,A}), 0.90 (3H, t, J 7.4, propyl 3-H_{3,B}); m/z (ES) [MNa]⁺ 238 (100%, [MNa]⁺).

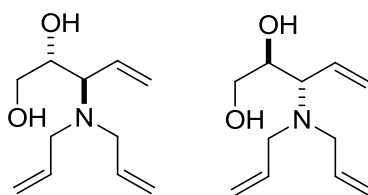
(4S,5R,6R) and (4R,5R,6R)-7-(dipropylamino)-4,5,6-trihydroxy-2,7-dioxoheptanoate DPAH⁶⁵



The diol **24** (220 mg, 1.02 mmol) was subjected to general ozonolysis conditions described previously. Methanol was removed *in vacuo* and the crude mixture was re-dissolved in 50 mM tris buffer (5.5 ml) to which sodium pyruvate (500 mg, 4.64 mmol) was added. The pH was adjusted to 7.4 by addition of NaOH (2 M) followed by addition of the NAL E192N variant (0.5 mg/ml in 50 mM tris buffer pH 7.4, 5 ml). The reaction was stirred for 24 hr then acidified to pH 3 with formic acid (2 M) and stirred for 30 min. The pH was then adjusted to 7.4 with NaOH (2 M) followed by the addition of Bakers' yeast (1.00 g) and the suspension was stirred for 16 h. The mixture was filtered through Celite® and the crude product was purified by Dowex® ion exchange (gradient elution 0 → 2 M formic acid in water) to give the sialic acid analogue **DPAH⁶⁵** (224 mg, 72%, (4S):(4R) 75:25) as a pale yellow glass; δ_{H} (500 MHz; D₂O) 4.58 (1H, d, J 9.6, 6-H), 3.95-3.87 (1H, m, 4-H), 3.60 (1H, t, J 9.5, 5-H), 3.46-3.28 (4H, m, 2 × propyl 1-H₂), 3.26-3.10 (4H, m, 2 × propyl 2-H₂), 2.18 (1H, dd, J 13.2 and 5.0, 3-H_A), 1.81 (1H, t, J 12.6, 3-H_B), 1.59-1.40 (6H, m, 2 × propyl 3-H₃); m/z (ES) [MH]⁺ 306.1 (100%, [MH]⁺). The characterisation data refers to the furanose ring form of the major diastereomer **DPAH-a**. See previous synthesis reports for full characterisation data for both diastereomers and both major and minor anomers and ring forms. The ratio of equilibrium species for the two diastereomers had previously been determined by 500 MHz ¹H NMR spectroscopy: (4S)-epimer - 46:33:14:7 and (4R)-epimer - 73:11:9:7.⁶⁵

Di-*p*-anisylmethylamine **36a**⁹²

4-4'-dimethoxybenzophenone (5.02 g, 20.7 mmol) and ammonium formate (7.72 g, 112 mmol) were stirred under argon at 185 °C for 4 h. Anhydrous magnesium chloride (0.14 g, 1.44 mmol) and formamide (3.15 ml, 61.8 mmol) were added and stirred for a further 2 h at 185 °C. The mixture was cooled and diluted with dichloromethane (500 ml), washed with water (200 ml) and the solvent was removed *in vacuo*. The residue was dissolved in HCl–methanol (1 M HCl, 55 ml) and heated under reflux for 2 h. Methanol was removed *in vacuo* and the residue was dissolved in water (50 ml) and extracted with toluene (50 ml). The aqueous fraction was made alkaline by the addition of NaOH (4 M) and extracted with toluene (3 × 50 ml). Combined organic layers were dried (MgSO₄) and the solvent removed *in vacuo*. Purification by recrystallisation from diethyl ether gave the amine **36a**⁹² as pale yellow crystals (2.38 g, 47%). m.p. 55.5–57.5 °C (diethyl ether) [lit. 59.5–60.0 °C]; *R_F*: 0.38 (10:90, MeOH–CHCl₃); δ_H (500 MHz; CDCl₃) 7.27 (4H, d, *J* 7.3, 2 × aryl 1-H), 6.84 (4H, d, *J* 6.8, 2 × aryl 2-H), 5.13 (1H, s, NH₂-CH), 3.77 (6H, s, 2 × OMe), 1.71 (2H, s, NH₂); HRMS Found: 227.1072, [C₁₅H₁₅O₂]⁺ requires 227.1067.

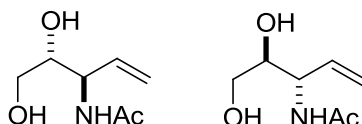
(2*R*,3*R*)- and (2*S*,3*S*)-3-[bis(prop-2-en-1-yl)amino]pent-4-en-1,2-diol **31b**

Vinylboronic acid dibutylester (0.82 ml, 3.77 mmol) was added to a solution of DL-glyceraldehyde (500 mg, 5.55 mmol) and diallyl amine (0.69 ml, 5.55 mmol) in 9:1 CH₂Cl₂–HFIP (30 ml) which had been heated to reflux. The mixture was heated under reflux for 18 h before being cooled to room temperature and the solvent removed *in vacuo* and the residue was purified by flash column chromatography (10:90 MeOH–CHCl₃) to give the *diallyl amine* **31b** (515 mg, 71%, d.r. >98:<2) as a yellow oil; *R_F*: 0.43 (10:90 MeOH–CH₂Cl₂); δ_H (500 MHz; MeOH) 5.89–5.78 (3H, m, 4-H and 2 × allyl 2-H),

Chapter 6 - Materials and Methods and Experimental

5.38 (1H, dd, J 10.3 and 2.1, 5-H_A), 5.25-5.13 (5H, m, 5-H_B and 2 × allyl 3-H), 3.83 (1H, dd, J 12.4 and 6.2, 2-H), 3.70 (1H, dd, J 11.0 and 5.6, 1-H_A), 3.54 (1H, dd, J 11.0 and 6.4, 1-H_B), 3.40 (2H, dd, J 14.2 and 4.5, 2 × allyl 1-H_A), 3.22 (1H, dd, J 9.1 and 7.7, 3-H), 2.94 (2H, dd, J 14.2 and 8.0, 2 × allyl 1-H_B); m/z (ES) [MH]⁺ 198.1 (100%, [MH]⁺).

N-[(3*R*,4*R*)- and *N*-[(3*S*,4*S*)-4,5-Dihydroxypent-1-en-3-yl]acetamide **39**⁷⁵



Method 1

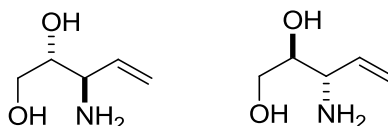
Vinylboronic acid dibutylester (0.44 ml, 2.00 mmol) was added to a solution of DL-glyceraldehyde (270 mg, 3.00 mmol) and the primary amine **36a** (740 mg, 3.00 mmol) in 9:1 CH₂Cl₂–HFIP (30 ml) which had been heated to reflux. The mixture heated under reflux for 3 days before being cooled to room temperature and the solvent removed *in vacuo* to give the intermediate amine **31a**. The residue was re-dissolved in 4:1 EtOH–H₂O (30 ml) to which TFA (1.3 ml) was added. This mixture was heated under reflux for 18 h before being cooled to room temperature and the solvents removed *in vacuo*. The residue was re-dissolved in MeOH (20 ml) to which NaHCO₃ (330 mg) and acetic anhydride (0.44 ml, 4.00 mmol) was added and the mixture was heated under reflux for 2 h. The mixture was cooled to room temperature, concentrated *in vacuo* and the residue purified by flash column chromatography (CH₂Cl₂–EtOH–NH₄OH 85:13:2) to give the diol **39**⁷⁵ (122 mg, 38%, d.r. >98:<2) as a pale cream amorphous solid; R_f : 0.14 (85:13:2, CH₂Cl₂–EtOH–NH₄OH); δ_H (500 MHz; CDCl₃) 8.09 (1H, s, NH), 5.95 (1H, ddd, J 17.2, 10.4 and 6.7, 2-H), 5.24 (2H, m, 1-H₂), 4.49 (1H, t, J 5.8, 3-H), 3.65 (1H, dd, J 10.8 and 5.3, 4-H), 3.57 (1H, dd, J 11.4 and 4.5, 5-H_A), 3.51 (1H, dd, J 11.4 and 6.4, 5-H_B), 2.01 (3H, s, acetyl CH₃); δ_C (75 MHz; CDCl₃) 171.3 (acetyl C=O), 134.4 (1-C), 117.8 (2-C), 73.5 (3-C), 62.9 (4-C), 53.9 (5-C), 23.3 (acetyl CH₃); m/z (ES) [MNa]⁺ 182 (100%, [MNa]⁺).

Method 2

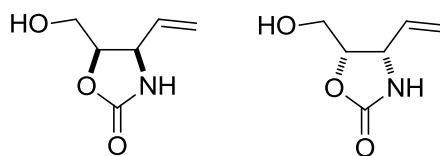
A solution of the diallylamine **31b** (295 mg, 1.5 mmol) in dry CH₂Cl₂ (10 ml) was added to a flask containing tetrakis(triphenylphosphine)palladium (34 mg, 0.03 mmol, 2

mol%) and *N, N'*-dimethylbarbituric acid (1.41 g, 9.00 mmol) which was heated to 35 °C and stirred under argon for 20 h, cooled to room temperature and concentrated *in vacuo*. The crude was dissolved in MeOH and NaHCO₃ (1.01 g, 12 mmol) and acetic anhydride (0.18 ml, 1.88 mmol) were added and the mixture heated under reflux for 1 h, cooled to room temperature, filtered and the filtrate was concentrated *in vacuo*. The crude residue was purified by flash column chromatography (CH₂Cl₂–EtOH–NH₄OH 85:13:2) to give the diol **39**⁷⁵ (224 mg, 91%) as a pale cream amorphous solid. spectroscopically identical to that obtained previously.

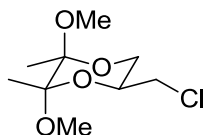
(2*S*,3*S*) and (2*R*,3*R*)-3-Aminopent-4-ene-1,2-diol **41**



The diallylamine **31b** (218 mg, 1.1 mmol) was dissolved in dry dichloromethane (10 ml) and transferred to a flame-dried flask containing tetrakis(triphenylphosphine) palladium (25 mg, 0.02 mmol) and *N, N'*-dimethylbarbituric acid (1.03 g, 6.6 mmol). The heterogeneous mixture was stirred at 30 °C for 20 h, the solvents were removed *in vacuo* and the crude mixture re-dissolved in methanol–water (2:1). HCl (2 M, 0.5 ml) was added and the mixture was purified by SCX ion exchange chromatography (5 g cartridge) eluting with methanol (50 ml) and NH₄OH (35 % v/v, 10 ml). NMR revealed a mixture of the fully and partially allyl deprotected amine, which were separated by flash column chromatography (CH₂Cl₂–EtOH–NH₄OH, 85:13:2) to give the *amine 41* (89 mg, 69%) as a yellow oil; *R_f*: 0.09 (85:13:2, CH₂Cl₂–EtOH–NH₄OH); δ_H (500 MHz; MeOH) 5.94 (1H, ddd, *J* 17.4, 10.4 and 7.3, 2-H), 5.24 (1H, dd, *J* 17.3 and 1.36, 1-H_B), 5.18 (1H, dd, *J* 10.4 and 1.0, 1-H_A), 3.63 (1H, dt, *J* 6.6 and 4.7, 4-H), 3.56 (2H, dd, *J* 5.8 and 1.7, 5-H₂), 3.40 (1H, dd, *J* 7.3 and 4.3, 3-H).

(4*R*,5*R*) and (4*S*,5*S*)-4-Ethenyl-5-(hydroxymethyl)-1,3-oxazolidin-2-one 42

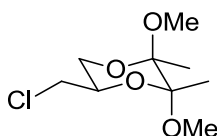
A solution of *p*-nitrophenyl chloroformate (615 mg, 3.05 mmol) in acetonitrile (1 ml) was added to a vigorously stirred solution of the amine **41** (143 mg, 1.22 mmol) and NaHCO₃ (512 mg, 6.1 mmol) in 2:1 water–acetonitrile (4 ml) at 0 °C and stirred for 12 h. The solvents were removed *in vacuo* and the remaining residue was extracted with methanol (3 × 20 ml), silica was added and the solvent removed *in vacuo* and the residue was loaded onto a column. (Gradient elution 1:99 MeOH–CHCl₃ → 10:90 MeOH–CHCl₃) to give the *oxazolidinone* **42** (112 mg, 64 %) as a colourless amorphous solid; *R_f*: 0.17 (9:1, CHCl₃–MeOH); δ_H (500 MHz; MeOH) 5.96 (1H, ddd, *J* 17.3, 10.3 and 7.2, 2-H), 5.37 (1H, dt, *J* 17.1 and 1.2, 1-H_B), 5.31 (1H, dt, *J* 10.3 and 1.1, 1-H_A), 4.74 (1H, ddd, *J* 8.6, 6.2 and 4.7, 4-H), 4.50 (1H, app. t, *J* 8.0, 3-H), 3.70 (2H, dd, *J* 5.4 and 2.4, 5-H); δ_C (75 MHz; MeOH) 161.6 (C=O), 134.6 (2-C), 119.3 (1-C), 81.4 (4-C), 61.8 (5-C), 58.2 (3-C); *m/z* (ES) [MNa]⁺ 166 (100%, [MNa]⁺); HRMS Found: 166.0491, [C₆H₉NO₃Na]⁺ requires 166.0475.

(2*S*,3*S*,5*S*)-5-(Chloromethyl)-2,3-dimethoxy-2,3-dimethyl-1,4-dioxane 44⁷²

Butanedione (4.5 ml, 52.0 mmol), trimethylorthoformate (6.9 ml, 63.3 mmol) and (±) camphor sulfonic acid (1.09 g, 4.70 mmol, 10 mol%) were added to a solution of (*S*)-(-)-3-chloro-1,2-propane diol (5.00 g, 45.2 mmol) in methanol (50 ml) and heated under reflux for 90 min. The reaction mixture was cooled to room temperature and triethylamine (0.7 ml) was added and the mixture allowed to stir at room temperature for a further 16 h. The reaction mixture was diluted with 1:1 sat. aqueous NaHCO₃–water (80 ml) and extracted with ether (3 × 80 ml). Combined organic fractions were washed with brine (80 ml), dried (MgSO₄) and the solvent removed *in vacuo* to give the dioxane **44**⁷² (6.10 g, 60%) as a pale yellow oil which was used without further

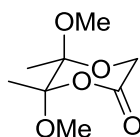
purification, however purification could be carried out by flash column chromatography (10:1 petrol–ether). R_F 0.19 (1:10 ether–petrol) $[\alpha]_D^{24}$: 158 (c. 1.40 in chloroform) [lit. 204 (c. 2.03 in chloroform)]; δ_H (500 MHz; $CDCl_3$) 4.08 (1H, dt, J 12.1 and 5.6, 5-H), 3.62-3.57 (2H, m, 6-H), 3.50 (1H, dd, J 11.3 and 6.4, CH_2Cl_A), 3.41 (1H, dd, J 11.1 and 6.4, CH_2Cl_B), 3.30 (3H, d, J 1.1, OMe_A), 3.27 (3H, d, J 1.1, OMe_B), 1.30 (3H, d, J 1.1, Me_A), 1.29 (3H, d, J 0.9, Me_B); HRMS Found: 247.0706, $[C_9H_{17}ClO_4Na]^+$ requires 247.0708.

(2*R*,3*R*,5*R*)-5-(Chloromethyl)-2,3-dimethoxy-2,3-dimethyl-1,4-dioxane *ent*-44⁷²



(*R*)-(+)-3-chloro-1,2-propane diol (15.0 g, 135.6 mmol) was treated under the condition described for the enantiomer to give the dioxane ***ent*-44⁷²** (24.4 g, 80%) as a pale yellow oil which was used without further purification; $[\alpha]_D^{24}$: -100.5 (c. 1.50 in chloroform) [lit. -204.1 (c. 2.03 in chloroform)]. Spectroscopically identical to that obtained for the enantiomer.

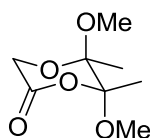
(5*S*,6*S*)-5,6-Dimethoxy-5,6-dimethyl-1,4-dioxan-2-one 33⁷²



Potassium *tert*-butoxide (4.98 g, 44.4 mmol) was added to a solution of the dioxane **44** (5.00 g, 22.2 mmol) in THF (45 ml) and the mixture was heated under reflux for 80 min before being cooled to room temperature, diluted with water (50 ml) and extracted with ether (3 × 50 ml). Combined organic fractions were washed with brine (50 ml), dried ($MgSO_4$) and the solvent removed *in vacuo*. The resulting alkene **45a** was dissolved in dichloromethane (150 ml) and subjected to ozonolysis conditions at -78 °C until the reaction was seen to have gone to completion by the appearance of a permanent blue colour. The reaction was quenched at room temperature with dimethyl sulfide (10 ml) and stirred under nitrogen until testing with starch iodide paper revealed peroxides had been fully quenched, at which point the solvents were

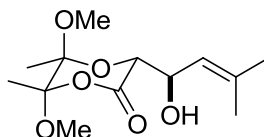
removed *in vacuo*. Purification by flash column chromatography (10:1 petrol–ether) gave the lactone **33**⁷² (1.23 g, 38%) as a pale yellow oil which solidified on cooling to 4 °C; R_F 0.17 (20:80 ether–petrol); $[\alpha]_D^{22}$: 124.8 (c. 1.30 in chloroform) [lit. 213.3 (c. 0.83 in chloroform)]; δ_H (500 MHz; CDCl₃) 4.28 (1H, d, J 17.8, 3-H_A), 4.13 (1H, d, J 17.8, 3-H_B), 3.43 (3H, s, OMe_A), 3.30 (3H, s, OMe_B), 1.49 (3H, s, Me_A), 1.38 (3H, s, Me_B); HRMS Found: 213.0739, [C₈H₁₄O₅Na]⁺ requires 213.0733.

(5R,6R)-5,6-Dimethoxy-5,6-dimethyl-1,4-dioxan-2-one ent-33⁷²



The dioxane **ent-44** (15.0 g, 66.6 mmol) was treated as described for the enantiomer to give the lactone **ent-33** (4.97 g, 40%) as a pale yellow oil which solidified on cooling to 4 °C; $[\alpha]_D^{24}$: -150.7 (c. 1.1 in chloroform) [lit. -212.1 (c. 1.07 in chloroform)]. Spectroscopically identical to that obtained for the enantiomer.

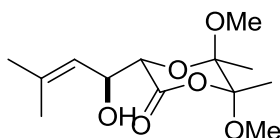
(3R,5S,6S)-3-((R)-1'-Hydroxy-3'-methylbut-2'-enyl)-5,6-dimethoxy-5,6-dimethyl-1,4-dioxan-2-one 49



Lithium hexamethyldisilazide (1.0 M in THF, 7.89 ml, 7.89 mmol) was added to a solution of the lactone **33** (1.00 g, 5.26 mmol) in dry THF and stirred for 15 min at -78 °C. 3-Methyl-2-butenal (0.61 ml, 6.32 mmol) was added and the mixture stirred for a further 10 min, followed by the addition of acetic acid (0.6 ml, 15.5 mmol). The mixture was allowed to warm to room temperature before being passed through a short plug of silica eluting with ether (125 ml). Solvents were removed *in vacuo* and the residue purified by flash column chromatography (40:60 ether–petrol) to give the alcohol **49** (1.22g, 85%, d.r. >98:<2) as a yellow oil; R_F 0.11 (40:60 ether–petrol); $[\alpha]_D^{24}$: 145 (c. 0.20 in chloroform); ν_{max}/cm^{-1} (film) 3466, 1736, 1681; δ_H (500 MHz; CDCl₃) 5.49 (1H, d, J 9.0, 2-H'), 4.76 (1H, dd, J 9.0, 3.0, 1-H'), 4.21 (1H, d, J 9.0, 3-H), 3.42 (3H, s, OMe_A), 3.33 (3H, s, OMe_B), 3.07 (1H, s, OH), 1.77 (3H, s, 4-H₃'_A), 1.72 (3H, s, 4-H₃'_B),

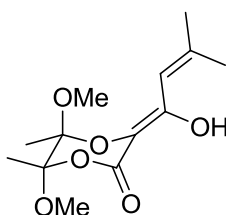
1.49 (3H, s, Me_A), 1.44 (3H, s, Me_B); δ_C (75 MHz; CDCl₃) 166.9 (2-C), 137.8 (3-C'), 121.4 (2-C'), 104.8 (5-C or 6-C), 98.2 (5-C or 6-C), 74.6 (3-C'), 69.3 (1-C'), 50.1 (OMe_A), 49.3 (OMe_B), 26.0 (4-C'_A), 18.4 (4-C'_B), 17.9 (Me_A), 16.8 (Me_B); HRMS Found: 297.132, [C₁₃H₂₂O₆Na]⁺ requires 297.1309.

(3*S*,5*R*,6*R*)-3-((*S*)-1'-Hydroxy-3'-methylbut-2'-enyl)-5,6-dimethoxy-5,6-dimethyl-1,4-dioxan-2-one *ent*-49



The lactone **ent-33** (2.00 g, 10.53 mmol) was treated as described for the enantiomer to give the *alcohol ent-49* (2.63 g, 91%, d.r. >98:<2) as a yellow oil; $[\alpha]_D^{24}$: -100.0 (c. 1.00 in chloroform). Spectroscopically identical to that obtained for the enantiomer.

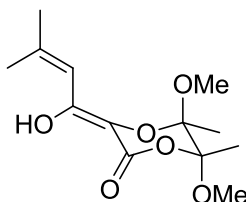
(5*S*,6*S*,*E*)-3-(1'-hydroxy-3'-methylbut-2'-enylidene)-5,6-dimethoxy-5,6-dimethyl-1,4-dioxan-2-one **50**



Lithium hexamethyldisilazide (1.0 M in THF, 15.7 ml, 15.7 mmol) was added to a solution of the lactone **33** (2.00 g, 10.5 mmol) in dry THF (48 ml) at -78 °C and the mixture stirred for 10 min. 3-methyl-2-butenyl chloride (1.4 ml, 12.6 mmol) was added and the mixture stirred for a further 60 min. Acetic acid (1.2 ml, 21.0 mmol) was added and the mixture allowed to warm to room temperature before being passed through a short plug of silica eluting with ether (250 ml) and removing the solvents *in vacuo*. Purification by flash column chromatography (10:90 ether-petrol) to give the *enol 50* (0.13 g, 23%) as a colourless-pale yellow amorphous solid; R_F 0.48 (40:60 ether-petrol) $[\alpha]_D^{24}$: 100.7 (c. 0.7 in chloroform); ν_{max}/cm^{-1} (film) 3448, 1748, 1648; δ_H (500 MHz; CDCl₃) 11.69 (1H, d, *J* 1.6, OH), 6.19 (1H, d, *J* 1.3, 2-H'), 3.44 (3H, s, OMe_A), 3.24 (3H, s, OMe_B), 2.14 (3H, s, 4-H₃'_A), 1.94 (3H, s, 4-H₃'_B), 1.53 (3H, s, Me_A), 1.49 (3H, s, Me_B); δ_C (75 MHz; CDCl₃) 166.2 (2-C), 159.9(1-C'), 149.5 (3-C), 113.3 (2-C'), 104.2 (5-C or 6-C),

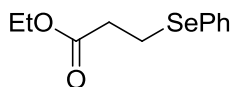
98.1 (5-C or 6-C), 50.7 (OMe_A), 49.0 (4-C'_A), 28.7 (4-C'_B), 20.9 (OMe_B), 17.5 (Me_A), 16.7 (Me_B).

(5*R*,6*R*,*E*)-3-(1'-Hydroxy-3'-methylbut-2'-enylidene)-5,6-dimethoxy-5,6-dimethyl-1,4-dioxan-2-one *ent*-50



The lactone ***ent*-33** (2.00 g, 10.5 mmol) was treated as described for the enantiomer to give the *enol ent*-50 (0.87 g, 30%) as a colourless-pale yellow amorphous solid; $[\alpha]_D^{24}$: -103.1 (c. 0.6 in chloroform). Spectroscopically identical to that obtained for the enantiomer.

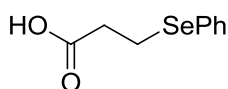
Ethyl-3-(phenylselanyl)propanoate 60⁹³



Sodium borohydride (1.04 g, 27.6 mmol) was added to a vigorously stirred solution of diphenyl diselenide (3.74 g, 12 mmol) in ethanol (450 ml) at 0 °C which was warmed to room temperature once addition was complete. **Caution: Hydrogen gas evolved.** Once the solution became colourless (approx. 10-20 min – up to a further 1 g of sodium borohydride was added if the solution did not become colourless) ethyl-3-chloropropionate was added and the mixture was heated to 60 °C and stirred for 6 h. The mixture was cooled to room temperature and water (15 ml) was added and approx. 75% of the ethanol was removed *in vacuo*. The remaining mixture was extracted with MTBE (3 × 100 ml), dried (MgSO₄) and the solvent removed *in vacuo*. The residue was purified by automated column chromatography (gradient elution 99:1 hexane–EtOAc → 90:10 hexane–EtOAc) to give the ester **60⁹³** (5.36 g, 87%) as a colourless-pale yellow oil; *R_f*: 0.3 (5:95, MTBE–hexane); δ_H (500 MHz; CDCl₃) 7.54-7.50 (2H, m, 2 × phenyl 3-H), 7.28-7.25 (3H, m, 2 × phenyl 2-H and phenyl 4-H), 4.13 (2H, q, *J* 7.1, ethyl 1-H₂), 3.10 (2H, t, *J* 7.5, 3-H₂), 2.71 (2H, t, *J* 7.5, 2-H₂), 1.25 (2H, t, *J* 7.1, ethyl

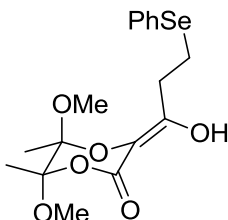
2-H₂); HRMS Found: 259.0232, [C₁₁H₁₅O₂⁸⁰Se]⁺ requires 259.0232 (isotope distribution as expected).

3-(Phenylselanyl)propanoic acid **61⁹³**



A solution of the ester **60** (7.00 g, 27.22 mmol) in THF (76.2 ml) was added to a 0.5 M aqueous solution of KOH (76.2 ml, 38.1 mmol) at 0 °C and stirred for 3 h. The reaction mixture was then extracted with MTBE (3 × 100 ml), and the aqueous layer acidified with conc. HCl_(aq) and re-extracted with MTBE (3 × 100 ml). Combined organic layers from the second extraction were washed with brine (100 ml), dried (MgSO₄) and the solvent removed *in vacuo*. Purification by recrystallisation from CH₂Cl₂ gave the acid **61**⁹³ (4.05 g, 66%) as colourless prisms; m.p. 49.6-54.2 °C (CH₂Cl₂) [lit. 45.0-46.0 °C (CH₂Cl₂-hexane)]; *R_F*: 0.53 (50:90, MeOH-CHCl₃); δ_H (500 MHz; CDCl₃) 7.53 (2H, dd, *J* 6.5 and 3.1, 2 × phenyl 3-H), 7.31-7.24 (3H, m, 2 × phenyl 2-H and phenyl 4-H), 3.08 (2H, t, *J* 7.4, 3-H), 2.77 (2H, t, *J* 7.4, 2-H).

(3*E*,5*S*,6*S*)-3-[1'-hydroxy-3'-(phenylselanyl)propylidene]-5,6-dimethoxy-5,6-dimethyl-1,4-dioxan-2-one **51**



A suspension of acid **61** (2.00 g, 8.80 mmol) in oxalyl chloride (1.49 ml, 17.6 mmol) was stirred at room temperature for 4 hr and the product was purified by distillation under vacuum (b.p. 175 °C, <0.1 mbar) to give acid chloride **48** as a colourless oil (1.93 g, 89%) which was used immediately due to its instability. LHMDS (1.0 M in THF, 3.94 ml, 3.94 mmol) was added to a solution of the lactone **33** (422 mg, 2.2 mmol) in dry THF (12 ml) which had been cooled to -78 °C and stirred for 15 min. The acid chloride **48** (781 mg, 3.16 mmol) was then added to a solution and stirred for 1 h at -78 °C. Acetic acid (0.3 ml, 5.26 mmol) was added and the mixture warmed to room temperature then filtered through a short plug of silica, eluting with MTBE (40 ml) and the solvents

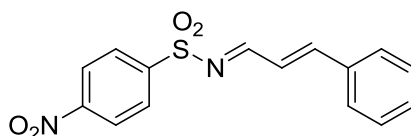
removed *in vacuo*. The residue was purified by automated column chromatography (gradient elution 10:90 → 40:60 MTBE–hexane) to give the *enol* **51** (575 mg, 65%, 1:1 keto-enol) as a yellow oil. R_F : enol - 0.2, keto - 0.08 (10:90, MTBE-hexane); $[\alpha]_D^{22}$: 95.3 (c. 0.20 in chloroform); Keto-enol ratio determined by separation of keto and enol forms by Biotage (see previously).

δ_H (500 MHz; $CDCl_3$):

enol - 11.32 (1H, s, OH), 7.58-7.46 (2H, m, 2 × phenyl 3-H), 7.28-7.23 (3H, m, 2 × phenyl 2-H and phenyl 4-H), 3.43 (3H, s, OMe_A), 3.15 (3H, s, OMe_B), 3.12-3.04 (2H, m, 3-H'), 2.84 (2H, t, J 8.0, 2-H'), 1.52 (3H, s, Me_A), 1.41 (3H, s, Me_B)

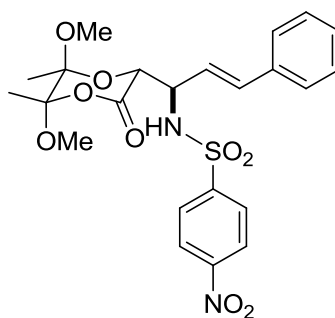
keto - 7.57-7.48 (2H, m, 2 × phenyl 3-H), 7.31-7.18 (3H, m, 2 × phenyl 2-H and phenyl 4-H), 4.67 (1H, s, H-3), 3.31 (3H, s, OMe_A), 3.31 (3H, s, OMe_B), 3.08 (2H, t, J 7.4, 3-H'), 2.79 (2H, t, J 7.6, 2-H'), 1.46 (3H, s, Me_A), 1.38 (3H, s, Me_B)

4-Nitro-*N*-[(*2E*)-3-phenylprop-2-en-1-ylidene]benzene-1-sulfonamide **34**



Borontrifluoro diethyletherate (194 μ l, 1.58 mmol, 8 mol%) was added to a refluxing solution of 4-nitrobenzenesulfonamide (4.00 g, 19.8 mmol) and cinnamaldehyde (2.49 ml, 19.8 mmol) in dry toluene (113 ml). **Caution: Effervescence occurs on addition of boron trifluoro diethyletherate.** The solution was heated under reflux for 3 days, cooled to room temperature and the solvent removed *in vacuo*. The residue was triturated from EtOAc to give the *imine* **34** (5.50 g, 88%) as a dark brown solid; R_F : 0.3 (20:80, EtOAc–petrol); δ_H (500 MHz; $CDCl_3$) 8.86 (1H, d, J 9.5, 1-H), 8.38 (2H, d, J 8.9, 2 × nosyl 3-H), 8.18 (2H, d, J 8.9, 2 × nosyl 3-H), 7.62-7.57 (3H, m, 2 × phenyl 3-H and 3-H), 7.51-7.42 (3H, m, 2 × phenyl 2-H and phenyl 4-H), 7.01 (1H, dd, J 15.8, 9.5, 2-H); δ_C (75 MHz; $CDCl_3$) 173.1 (1-C), 156.0 (3-C), 150.5 (nosyl-1-C or nosyl 4-C), 144.4 (nosyl-1-C or nosyl 4-C), 133.9 (phenyl 1-C), 132.3 (phenyl 4-C), 129.3 (nosyl 2-C or nosyl 3-C), 129.2 (2 × phenyl 2-C), 129.0 (2 × phenyl 3-C), 124.34 (nosyl 2-C or nosyl 3-C), 124.31 (2-C); HRMS Found: 317.0592, $[C_{15}H_{13}N_2O_4S]^+$ requires 317.0591.

N*-[(1'*R*,2'*E*)-1'-[(2*R*,5*S*,6*S*)-5,6-Dimethoxy-5,6-dimethyl-3-oxo-1,4-dioxan-2-yl]-3'-phenylprop-2'-en-1'-yl]-4-nitrobenzene1'-sulfonamide **35*

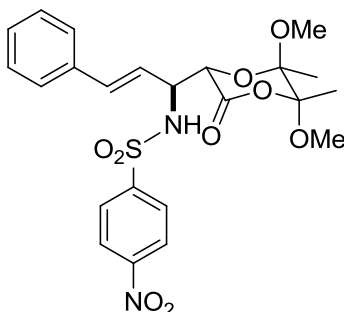


Lithium hexamethyldisilazide (1.0 M in THF, 2.4 ml, 2.4 mmol) was added to a solution of the lactone **33** (300 mg, 1.6 mmol) in THF (5 ml) at $-78\text{ }^{\circ}\text{C}$ and stirred for 15 min. A solution of the imine **34** (500 mg, 1.6 mmol) in THF (10 ml) was added to the enolate solution and the reaction stirred for 1 h at $-78\text{ }^{\circ}\text{C}$ before being quenched with acetic acid (0.4 ml) and filtered through a short plug of silica, eluting with ether. The solvents were removed *in vacuo* and the resulting crude material was purified by flash column chromatography (20:80 EtOAc–petrol). The excess *p*-nosyl sulfonamide was removed by dissolving the residue in chloroform, filtering under vacuum and concentrating the filtrate *in vacuo* to give the lactone **35** (643 mg, 79%, d.r. 83:17) as a sticky yellow-orange solid; R_F : 0.43 (1:1, petrol–EtOAc); $[\alpha]_D^{22}$: 92.9 (c. 0.50 in chloroform); $\nu_{\text{max}}/\text{cm}^{-1}$ (film) 3271, 3106, 2951, 1748, 1530, 1450; δ_{H} (500 MHz; CDCl_3) 8.15 (2H, d, J 8.8, 2 \times nosyl 2-H), 7.98 (2H, d, J 8.7, 2 \times nosyl 3-H), 7.23–7.20 (3H, m, 2 \times phenyl 3-H and phenyl 4-H), 7.09–7.05 (2H, m, 2 \times phenyl 2-H), 6.32 (1H, d, J 16.0, 3-H'), 5.82 (1H, d, J 7.2, NH), 5.80 (1H, dd, J 16.0 and 9.2, 2-H'), 4.55–4.49 (1H, m, 1-H'), 4.39 (1H, d, J 3.1, 2-H), 3.32 (3H, s, OMe_A), 3.20 (3H, s, OMe_B), 1.45 (3H, s, Me_A), 1.43 (3H, s, Me_B); δ_{C} (75 MHz; CDCl_3) 165.9 (3-C'), 149.7 (nosyl 4-C), 146.4 (nosyl 1-C), 135.2 (phenyl 1-C), 135.1 (3-C'), 128.8 (2 \times nosyl 3-C), 128.6 (2 \times phenyl 3-C and phenyl 4-C), 126.3 (2 \times phenyl 2-C), 124.1 (2 \times nosyl 2-C), 122.3 (2-C'), 105.4 (6-C), 98.6 (5-C), 73.6 (2-C), 58.6 (1-C'), 50.2 (OMe_A), 49.5 (OMe_B), 17.7 (Me_A), 16.8 (Me_B); HRMS Found: 529.1260, $[\text{C}_{23}\text{H}_{26}\text{N}_2\text{O}_9\text{SNa}]^+$ requires 529.1251. The diastereomeric ratio was determined by the

Chapter 6 - Materials and Methods and Experimental

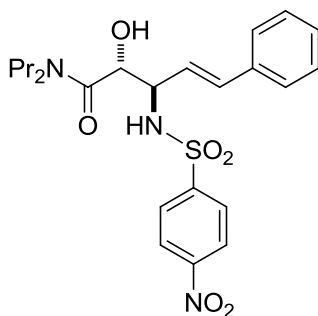
relative integration of the peaks at 4.55-4.49 (1H, m, 1-H^{'maj}) and 4.68-4.60 (1H, m, 1-H^{'min}) in the 500 MHz ¹H NMR spectrum.

***N*-[(1'*S*,2'*E*)-1'-[(2*S*,5*R*,6*R*)-5,6-Dimethoxy-5,6-dimethyl-3-oxo-1,4-dioxan-2-yl]-3'-phenylprop-2'-en-1'-yl]-4-nitrobenzene1'-sulfonamide *ent*-35**



The lactone *ent*-33 (2.70 g, 14.2 mmol) was treated as described for the enantiomer to give the lactone *ent*-35 (6.52 g, 91%, d.r. 83:17) as a sticky yellow-orange solid; $[\alpha]_{\text{D}}^{22}$: -39.8 (c. 1.30 in chloroform). Spectroscopically identical to that obtained for the enantiomer.

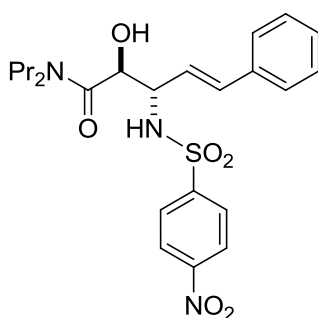
(2*R*,3*R*,4*E*)-2-Hydroxyl-3-[(4-nitrobenzene)sulfonamide]-5-phenyl-*N,N*-dipropylpent-4-enamide 53



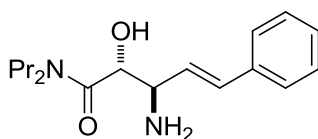
Trimethylaluminium (2.00 M in hexane, 1.0 ml, 2.00 mmol) was added to a solution of dipropylamine (273 μ l, 2.00 mmol) in dry CH₂Cl₂ (5 ml) and stirred at room temperature for 15 min. The lactone **35** (0.50 g, 1.00 mmol) was dissolved in the minimum amount of CH₂Cl₂ and added to the stirred solution of Me₂AlNPr₂ and the mixture was warmed to 40 °C, stirred for 2 h, cooled to room temperature and quenched by addition of 1 M HCl_(aq) (1 ml). **Caution: addition of HCl results in a vigorous effervescent reaction.** The reaction mixture was extracted with CH₂Cl₂ (3 \times 30 ml), dried (Na₂SO₄) and the solvent removed *in vacuo*. The residue was dissolved in 1:1 MeCN–water (50 ml) to which TFA (1.2 ml) was added and the mixture stirred at room

temperature for 24 h, poured into EtOAc, separated and the aqueous layer extracted with EtOAc (2 × 30 ml). Combined organic layers were dried (MgSO₄) and the solvent removed *in vacuo*. Purification by flash column chromatography (30:70 EtOAc–petrol) to give the *sulfonylamide* **53** (324 mg, 88%) as a dark orange/yellow solid; *R_f*: 0.37 (1:1, petrol-EtOAc); m.p. 121-123 °C (petrol–EtOAc); $[\alpha]_D^{22}$: 45 (c. 0.80 in chloroform); $\nu_{\max}/\text{cm}^{-1}$ (film) 3203, 2969, 1645, 1532; δ_{H} (500 MHz; CDCl₃) 8.13 (2H, d, *J* 8.5, 2 × nosyl 2-H), 7.99 (2H, d, *J* 8.5, 2 × nosyl 3-H), 7.20 (3H, s, 2 × phenyl 2-H and phenyl 4-H), 7.05-6.96 (2H, m, 2 × phenyl 3-H), 6.12 (1H, d, *J* 15.9, 5-H), 5.64 (1H, dd, *J* 15.8 and 8.1, 4-H), 4.16 (1H, d, *J* 2.1, 2-H), 4.29 (1H, d, *J* 8.1, 3-H), 3.61-3.51 (1H, m, propyl 1-H_A), 3.37-3.27 (1H, m, propyl 1-H_B), 3.25-3.14 (1H, m, propyl-1-H_C), 3.03-2.90 (1H, m, propyl 1-H_D), 1.71-1.55 (2H, m, propyl 2-H_{2,A}), 1.51-1.40 (2H, m, propyl 2-H_{2,B}), 0.94 (3H, t, *J* 7.3, propyl 3-H_{3,A}), 0.82 (3H, t, *J* 7.3, propyl 3-H_{3,B}); δ_{C} (75 MHz; MeOD) 172.4 (1-C), 151.0 (nosyl 4-C), 148.8 (nosyl 1-C), 137.2 (phenyl 1-C), 135.2 (phenyl 5-C), 129.7 (2 × phenyl 2-C), 129.5 (2 × phenyl 3-C), 129.1 (phenyl 4-C), 127.3 (2 × nosyl 3-C), 125.2 (2 × nosyl 2-C), 124.2 (4-C), 72.3 (2-C), 60.7 (3-C), 50.3 (propyl 1-C_A), 49.1 (propyl 1-C_B), 23.4 (propyl 2-C_A), 21.8 (propyl 2-C_B), 11.7 (propyl 3-C_A), 11.4 (propyl 3-C_B); HRMS Found: 476.1862, [C₂₃H₃₀N₃O₆S]⁺ requires 476.185.

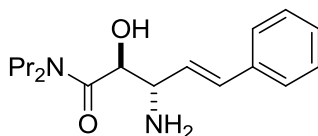
(2*S*,3*S*,4*E*)-2-Hydroxy-3-[(4-nitrobenzene)sulfonamide]-5-phenyl-*N,N*-dipropylpent-4-enamide *ent*-53



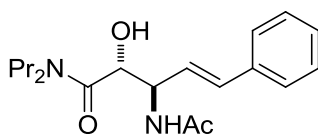
The lactone *ent*-**35** (3.00 g, 5.93 mmol) was treated as described for the enantiomer to give the *sulfonylamide* *ent*-**53** (2.19 g, 78%) as a dark orange/yellow solid; $[\alpha]_D^{22}$: -48.7 (c. 1.7, CHCl₃). Spectroscopically identical to that obtained for the enantiomer.

(2R,3R,4E)-3-Amino-2-hydroxy-5-phenyl-N,N-dipropylpent-4-enamide 54

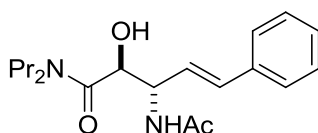
Thiophenol (300 μ l, 2.97 mmol) and 1,8-diazabicycloundec-7-ene (600 μ l, 3.96 mmol) were added to a solution of the sulfonylamide **53** (470 mg, 0.99 mmol) in MeCN (4 ml) and stirred at room temperature for 16 h. The reaction mixture was concentrated *in vacuo* and purified by flash column chromatography (gradient elution 5:95 EtOH–CH₂Cl₂ \rightarrow 5:5:90 sat. NH₃ in MeOH–EtOH–CH₂Cl₂) to give *amine 54* (255 mg, 89%) as a pale yellow viscous oil; R_F : 0.18 (5:95, EtOH–CH₂Cl₂); $[\alpha]_D^{22}$: 55.1 (c. 0.90 in chloroform); $\nu_{\max}/\text{cm}^{-1}$ (film) 3277, 2965, 1638; δ_H (500 MHz; CDCl₃) 7.34–7.20 (5H, m, 2 \times phenyl 2-H, 2 \times phenyl 3-H and phenyl 4-H), 6.52 (1H, d, J 15.9, 5-H), 6.12 (1H, dd, J 15.9 and 7.9, 4-H), 4.60 (1H, d, J 3.2, 2-H), 3.88 (2H, s, NH₂), 3.82 (1H, dd, J 7.7 and 2.8, 3-H), 3.60–3.51 (1H, m, propyl 1-H_A), 3.39–3.31 (1H, m, propyl 1-H_B), 3.20–3.12 (1H, m, propyl 1-H_C), 3.01–2.93 (1H, m, propyl-1-H_D), 1.63–1.54 (2H, m, propyl 2-H_{2A}), 1.52–1.45 (2H, m, propyl 2-H_{2B}), 0.90 (3H, t, J 7.4, propyl-3-H_{3A}), 0.93 (3H, t, J 7.4, propyl 3-H_{3B}); δ_C (75 MHz; CDCl₃) 171.0 (1-C), 133.2 (5-C), 128.9 (phenyl 1-C), 128.5 (2 \times phenyl 2-C), 127.9 (phenyl 4-C), 126.6 (2 \times phenyl 3-C), 126.0 (4-C), 70.2 (2-C), 56.8 (3-C), 48.8 (propyl 1-C_A), 47.6 (propyl 1-C_B), 22.1 (propyl 2-C_A), 20.7 (propyl 2-C_B), 11.4 (propyl 3-C_A), 11.1 (propyl 3-C_B); HRMS Found: 291.2067, [C₁₇H₂₇N₂O₂]⁺ requires 291.2067.

(2S,3S,4E)-3-Amino-2-hydroxy-5-phenyl-N,N-dipropylpent-4-enamide ent-54

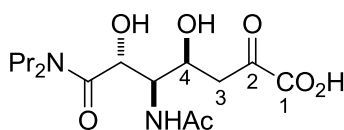
The sulfonylamide **ent-53** (2.00 g, 4.21 mmol) was treated as described for the enantiomer to give *amine ent-54* (1.06 g, 88%) as a dark orange/yellow viscous oil; $[\alpha]_D^{22}$: –30.5 (c. 1.20 in chloroform). Spectroscopically identical to that obtained for the enantiomer.

(2R,3R,4E)-3-Acetamido-2-hydroxy-5-phenyl-N,N-dipropylpent-4-enamide 24

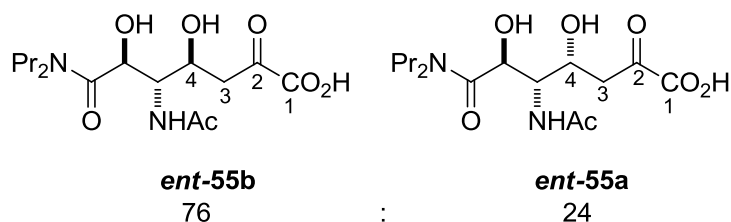
A solution of the amine **54** (225 mg, 0.77 mmol), NaHCO₃ (520 mg, 6.16 mmol) and acetic anhydride (0.11 ml, 1.16 mmol) in methanol (5 ml) was heated under reflux for 1 h before being cooled to room temperature, filtered and the solvent removed *in vacuo*. Purification by flash column chromatography (80:20 EtOAc–petrol) to give the *dipropylamide* **24** (228 mg, 89%) as a pale yellow/colourless amorphous solid; *R_F*: 0.16 (80:20, EtOAc–petrol); $[\alpha]_D^{22}$: 29.1 (c. 1.30 in chloroform); $\nu_{\max}/\text{cm}^{-1}$ (film) 3234, 1628; δ_{H} (500 MHz; CDCl₃) 7.32-7.27 (4H, m, 2 × phenyl 2-H and 2 × phenyl 3-H), 7.24-7.20 (1H, m, phenyl 4-H), 6.53 (1H, d, *J* 15.9, 5-H), 6.36 (1H, d, *J* 8.4, NH), 6.05 (1H, dd, *J* 15.9 and 7.2, 4-H), 4.85-4.81 (1H, m, 3-H), 4.59 (1H, d, *J* 2.2, 2-H), 3.68-3.56 (2H, m, propyl 1-H_{2,A}), 3.30-3.23 (1H, m, propyl 1-H_B), 3.01-2.94 (1H, m, propyl 1-H_C), 2.06 (3H, s, acetyl CH₃), 1.70-1.60 (2H, m, propyl 2-H_{2,A}), 1.57-1.47 (2H, m, propyl 2-H_{2,B}), 0.97 (3H, t, *J* 7.4, propyl 3-H_{3,A}), 0.85 (3H, t, *J* 7.4, propyl 3-H_{3,B}); δ_{C} (75 MHz; CDCl₃) 170.4 (amide-C=O), 169.8 (acetyl C=O), 136.2 (phenyl 1-C), 134.0 (5-C), 128.6 (2 × phenyl 2-C), 128.0 (phenyl 4-C), 126.6 (2 × phenyl 3-C), 122.5 (4-C), 70.3 (2-C), 53.7 (3-C), 48.4 (propyl 1-C_A), 47.5 (propyl 1-C_B), 23.4 (acetyl CH₃), 22.1 (propyl 2-C_A), 20.7 (propyl 2-C_B), 11.4 (propyl 3-C_A), 11.0 (propyl 3-C_B); HRMS Found: 333.2165, [C₁₉H₂₉N₂O₃]⁺ requires 333.2173.

(2S,3S,4E)-3-Acetamido-2-hydroxy-5-phenyl-N,N-dipropylpent-4-enamide ent-24

The amine **ent-54** (1.39 g, 4.8 mmol) was treated as described for the enantiomer to give the *dipropylamide* **ent-25** (0.88 g, 56%) as a pale yellow/colourless amorphous solid; $[\alpha]_D^{22}$: -34.4 ° (c. 0.90 in chloroform). Spectroscopically identical to that obtained for the enantiomer.

(4*R*,5*R*,6*R*)-7-(Dipropylamino)-5-acetamido-4,6-dihydroxy-2,7-dioxoheptanoate 55a

The dipropylamide **24** (150 mg, 0.4 mmol) subjected to general ozonolysis conditions described previously. Methanol was removed *in vacuo* and the crude mixture was re-dissolved in 50 mM tris buffer (5 ml) to which sodium pyruvate (88 mg, 0.8 mmol) was added. The pH was adjusted to 7.4 by addition of NaOH (2 M) followed by addition of the NAL E192N variant (1 mg/ml in 50 mM tris buffer pH 7.4, 1 ml). The reaction was stirred for 24 h then acidified to pH 3 with formic acid (2 M) and allowed to stir for 30 min. The pH was then adjusted to 7.4 with NaOH (2 M) followed by the addition of baker's yeast (200 mg) and stirred for 16 h. The mixture was filtered through Celite® and the crude product was purified by Dowex® ion exchange (gradient elution 0 → 2M formic acid in water) to give the *sialic acid analogue 55* (57 mg, 41 %, d.r. >98:<2) as a pale yellow glass; δ_{H} (500 MHz; D₂O) 4.83 (1H, d, *J* 10.3, 6-H), 4.11 (1H, td, *J* 11.2, 10.9 and 4.5, 4-H), 4.00 (1H, t, *J* 10.2, 5-H), 3.59-3.50 (2H, m, propyl 1-H_{2,A}), 3.29-3.22 (1H, m, propyl 1-H_C), 3.03-2.96 (1H, m, propyl 1-H_D), 2.35 (1H, dd, *J* 13.1, 4.5, 3-H_{eq}), 1.88 (3H, s, acetyl-CH₃), 1.99-1.92 (1H, m, 3-H_{ax}), 1.68-1.57 (2H, m, propyl 2-H_{2,A}), 1.53-1.43 (2H, m, propyl 2-H_{2,B}), 0.87 (3H, t, *J* 7.4, propyl 3_{3,A}), 0.83 (3H, t, *J* 7.4, propyl 3-H_{3,B}); δ_{C} (75 MHz; D₂O) 174.0 (acetyl C=O), 172.1 (1-C), 169.0 (7-C), 95.9 (2-C), 68.0 (6-C), 65.7 (4-C), 54.1 (5-C), 49.9 (propyl 1-C_B), 48.7 (propyl 1-C_A), 38.7 (3-C), 22.1 (propyl 2-C_A), 21.9 (acetyl-CH₃), 20.0 (propyl 2-C_B), 10.5 (propyl 3-C_B), 10.2 (propyl 3-C_A); HRMS Found: 345.1682, [C₁₅H₂₅N₂O₇]⁻ requires 345.1667. The product was isolated as a single diastereomer which exists as one pyranose ring form as determined by 500MHz ¹H NMR.

(4R,5S,6S) and (4S,5S,6S) -7-(Dipropylamino)-5-acetamido-4,6-dihydroxy-2,7-dioxoheptanoate ent-55

The dipropylamide **ent-25** (100 mg, 0.3 mmol) subjected to general ozonolysis conditions described previously. Methanol was removed *in vacuo* and the crude mixture was re-dissolved in 50 mM tris buffer (3.5 ml) to which sodium pyruvate (66 mg, 0.6 mmol) was added. The pH was adjusted to 7.4 by addition of NaOH (2 M) followed by addition of the NAL E192N variant (0.8 mg/ml in 50 mM tris buffer pH 7.4, 4 ml). The reaction was stirred under nitrogen for 24 h. The reaction was acidified to pH 3 with formic acid (2 M) and allowed to stir for 30 min. The pH was then adjusted to 7.4 with NaOH (2 M) followed by the addition of Bakers' yeast (150 mg) and stirred for 16 h. The mixture was filtered through Celite® and the crude product was purified by Dowex® ion exchange (gradient elution 0 → 2M formic acid in water) to give the *sialic acid analogue ent-55* as a pale yellow glass, which was then further purified by mass directed HPLC. (9 mg, 9%, (4S):(4R) 76:24); δ_{H} (500 MHz; D₂O)* 5.03 (1H, d, *J* 10.6, 6-H^{4S,maj}), 5.00 (1H, d, *J* 9.6, 6-H^{4S,min}), 4.75 (1H, d, *J* 10.2, 6-H^{4R}), 4.23 (1H, dd, *J* 10.6 and 3.1, 5-H^{4S}), 4.12 (1H, t, *J* 3.0, 4-H^{4S}), 4.04-4.06 (1H, m, 4-H^{4R}), 3.94 (1H, t, *J* 10.2, 5-H^{4R}), 3.57-3.47 (2H, m, 2 × propyl 1-H_{2,A}^{4S}), 3.42-3.33 (2H, m, propyl H-1₂^{4R}), 3.23-3.16 (1H, m, propyl 1-H_C^{4S}), 3.07-2.99 (1H, m, propyl 1-H_C^{4R}), 2.97-2.90 (1H, m, propyl 1-H_D^{4S}), 2.26 (1H, dd, *J* 13.1 and 4.5, 3-H_{eq}^{4R}), 2.17-2.15 (1H, m, 3-H_{eq}^{4S,maj}), 2.12-2.09 (1H, m, 3-H_{eq}^{4S,min}), 2.01-1.93 (1H, m, 3-H_{ax}^{4S}), 1.90 (3H, s, acetyl CH₃^{4R}), 1.90-1.89 (1H, m, 3-H_{ax}^{4R}), 1.19 (3H, s, acetyl CH₃^{4S}), 1.62-1.52 (2H, m, propyl 2-H_{2,A}), 1.46-1.52 (2H, m, propyl 2-H_{2,B}), 0.83 (3H, t, *J* 7.4, propyl 3-H_{3,B}), 0.78 (3H, t, *J* 7.4, propyl 3-H_{3,B}) δ_{C} (75 MHz; D₂O) 174.0 (acetyl C=O^{4R}), 173.3 (acetyl C=O^{4S}), 172.0 (1-C^{4R}), 169.6 (7-C^{4S}), 169.0 (7-C^{4R}), 95.9 (2-C^{4R}), 95.3 (2-C^{4S}), 68.8 (6-C^{4S,min}), 68.0 (6-C^{4R}), 65.4 (4-C^{4R}), 64.5 (4-C^{4S}), 64.4 (6-C^{4S,maj}), 54.1 (5-C^{4R}), 49.7 (propyl 1-C_A^{4S}), 49.5 (5-C^{4S}), 49.4 (2 × propyl 1-C^{4R}), 48.5

* Superscript abbreviations in NMR characterisation data: 4S and 4R refer to the diastereomer, and *maj* and *min* refer to the major and minor anomer. When unspecified, assume that the peak described both of the diastereomers/anomers.

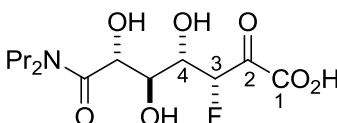
Chapter 6 - Materials and Methods and Experimental

(propyl 1-C_B,^{4S}), 39.0 (3-C^{4S,min}), 38.7 (3-C^{4R}), 36.4 (3-C^{4S,maj}), 22.1 (acetyl CH₃,^{4R}), 21.9 (acetyl CH₃,^{4S}), 21.8 (propyl 2-C_A), 19.9 (propyl 2-C_B), 10.4 (propyl 3-C_B), 10.2 (propyl 3-C_A); HRMS Found: 346.1718, [C₁₅H₂₆N₂O₇]⁻ requires 346.174; The diastereomeric ratio was determined by comparison of the relative integrals of the peaks at 4.12 (1H, t J 3.0, 4-H^{4R}) and 4.04-4.06 (1H, m, 4-H^{4S}) The major diastereomer **ent-55b** was observed as 60:40 mixture of anomers, which was determined by comparison of the peaks for 6-H in the 500 MHz ¹H NMR spectrum. The minor diastereomer **ent-55a** was observed as a single anomer and was found to be spectroscopically identical to the enantiomer **55a**.

6.3.1 General method for synthesis of fluorinated sialic acid analogues

The alkene was cleaved under standard ozonolysis condition (see Section 6.2.1). Methanol was removed *in vacuo* and the crude mixture was re-dissolved in 50 mM tris buffer (1.2 ml per 0.1 mmol aldehyde) to which sodium fluoropyruvate (0.5-1 eq.) was added. The pH was adjusted to 7.4 by addition of NaOH (2 M) followed by addition of the NAL variant (in 50 mM tris buffer, 2-4 mg per 0.1 mmol aldehyde). The reaction was allowed to stir under nitrogen for 24 h. The mixture was frozen, thawed and filtered through Celite® and the product was isolated by ion exchange chromatography using Dowex® resin (gradient elution 0 → 2 M formic acid in water) or SAX resin cartridges (gradient elution 0 → 2 M formic acid in MeOH)

(3R,4S,5S,6R)-7-(dipropylamino)-3-fluoro-4,5,6-trihydroxy-2,7-dioxoheptanoate **23b**



Reaction was carried out as described in the general experimental Section 6.3.1 using the alkene **24** (222 mg, 1.03 mmol), sodium fluoropyruvate (88 mg, 0.69 mmol) and the NAL E192N/T167V/S208V variant. The crude product was purified by ion exchange to give the *fluorinated sialic acid analogue* **23b** (90 mg, 41%, d.r. >98:<2) as a yellow glass. Purification by reverse-phase HPLC, retention time 31.0 min; δ_{H} (500 MHz, D₂O) 5.03 (1H, dd, ²J_{HF} 52.0, ³J_{HH} 5.5, 3-H^{min,pyran}), 4.86 (1H, dd, ²J_{HF} 48.1, ³J_{HH} 7.3, H-3^{min,furan}), 4.85 (1H, dd, ²J_{HF} 49.7, ³J_{HH} 4.8, 3-H^{maj,pyran}), 4.75 (1H, d, ³J_{HH} 5.4, 6-H^{min,furan}), 4.72 (1H,

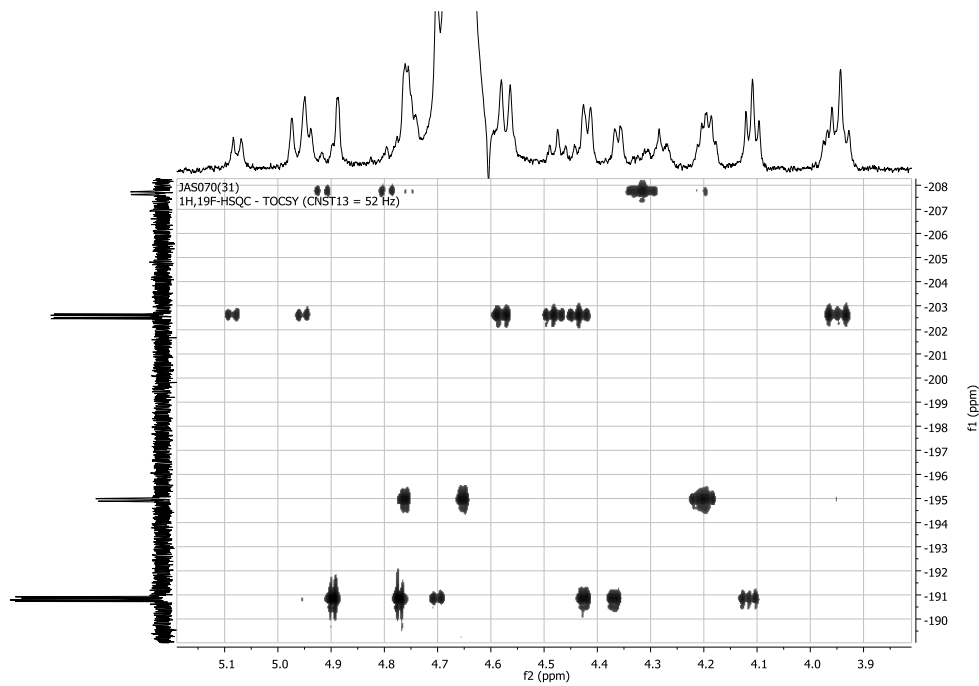
Chapter 6 - Materials and Methods and Experimental

d, $^2J_{\text{HF}}$ 44.2, H-3^{*maj,furan*}), 4.65 (1H, d, $^3J_{\text{HH}}$ 6.1, 6-H^{*maj,pyran*}), 4.57 (1H, d, $^3J_{\text{HH}}$ 7.2, 6-H^{*min,pyran*}), 4.46 (1H, dd, $^3J_{\text{HF}}$ 18.7, $^3J_{\text{HH}}$ 5.6, 4-H^{*min,pyran*}), 4.39 (1H, dd, $^3J_{\text{HF}}$ 22.4, $^3J_{\text{HH}}$ 3.7, 4-H^{*maj,pyran*}), 4.30 (1H, td, $^3J_{\text{HH}}$ 7.7 and 3.4, H-4^{*min,furan*}), 4.18 (1H, dd, $^3J_{\text{HH}}$ 8.6 and 5.1, H-5^{*min,furan*}), 4.12 (1H, t, $^3J_{\text{HH}}$ 5.0, 5-H^{*maj,pyran*}), 4.02 (1H, app. t, $^3J_{\text{HH}}$ 7.4, H-4^{*maj,furan*}), 3.96 (1H, m, H-5^{*maj,furan*}), 3.95 (1H, dd, $^3J_{\text{HH}}$ 6.4, 5-H^{*min,pyran*}); 3.43-2.99 (4H, m, 2 × propyl 1-H₂), 1.58-1.37 (4H, m, 2 × propyl 2-H₂), 0.99-0.66 (6H, m, 2 × propyl 3-H₃); δ_{F} (395 MHz, D₂O) -190.5 (d, $^2J_{\text{HF}}$ 50.5, $^3J_{\text{HF}}$ 24.0, 3-F^{*maj,pyran*}), -194.5 (d, $^2J_{\text{HF}}$ 43.7, $^3J_{\text{HF}}$ 4.7, 3-F^{*maj,furan*}), -201.9 (d, $^2J_{\text{HF}}$ 53.1, $^3J_{\text{HF}}$ 18.7, 3-F^{*min,pyran*}), -207.4 (d, $^2J_{\text{HF}}$ 48.5, $^3J_{\text{HF}}$ 10.1, 3-F^{*min,furan*});* m/z (ES) [MH]⁺ 324.1 (100 % [MH]⁺). The fluorinated sialic acid analogues **23b** was observed as a mixture of equilibrium ring forms (pyranose and furanose), which both existed as major and minor anomers with a ratio of 37:29:23:11 major pyranose to minor pyranose to major furanose to minor furanose. The ratio of equilibrium species was determined by analysis of the 395 MHz ¹⁹F NMR spectrum and the reaction was seen to be completely diastereoselective under the reaction conditions to within the sensitivity of 395 MHz ¹⁹F NMR spectroscopy. The ¹H NMR spectrum was indirectly obtained by ¹⁹F/¹H HSQC-TOCSY.

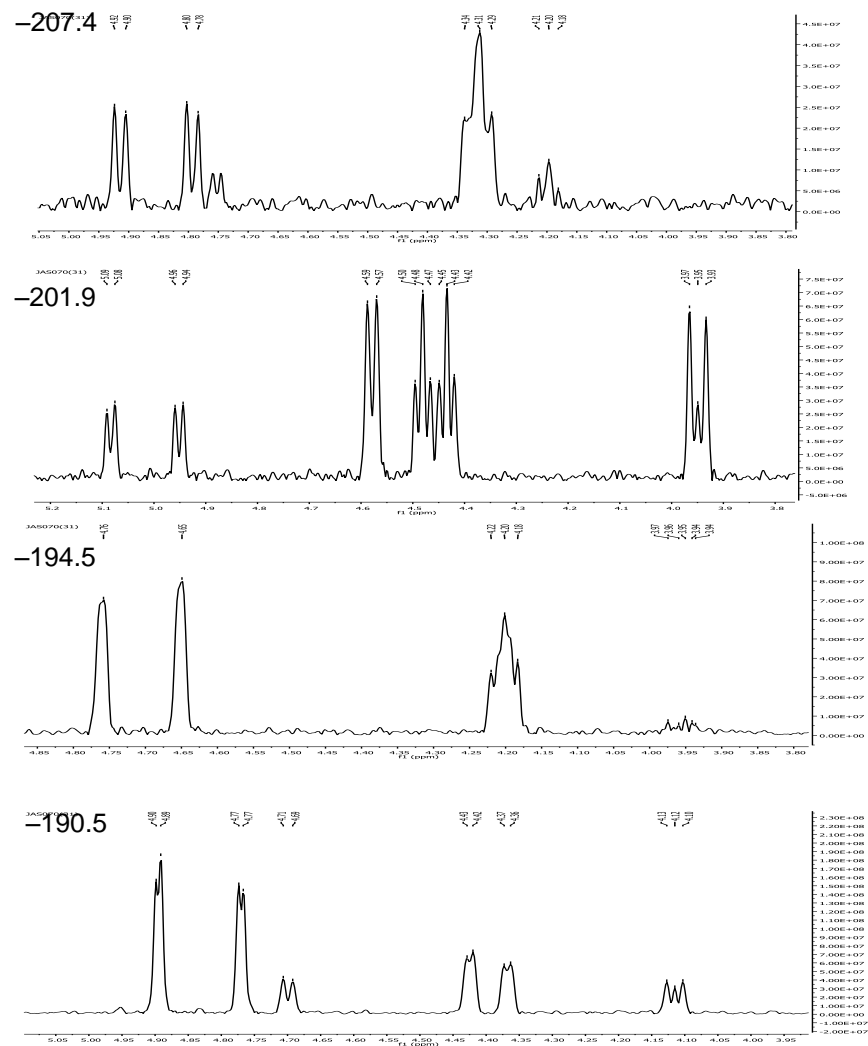
* Superscript abbreviations in NMR characterisation data: *maj* and *min* refer to the major and minor anomer and *pyran* and *furan* refers to the pyranose and furanose ring form. When unspecified, assume that the peak described both of the anomers/ring forms.

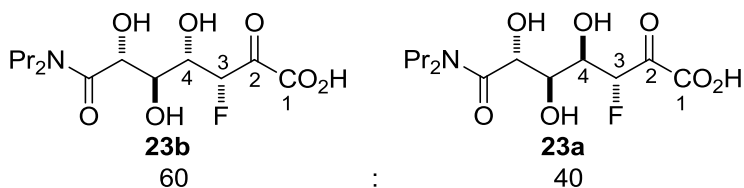
(3*R*,4*S*,5*S*,6*R*)-7-(dipropylamino)-3-fluoro-4,5,6-trihydroxy-2,7-dioxoheptanoate 23b NMR spectra

¹H/¹⁹F-HSQC-TOCSY

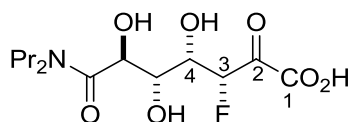


Extracted ¹H-NMR spectra



(3R,4S,5S,6R) and **(3R,4R,5S,6R)-7-(dipropylamino)-3-fluoro-4,5,6-trihydroxy-2,7-dioxoheptanoate 23**

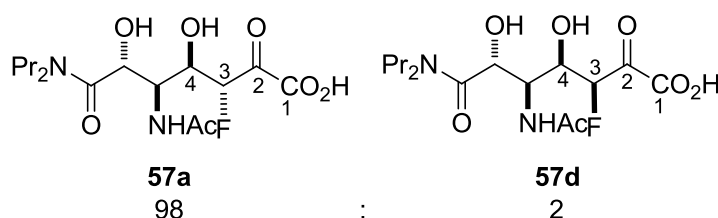
Reaction was carried out as described in the general experimental Section 6.3.1 using the alkene **24** (314 mg, 1.58 mmol), sodium fluoropyruvate (202 mg, 1.58 mmol) and the NAL E192N variant. A mixture of *products 23b and 23a* (171 mg, 33%, **23b:23a** 60:40) were isolated by ion exchange as a yellow glass. Purification by reverse-phase HPLC: **23a** retention time 28.7 min, **23b** retention time 31.0 min. The spectroscopic data for the product **23b** was found to be identical to that described previously. The product **23a** was observed as 92:8 mixture of anomers of a pyranose ring and the spectroscopic data is presented as follows; δ_{H} (500 MHz, D₂O) 4.78 (1H, dd, $^2J_{\text{HF}}$ 49.9, $^3J_{\text{HH}}$ 3.4, 3-H), 4.57 (1H, d, $^3J_{\text{HH}}$ 9.2, 6-H), 3.97-3.90 (1H, m, 4-H), 3.88 (1H, t, $^3J_{\text{HH}}$ 9.7, 5-H), 3.42-3.08 (4H, m, 2 × propyl 1-H₂), 1.58-1.38 (4H, m, 2 × propyl 2-H₂), 0.78-0.68 (6H, m, 2 × propyl 3-H₃); δ_{F} (395 MHz, D₂O) -206.0 (1F, dd, $^2J_{\text{HF}}$ 49.9, $^3J_{\text{HF}}$ 32.5, 3-F^{maj}), -216.8 (1F, dd, $^2J_{\text{HF}}$ 51.4, $^3J_{\text{HF}}$ 32.8, 3-F^{min}); *m/z* (ES) [MH]⁺ 324.1 (100 % [MH]⁺). The ratio of diastereomers was determined by analysis of the 395 MHz ¹⁹F NMR spectrum.

(3R,4S,5R,6S)-7-(dipropylamino)-3-fluoro-4,5,6-trihydroxy-2,7-dioxoheptanoate ent-23d

Reaction was carried out as described in the general experimental Section 6.3.1 using the alkene **ent-24** (202 mg, 0.93 mmol, supplied by Thomas Harman), sodium fluoropyruvate (119 mg, 0.93 mmol) and the NAL E192N/T167V/S208V variant. The crude product was isolated by ion exchange to give the *fluorinated sialic acid analogue ent-23d* (155 mg, 52%, d.r. >98:<2) as a colourless glass. One pyranose ring form was observed as a single anomer. δ_{H} (500 MHz, D₂O) 4.62 (1H, d, $^3J_{\text{HH}}$ 9.7, 6-H), 4.60 (1H, dd, $^2J_{\text{HF}}$ 49.3, $^3J_{\text{HH}}$ 9.3, 3-H), 3.95 (1H, dt, $^3J_{\text{HF}}$ 13.3, $^3J_{\text{HH}}$ 9.4, 4-H), 3.78 (1H, t, $^3J_{\text{HH}}$ 9.5, 5-H),

3.42-3.12 (4H, m, 2 × propyl 1-H₂), 1.60-1.39 (4H, m, 2 × propyl 2-H₂), 0.83-0.70 (6H, m, 2 × propyl 3-H₃); δ_F (395 MHz, D₂O) -199.8 (1F, dd, ²J_{HF} 49.3, ³J_{HF} 13.3, 3-F); *m/z* (ES) [MH]⁺ 324.1 (100 % [MH]⁺). The reaction was found to be completely diastereoselective under the conditions described to within the sensitivity of 395 MHz ¹⁹F NMR spectroscopy.

(3*R*,4*R*,5*S*,6*R*)-7-(dipropylamino)-5-acetamido-3-fluoro-4,6-dihydroxy-2,7-dioxoheptanoate **57a**



Reaction was carried out as described in the general experimental Section 6.3.1 using the alkene **25** (100 mg, 0.3 mmol), sodium fluoropyruvate (38 mg, 0.3 mmol) and the NAL E192N variant. The product was purified first by Dowex[®] ion exchange then mass directed HPLC to give the *fluorinated sialic acid analogue 57* (5.3 mg, 5%, **57a:57d** 98:2). The product **57a** was observed as mixture of anomers in a 97:3 ratio. δ_H (500 MHz; D₂O) 4.95 (1H, dd, ²J_{HF} 49.0, ³J_{HH} 2.1, 3-H^{min}), 4.90 (1H, dd, ²J_{HF} 49.2, ³J_{HH} 2.2, 3-H^{maj}), 4.84 (1H, d, ³J_{HH} 10.0, 6-H^{min}), 4.83 (1H, d, ³J_{HH} 10.0, 6-H^{maj}), 4.23 (1H, t, ³J_{HH} 9.9, 5-H^{maj}), 4.22 (1H, t, ³J_{HH} 9.9, 5-H^{min}), 4.17 (1H, ddd, ³J_{HF} 29.1, ³J_{HH} 10.9 and 2.2, 4-H^{min}), 4.16 (1H, ddd, ³J_{HF} 29.1, ³J_{HH} 10.9 and 2.2, 4-H^{maj}), 3.55-3.43 (2H, m, propyl 1-H_{2,A}), 3.25-3.18 (1H, m, propyl 1-H_C), 3.00-2.93 (1H, m, propyl 1-H_D), 1.91 (3H, s, acetyl-CH₃), 1.62-1.51 (2H, m, propyl 2-H_A), 1.48-1.39 (2H, m, propyl 2-H_B), 0.81 (3H, t, ³J_{HH} 7.7, propyl 3-H_A), 0.78 (3H, t, ³J_{HH} 7.5, propyl 3-H_B); δ_C (75 MHz; D₂O) 174.1 (acetyl-C=O), 170.8 (1-C), 168.7 (7-C), 95.4 (2-C), 89.7 (d, ¹J_{CF} 178.0, 3-C), 67.6 (6-C), 66.9 (5-C), 66.8 (4-C), 49.8 (propyl 1-C_A), 48.7 (propyl 1-C_B), 22.1 (propyl 2-C_A), 21.9 (acetyl-CH₃), 20.1 (propyl 2-C_A), 10.5 (propyl 3-C_B), 10.3 (propyl 3-C_A); δ_F (296 MHz, D₂O) -199.2 (1F, dd, ²J_{HF} 49.3, ³J_{HF} 10.4, 3-F^{3*S*4*R*}), -207.8 (1F, dd, ²J_{HF} 49.0, ³J_{HF} 29.1, 3-F^{3*R*4*R*,*min*}), -218.5 (1F, dd, ²J_{HF} 50.2, ³J_{HF} 28.8, 3-F^{3*R*4*R*,*maj*}).^{*} HRMS Found: 363.1565, [M]-H⁺ requires 363.1573.

^{*} Superscript abbreviations in NMR characterisation data: “3*R*4*R*” and “3*S*4*R*” refer to the **57a** and **57d** diastereomers respectively. “*maj*” and “*min*” refer to the major and

Chapter 6 - Materials and Methods and Experimental

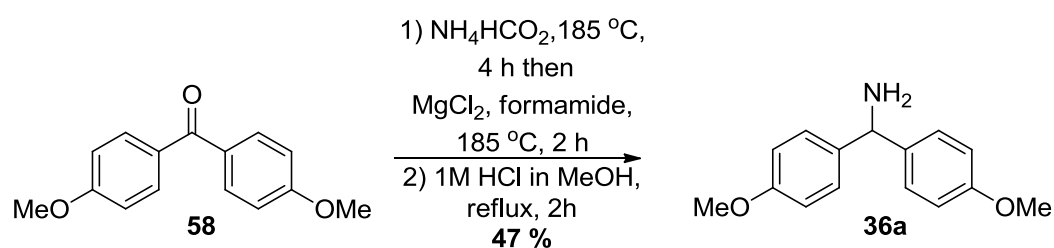
The ratio of anomers and diastereomers was determined by analysis of the 296 MHz ^{19}F NMR. The product **57d** could not be characterised by ^1H NMR or ^{13}C NMR so the configuration was predicted by correlation of the ^{19}F NMR spectroscopy data with a related product (product **ent-23d**) with the same relative configuration.

minor anomer. When unspecified, assume that the peak described both of the anomers. Only 296 MHz ^{19}F NMR has been used to characterise the product **57d**.

Appendix 1 - Synthesis of non-commercial available reagents

A1.1 Synthesis of primary amine used in the Petasis reaction

The primary amine **36a**, used in the Petasis reaction described in Section 2.3.2, was synthesised by melting 4-4'-dimethoxybenophenone **58** with ammonium formate, followed by the addition of magnesium chloride and formamide. Refluxing in acidic methanol and recrystallisation from diethyl ether gave the primary amine **36a** in a 47% overall yield (Scheme A:1).⁹²



Scheme A:1 - Synthesis of the primary amine **36a** used in the optimisation of the Petasis reaction described in Section 2.3.2.

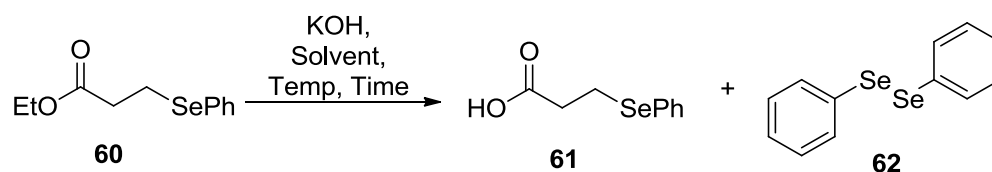
A1.2 Optimisation of the synthesis of the selenyl acid chloride

Synthesis of the selenyl acid chloride used in the Claisen reaction of the lactone **33** (Section 2.3.3) was synthesised in three steps from the chloro ester **59**. The conversion of the chloro ester **59** to the selenyl-ether **60** was carried out as described in the literature by reaction with the phenylselenide dimer under reducing conditions to give the intermediate ester **60** in an 86% yield.⁹³ However, hydrolysis of the ester resulted in cleavage of the carbon-selenium bond under the conditions described in the literature.⁹³ The reaction conditions were optimised with the aid of analytical HPLC, which was calibrated with a sample of known concentration of the selenyl-ether **60**, the acid **61** and diphenyldiselenide **62**. By using the analytical HPLC it was possible to follow the reactions under various conditions and monitor the rate of conversion to the acid and the rate of decomposition. Table A:1 show the conditions screened along with both the conversion to the acid **61** after 90 minutes and the decomposition to diphenyldiselenide **62** after 90 minutes. Chart A:1 shows the plots of disappearance of selenyl-ether **60** (blue) and the appearance of the acid **61** (green) and diphenyldiselenide **62** (red). Increased reaction temperatures and higher

Appendix

concentrations of ester **60** resulted in a faster rate of decomposition. However, very low concentrations of ester **60** also favoured decomposition. The optimised condition for synthesis of the acid **61** were found to be potassium hydroxide in 1:1 THF–water with the temperature carefully controlled in a jacketed vessel at 0 °C to prevent the elimination of diphenyldiselenide **62**.

Table A:1 - Optimisation of the conditions for the hydrolysis of ester 60



Reaction number	Solvent	Temp /°C	Initial concentration of 60/mg ml ⁻¹	Conversion to 61 after 90 min %	Decomposition to 62 after 90 min %
1	EtOH–water (98:2)	0	4	1.5	30.0
2	Water–THF (1:1)	22	46.3	55.2	27.7
3	Water–THF (1:1)	22	23.1	51.4	24.7
4	Water–THF (1:1)	0	46.3	43.5	19.8

Appendix

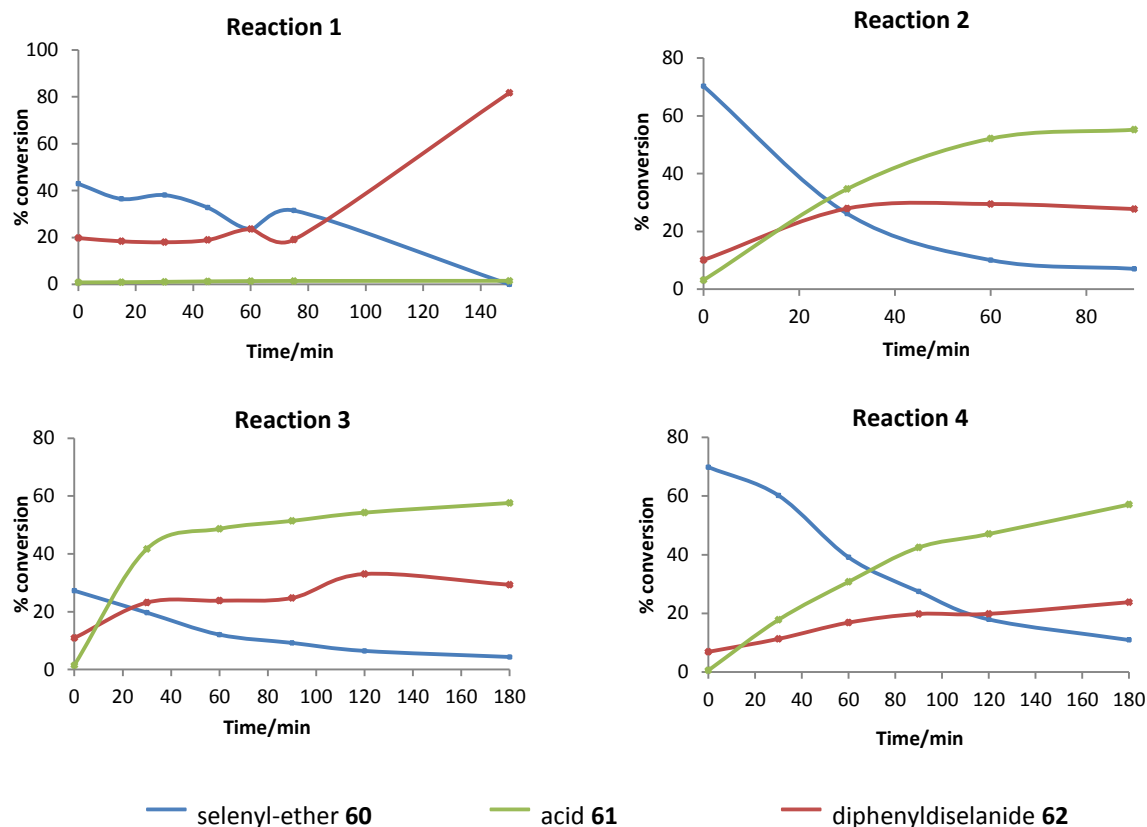
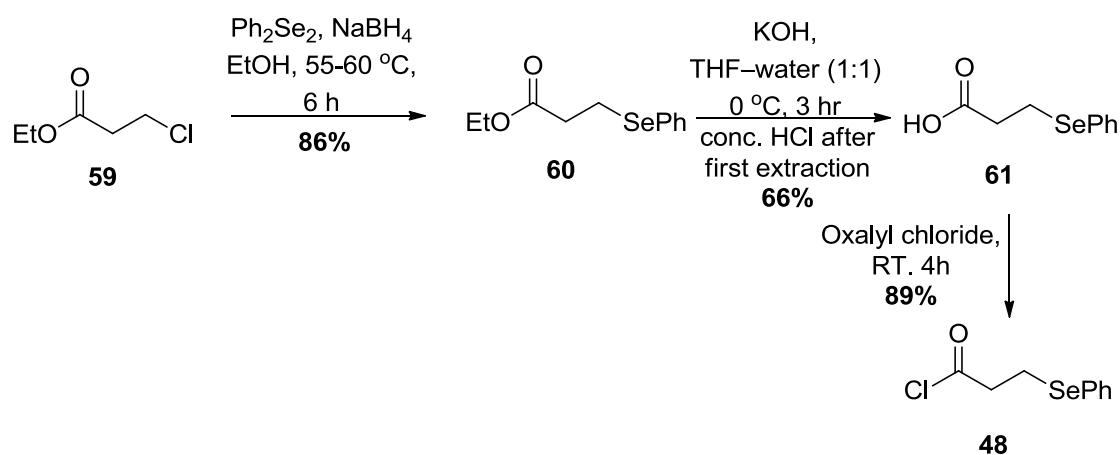


Chart A:1 - Optimisation of the hydrolysis of the ester **60** to give the acid **62**, while reducing the decomposition to diphenyldiselenide.

Scheme A:2 outlines the optimised conditions for the synthesis of the acid chloride **48**. The acid chloride **48** was synthesised by reacting the acid **61** with oxalyl chloride, followed by distillation.⁹⁴ The acid chloride **48** was used immediately in the Claisen reaction with the lactone **33** (Section 2.3.3)

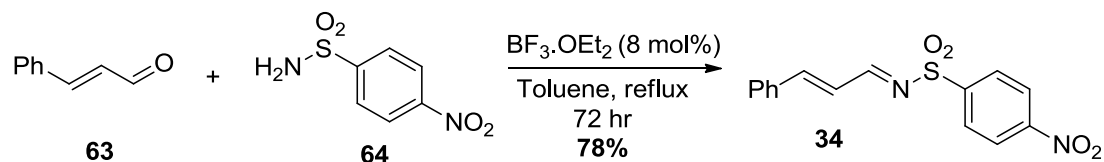


Scheme A:2 - Synthesis of non-commercially available reaction partners of the lactone **33** 1) Optimised synthesis of the selenyl acid chloride **48** used in the Claisen reaction with the lactone **33**.

Appendix

A1.3 Synthesis of the imine used in the Mannich reaction

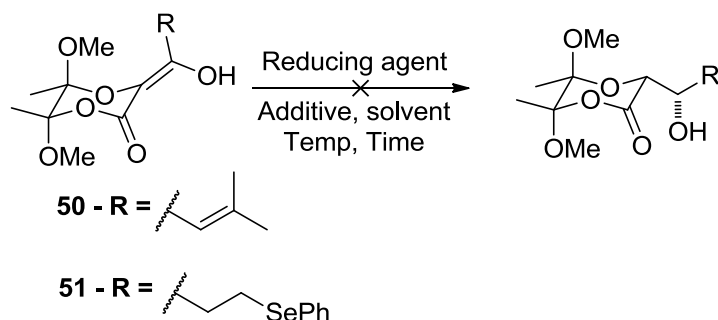
The imine **34** (see Section 2.3.3) was synthesised in a single step from cinnamaldehyde **63** and *p*-nitrobenzene sulfonamide **64** in refluxing toluene with catalytic boron trifluoride etherate. The resulting imine **34** was triturated from ethyl acetate and isolated in 78% yield (Scheme A:3).



Scheme A:3 - Synthesis of non-commercially available reaction partners of the lactone **33** 2) Synthesis of the imine **34** used in the Mannich reaction with lactone **33**

Appendix 2 - Unsuccessful reduction of enol products **50** and **51**

Section 2.3.3 described a selection of examples of reactions of the lactone **33**. One example was a Claisen-type condensation between the lactone **33** and two different acid chlorides **47** and **48**. Literature precedent⁸⁰ suggested that it ought to be possible to reduce the resulting enol **50/51** to the alcohol (Scheme A:4), however no suitable conditions were found.



Scheme A:4 - Unsuccessful reduction of Claisen-type condensation products **50 and **51**.**

Table A:2 outlines all of the reduction conditions attempted for enol **50** and **51**. Entry 1 and Entry 9 replicate the conditions described in the literature.⁸⁰ In the case of the enol **50** (Entry 1), the conjugate reduction product was formed in a complex mixture with starting material and decomposition by-products. In the case of the enol **51** (Entry 9), a complex mixture with no evidence of enol reduction was formed.

Entries 2-8 are all variations of Luche conditions, where CeCl_3 is used as an additive with sodium borohydride as the reducing agent. Luche conditions are known to selectively reduce α,β -unsaturated ketones to give allyl alcohols.⁹⁵ In all cases either a complex mixture was formed or no reaction was observed. Some success was observed when the reaction was cooled to -78°C (Entries 6 and 7), but still only a very small quantity of product was observed and the purity was very poor. It was predicted that the reason for difficulty in carrying out the reduction was that, even under Luche conditions, conjugate reduction was taking place.

In an attempt to avoid the problem of conjugate reduction, the enol **51** was synthesised with the intention that the selenyl-ether functional group would act as a "masked" double bond, which would allow the required double bond functionality to be revealed later.⁸² However, the enol **51** also proved difficult to reduce and in most

Appendix

cases, no reaction took place or a complex mixture was observed. This was most likely due to the decomposition.

Appendix

Table A:2 - Reduction conditions attempted for enol-lactones 50 and 51

Entry	Enol	Reducing agent ^{a-e} and additives	Solvent	Temp /°C	Time /h	Comments
1	50	NBu ₄ BH ₄ ^a	CH ₂ Cl ₂	0 to RT	5.25	Conjugate reduction product observed ^f
2	50	NaBH ₄ ^b , CeCl ₃ ·7H ₂ O	MeOH-CH ₂ Cl ₂ 1:1	- 70 to - 30	1	Complex mixture ^f
3	50	K-selectride ^b	THF	- 78	120	No reaction ^g
4	50	NaBH ₄ ^c , CeCl ₃ ·7H ₂ O	MeOH	RT	0.6	No product observed ^h
5	50	NaBH ₄ ^c , CeCl ₃ ·7H ₂ O	MeOH	- 70 to - 30	4	No product observed ^f
6	50	NaBH ₄ ^d , CeCl ₃ ·7H ₂ O	MeOH	- 78	4	<4% yield of impure product ^f
7	50	NaBH ₄ ^a , CeCl ₃ ·7H ₂ O	MeOH	- 78 to RT	72	<10% yield of impure product ^f
8	50	NBu ₄ BH ₄ ^a , CeCl ₃ ·7H ₂ O	MeOH-CH ₂ Cl ₂ 1:1	- 78	72	Complex mixture ^f
9	51	NBu ₄ BH ₄ ^a	CH ₂ Cl ₂	0 to RT	5.25	Complex mixture ^f
10	51	NaBH ₄ ^e	EtOH	0	3	Complex mixture ^f
11	51	NaBH ₄ ^d , CeCl ₃ ·7H ₂ O	MeOH	- 78	-	No reaction ^g
12	51	NBu ₄ BH ₄ ^d	CH ₂ Cl ₂	0	5	No reaction ^g
13	51	NBu ₄ BH ₄ ^d	CH ₂ Cl ₂	- 78	4	No reaction ^f
14	51	NaBH ₄ ^d	EtOH	- 78	1.5	No reaction ^f
15	51	NaBH ₄ ^d	EtOH	0	1.5	Complex mixture ^f

a-e) Equivalents of reducing agent used. Where an additive was used, equimolar equivalents of reducing agent and additive were used. a) 2.2 equivalents b) 1.5 equivalents c) 1.0 equivalents d) 1.1 equivalents e) 2.0 equivalents f) By analysing the ¹H-NMR spectrum of the crude product g) No reaction was observed by TLC h) No product observed by LC-MS

Appendix 3 - Monitoring the reaction between aldehyde variants and pyruvate by 500 MHz ^1H NMR spectroscopy

The following Section is the data used to determine the kinetic selectivity of the NAL variants towards **AHOB** and pyruvate (Section 3.1.4). The NAL variant-catalysed reactions between **AHOB** and pyruvate were monitored by 500 MHz ^1H NMR spectroscopy. Chart A:2 represents the calculated conversions at each time point in the NAL E192N-catalysed reaction of **AHOB** and pyruvate.

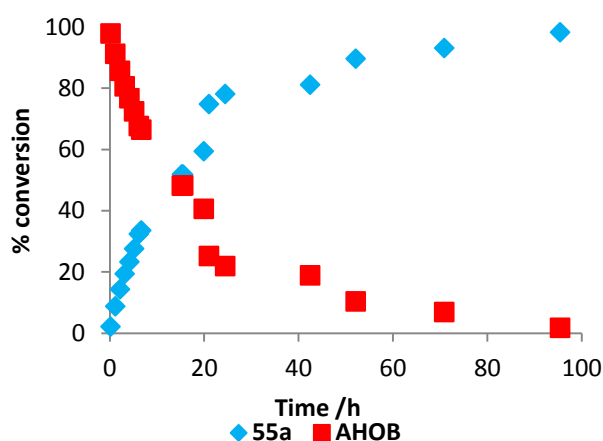


Chart A:2 - Representation of the percentage disappearance of **AHOB** and appearance of diastereomer **55a** calculated from the relative integrals measured at a series of time points in the NAL E192N-catalysed reaction of **AHOB** and pyruvate.

The conversion in the NAL E192N-catalysed reaction of **ent-AHOB** and pyruvate was made more challenging because the reaction was very slow, so the decomposition of **ent-AHOB** made it difficult to reliably measurement the reaction rate. A series of time points from the 500 MHz ^1H NMR spectroscopy time-course is shown in Figure A:1, and it is possible to see that the peaks corresponding to **AHOB** are decomposing faster than the peaks corresponding to product **ent-55b** (highlighted in green) are appearing. After ozonolysis of the aldehyde precursor **ent-25**, there is always a small amount of benzaldehyde remaining, which does not participate in the enzyme reaction. The peaks corresponding to benzaldehyde are highlighted in purple. The contaminating benzaldehyde was therefore used as an internal standard in order to estimate the loss of **AHOB** due to decomposition. The full time-course data is shown in Chart A:3.

Appendix

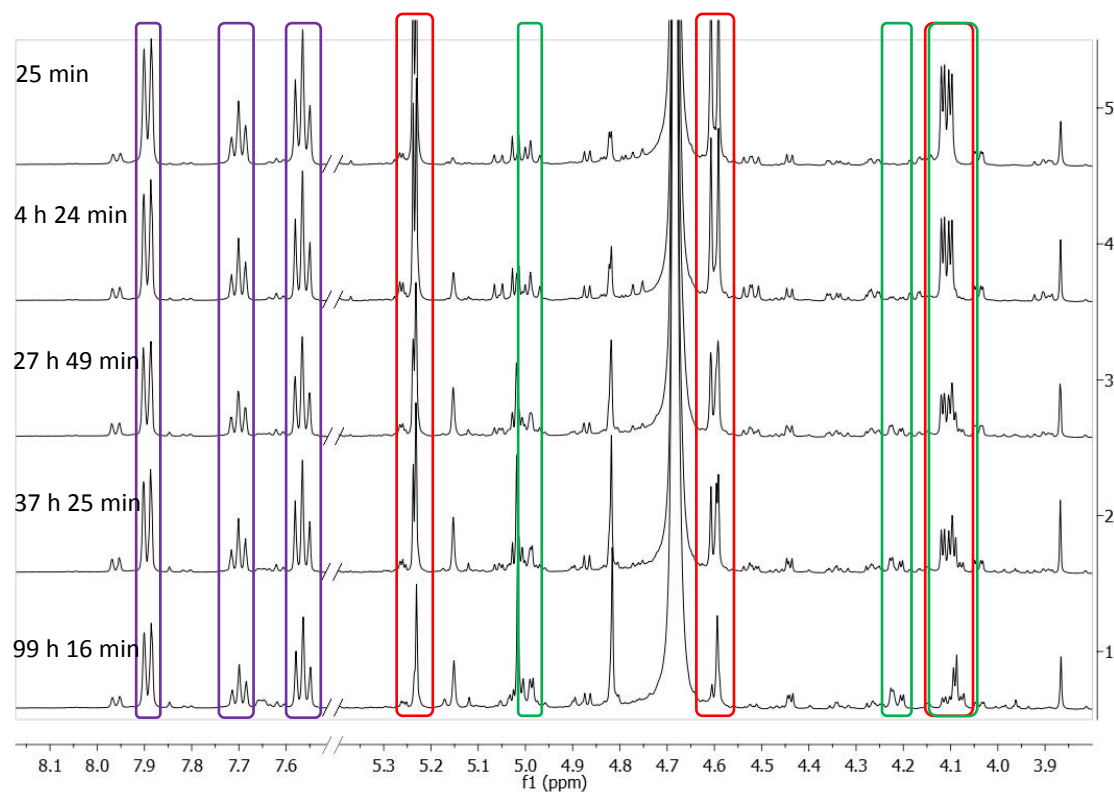


Figure A:1 - Illustration of the change in intensity of the peaks corresponding to *ent*-AHOB (red) and the product of the NAL E192N-catalysed reaction *ent*-55b (green) over time by 500 MHz ¹H NMR spectroscopy. Decomposition was estimated by measuring by using the peaks corresponding to the benzaldehyde by-product (purple) as an internal standard.

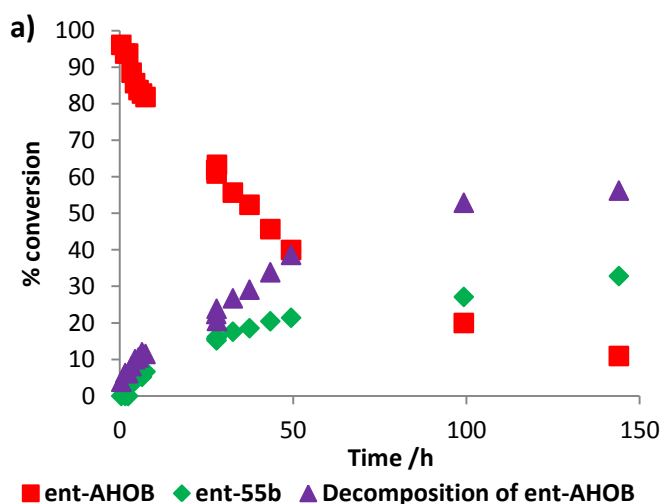


Chart A:3 - Representation of the percentage disappearance of *ent*-AHOB and appearance of diastereomer *ent*-55b calculated from the relative integrals measured at a series of time points in the NAL E192N-catalysed reaction of *ent*-AHOB and pyruvate.

Appendix 4 - ^{19}F NMR spectra from the reactions of AHOB and fluoropyruvate

The following Section shows the 296 MHz ^{19}F NMR used in the characterisation of the products of the NAL-catalysed reaction of **AHOB** and fluoropyruvate (Section 4.2.2). Figure A:2 shows the 296 MHz ^{19}F NMR spectra of the products after ion exchange purification for the reaction between **AHOB** and fluoropyruvate catalysed by NAL E192N (Figure A:2a) and E192N/T167G (Figure A:2b) and between *ent*-**AHOB** and fluoropyruvate catalysed by NAL E192N (Figure A:2c) and E192N/T167G (Figure A:2d). The first thing to note is that, as would be expected from the conversions recorded in Section 4.2.1 (Table 4.2), most of the samples are very weak and the fluoropyruvate peak (highlighted in orange) dwarfs the doublet of doublets (highlighted in red or green) and the reaction products are difficult to distinguish from the noise. Across the four reactions, two different products are identified, one characterised by a peak at -207.9 ppm (red) and a second at -200.9 ppm (green). Upon HPLC purification, a peak at -218.5 ppm was identified, which corresponded to the minor anomer of the product characterised by the peak at -207.9 ppm.

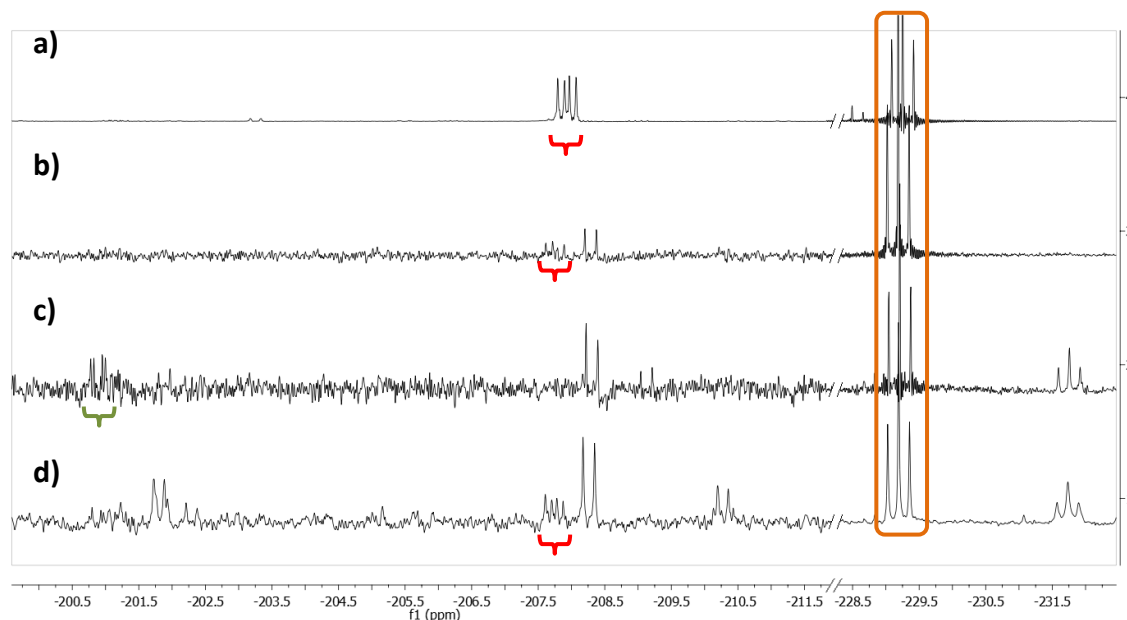


Figure A:2 – 296 MHz ^{19}F NMR of products isolated after ion exchange of the reactions between fluoropyruvate and AHOB/*ent*-AHOB catalysed by the NAL variants. The conversion is low in all cases so there is a large peak for fluoropyruvate (highlighted orange) however two different diastereomers were identified as diagnostic doublet of doublets at -207.9 ppm (red) and -200.9 ppm (green) a) AHOB catalysed by E192N b) AHOB catalysed by E192N/T167G c) *ent*-AHOB catalysed by E192N d) *ent*-AHOB catalysed by E192N/T167G

Appendix 5 - Monitoring the reaction between aldehyde variants and fluoropyruvate by 296 MHz ^{19}F NMR spectroscopy

The following Sections show the data used to calculate initial rates of NAL-catalysed reaction of the aldehyde analogues and fluoropyruvate and the diastereoselectivity of the enzymes. (For the initial rates see Section 4.4.1 and for the calculated kinetic ratios see Section 4.4.2) The NAL variant-catalysed reactions between the aldehyde analogues and fluoropyruvate were monitored by 296 MHz ^{19}F NMR spectroscopy. The main body of the thesis shows two examples of the plots of conversion of fluoropyruvate and appearance of fluorinated product **23** and **57** over time. These plots were used to calculate the initial rates of reaction and the kinetic ratio of products. The following plots show the conversions calculated from relative integrals for all of the combinations of NAL variants and aldehyde analogues.

A5.1 Reactions of AHOB/*ent*-AHOB and fluoropyruvate

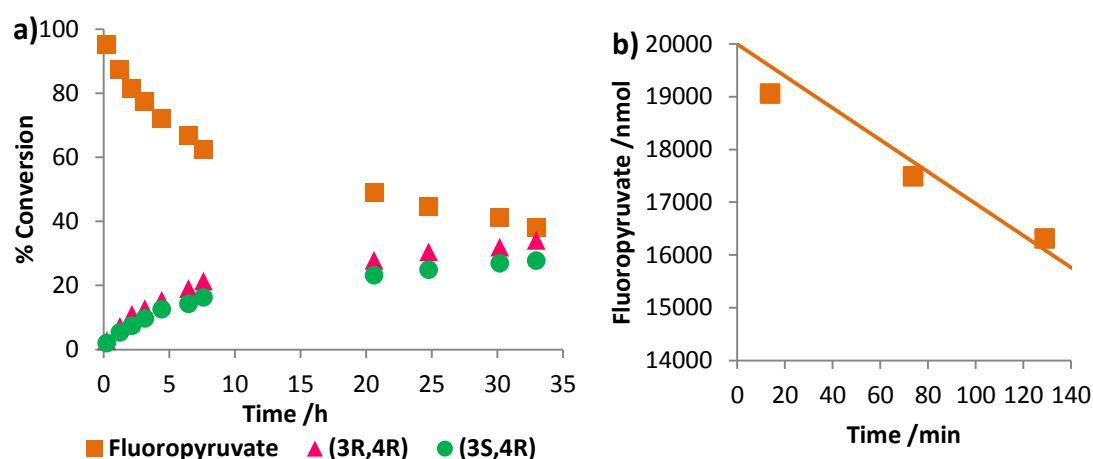


Chart A:4 - A plot of the appearance of the products of the NAL E192N -catalysed reaction of AHOB and fluoropyruvate and the disappearance of fluoropyruvate. The conversion was calculated from the relative integrals of the 296 MHz ^{19}F NMR spectra recorded at suitable time intervals. a) Representation of the percentage disappearance of fluoropyruvate and the percentage appearance of product over the full reaction time. b) Linear points of the disappearance of fluoropyruvate. The initial gradient was used to calculate the initial rate of the reaction. In this reaction, the fluoropyruvate is disappearing at a rate of 30 nmol/min.

Appendix

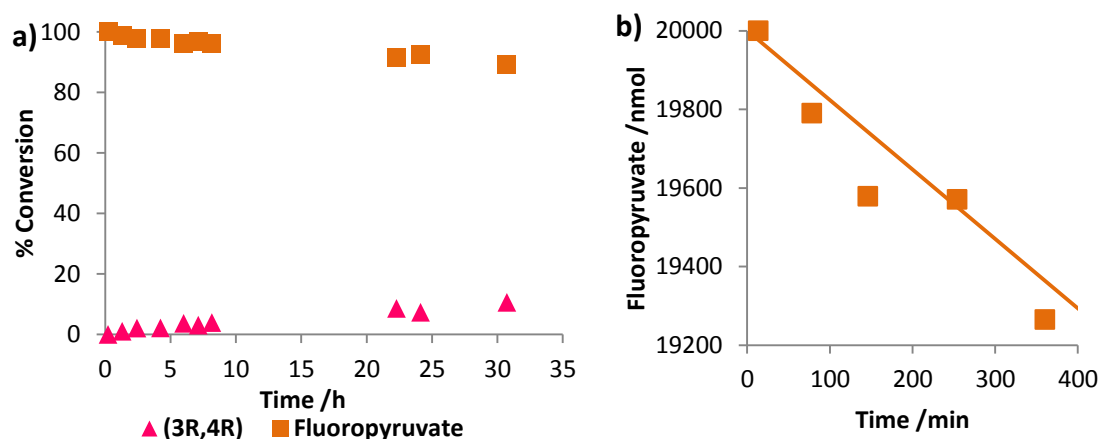


Chart A:5 - A plot of the appearance of the product of the NAL E192N/T167G-catalysed reaction of AHOB and fluoropyruvate and the disappearance of fluoropyruvate. The conversion was calculated from the relative integrals of the 296 MHz ^{19}F NMR spectra recorded at suitable time intervals. a) Representation of the percentage disappearance of fluoropyruvate and the percentage appearance of product over the full reaction time. b) Linear points of the disappearance of fluoropyruvate. The initial gradient was used to calculate the initial rate of the reaction. In this reaction, the fluoropyruvate is disappearing at a rate of 1.8 nmol/min.

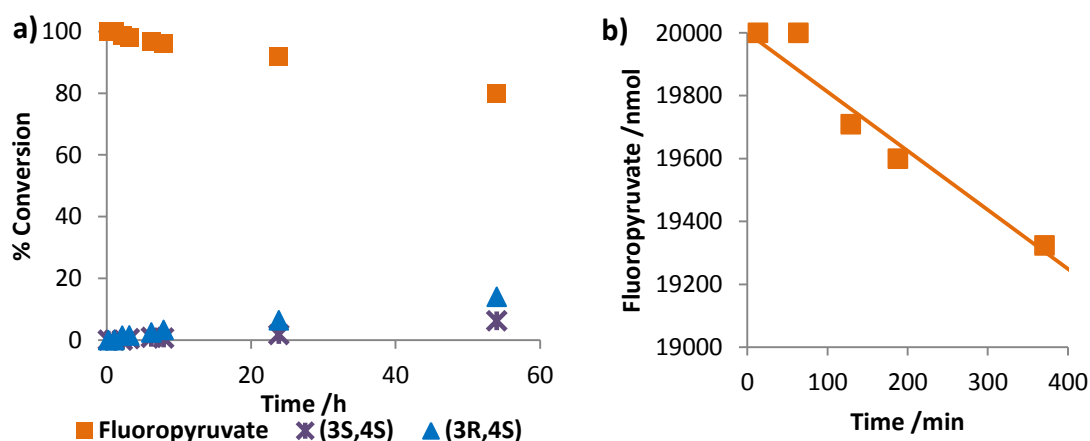


Chart A:6 - A plot of the appearance of the products of the NAL E192N-catalysed reaction of *ent*-AHOB and fluoropyruvate and the disappearance of fluoropyruvate. The conversion was calculated from the relative integrals of the 296 MHz ^{19}F NMR spectra recorded at suitable time intervals. a) Representation of the percentage disappearance of fluoropyruvate and the percentage appearance of product over the full reaction time. b) Linear points of the disappearance of fluoropyruvate. The initial gradient was used to calculate the initial rate of the reaction. In this reaction, the fluoropyruvate is disappearing at a rate of 1.9 nmol/min.

Appendix

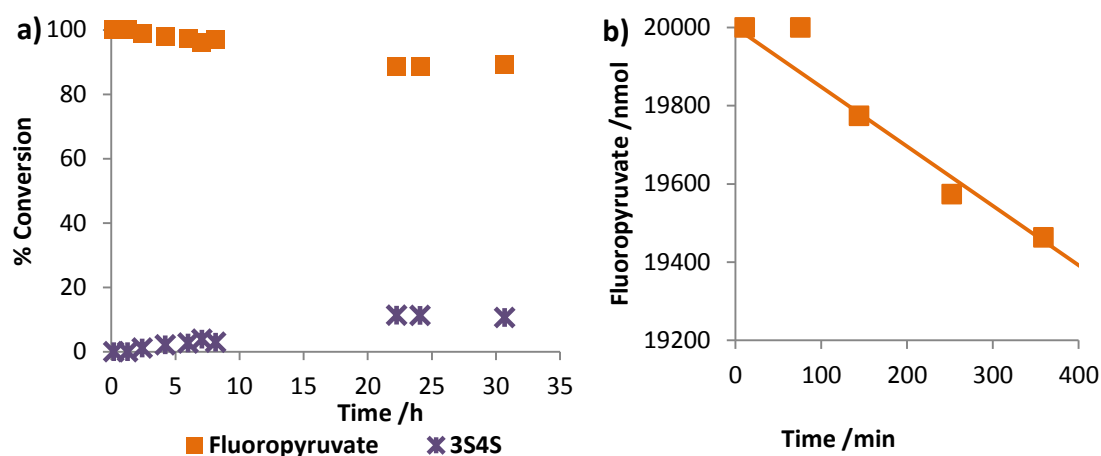


Chart A:7 - A plot of the appearance of the product of the NAL E192N/T167G-catalysed reaction of *ent*-AHOB and fluoropyruvate and the disappearance of fluoropyruvate. The conversion was calculated from the relative integrals of the 296 MHz ^{19}F NMR spectra recorded at suitable time intervals. a) Representation of the percentage disappearance of fluoropyruvate and the percentage appearance of product over the full reaction time. b) Linear points of the disappearance of fluoropyruvate. The initial gradient was used to calculate the initial rate of the reaction. In this reaction, the fluoropyruvate is disappearing at a rate of 1.5 nmol/min.

A5.2 Reaction of DHOB/*ent*-DHOB and fluoropyruvate

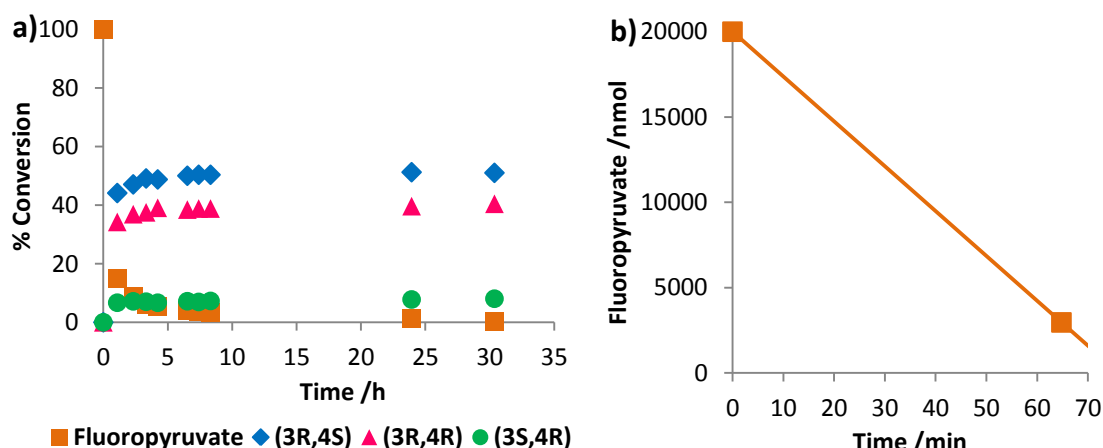


Chart A:8 - A plot of the appearance of the products of the NAL E192N-catalysed reaction of DHOB and fluoropyruvate and the disappearance of fluoropyruvate. The conversion was calculated from the relative integrals of the 296 MHz ^{19}F NMR spectra recorded at suitable time intervals. a) Representation of the percentage disappearance of fluoropyruvate and the percentage appearance of product over the full reaction time. b) Linear points of the disappearance of fluoropyruvate. The initial gradient was used to calculate the initial rate of the reaction. In this reaction, the fluoropyruvate is disappearing at a rate of >263 nmol/min.

Appendix

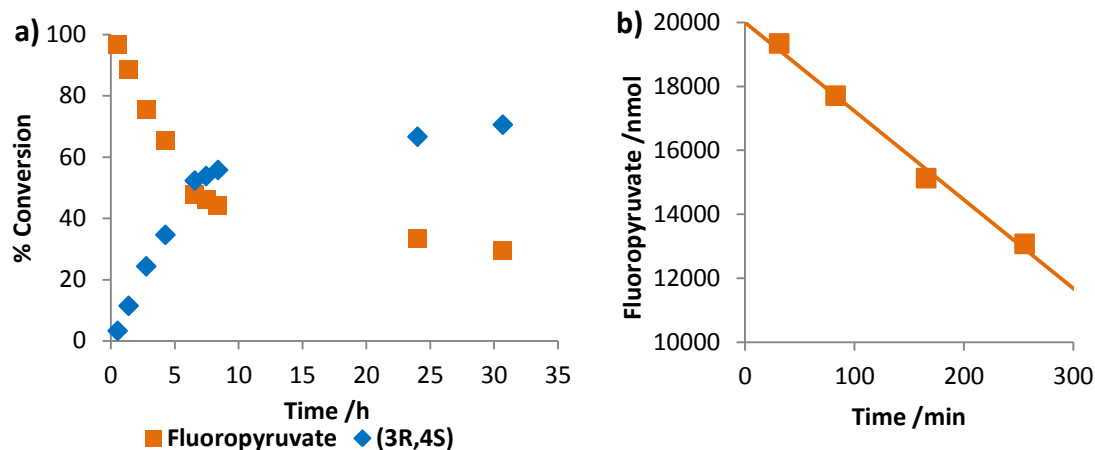


Chart A:9 - A plot of the appearance of the product of the NAL E192N/T167V/S208V-catalysed reaction of DHOB and fluoropyruvate and the disappearance of fluoropyruvate. The conversion was calculated from the relative integrals of the 296 MHz ^{19}F NMR spectra recorded at suitable time intervals. a) Representation of the percentage disappearance of fluoropyruvate and the percentage appearance of product over the full reaction time. b) Linear points of the disappearance of fluoropyruvate. The initial gradient was used to calculate the initial rate of the reaction. In this reaction, the fluoropyruvate is disappearing at a rate of 28 nmol/min.

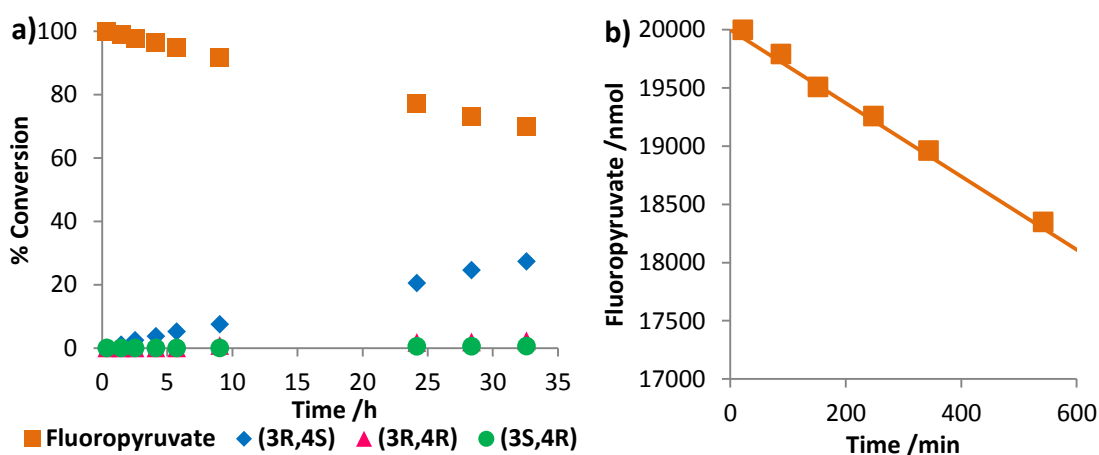


Chart A:10 - A plot of the appearance of the products of the NAL E192N/T167G-catalysed reaction of DHOB and fluoropyruvate and the disappearance of fluoropyruvate. The conversion was calculated from the relative integrals of the 296 MHz ^{19}F NMR spectra recorded at suitable time intervals. a) Representation of the percentage disappearance of fluoropyruvate and the percentage appearance of product over the full reaction time. b) Linear points of the disappearance of fluoropyruvate. The initial gradient was used to calculate the initial rate of the reaction. In this reaction, the fluoropyruvate is disappearing at a rate of 3.2 nmol/min.

Appendix

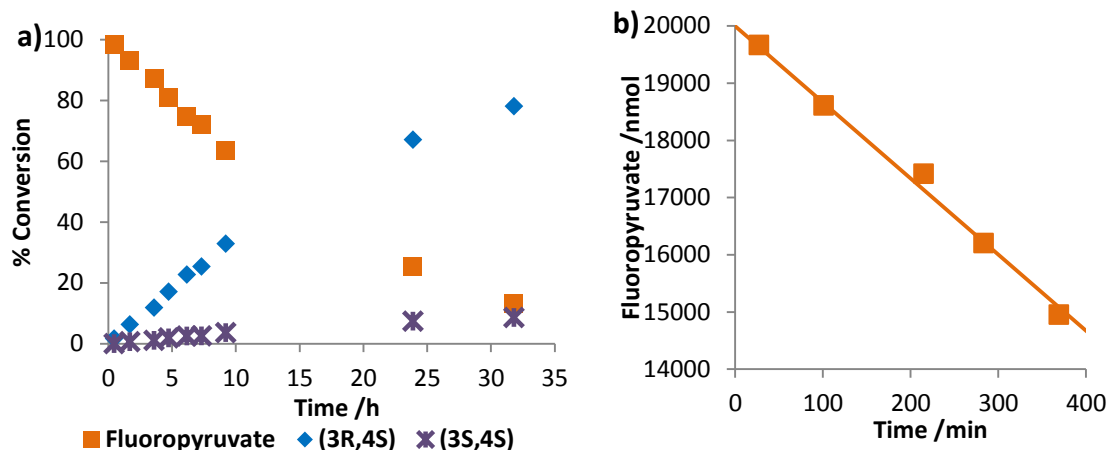


Chart A:11 - A plot of the appearance of the products of the NAL E192N-catalysed reaction of *ent*-DHOB and fluoropyruvate and the disappearance of fluoropyruvate. The conversion was calculated from the relative integrals of the 296 MHz ^{19}F NMR spectra recorded at suitable time intervals. a) Representation of the percentage disappearance of fluoropyruvate and the percentage appearance of product over the full reaction time. b) Linear points of the disappearance of fluoropyruvate. The initial gradient was used to calculate the initial rate of the reaction. In this reaction, the fluoropyruvate is disappearing at a rate of 13 nmol/min.

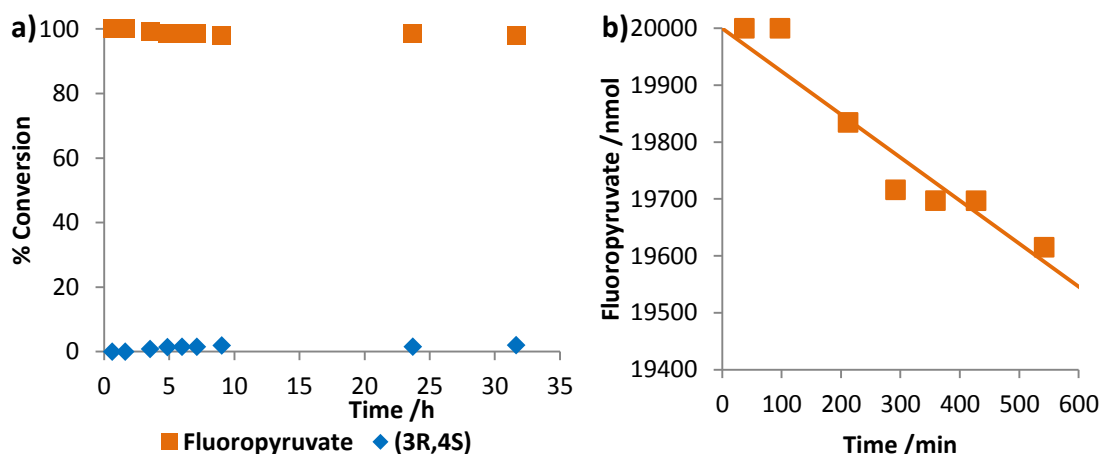


Chart A:12 - A plot of the appearance of the product of the NAL E192N/T167V/S208V-catalysed reaction of *ent*-DHOB and fluoropyruvate and the disappearance of fluoropyruvate. The conversion was calculated from the relative integrals of the 296 MHz ^{19}F NMR spectra recorded at suitable time intervals. a) Representation of the percentage disappearance of fluoropyruvate and the percentage appearance of product over the full reaction time. b) Linear points of the disappearance of fluoropyruvate. The initial gradient was used to calculate the initial rate of the reaction. In this reaction, the fluoropyruvate is disappearing at a rate of 0.76 nmol/min.

Appendix

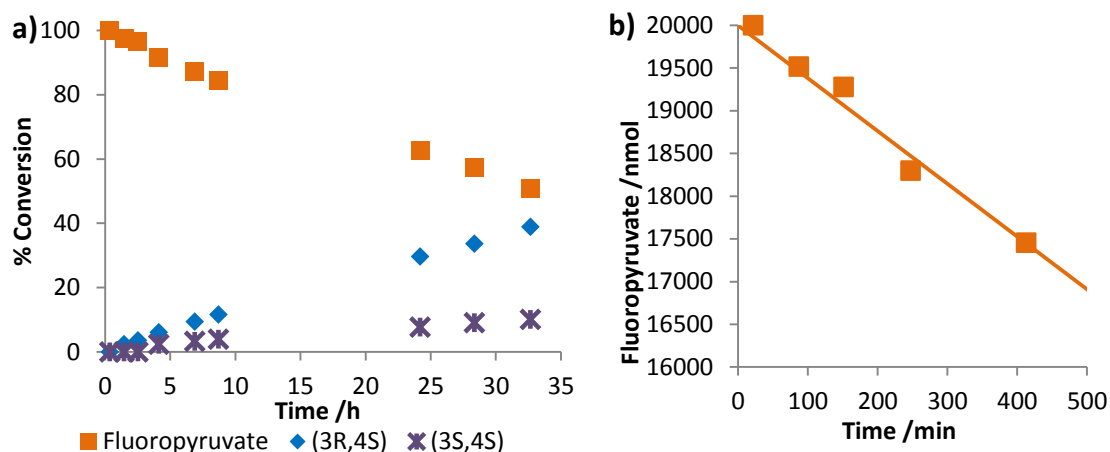


Chart A:13 - A plot of the appearance of the products of the NAL E192N/T167G-catalysed reaction of *ent*-DHOB and fluoropyruvate and the disappearance of fluoropyruvate. The conversion was calculated from the relative integrals of the 296 MHz ^{19}F NMR spectra recorded at suitable time intervals. a) Representation of the percentage disappearance of fluoropyruvate and the percentage appearance of product over the full reaction time. b) Linear points of the disappearance of fluoropyruvate. The initial gradient was used to calculate the initial rate of the reaction. In this reaction, the fluoropyruvate is disappearing at a rate of 6.2 nmol/min.

A5.3 Rate of NAL E192N catalysed reaction: Pyruvate Vs fluoropyruvate

Chart A:14a and b show the data used to compare the initial rate of the NAL E192N-catalysed reaction of **AHOB** and pyruvate with **AHOB** and fluoropyruvate (see Section 4.4.1).

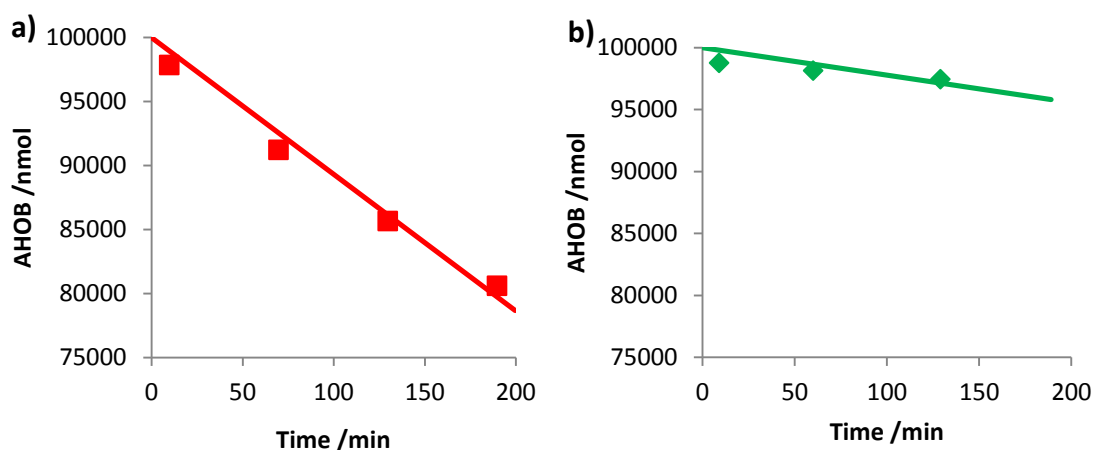


Chart A:14 - Comparison of the rate of reaction of AHOB with pyruvate Vs fluoropyruvate. AHOB was the limiting reagent. a) Linear points of the disappearance of AHOB in the reaction with pyruvate. The initial gradient was used to calculate the initial rate of the reaction. In this reaction, the AHOB disappeared at a rate of 161 nmol/min. b) Linear points of the disappearance of AHOB in the reaction with fluoropyruvate. The initial gradient was used to calculate the initial rate of the reaction. In this reaction, the AHOB disappeared at a rate of 22 nmol/min.

References

1. C. Jackel and D. Hilvert, *Curr. Opin. Biotech.*, 2010, **21**, 753-759.
2. A. Fersht, *Enzyme structure and mechanism (second edition)*, W H Freeman, 1985.
3. T. Hudlicky and J. W. Reed, *Chem. Soc. Rev.*, 2009, **38**, 3117-3132.
4. M. Wang, T. Si and H. Zhao, *Bioresource Technol.*, 2012, **115**, 117-125.
5. S. Panke, M. Held and M. Wubbolts, *Curr. Opin. Biotech.*, 2004, **15**, 272-279.
6. R. Wohlgemuth, *Curr. Opin. Microbio.*, 2010, **13**, 283-292.
7. T. H. Osterheld and J. I. Brauman, *J. Am. Chem. Soc.*, 1990, **112**, 2014-2016.
8. S. F. Royer, L. Haslett, S. J. Crennell, D. W. Hough, M. J. Danson and S. D. Bull, *J. Am. Chem. Soc.*, 2010, **132**, 11753-11758.
9. S. Panke and M. Wubbolts, *Curr. Opin. Chem. Bio.*, 2005, **9**, 188-194.
10. A. S. Eustaquio, D. O'Hagan and B. S. Moore, *J. Nat. Prod.*, 2010, **73**, 378-382.
11. K. K. J. Chan, D. O'Hagan and A. H. David, in *Methods in Enzymology*, Academic Press, Editon edn., 2012, vol. 516, pp. 219-235.
12. M. Sanada, T. Miyano, S. Iwadare, J. M. Williamson, B. H. Arison, J. L. Smith, A. W. Douglas, J. M. Liesch and E. Inamine, *J. antibio.*, 1984, **39**, 259-265.
13. D. O'Hagan, *J. Fluorine Chem.*, 2006, **127**, 1479-1483.
14. C. Schaffrath, H. Deng and D. O'Hagan, *FEBS Letters*, 2003, **547**, 111-114.
15. H. Deng and D. O'Hagan, *Curr. Opin. Chem. Bio.*, 2008, **12**, 582-592.
16. H. A. Chokhawala, H. Cao, H. Yu and X. Chen, *J. Am. Chem. Soc.*, 2007, **129**, 10630-10631.
17. W. K. Hagmann, *J. Med. Chem.*, 2008, **51**, 4359-4369.
18. D. O'Hagan, *J. Fluorine Chem.*, 2010, **131**, 1071-1081.
19. T. Angata and A. Varki, *Chem. Rev.*, 2002, **102**, 439-470.
20. M. M. Fuster and J. D. Esko, *Nat. Rev. Cancer*, 2005, **5**, 526-542.
21. J. M. Woods, R. C. Bethell, J. A. V. Coates, N. Healy, S. A. Hiscox, B. A. Pearson, D. M. Ryan, J. Ticehurst, J. Tilling, S. M. Walcott and C. R. Penn, *Antimicrob. Agents Ch.*, 1993, **37**, 1473-1479.
22. F. G. Hayden, J. J. Treanor, R. F. Betts, M. Lobo, J. D. Esinhart and E. K. Hussey, *J. Am. Med. Assoc.*, 1996, **275**, 295-299.
23. D. M. Ryan, J. Ticehurst and M. H. Dempsey, *Antimicrob. Agents Chem.*, 1995, **39**, 2583-2584.
24. C. U. Kim, W. Lew, M. A. Williams, H. T. Liu, L. J. Zhang, S. Swaminathan, N. Bischofberger, M. S. Chen, D. B. Mendel, C. Y. Tai, W. G. Laver and R. C. Stevens, *J. Am. Chem. Soc.*, 1997, **119**, 681-690.
25. W. Li, P. A. Escarpe, E. J. Eisenberg, K. C. Cundy, C. Sweet, K. J. Jakeman, J. Merson, W. Lew, Matt Williams, L. Zhang, C. U. Kim, N. Bischofberger, M. S. Chen and M. D. B., *Antimicrob. Agents Ch.*, 1998, **42**, 647-653.
26. P. W. Smith, S. L. Sollis, P. D. Howes, P. C. Cherry, I. D. Starkey, K. N. Cobley, H. Weston, J. Scicinski, A. Merritt, A. Whittington, P. Wyatt, N. Taylor, D. Green, R. Bethell, S. Madar, R. J. Fenton, P. J. Morley, T. Pateman and A. Beresford, *J. Med. Chem.*, 1998, **41**, 787-797.
27. N. R. Taylor, A. Cleasby, O. Singh, T. Skarzynski, A. J. Wonacott, P. W. Smith, S. L. Sollis, P. D. Howes, P. C. Cherry, R. Bethell, P. Colman and J. Varghese, *J. Med. Chem.*, 1998, **41**, 798-807.

References

28. T. Woodhall, G. Williams, A. Berry and A. Nelson, *Angew. Chem. Int. Ed.*, 2005, **44**, 2109-2112.
29. <http://www.drugs.com/stats/top100/2012/sales>, Accessed 02.08.2013.
30. <http://www.drugs.com/stats/top100/2011/sales>, Accessed 02.08.2013.
31. F. M. D. Ismail, *J. Fluorine Chem.*, 2002, **118**, 27-33.
32. K. Muller, C. Faeh and F. Diederich, *Science*, 2007, **317**, 1881-1886.
33. W. R. Dolbier, *Guide to Fluorine NMR for Organic Chemists*, Wiley, New Jersey, 2009.
34. D. O'Hagan, H. S. Rzepa, M. Schuler and A. M. Z. Slawin, *Beilstein J. Org. Chem.*, 2006, **2**, 19.
35. C. R. S. Briggs, M. H. Allen, D. O'Hagan, D. J. Tozer, A. M. Z. Slawin, A. E. Goeta and J. A. K. Howard, *Org. Biomol. Chem.*, 2004, **2**, 732-840.
36. G. Zhong, J. Fan and C. F. Barbas lii, *Tetrahedron Lett.*, 2004, **45**, 5681-5684.
37. X.-Y. Xu, Y.-Z. Wang and L.-Z. Gong, *Org. Lett.*, 2007, **9**, 4247-4249.
38. X.-Y. Xu, Y.-Z. Wang, L.-F. Cun and L.-Z. Gong, *Tetrahedron-Asymm.*, 2007, **18**, 237-242.
39. S. Bowles, M. M. Campbell, M. Sainsbury and G. M. Davies, *Tetrahedron Lett.*, 1989, **30**, 3711-3714.
40. W. J. Middleton, *J. Org. Chem.*, 1975, **40**, 574-578.
41. L. Hunter, D. O'Hagan and A. M. Z. Slawin, *J. Am. Chem. Soc.*, 2006, **128**, 16422-16423.
42. K. L. Kirk, *Org. Process Res. Dev.*, 2008, **12**, 305-321.
43. V. A. Brunet and D. O'Hagan, *Angew. Chem. Int. Ed.*, 2008, **47**, 1179-1182.
44. M. Tredwell and V. Gouverneur, *Org. Biomol. Chem.*, 2006, **4**, 26-32.
45. G. T. Giuffredi, S. Purser, M. Sawicki, A. L. Thompson and V. Gouverneur, *Tetrahedron-Asymm.*, 2009, **20**, 910-920.
46. S. M. Kim, H. R. Kim and D. Y. Kim, *Org. Lett.*, 2005, **7**, 2309-2311.
47. H.-F. Wang, H.-F. Cui, Z. Chai, P. Li, C.-W. Zheng, Y.-Q. Yang and G. Zhao, *Chem.-Euro. J.*, 2009, **15**, 13299-13303.
48. M. Marigo, D. Fielenbach, A. Braunton, A. Kjærsgaard and K. A. Jørgensen, *Angew. Chem. Int. Ed.*, 2005, **44**, 3703-3706.
49. S. C. Wilkinson, O. Lozano, M. Schuler, M. C. Pacheco, R. Salmon and V. Gouverneur, *Angew. Chem. Int. Ed.*, 2009, **48**, 7083-7086.
50. M. Tredwell, K. Tenza, M. C. Pacheco and V. r. Gouverneur, *Org. Lett.*, 2005, **7**, 4495-4497.
51. B. Greedy, J.-M. Paris, T. Vidal and V. Gouverneur, *Angew. Chem. Int. Ed.*, 2003, **42**, 3291-3294.
52. M. D. Burkart, Z. Zhang, S.-C. Hung and C.-H. Wong, *J. Am. Chem. Soc.*, 1997, **119**, 11743-11746.
53. K. Aisaka, A. Igarashi, K. Yamaguchi and T. Uwajima, *Biochem. J.*, 1991, **276**, 541-546.
54. C.-H. Wong and G. M. Whitesides, *Enzymes in Synthetic Organic Chemistry*, Pergamon, 1994.
55. A. Bolt, A. Berry and A. Nelson, *Arch. Biochem. Biophys.*, 2008, **474**, 318-330.
56. J. A. R. G. Barbosa, B. J. Smith, R. DeGori, H. C. Ooi, S. M. Marcuccio, E. M. Campi, W. R. Jackson, R. Brossmer, M. Sommer and M. C. Lawrence, *J. Mol. Biol.*, 2000, **303**, 405-421.
57. A. D. Daniels, PhD Thesis, University of Leeds, 2012.

References

58. A. Theodossis, H. Walden, E. J. Westwick, H. Connaris, H. J. Lamble, D. W. Hough, M. J. Danson and G. L. Taylor, *J. Biol. Chem.*, 2004, **279**, 43886-43892.
59. Y. Uchida, Y. Tsukada and T. Sugimori, *J. Biochem.*, 1984, **96**, 507-522
60. R. Gantt, S. Millner and S. B. Binkley, *Biochemist.*, 1964, **3**, 1952-1960.
61. J. Beliczey, U. Kragl, A. Liese, C. Wandrey, K. Hamacher, H. H. Coenen and T. Tierling, US Patent 6355453, 2002.
62. A. G. Watts and S. G. Withers, *Can. J. Chem.*, 2004, **82**, 1581-1588.
63. C. Windle, University of Leeds, Leeds, unpublished data, 2012.
64. G. J. Williams, T. Woodhall, A. Nelson and A. Berry, *Protein. Eng. Des. Selec.*, 2005, **18**, 239-246.
65. T. Woodhall, G. Williams, A. Berry and A. Nelson, *Org. Biomol. Chem.*, 2005, **3**, 1795-1800.
66. I. Campeotto, A. H. Bolt, T. A. Harman, C. Dennis, C. H. Trinh, S. E. V. Phillips, A. Nelson, A. R. Pearson and A. Berry, *J. Mol. Biol.*, 2010, **404**, 56-69.
67. G. J. Williams, T. Woodhall, L. M. Farnsworth, A. Nelson and A. Berry, *J. Am. Chem. Soc.*, 2006, **128**, 16238-16247.
68. G. J. Williams, S. Domann, A. Nelson and A. Berry, *Proc. Nat. Acd. Sci. U.S.A.*, 2003, **100**, 3143-3148.
69. T. Harman, PhD Thesis, University of Leeds, 2010.
70. A. Kinnell, T. Harman, M. Bingham, A. Berry and A. Nelson, *Tetrahedron*, 2012, **68**, 7719-7722.
71. T. Woodhall, PhD Thesis, University of Leeds, 2004.
72. S. V. Ley, E. Diez, D. J. Dixon, R. T. Guy, P. Michel, G. L. Nattrass and T. D. Sheppard, *Org. Biomol. Chem.*, 2004, **2**, 3608-3617.
73. N. A. Petasis and I. A. Zavalov, *J. Am. Chem. Soc.*, 1998, **120**, 11798-11799.
74. J. Tao and S. Li, *Chin. J. Chem.*, 2010, **28**, 41-49.
75. Z. Hong, L. Lui, C.-C. Hsu and C.-H. Wong, *Angew. Chem. Int. Ed.*, 2006, **45**, 7417-7421.
76. J.-F. Soule, A. Mathieu, S. Norsikian and J.-M. Beau, *Org. Lett.*, 2010, **12**, 5322-5325.
77. T. J. Southwood, M. C. Curry and C. A. Hutton, *Tetrahedron*, 2006, **62**, 236-242.
78. K. K. Nanda and B. Wesley Trotter, *Tetrahedron Lett.*, 2005, **46**, 2025-2028.
79. Z. Hong, L. Liu, C.-C. Hsu and C.-H. Wong, *Angew. Chem. Int. Ed.*, 2006, **45**, 7417-7421.
80. S. V. Ley, D. J. Dixon, R. T. Guy, M. A. Palomero, A. Polara, F. Rodriguez and T. D. Sheppard, *Org. Biomol. Chem.*, 2004, **2**, 3618-3627.
81. M. Penso, F. Foschi, S. Pellegrino, A. Testa and M. L. Gelmi, *J. Org. Chem.*, 2012, **77**, 3454-3461.
82. R. B. Grossman, *J. Org. Chem.*, 1997, **62**, 1906-1908.
83. A. Basha, M. Lipton and S. M. Weinreb, *Tetrahedron Lett.*, 1977, **18**, 4171-4172.
84. P.-Q. Huang, X. Zheng and X.-M. Deng, *Tetrahedron Lett.*, 2001, **42**, 9039-9041.
85. A. H. Bolt, PhD Thesis, University of Leeds, 2009.
86. M. Karplus, *J. Am. Chem. Soc.*, 1963, **85**, 2870-2871.
87. D. H. Williams and I. Fleming, *Spectroscopic methods in organic chemistry*, Fifth Edition edn., McGraw Hill, 1995.
88. N. Timms, C. L. Windle, A. Polyakova, J. R. Ault, C. H. Trinh, A. R. Pearson, A. Nelson and A. Berry, *ChemBioChem.*, 2013, **14**, 474-481.

References

89. F. Gassa, A. Contini, G. Fontana, S. Pellegrino and M. L. Gelmi, *J. Org. Chem.*, 2010, **75**, 7099-7106.
90. L. You and F. H. Arnold, *Protein Eng.* 1996, **9**, 77-83.
91. M. R. Wilkins, E. Gasteiger, A. Bairoch, J.-C. Sanchez, K. L. Williams, R. D. Appel and D. F. Hochstrasser, in *Methods in Molecular Biology; 2-D proteome analysis protocols*, Humana Press Inc, 1999, vol. 112, p. 531.
92. Y. It, Y. Kobayashi, T. Kawabata, M. Takase and S. Terashimaa, *Tetrahedron*, 1989, **45**, 5767-5790.
93. A. Bhalla, S. Sharma, K. K. Bhasin and S. S. Bari, *Synthetic Commun.*, 2007, **37**, 783-793.
94. H. Mastalerz, M. Menard, V. Vinet, J. Desiderio, J. Fung-Tomc, R. Kessler and Y. Tsai, *J. Med. Chem.*, 1988, **31**, 1190-1196.
95. J.-L. Luche, *J. Am. Chem. Soc.*, 1978, **100**, 2226-2227.